

**NMR STUDIES OF THE THERMAL AND PHOTOCHEMICAL
REACTIONS OF CYCLOPENTADIENYL RUTHENIUM
COMPLEXES**

By

Johnathan Lee Clark

A thesis submitted for the degree of Doctor of Philosophy

University of York

Department of Chemistry

September

2011

Abstract

The research reported in this thesis primarily focuses on the thermal and photochemical reactions of half-sandwich ruthenium complexes. The photochemical reactions employ the use of *ex situ* and *in situ* UV irradiation of the complexes. The latter of these techniques allows for samples to be irradiated within an NMR spectrometer, the principal method used to monitor reactions when highly unstable products result.

The reactivity of $[\text{CpRu}(\text{PPh}_3)_2\text{Cl}]$ towards a range of substrates is first described, where the thermal and photochemical (applying the *ex situ* method) reactions are contrasted. Replacement of PPh_3 by a range of 2-electron donors, including CO , PEt_3 , ethene and ${}^t\text{BuNC}$ was achieved. Similar treatment is given to the complex, $[\text{CpRu}(\text{PPh}_3)_2\text{H}]$. However, this hydride complex proved to be slow to react and only minimal conversion to products was achieved, even using photochemical methods.

The reactivity of $\text{CpRu}(\text{PPh}_3)_2\text{Me}$ toward a range of 2 electron donors was considered in greater detail, particularly its ability to activate Si-H, H-H and C-H adducts under photochemical conditions. Low temperature photochemical techniques, using the *in situ* method, were employed to determine that both Si-H and C-H bond activation is undertaken by the fragment $[\text{CpRu}(\kappa^2\text{-}2\text{-C}_6\text{H}_4\text{PPh}_2)]$. This fragment was shown to activate the C-H bonds of solvent molecules, and form Ru(IV) complexes $[\text{CpRu}(\text{PPh}_3)(\text{sol})(\text{SiEt}_3)\text{H}]$, where sol = C-H activated solvent, e.g. THF) which were stable at room temperature. The substitution of PPh_3 occurs in an analogous fashion to that of the chloride derivative. However, the rate of conversion was increased but no evidence for migration of either CO or ethene into the RuMe bond was observed.

The η^3 -coordinated complexes, $[\text{CpRu}(\text{PPh}_3)(\eta^3\text{-Si}(\text{Me}_2)\text{-CH=CH}_2)]$, $[\text{CpRu}(\text{PPh}_3)(\eta^3\text{-CH}_2\text{C}_2\text{H}_3)]$, $[\text{CpRu}(\text{PPh}_3)(\eta^3\text{-CH}_2\text{C}_6\text{H}_5)]$ and $[\text{CpRu}(\text{PPh}_3)(\eta^3\text{-CH}_2\text{C}_{10}\text{H}_7)]$ were synthesised. In the cases of $[\text{CpRu}(\text{PPh}_3)(\eta^3\text{-CH}_2\text{C}_2\text{H}_3)]$ and $[\text{CpRu}(\text{PPh}_3)(\eta^3\text{-CH}_2\text{C}_6\text{H}_5)]$, thermal and photochemical reaction was initiated with substrates to generate the corresponding η^1 substituted derivatives. These products were characterised by NMR techniques.

Finally, the ability of the fragment, $[\text{CpRh}(\text{NR}_3)]$, to C-H activate benzene was considered. NMR data were collected for the low stability products of the photochemical reaction which strongly indicated that this auxiliary is capable of C-H bond activation. Due to working at low temperatures (233 K) and the large amounts of amine required to generate $[\text{CpRh}(\text{NR}_3)]$, full characterisation by NMR of these species was not attained.

Contents

1 Introduction	1
1.1 General Introduction	1
1.2 Activation of R-H bonds (where R = Si, H or C)	2
1.2.1 Si-H activation	2
1.2.1.1 Oxidative addition and metathesis reaction pathways	2
1.2.1.2 Classical and nonclassical products of oxidative addition	3
1.2.1.3 σ -CAM (σ -complex assisted metathesis) reaction	5
1.2.1.4 Hydrosilation	5
1.2.1.5 Polymerisation	10
1.2.2 H-H activation	12
1.2.2.1 Oxidative addition pathway	12
1.2.3 C-H activation	15
1.2.3.1 Oxidative addition pathway	16
1.2.3.2 Agostic interactions	18
1.3 Reactions of cyclopentadienyl ruthenium complexes	20
1.4 The role of phosphine ligands in organometallic complexes	26
1.5 Photochemically induced reactivity	29
1.5.1 Low temperature photochemistry	30
1.6 The role of NMR spectroscopy in organometallic chemistry	31
1.6.1 NOE	31
1.6.2 Dynamic NMR spectroscopy	33
1.7 Studies described in this thesis	35
2 Thermal and photochemical reactions of CpRu(PPh₃)₂Cl	37
2.1 Introduction	37
2.2 Overview	38
2.3 Synthesis and characterisation of CpRu(PPh ₃) ₂ Cl	38
2.3.1 Synthesis of CpRu(PPh ₃) ₂ Cl	38
2.3.2 NMR characterisation of CpRu(PPh ₃) ₂ Cl	38
2.4 Thermal and photochemical reactions of CpRu(PPh ₃) ₂ Cl with substrates	41
2.4.1 Reactions of CpRu(PPh ₃) ₂ Cl with PEt ₃	41
2.4.1.1 Thermally initiated reaction of CpRu(PPh ₃) ₂ Cl with PEt ₃	41
2.4.1.2 Photochemical reaction of CpRu(PPh ₃) ₂ Cl with PEt ₃	46

2.4.2	Reactions of CpRu(PPh ₃) ₂ Cl with CO	47
2.4.2.1	Thermally initiated reactions of CpRu(PPh ₃) ₂ Cl with CO	47
2.4.2.2	Photochemical reaction of CpRu(PPh ₃) ₂ Cl with CO	48
2.4.3	Reactions of CpRu(PPh ₃) ₂ Cl with ^t BuNC	49
2.4.3.1	Thermally initiated reactions of CpRu(PPh ₃) ₂ Cl with ^t BuNC	49
2.4.3.2	Photochemical reaction of CpRu(PPh ₃) ₂ Cl with ^t BuNC	50
2.4.3.3	Synthesis of CpRu(PPh ₃)(CNBu ^t)Cl	52
2.4.4	Reactions of CpRu(PPh ₃) ₂ Cl with HSiEt ₃	52
2.4.4.1	Thermally initiated reactions of CpRu(PPh ₃) ₂ Cl with HSiEt ₃	52
2.4.4.2	Photochemical reaction of CpRu(PPh ₃) ₂ Cl with HSiEt ₃	53
2.4.5	Reactions of CpRu(PPh ₃) ₂ Cl with H ₂	54
2.4.5.1	Thermally initiated reactions of CpRu(PPh ₃) ₂ Cl with H ₂	54
2.4.5.2	Photochemical reaction of CpRu(PPh ₃) ₂ Cl with H ₂	54
2.4.6	Reactions of CpRu(PPh ₃) ₂ Cl with C ₂ H ₄	55
2.4.6.1	Thermally initiated reactions of CpRu(PPh ₃) ₂ Cl with C ₂ H ₄	55
2.4.6.2	Photochemical reaction of CpRu(PPh ₃) ₂ Cl with C ₂ H ₄	55
2.4.7	Reactions of CpRu(PPh ₃) ₂ Cl with C ₁₀ H ₈	57
2.4.7.1	Thermally initiated reactions of CpRu(PPh ₃) ₂ Cl with C ₁₀ H ₈	57
2.4.7.2	Photochemical reaction of CpRu(PPh ₃) ₂ Cl with C ₁₀ H ₈	58
2.5	Conclusions	60
2.6	NMR Characterisation data	62
3	Thermal and low temperature reactions of CpRu(PPh₃)₂Me	71
3.1	Introduction	71
3.1.1	Context	73
3.2	Synthesis and characterisation of CpRu(PPh ₃) ₂ Me	73
3.2.1	Synthesis of CpRu(PPh ₃) ₂ Me	73
3.2.2	NMR characterisation of CpRu(PPh ₃) ₂ Me	73
3.3	Synthesis and characterisation of CpRu(PPh ₃)(κ ² -2-C ₆ H ₄ PPh ₂)	75
3.3.1	Synthesis of CpRu(κ ² -2-C ₆ H ₄ PPh ₂)(PPh ₃)	75
3.3.2	NMR characterisation of CpRu(PPh ₃)(κ ² -2-C ₆ H ₄ PPh ₂)	75
3.3.3	The role of CpRu(PPh ₃)(κ ² -2-C ₆ H ₄ PPh ₂)	76
3.4	The thermal and photochemical reactions of CpRu(PPh ₃) ₂ Me	77
3.4.1	Reactions with PEt ₃	77
3.4.1.1	Thermal reactions of CpRu(PPh ₃) ₂ Me with PEt ₃	77

3.4.1.2	Photolysis of CpRu(PPh ₃) ₂ Me with PEt ₃	78
3.4.1.3	Photolysis of CpRu(PPh ₃) ₂ Me with PEt ₃ at 198 K	80
3.4.2	Photochemical reactivity of CpRu(PPh ₃) ₂ Me with solvents	83
3.4.2.1	Low temperature photolysis with THF	83
3.4.2.2	Low temperature photolysis with acetone	90
3.4.2.3	Low temperature photolysis with methanol	90
3.4.3	Reactions with CO	90
3.4.3.1	Thermal reactions of CpRu(PPh ₃) ₂ Me with CO	91
3.4.3.2	Photolysis of CpRu(PPh ₃) ₂ Me with CO	93
3.4.4	Reactions with ^t BuNC	94
3.4.5	Photolysis with arenes	96
3.4.5.1	Reactions with naphthalene	97
3.4.5.2	Thermal reactions with naphthalene	98
3.4.5.3	Photochemical reaction with naphthalene	98
3.4.6	Reactions with ethene	102
3.4.6.1	Thermal reactions with ethene	102
3.4.6.2	Photochemical reaction with ethene	103
3.4.6.3	Determination of the rate of rotation for the η ² -ethene moiety	106
3.4.7	Reactions with DMSO	109
3.4.7.1	Photochemical reaction with DMSO	109
3.4.8	Reactions with pyridine	112
3.4.8.1	Thermal reactions with pyridine	112
3.4.8.2	Photochemical reactions with pyridine	112
3.4.9	Reactions with H ₂	115
3.4.9.1	Thermal reaction with H ₂	116
3.4.9.2	Photochemical reaction with H ₂	117
3.4.10	Reactions with HSiEt ₃	120
3.4.10.1	Thermal reaction with HSiEt ₃	120
3.4.10.2	Photochemical reaction with HSiEt ₃	122
3.4.10.3	Photolysis of CpRu(PPh ₃) ₂ Me with HSiEt ₃ at 298 K	123
3.4.10.4	Attempted synthesis of CpRu(PPh ₃) ₂ SiEt ₃	128
3.4.10.5	Photolysis of CpRu(PPh ₃) ₂ Me with HSiEt ₃ at low temperature	129
3.4.10.6	Formation of CpRu(PPh ₃) ₂ H	132
3.4.10.7	Formation of the metallated complex, Cp(SiEt ₂ {CHCH ₃ }) ₂ H	135

3.4.10.8	Summary of the silane reactions	137
3.4.11	Attempts to selectively sequester PPh ₃ using sulfur and oxygen	138
3.4.11.1	Reactions involving sulfur and oxygen	139
3.4.12	Determination of the orthometallation pathway	141
3.5	Conclusions	144
3.6	NMR characterisation data	147
4	Thermal and photochemical reactions of CpRu(PPh₃)₂H	173
4.1	Introduction	173
4.2	Overview	175
4.3	Synthesis and characterisation of CpRu(PPh ₃) ₂ H	176
4.4	Thermal and photochemical reactions of CpRu(PPh ₃) ₂ H with substrates	177
4.4.1	Reactions of CpRu(PPh ₃) ₂ H with PEt ₃	177
4.4.1.1	Thermally initiated reaction	177
4.4.1.2	Photochemical reaction	178
4.4.2	Reactions of CpRu(PPh ₃) ₂ H with CO	179
4.4.2.1	Thermally initiated reaction	179
4.4.2.2	Photochemical reaction	179
4.4.3	Reactions of CpRu(PPh ₃) ₂ H with ^t BuNC	181
4.4.3.1	Thermal and photochemical reaction	181
4.4.4	Reactions of CpRu(PPh ₃) ₂ H with HSiEt ₃	182
4.4.4.1	Thermally initiated reaction	182
4.4.4.2	Photochemical reaction	183
4.4.5	Reactions of CpRu(PPh ₃) ₂ H with H ₂	183
4.4.6	Reactions of CpRu(PPh ₃) ₂ H with ethene	183
4.4.7	Reactions of CpRu(PPh ₃) ₂ H with naphthalene	184
4.5	Conclusions	185
4.6	NMR characterisation data	186
5	Synthesis, characterisation and photochemistry of ruthenium complexes containing η^1 and η^3-ligands	191
5.1	Introduction	191
5.1.1	Context	194

5.1.2	Synthetic routes to $\text{CpRu}(\text{PPh}_3)(\eta^3\text{-Si}(\text{Me})_2\text{-CH=CH}_2)$, $\text{CpRu}(\text{PPh}_3)(\eta^3\text{-CH}_2\text{C}_2\text{H}_3)$, $\text{CpRu}(\text{PPh}_3)(\eta^3\text{-CH}_2\text{C}_6\text{H}_5)$ and $\text{CpRu}(\text{PPh}_3)(\eta^3\text{-CH}_2\text{C}_{10}\text{H}_7)$	196
5.2	Formation of $\text{CpRu}(\text{PPh}_3)(\eta^3\text{-Si}(\text{Me})_2\text{-CH=CH}_2)$	197
5.3	Synthesis and characterisation of $\text{CpRu}(\text{PPh}_3)(\eta^3\text{-CH}_2\text{C}_2\text{H}_3)$	203
5.3.1	Synthesis of $\text{CpRu}(\text{PPh}_3)(\eta^3\text{-CH}_2\text{C}_2\text{H}_3)$	204
5.3.2	NMR characterisation of $\text{CpRu}(\text{PPh}_3)(\eta^3\text{-CH}_2\text{C}_2\text{H}_3)$	204
5.3.2.1	NMR characterisation of $\text{CpRu}(\text{PPh}_3)_2(\text{CH}_2\text{C}_2\text{H}_3)$	206
5.3.3	Thermal and photochemical reactions of $\text{CpRu}(\text{PPh}_3)(\eta^3\text{-CH}_2\text{C}_2\text{H}_3)$	206
5.3.3.1	Thermal reaction of $\text{CpRu}(\text{PPh}_3)(\eta^3\text{-CH}_2\text{C}_2\text{H}_3)$ with CO	206
5.3.3.2	Photolysis of $\text{CpRu}(\text{PPh}_3)(\eta^3\text{-CH}_2\text{C}_2\text{H}_3)$ with CO	208
5.3.3.3	Thermal reaction of $\text{CpRu}(\text{PPh}_3)(\eta^3\text{-CH}_2\text{C}_2\text{H}_3)$ with H_2	209
5.3.3.4	Photolysis of $\text{CpRu}(\text{PPh}_3)(\eta^3\text{-CH}_2\text{C}_2\text{H}_3)$ with H_2	209
5.3.3.5	Thermal reaction of $\text{CpRu}(\text{PPh}_3)(\eta^3\text{-CH}_2\text{C}_2\text{H}_3)$ with ethene	211
5.3.3.6	Photolysis of $\text{CpRu}(\text{PPh}_3)(\eta^3\text{-CH}_2\text{C}_2\text{H}_3)$ with ethene	211
5.3.3.7	Reaction of $\text{CpRu}(\text{PPh}_3)(\eta^3\text{-CH}_2\text{C}_2\text{H}_3)$ with naphthalene	213
5.3.3.8	Thermal reaction of $\text{CpRu}(\text{PPh}_3)(\eta^3\text{-CH}_2\text{C}_2\text{H}_3)$ with HSiEt_3	214
5.3.3.9	Photolysis of $\text{CpRu}(\text{PPh}_3)(\eta^3\text{-CH}_2\text{C}_2\text{H}_3)$ with HSiEt_3	214
5.4	Synthesis and characterisation of $\text{CpRu}(\text{PPh}_3)(\eta^3\text{-CH}_2\text{C}_6\text{H}_5)$	215
5.4.1	Synthesis of $\text{CpRu}(\text{PPh}_3)_2(\text{CH}_2\text{C}_6\text{H}_5)$	216
5.4.2	NMR characterisation of $\text{CpRu}(\text{PPh}_3)_2(\text{CH}_2\text{C}_6\text{H}_5)$	216
5.4.3	Formation of $\text{CpRu}(\text{PPh}_3)(\eta^3\text{-CH}_2\text{C}_6\text{H}_5)$	218
5.4.4	NMR characterisation of $\text{CpRu}(\text{PPh}_3)(\eta^3\text{-CH}_2\text{C}_6\text{H}_5)$	218
5.4.5	Thermal and photochemical reactions of $\text{CpRu}(\text{PPh}_3)(\eta^3\text{-CH}_2\text{C}_6\text{H}_5)$	220
5.4.5.1	Thermal reaction of $\text{CpRu}(\text{PPh}_3)(\eta^3\text{-CH}_2\text{C}_6\text{H}_5)$ with CO	220
5.4.5.2	Photolysis of $\text{CpRu}(\text{PPh}_3)(\eta^3\text{-CH}_2\text{C}_6\text{H}_5)$ with CO	221
5.4.5.3	Thermal reaction of $\text{CpRu}(\text{PPh}_3)(\eta^3\text{-CH}_2\text{C}_6\text{H}_5)$ with H_2	222
5.4.5.4	Photolysis of $\text{CpRu}(\text{PPh}_3)(\eta^3\text{-CH}_2\text{C}_6\text{H}_5)$ with H_2	222
5.4.5.5	Photolysis of $\text{CpRu}(\text{PPh}_3)(\eta^3\text{-CH}_2\text{C}_6\text{H}_5)$ with ethene	222
5.4.5.6	Photolysis of $\text{CpRu}(\text{PPh}_3)(\eta^3\text{-CH}_2\text{C}_6\text{H}_5)$ with naphthalene	224
5.4.5.7	Photolysis of $\text{CpRu}(\text{PPh}_3)(\eta^3\text{-CH}_2\text{C}_6\text{H}_5)$ with HSiEt_3	225
5.5	Synthesis and characterisation of $\text{CpRu}(\text{PPh}_3)_2(\text{CH}_2\text{C}_{10}\text{H}_7)$	226
5.5.1	Synthesis of $\text{CpRu}(\text{PPh}_3)_2(\text{CH}_2\text{C}_{10}\text{H}_7)$	226
5.5.2	NMR characterisation of $\text{CpRu}(\text{PPh}_3)_2(\text{CH}_2\text{C}_{10}\text{H}_7)$	226
5.6	Conclusions	228

5.7 NMR characterisation data	230
6 Low temperature photochemical reactions of CpRh(η^2-C₂H₄)₂	247
6.1 Introduction	247
6.1.1 Context	249
6.2 Characterisation of CpRh(η^2 -C ₂ H ₄) ₂	252
6.3 Photochemical reactions of CpRh(η^2 -C ₂ H ₄) ₂ with tributylamine and tripentylamine	252
6.3.1 Photochemical reactions of CpRh(η^2 -C ₂ H ₄) ₂ with tributylamine and protio benzene	255
6.3.2 Photochemical reactions of CpRh(η^2 -C ₂ H ₄) ₂ with tributylamine and d ₆ -benzene	259
6.3.3 Photochemical reactions of CpRh(η^2 -C ₂ H ₄) ₂ with triethylamine and benzene	259
6.4 Conclusions	260
6.5 NMR characterisation data	261
7 Experimental methods	265
7.1 General experimental	265
7.1.1 Solvents, reagents and equipment	265
7.1.2 NMR spectroscopy	266
7.1.2.1 NMR sample preparation	266
7.1.3 Mass spectrometry	267
7.1.4 UV spectroscopy	268
7.1.5 Infrared spectroscopy	268
7.2 Synthesis of starting complexes / reactions	270
7.2.1 Methods for Chapter 2	270
7.2.1.1 Preparation of CpRu(PPh ₃) ₂ Cl	270
7.2.1.2 Reactions of CpRu(PPh ₃) ₂ Cl	271
7.2.1.3 Preparation of CpRu(PEt ₃) ₂ Cl	272
7.2.1.4 Preparation of CpRu(PPh ₃)(CO)Cl	272
7.2.1.5 Preparation of CpRu(CNBu ^t) ₂ Cl	273
7.2.2 Methods for Chapter 3	273
7.2.2.1 Preparation of CpRu(PPh ₃) ₂ Me	273
7.2.2.2 Preparation of CpRu(PPh ₃)(κ^2 -2-C ₆ H ₄ PPh ₂)	274

7.2.2.3	Preparation of DSiEt_3	274
7.2.2.4	Reactions of $\text{CpRu}(\text{PPh}_3)_2\text{Me}$	275
7.2.2.5	Preparation of $\text{CpRu}(\text{PPh}_3)_2(\text{C}_{10}\text{H}_7)$	275
7.2.3	Methods for Chapter 4	276
7.2.3.1	Preparation of $\text{CpRu}(\text{PPh}_3)_2\text{H}$	276
7.2.3.2	Reactions of $\text{CpRu}(\text{PPh}_3)_2\text{H}$	276
7.2.3.3	Preparation of $\text{CpRu}(\text{PPh}_3)(\text{CO})\text{H}$	277
7.2.4	Methods for Chapter 5	278
7.2.4.1	Preparation of $\text{HSi}(\text{Me})_2\text{C}_2\text{H}_3$	278
7.2.4.2	Reaction of $\text{CpRu}(\text{PPh}_3)_2\text{Me}$ with dimethylvinylsilane	279
7.2.4.3	Preparation of Grignard reagents	279
7.2.4.4	Preparation of $\text{CpRu}(\text{PPh}_3)_2\text{R}$ (R = vinyl, benzyl or methyl-1-naphthyl)	280
7.2.4.5	Preparation of $\text{CpRu}(\text{PPh}_3)(\eta^3\text{-CH}_2\text{C}_6\text{H}_5)$	281
7.2.4.6	Reactions of $\text{CpRu}(\text{PPh}_3)(\eta^3\text{-CH}_2\text{C}_2\text{H}_3)$ and $\text{CpRu}(\text{PPh}_3)(\eta^3\text{-CH}_2\text{C}_6\text{H}_5)$	281
7.2.4.7	Preparation of sodium/mercury amalgam	282
7.2.4.8	Attempted η^3 -ligand complex synthesis using sodium/mercury amalgam	282
7.2.5	Methods for Chapter 6	283
7.2.5.1	Preparation of $\text{CpRh}(\eta^2\text{-C}_2\text{H}_4)_2$	283
7.3	Photolysis	284
7.3.1	<i>In situ</i> photolysis setup (LASER)	284
7.3.2	<i>In situ</i> photolysis setup (fibre-optic)	286
7.3.3	<i>Ex situ</i> photolysis setup	287
7.4	Calculation of rate constants using NMR data	288
Abbreviations		295
References		297

List of Figures

Chapter 1

Figure 1.1	<i>The metathesis of a Si-H adduct to a metal centre</i>	2
Figure 1.2	<i>The oxidative addition of a Si-H adduct to a metal centre, with typical Si-H bond lengths</i>	3
Figure 1.3	<i>Classical (a) and nonclassical (b) metal-silane complexes</i>	3
Figure 1.4	<i>σ-CAM mechanism</i>	5
Figure 1.5	<i>Generalised depiction of the Chalk-Harrod mechanism for hydrosilation</i>	6
Figure 1.6	<i>The silyl migration variant of the Chalk-Harrod mechanism</i>	7
Figure 1.7	<i>Formation of vinylsilane as a by-product of metal catalysed hydrosilation</i>	7
Figure 1.8	<i>Catalytic hydrosilation using $\text{CpRh}(\text{C}_2\text{H}_4)\text{SiEt}_3(\text{H})$ – The Duckett-Pertutz mechanism</i>	8
Figure 1.9	<i>Proposed catalytic hydrosilation cycle for $[\text{Cp}^*(\text{H})_2(\text{P}^i\text{Pr}_3)\text{Ru}=\text{Si}(\text{H})\text{Ph}.\text{Et}_2\text{O}]^+ [\text{B}(\text{C}_6\text{F}_5)_4]^-$</i>	9
Figure 1.10	<i>Hydrosilation of carbonyl compounds by $[\text{CpRu}(\text{N}\equiv\text{CMe})_2(\text{P}^i\text{Pr}_3)]^+$, and the subsequent formation of a σ-bound cationic silane complex, and silylium cation</i>	9
Figure 1.11	<i>Methods of polysilane synthesis</i>	10

Figure 1.12	Generalised mechanism for the transition metal catalysed formation of polysilanes	11
Figure 1.13	Catalytic hydrogenation of alkenes using Wilkinson's catalyst	12
Figure 1.14	Depiction of the oxidative addition pathway for the H-H adduct and the average H-H bond length of the intervening complexes	13
Figure 1.15	Metal-hydrogen bonding for dihydrogen complexes	14
Figure 1.16	The catalytic addition of an olefin to an aromatic compound using $Ru(H)_2(CO)(PPh_3)_3$	15
Figure 1.17	The photochemically induced cyclometallation of $Cp^*Ir(PPh_3)(H)_2$	16
Figure 1.18	The oxidative addition of a C-H adduct to a metal centre	16
Figure 1.19	Photochemical C-D activation of benzene by $Cp^*Rh(PMe_3)(H)_2$	18
Figure 1.20	The agostic interaction of $W(CO)_3(PCy_3)_2$	19
Figure 1.21	The agostic interaction of a C-H adduct with a metal centre	19
Figure 1.22	Examples of ruthenium half-sandwich complexes	20
Figure 1.23	Photochemically initiated isomerisation of silane moieties of $CpFe(CO)_2R$ complexes	21

Figure 1.24	Examples of photochemical reactions of the bimetallic complex $[\text{CpRu}(\text{CO})_2]_2$	22
Figure 1.25	The synthesis and reactions of $\text{CpRu}(\text{CO})_2\text{H}$ and $\text{CpRu}(\text{CO})_2\text{Me}$	23
Figure 1.26	The synthesis and reactions of $\text{CpRu}(\text{PPh}_3)_2\text{Cl}$	24
Figure 1.27	Cyclometallated intermediates formed prior to arene C-H bond activation	24
Figure 1.28	Attempt to form ethylbenzene catalytically using $\text{CpRu}(\text{PPh}_3)_2\text{Me}$	25
Figure 1.29	Catalytic isomerisation of alkenyl alcohols to aldehydes (and ketones) using $\text{CpRu}(\text{PPh}_3)_2\text{Cl}$	25
Figure 1.30	Metal-phosphorous bonding for phosphine bound complexes	26
Figure 1.31	General order of π acidity for phosphine ligands	26
Figure 1.32	Depiction of the Tolman cone angle (θ) for sterically hindered phosphines	27
Figure 1.33	Tolman map correlating the electronic and steric factors of phosphine ligands	28
Figure 1.34	Relaxation pathways for a two spin system	32
Figure 1.35	The two isomers of $\text{CpMo}(\text{MeN}=\text{CPhNMeCHPh})(\text{CO})_2$	33
Figure 1.36	Basic pulse sequence for EXSY / NOESY 2D NMR experiment	33

Chapter 2

Figure 2.1	Structure of $\text{CpRu}(\text{PPh}_3)_2\text{Cl}$	39
Figure 2.2	^{31}P NMR spectrum of $\text{CpRu}(\text{PPh}_3)_2\text{Cl}$ in d_6 -benzene	39
Figure 2.3	^1H NMR spectrum of $\text{CpRu}(\text{PPh}_3)_2\text{Cl}$ in d_6 -benzene	40
Figure 2.4	Interconversion of chiral structures, about the metal centre, via coordinatively unsaturated pyramidal intermediates	40
Figure 2.5	$^{31}\text{P}\{^1\text{H}\}$ NMR spectrum obtained after the thermal reaction of $\text{CpRu}(\text{PPh}_3)_2\text{Cl}$ with PEt_3 at 323 K, after irradiation had proceeded for 24 hours	42
Figure 2.6	Overlaid short and long range $^1\text{H}/^{13}\text{C}$ HMQC NMR spectra which depict the signals of the phenyl protons and carbons of the triphenylphosphine ligand	44
Figure 2.7	Depiction of a basic $^1\text{H}/^{13}\text{C}$ HMQC NMR pulse sequence	44
Figure 2.8	Depiction of the mono and bis-substituted phosphine complexes, $\text{CpRu}(\text{PPh}_3)(\text{PEt}_3)\text{Cl}$ and $\text{CpRu}(\text{PEt}_3)_2\text{Cl}$	45
Figure 2.9	Illustration of the mono carbonyl substituted product $\text{CpRu}(\text{CO})_2\text{Cl}$	48
Figure 2.10	$^1\text{H}/^{13}\text{C}$ HMQC spectrum showing the tertiary carbons for the free $^t\text{BuNC}$, and that of the complex, $\text{CpRu}(\text{PPh}_3)(\text{CNBu}^t)\text{Cl}$	50
Figure 2.11	Depiction of the mono and bis-substituted isocyanide complexes, $\text{CpRu}(\text{PPh}_3)(\text{CNBu}^t)\text{Cl}$ and $\text{CpRu}(\text{CNBu}^t)_2\text{Cl}$	51

Figure 2.12	<i>¹H NMR spectrum highlighting the low intensity peaks corresponding to the coordinated ethene protons</i>	56
Figure 2.13	<i>CpRu(PPh₃)(η²-C₂H₄)Cl</i>	57
Figure 2.14	<i>The equilibrium between coordinated and activated complexes, Cp[*]Rh(PMe₃)(η²-C₁₀H₈) and Cp[*]Rh(PMe₃)(C₁₀H₇)H, as determined by Jones et al. using deuterium labelling experiments</i>	59
Figure 2.15	<i>Possible structures for CpRu(PPh₃)(η²-C₁₀H₈)Cl</i>	59

Chapter 3

Figure 3.1	<i>Proposed mechanism for the replacement of alkyl moieties at CpRu(PPh₃)₂Me by benzene</i>	71
Figure 3.2	<i>The replacement of the alkyl moiety of CpRu(PPh₃)₂Me by benzene via an orthometallation mechanism (illustrated for benzene, proposed to be general)</i>	72
Figure 3.3	<i>¹H NMR spectrum of CpRu(PPh₃)₂Me with Cp and Me resonances indicated</i>	74
Figure 3.4	<i>Structure of CpRu(PPh₃)₂Me</i>	74
Figure 3.5	<i>A ¹H/³¹P HMQC NMR spectrum showing the coupling between the ³¹P signal at δ -16.9 and the corresponding phenyl protons</i>	76
Figure 3.6	<i>Structure of CpRu(PPh₃)(κ²-2-C₆H₄PPh₂)</i>	76
Figure 3.7	<i>Structure of CpRu(PEt₃)₂Me</i>	78

Figure 3.8	A plot of the relative ^{31}P resonances over time, for the photochemically formed products of the reaction between $\text{CpRu}(\text{PPh}_3)_2\text{Me}$ and PEt_3 , at 298 K	79
Figure 3.9	A plot of the relative ^{31}P resonances over time, for the photochemically formed products of the reaction between $\text{CpRu}(\text{PPh}_3)_2\text{Me}$ and PEt_3 , at 193 K	81
Figure 3.10	Structure of $\text{CpRu}(\text{PPh}_3)(\text{PEt}_3)\text{Me}$	82
Figure 3.11	$^{31}\text{P}\{^1\text{H}\}$ NMR spectrum showing the ^{31}P signals corresponding to $\text{CpRu}(\text{PPh}_3)(\text{THF})\text{Me}$ and $\text{CpRu}(\text{PPh}_3)_2(\text{C}_4\text{H}_7\text{O})$, following 5 hours of photolysis	85
Figure 3.12	Structure of $\text{CpRu}(\text{PPh}_3)(\text{C}_4\text{H}_8\text{O})\text{Me}$ and $\text{CpRu}(\text{PPh}_3)_2(\text{C}_4\text{H}_7\text{O})$	86
Figure 3.13	A plot of the relative ^{31}P resonances over time, for the photochemically formed products of the reaction between $\text{CpRu}(\text{PPh}_3)_2\text{Me}$ and THF , at 193 K	87
Figure 3.14	^1H spectra depicting the increasing intensity of the signal corresponding to liberated methane	89
Figure 3.15	Structure of $\text{CpRu}(\text{PPh}_3)(\text{CO})\text{Me}$	92
Figure 3.16	$^{13}\text{C}\{^1\text{H}\}$ NMR focusing on the doublet carbonyl signal	92
Figure 3.17	$^1\text{H}/^{13}\text{C}$ HMQC of Methyl moiety of $\text{CpRu}(\text{PPh}_3)(\text{CO})\text{Me}$	92
Figure 3.18	A plot of the relative ^{31}P resonances over time, for the photochemically formed products of the reaction between $\text{CpRu}(\text{PPh}_3)_2\text{Me}$ and CO , at 193 K	94
Figure 3.19	Structure of $\text{CpRu}(\text{PPh}_3)(\text{CNBu}^t)\text{Me}$	95

Figure 3.20	A plot of the relative ^{31}P resonances over time, for the photochemically formed products of the reaction between $\text{CpRu}(\text{PPh}_3)_2\text{Me}$ and $^1\text{BuNC}$, at 193 K	95
Figure 3.21	Photochemical products of reaction of $\text{CpRu}(\text{PPh}_3)_2\text{Me}$ with toluene	96
Figure 3.22	$^{31}\text{P}\{^1\text{H}\}$ NMR spectrum showing the ^{31}P signals of the activated toluene products	97
Figure 3.23	A plot of the relative ^{31}P resonances over time, for the photochemically formed products of the reaction between $\text{CpRu}(\text{PPh}_3)_2\text{Me}$ and C_{10}H_8 , at 193 K	99
Figure 3.24	Feasible binding modes of the naphthalene ligand to the ruthenium centre	100
Figure 3.25	$^{31}\text{P}\{^1\text{H}\}$ NMR spectrum showing the relative conversion of $\text{CpRu}(\text{PPh}_3)_2\text{Me}$ to the two isomeric forms of $\text{CpRu}(\text{PPh}_3)(\eta^2\text{-C}_{10}\text{H}_8)\text{Me}$	101
Figure 3.26	A plot of the relative ^{31}P resonances over time, for the photochemically formed products of the reaction between $\text{CpRu}(\text{PPh}_3)_2\text{Me}$ and C_2H_4 , at 193 K	104
Figure 3.27	^1H NMR spectrum for $\text{CpRu}(\text{PPh}_3)(\text{C}_2\text{H}_4)\text{Me}$	105
Figure 3.28	Structure of $\text{CpRu}(\text{PPh}_3)(\eta^2\text{-C}_2\text{H}_4)\text{Me}$	105
Figure 3.29	Ethene rotation in $\text{CpRu}(\text{PPh}_3)(\eta^2\text{-C}_2\text{H}_4)\text{Me}$	106
Figure 3.30	Eyring plot for the rate of rotation of for the ethene moiety $\text{CpRu}(\text{PPh}_3)(\eta^2\text{-C}_2\text{H}_4)\text{Me}$	108
Figure 3.31	Structure of $\text{CpRu}(\text{PPh}_3)(\text{S}(\text{O})\text{Me}_2)\text{Me}$	111

Figure 3.32	A plot of the relative ^{31}P resonances over time, for the photochemically formed products of the reaction between $\text{CpRu}(\text{PPh}_3)_2\text{Me}$ and DMSO , at 193 K	111
Figure 3.33	A plot of the relative ^{31}P resonances over time, for the photochemically formed products of the reaction between $\text{CpRu}(\text{PPh}_3)_2\text{Me}$ and $\text{C}_5\text{H}_5\text{N}$, at 193 K	113
Figure 3.34	Formation of $\text{CpRu}(\text{PPh}_3)_2\text{H}$ and $\text{CpRu}(\text{PPh}_3)(\text{H})_3$, proposed by Davies et al.	115
Figure 3.35	Structure of $\text{CpRu}(\text{PPh}_3)_2\text{H}$	116
Figure 3.36	Depiction of the two possible geometries for $\text{CpRu}(\text{PPh}_3)(\text{H})_3$	118
Figure 3.37	Structure of $\text{cis-Ru}(\text{PPh}_3)_4(\text{H})_2$, and the accompanying doublet of triplets hydride resonance (overlapped by the doublet hydride signal of $\text{CpRu}(\text{PPh}_3)(\text{H})_3$)	119
Figure 3.38	Structure of $\text{CpRu}(\text{PPh}_3)_2\text{SiEt}_3$	121
Figure 3.39	Structure of $\text{CpRu}(\text{PPh}_3)(\text{SiEt}_3)_2\text{H}$	122
Figure 3.40	Hydride ^1H resonances for the products of the photochemical reaction of $\text{CpRu}(\text{PPh}_3)_2\text{Me}$ with HSiEt_3 in THF	123
Figure 3.41	Hydride ^1H resonances for the products of the photochemical reaction of $\text{CpRu}(\text{PPh}_3)_2\text{Me}$ with HSiEt_3 in cyclohexane	124
Figure 3.42	Relative order of M-C bond stability for metal alkane complexes, determined by Jones and Feher	125

Figure 3.43	Structure for $\text{CpRu}(\text{PPh}_3)(\text{SiEt}_3)(\text{R})\text{H}$ (where $\text{R} = \text{C}_6\text{D}_{11}$, $\text{C}_4\text{D}_7\text{O}$ or C_7D_7)	126
Figure 3.44	Two possible cyclohexyl binding modes for $\text{CpRu}(\text{PPh}_3)(\text{SiEt}_3)(\text{Cy})\text{H}$	126
Figure 3.45	Possible equilibrium between isomers of cyclohexyl complexes, suggested by Ball et al.	127
Figure 3.46	Some of the possible isomers for the stereogenic $\text{Ru}(\text{IV})$ centre	128
Figure 3.47	Structure of $\text{CpRu}(\kappa^2\text{-}2\text{-C}_6\text{H}_4\text{PPh}_2)(\text{SiEt}_3)\text{H}$	130
Figure 3.48	The reaction pathway proposed by Lemke et al.	130
Figure 3.49	The two possible mechanistic routes towards the formation of the observed complex, $\text{CpRu}(\kappa^2\text{-}2\text{-C}_6\text{H}_4\text{PPh}_2)(\text{SiEt}_3)\text{D}$, using DSiEt_3 as a reporter ligand	131
Figure 3.50	Structure of $\text{CpRu}(\text{PPh}_3)_2\text{H}$	132
Figure 3.51	Possible Cp ring-slip mechanism	133
Figure 3.52	Magnified region of the ^1H NMR spectrum showing the triplet signal associated with $\text{CpRu}(\text{PPh}_3)_2\text{H}$ (major resonance) and a second overlapping minor triplet signal	133
Figure 3.53	Possible reaction pathways for bond activation	134
Figure 3.54	A depiction of the general structure of the substituted phosphine ligand (where $\text{R} = ^2\text{H}$ or SiEt_3)	135
Figure 3.55	2D NOESY NMR experiment recorded for $\text{CpRu}(\text{SiEt}_2\{\text{CHCH}_3\})_2\text{H}$	136

Figure 3.56	The structure of $\text{CpRu}(\text{SiEt}_2\{\text{CHCH}_3\})_2\text{H}$	137
Figure 3.57	A plot of the relative ^1H NMR Cp resonances over time, for the photochemically formed silane product complexes	138
Figure 3.58	^1H NMR spectrum showing the magnitude of the previously low intensity hydride signal for $\text{CpRu}(\text{SiEt}_2\{\text{CHCH}_3\})_2\text{H}$, compared with the other product resonances within the sample	141
Figure 3.59	Orthometallation and non-orthometallation routes to lead to C-H activation	142

Chapter 4

Figure 4.1	Formation of the deuteride and protio complexes, $\text{CpRu}(\text{PPh}_3)_2\text{D}$ and $\text{CpRu}(\text{PPh}_3)_2\text{H}$, via an alkoxy intermediate	174
Figure 4.2	“Trapped” alkoxy complex, $[\text{CpRu}(\text{PPh}_3)_2(\text{OCD}_3)]^+ \text{BPh}_4^-$	174
Figure 4.3	^1H NMR spectrum recorded for $\text{CpRu}(\text{PPh}_3)_2\text{H}$ in d_6 -benzene	176
Figure 4.4	The structure of $\text{CpRu}(\text{PPh}_3)_2\text{H}$	177
Figure 4.5	Structure of $\text{CpRu}(\text{PPh}_3)(\text{PEt}_3)\text{H}$	178
Figure 4.6	^1H NMR spectrum for the synthesised $\text{CpRu}(\text{PPh}_3)(\text{CO})\text{H}$	180
Figure 4.7	$^1\text{H}/^{31}\text{P}$ HMQC for the synthesised $\text{CpRu}(\text{PPh}_3)(\text{CO})\text{H}$	180
Figure 4.8	Structure of $\text{CpRu}(\text{PPh}_3)(\text{CO})\text{H}$	181

Figure 4.9	Structure of $\text{CpRu}(\text{PPh}_3)(\text{CNBu}^t)\text{H}$	182
Figure 4.10	$^{13}\text{C}\{^1\text{H}\}$ NMR spectrum of $\text{CpRu}(\text{PPh}_3)(\text{CNBu}^t)\text{H}$, showing the relative conversion from $\text{CpRu}(\text{PPh}_3)_2\text{H}$	182

Chapter 5

Figure 5.1	Example of the binding modes for complexes containing allyl ligands	191
Figure 5.2	Examples of known ruthenium complexes with coordinated η^3 ligands	192
Figure 5.3	Figure 5.3 Thermal and photochemical reactions of $[\text{CpRu}(\eta^6\text{-naphthalene})]\text{PF}_6$	193
Figure 5.4	Activation pathways of $[\text{CpRu}(\text{PPh}_3)\text{Me}]$ with H-H or H-Si bonds	194
Figure 5.5	Structure of $\text{CpRu}(\text{PPh}_3)(\eta^3\text{-Si}(\text{Me})_2\text{-CH=CH}_2)$	200
Figure 5.6	^1H NMR spectra showing the hydride signals (for the activated tolyl product, analogous to those described in Chapter 3) and the major product proton signals – highlighting the abundance of products formed	201
Figure 5.7	A plot of the relative ^{31}P resonances over time, for the photochemically formed products of the reaction between $\text{CpRu}(\text{PPh}_3)_2\text{Me}$ and dimethylvinylsilane	202
Figure 5.8	^1H COSY NMR experiment showing the coupling between the coordinated allyl protons	205
Figure 5.9	The structure of $\text{CpRu}(\text{PPh}_3)(\eta^3\text{-CH}_2\text{-CH=CH}_2)$	205

Figure 5.10	Structure of $\text{CpRu}(\text{PPh}_3)(\text{CO})(\text{CH}_2\text{CH}=\text{CH}_2)$	207
Figure 5.11	Structure of $\text{CpRu}(\text{PPh}_3)(\text{H})_3$	210
Figure 5.12	A recorded $^{31}\text{P}\{^1\text{H}\}$ NMR spectrum for $\text{CpRu}(\text{PPh}_3)(\text{H})_3$	211
Figure 5.13	Structure of $\text{CpRu}(\text{PPh}_3)(\text{CH}_2\text{-CH}=\text{CH}_2)(\eta^2\text{-C}_2\text{H}_4)$	212
Figure 5.14	Structure of $\text{CpRu}(\text{PPh}_3)(\eta^2\text{-C}_{10}\text{H}_8)(\text{CH}_2\text{-CH}=\text{CH}_2)$	213
Figure 5.15	Structure of $\text{CpRu}(\text{PPh}_3)(\text{SiEt}_3)_2\text{H}$	215
Figure 5.16	A $^1\text{H}/^{31}\text{P}$ HMQC NMR spectrum for $\text{CpRu}(\text{PPh}_3)_2(\text{CH}_2\text{C}_6\text{H}_5)$	217
Figure 5.17	Structure of $\text{CpRu}(\text{PPh}_3)_2(\text{CH}_2\text{C}_6\text{H}_5)$	217
Figure 5.18	$\text{CpRu}(\text{PPh}_3)(\eta^3\text{-CH}_2\text{C}_6\text{H}_5)$	219
Figure 5.19	Structure of $\text{CpRu}(\text{PPh}_3)(\text{CO})(\text{CH}_2\text{C}_6\text{H}_5)$	221
Figure 5.20	Structure of $\text{CpRu}(\text{PPh}_3)(\text{C}_2\text{H}_4)(\text{CH}_2\text{C}_6\text{H}_5)$	223
Figure 5.21	Structure of $\text{CpRu}(\text{PPh}_3)(\eta^2\text{-C}_{10}\text{H}_8)(\text{CH}_2\text{-C}_6\text{H}_5)$	224
Figure 5.22	Structure of $\text{CpRu}(\text{PPh}_3)_2(\text{CH}_2\text{C}_{10}\text{H}_7)$	226

Chapter 6

Figure 6.1	Photochemical substitution reactions of $\text{CpRh}(\eta^2\text{-C}_2\text{H}_4)_2$	248
Figure 6.2	Comparison of the ability of the fragments $[\text{CpRh}(\text{CO})]$ and $[\text{CpRh}(\text{C}_2\text{H}_4)]$ to C-H activate methane	249
Figure 6.3	Proposed scheme of reactivity for the work covered in this chapter, based on DFT calculations	250
Figure 6.4	Energy profiles for the activation of benzene by $[\text{CpRh}(\text{C}_2\text{H}_4)]$ and $[\text{CpRh}(\text{NMe}_3)]$, calculated by Dr. Joaquín López-Serrano using DFT methods	251
Figure 6.5	^1H NMR spectra showing the conversion of $\text{CpRh}(\text{NBu}_3)(\text{C}_2\text{H}_4)$ to $\text{CpRh}(\text{NBu}_3)_2$	253
Figure 6.6	^1H NMR Spectrum, focusing on the phenyl region	255
Figure 6.7	^1H NMR spectrum focusing on the hydride doublet signal of $\text{CpRh}(\text{NBu}_3)(\text{Ph})\text{H}$	256
Figure 6.8	General conditions for the C-H activation of benzene by this system	256
Figure 6.9	^1H NMR spectrum showing the product signals and free amine peaks	257
Figure 6.10	^1H NMR of hydride region	258

Chapter 7

Figure 7.1	Mass spectrum obtained for the sample containing $\text{CpRu}(\text{PPh}_3)(\eta^3\text{-Si}(\text{Me})_2\text{C}_2\text{H}_4)$ and $\text{CpRu}(\text{PPh}_3)_2(\text{Si}(\text{Me})_2\text{C}_2\text{H}_4)$	267
Figure 7.2	Mass spectrum obtained for the sample containing $\text{CpRu}(\text{CNBu}^t)_2\text{Cl}$	268
Figure 7.3	IR spectrum for $\text{CpRu}(\text{PPh}_3)(\text{H})_3$ – not isolated, contains residual $\text{CpRu}(\text{PPh}_3)_2\text{H}$, $\text{Ru}(\text{PPh}_3)_4(\text{H})_2$ and benzene	269
Figure 7.4	IR spectrum for $\text{CpRu}(\text{PPh}_3)(\text{CO})(\text{CH}_2\text{-CH=CH}_2)$ with residual THF	269
Figure 7.5	IR spectrum for $\text{CpRu}(\text{PPh}_3)(\text{CO})\text{Me}$ with residual benzene	270
Figure 7.6	Cut-away view of the modified NMR probe and LASER set-up used for in situ photolysis experiments	285
Figure 7.7	Cut-away view of the modified NMR probe and UV lamp setup used for ex situ photolysis experiments	288
Figure 7.8	Plot of the mixing time against the relative peak intensities for the experimentally obtained and calculated values of A and B	292

List of Tables

Chapter 2

Table 2.1	<i>NMR data for $\text{CpRu}(\text{PPh}_3)_2\text{Cl}$</i>	62
Table 2.2	<i>NMR data for $\text{CpRu}(\text{PPh}_3)(\text{PEt}_3)\text{Cl}$</i>	63
Table 2.3	<i>NMR data for $\text{CpRu}(\text{PEt}_3)_2\text{Cl}$</i>	64
Table 2.4	<i>NMR data for $\text{CpRu}(\text{PPh}_3)(\text{CO})\text{Cl}$</i>	65
Table 2.5	<i>NMR data for $\text{CpRu}(\text{PPh}_3)(\text{CNBu}^t)\text{Cl}$</i>	66
Table 2.6	<i>NMR data for $\text{CpRu}(\text{}^t\text{BuNC})_2\text{Cl}$</i>	67
Table 2.7	<i>NMR data for $\text{CpRu}(\text{PPh}_3)(\eta^2\text{-C}_2\text{H}_4)\text{Cl}$</i>	68
Table 2.8	<i>NMR data for $\text{CpRu}(\text{PPh}_3)(\eta^2\text{-C}_{10}\text{H}_8)\text{Cl}$</i>	69

Chapter 3

Table 3.1	<i>The exchange rates for the ethene rotation at varying temperatures</i>	107
Table 3.2	<i>Parameters for the rotation of the ruthenium-bound ethene</i>	108
Table 3.3	<i>Second order rate constants for the reaction of substrates with a transient intermediate formed from the flash photolysis of $\text{cis-Ru}(\text{PMe}_3)_4(\text{H})_2$ in cyclohexane</i>	143
Table 3.4	<i>NMR data for $\text{CpRu}(\text{PPh}_3)_2\text{Me}$</i>	147
Table 3.5	<i>NMR data for $\text{CpRu}(\text{PPh}_3)(\kappa^2\text{-2-C}_6\text{H}_4\text{PPh}_2)$</i>	148

Table 3.6	<i>NMR data for CpRu(PEt₃)₂Me</i>	149
Table 3.7	<i>NMR data for CpRu(PPh₃)(PEt₃)Me</i>	150
Table 3.8	<i>NMR data for CpRu(PPh₃)(OC₄H₈)Me</i>	151
Table 3.9	<i>NMR data for CpRu(PPh₃)₂(OC₄H₇)</i>	152
Table 3.10	<i>NMR data for CpRu(PPh₃)(CO)Me</i>	153
Table 3.11	<i>NMR data for CpRu(PPh₃)(^tBuNC)Me</i>	154
Table 3.12	<i>NMR data for CpRu(PPh₃)₂(o-tolyl)</i>	155
Table 3.13	<i>NMR data for CpRu(PPh₃)₂(m-tolyl)</i>	156
Table 3.14	<i>NMR data for CpRu(PPh₃)₂(p-tolyl)</i>	157
Table 3.15	<i>NMR data for CpRu(PPh₃)₂Ph</i>	158
Table 3.16	<i>NMR data for CpRu(PPh₃)(C₁₀H₇)Me - Major isomer</i>	159
Table 3.17	<i>NMR data for CpRu(PPh₃)(C₁₀H₇)Me – Minor isomer</i>	160
Table 3.18	<i>NMR data for CpRu(PPh₃)(C₂H₄)Me</i>	161
Table 3.19	<i>NMR data for CpRu(PPh₃)(OS(CH₃)₂)Me</i>	162
Table 3.20	<i>NMR data for CpRu(PPh₃)(NC₅H₅)Me</i>	163
Table 3.21	<i>NMR data for CpRu(PPh₃)₂(NC₅H₄)</i>	164
Table 3.22	<i>NMR data for CpRu(PPh₃)H₃ (C_{3v})</i>	165
Table 3.23	<i>NMR data for CpRu(PPh₃)₂H</i>	166

Table 3.24	<i>NMR data for CpRu(PPh₃)(SiEt₃)₂H</i>	167
Table 3.25	<i>NMR data for CpRu(PPh₃)₂(SiEt₃)</i>	168
Table 3.26	<i>NMR data for CpRu(PPh₃)(SiEt₃)(C₆H₁₁)H</i>	169
Table 3.27	<i>NMR data for CpRu(κ^2-2-C₆H₄PPh₂)(SiEt₃)H</i>	170
Table 3.28	<i>NMR data for CpRu(SiEt₂{CHCH₃})₂H</i>	171

Chapter 4

Table 4.1	<i>NMR data for CpRu(PPh₃)₂H</i>	186
Table 4.2	<i>NMR data for CpRu(PPh₃)(PEt₃)H</i>	187
Table 4.3	<i>NMR data for CpRu(PEt₃)₂H</i>	188
Table 4.4	<i>NMR data for CpRu(PPh₃)(CO)H</i>	189
Table 4.5	<i>NMR data for CpRu(PPh₃)(CNBu^t)H</i>	190

Chapter 5

Table 5.1	<i>NMR data for CpRu(PPh₃)(η^3-Si(Me)₂C₂H₃)</i>	230
Table 5.2	<i>NMR data for CpRu(PPh₃)₂(Si(Me)₂C₂H₃)</i>	231
Table 5.3	<i>NMR data for CpRu(PPh₃)(η^3-CH₂CH=CH₂)</i>	232
Table 5.4	<i>NMR data for CpRu(PPh₃)₂(CH₂CH=CH₂)</i>	233
Table 5.5	<i>NMR data for CpRu(PPh₃)(CO)(CH₂CH=CH₂)</i>	234

Table 5.6	<i>NMR data for CpRu(PPh₃)H₃ (C_{3v})</i>	235
Table 5.7	<i>NMR data for CpRu(PPh₃)(SiEt₃)₂H</i>	236
Table 5.8	<i>NMR data for CpRu(PPh₃)(η²-C₂=H₄)(CH₂CH=CH₂)</i>	237
Table 5.9	<i>NMR data for CpRu(PPh₃)(η²-C₁₀H₈)(CH₂CH=CH₂)</i>	238
Table 5.10	<i>NMR data for CpRu(PPh₃)₂(CH₂Ph)</i>	239
Table 5.11	<i>NMR data for CpRu(PPh₃)(η³-CH₂Ph)</i>	240
Table 5.12	<i>NMR data for CpRu(PPh₃)(CO)(CH₂Ph)</i>	241
Table 5.13	<i>NMR data for CpRu(PPh₃)(η²-C₂=H₄)(CH₂Ph)</i>	242
Table 5.14	<i>NMR data for CpRu(PPh₃)(η²-C₁₀H₈)(CH₂Ph)</i>	243
Table 5.15	<i>NMR data for CpRu(PPh₃)₂(CH₂C₁₀H₇)</i>	244
Table 5.16	<i>NMR data for CpRu(PPh₃)(η³-CH₂C₁₀H₇)</i>	245

Chapter 6

Table 6.1	<i>NMR data for CpRh(C₂H₄)₂</i>	261
Table 6.2	<i>NMR data for CpRh(NBu₃)(Ph)H</i>	262
Table 6.3	<i>NMR data for CpRh(NPe₃)(Ph)H</i>	263
Table 6.4	<i>NMR data for CpRh(NEt₃)(Ph)H</i>	264

Chapter 7

Table 7.1	<i>Quantities of reagents used in the thermal and photochemical reactions with $\text{CpRu}(\text{PPh}_3)_2\text{Cl}$</i>	271
Table 7.2	<i>Quantities of reagents used in the thermal and photochemical reactions with $\text{CpRu}(\text{PPh}_3)_2\text{Me}$</i>	275
Table 7.3	<i>Quantities of reagents used in the thermal and photochemical reactions with $\text{CpRu}(\text{PPh}_3)_2\text{H}$</i>	277
Table 7.4	<i>Quantities of chloro compounds used in the synthesis of their corresponding Gignard reagents</i>	280
Table 7.5	<i>Tabulated yield data for the product complexes</i>	281
Table 7.6	<i>Quantities of chloro compounds used in the amalgam reactions</i>	283
Table 7.7	<i>Peak intensities (%) for the reversible conversion of resonances A to B for a range of varying mixing times</i>	289
Table 7.8	<i>Simulated data points</i>	290
Table 7.9	<i>Calculation of error for the experimentally obtained values, for the intensities of peaks A and B, over a range of varying mixing times</i>	291
Table 7.10	<i>Rate constant data for the interconversion of signals A and B</i>	292
Table 7.11	<i>Revised Rate constant data</i>	293
Table 7.12	<i>Calculation of error for the experimentally obtained values, for the photochemical reaction of pyridine with $\text{CpRu}(\text{PPh}_3)_2\text{Me}$ at 198 K</i>	293

Acknowledgements

I am deeply grateful to my supervisor, Professor Simon Duckett, for providing me with the opportunity to work on this thoroughly enjoyable project. I am also thankful for his guidance, advice and unwavering support throughout the course of my research.

Thank you to the past and present members of the SBD research group, who have made the past four years in the lab an enjoyable experience. Particular thanks to Ana, Catherine, Janet and Steve, whose enlightening discussions regarding *in situ* photochemistry, proved invaluable during the early stages of my research. My sincerest thanks go to the present / former postdocs of the SBD group: Joaquín, Jose, Juan, Iman, Mike, Ralph and Ryan, for their guidance and expertise.

I would also like to thank the Centre for Magnetic Resonance for providing the funding necessary for my project over the past four years. Also my deepest thanks to Heather and David of the NMR service, who provided many insightful discussions and assistance regarding NMR techniques, in addition to making my time with the NMR service pleasant and enjoyable.

Finally, I am immeasurably grateful to my parents, whose encouragement and support has helped immensely over the years.

Declaration

The work presented in this thesis is the original work of the author, with the exception of specific references made to other literature sources. Work contained within this thesis has not been submitted for any other degree.

A handwritten signature in black ink, appearing to read "J. Clark". The signature is written in a cursive style with a large, looping initial "J".

Johnathan L. Clark

“I may not have gone where I intended to go, but I think I have ended up where I needed to be”

- Dirk Gently

The Long Dark Tea-time of the Soul
by Douglas Adams

Chapter 1

Introduction

1.1 General Introduction

Much of the interest surrounding the research of organometallic complexes lies in the metal centres ability to activate small organic molecules.¹ Such characteristics may be exploited by catalytic processes to convert readily available substrates into commercially valuable compounds.² These compounds may otherwise be difficult or impossible to manufacture on a large scale, using traditional organic synthetic methods. A principal reaction step in organometallic catalysis is often that of oxidative addition, whereby C-H, H-H and Si-H bonds are cleaved and bound to the metal centre.³

Many studies have been conducted to investigate oxidative addition reactions.^{4,5} In the case of cyclopentadienyl rhodium complexes (e.g. [CpRh(C₂H₄)₂]) these reactions have been probed using thermal and photochemical methods.⁶⁻⁸ Related cyclopentadienyl ruthenium bis-phosphine complexes have also been widely studied in the literature.^{9,10} However, their thermally induced reactivity has been the primary focus of such studies, while their photochemical activity has been mainly ignored.

The potential advantage of oxidative activations at the ruthenium centre of such cyclopentadienyl complexes is that there is an additional reaction site when compared with the rhodium analogues mentioned above. When vacant, this position provides the potential to produce more varied products and allow for catalytic behaviour. In this case the route to oxidative addition is facilitated by the labile nature of the phosphine ligand¹¹ and associated access to a 16 electron reaction intermediate with a vacant site for subsequent addition.

The intention of this thesis is to explore the photochemical activity for cyclopentadienyl ruthenium bis-phosphine complexes (and cyclopentadienyl rhodium complexes in

chapter 6). The use of photochemical reaction inducement as opposed to a thermal reaction is envisioned to lead to the formation of previously inaccessible novel complexes. In addition, low temperature *in situ* photochemistry^{12, 13} will be employed to stabilise reaction intermediates in these reactions that are subsequently structurally characterised by NMR techniques.

1.2 Activation of R-H bonds (where R = Si, H or C)

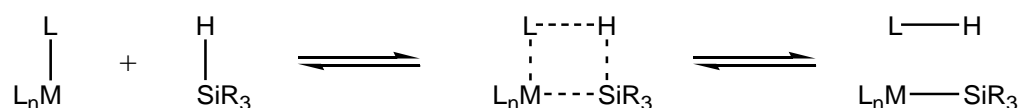
1.2.1 Si-H activation

Research into the activation of Si-H bonds has been of great interest mostly due to the key involvement of this reaction step in the industrial hydrosilation process¹⁴ (see section 1.2.1.4). A key feature of hydrosilation is the oxidative addition of a Si-H bond and migration of the hydride to an unsaturated centre followed by elimination. Research into Si-H bond activation has therefore enhanced the understanding of similar C-H and H-H activation pathways.^{15, 16} Interestingly, studies on the process of Si-H bond activation revealed the existence of stable σ -bound intermediates.

1.2.1.1 Oxidative addition and metathesis reaction pathways

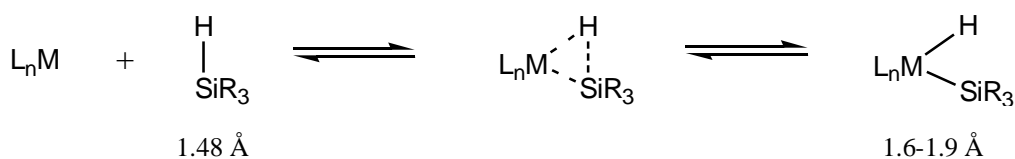
Activation of Si-H bonds to a metal centre typically occurs by either of two modes: metathesis (Figure 1.1) or oxidative addition (Figure 1.2).

Figure 1.1 The metathesis of a Si-H adduct to a metal centre



For bond metathesis, the sigma bond of the coordinated ligand “L” is replaced with the sigma bond of the incoming silyl group. This occurs through a four-centre mechanism, which unlike the oxidative addition mechanism, does not result in a change in the oxidation state of the metal centre (Figure 1.1).

Figure 1.2 The oxidative addition of a Si-H adduct to a metal centre, with typical Si-H bond lengths

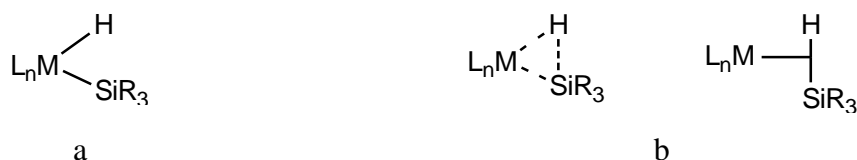


Oxidative addition of an Si-H moiety requires that the metal centre increases its oxidation state by two units, and is observed most often for the late transition metals, which have access to higher oxidation states (e.g. Ru(II) \rightarrow Ru(IV)). Conversely, early transition metals primarily exist at their highest oxidation state (owing to their highly ionic character), which restricts these metal centres from increasing their oxidation states further, and undergoing reaction via the oxidative addition pathway. For these reasons, it is generally assumed that early transition metals proceed via a metathesis route, while late transition metals follow an oxidative addition pathway.^{14, 17}

1.2.1.2 Classical and nonclassical products of oxidative addition

It should therefore now be clear that products formed via the oxidative addition route fall into two categories, often referred to as classical (Figure 1.3, a) and nonclassical (Figure 1.3, b) complexes.

Figure 1.3 Classical (a) and nonclassical (b) metal-silane complexes



The nonclassical complexes may be viewed as an ‘incomplete’ form of the oxidative addition pathway, and arise as a consequence of σ donation to the metal centre. The tendency of these σ (or η^2) complexes to be formed over their classical counterparts is influenced heavily by the degree of back bonding by the metal.¹⁸ Studies reported in

the literature have determined that increased back bonding favours the formation of classical complexes.¹⁹ With increasing π -basicity of the Si-H adduct, the likelihood of complete oxidative addition is reduced, owing to the higher energy requirement to cleave the Si-H bond.

The degree of back bonding may be tuned by adjusting the ligands coordinated to the metal centre so as to increase the electron density of the metal to favour the formation of a classical complex. Alternatively, increasing the number of electron withdrawing groups on the metal would achieve the same effect. Additionally, the substituents of the silane may be replaced with strong electron withdrawing groups (e.g. Cl). This would consequently increase the back donation from the metal owing to the lowered energy of the σ^* orbital.^{14, 20} It should also be noted that increasing the contribution of electron density from the Si-H adduct to the metal centre also favours the formation of a classical complex. This sigma interaction with the metal centre reduces the electron participation of within the Si-H bond, hence weakening the bond.

Typically a stable 18 electron species must undergo ligand dissociation (lowering to a 16 electron complex) prior to the oxidative addition of a Si-H adduct. There are numerous examples reported in the literature where this process is described to occur either thermally or photochemically.^{14, 16, 21, 22}

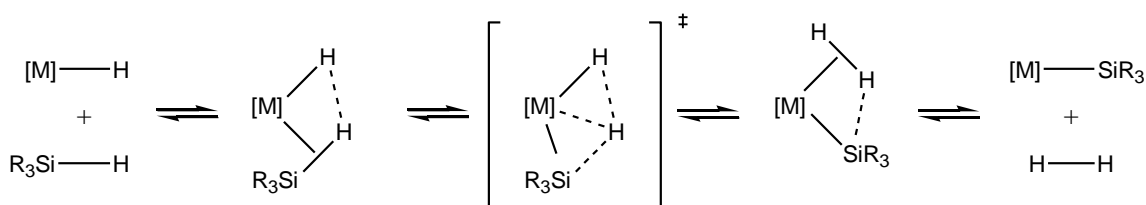
The Si-H bond is weaker than both the H-H and C-H bonds, owing to the greater Si-H σ^* accessibility towards metal centres, Si-H bonds are consequently better pi acceptors and sigma donors due to the greater Si-H basicity.²³

Determination of the metal – silane binding mode can be made using the J_{SiH} coupling constants obtained using NMR spectroscopy. A J_{SiH} value of approximately 200 Hz is expected for free silane, while σ complexes generally have values of less than 100 Hz.^{19, 23} Complexes which have completely undergone oxidative addition more commonly have J_{SiH} values of ~ 20 Hz.¹⁶ However, examples are known where products of full oxidative addition have higher values (e.g. $(\text{C}_5\text{H}_4\text{Me})(\text{CO})_2\text{Mn}(\text{HSiCl}_3)$ with a J_{SiH} of 54.8 Hz).²⁴

1.2.1.3 σ -CAM (σ -complex assisted metathesis) reaction

The σ -CAM mechanism provides an additional reaction pathway for late transition metal complexes by utilising both σ -complexation and metathesis. This is achieved through the interconversion of σ ligands, without a change in oxidation state for the complexes involved. Figure 1.4 demonstrates this overall process in a generalised depiction.

Figure 1.4 σ -CAM mechanism



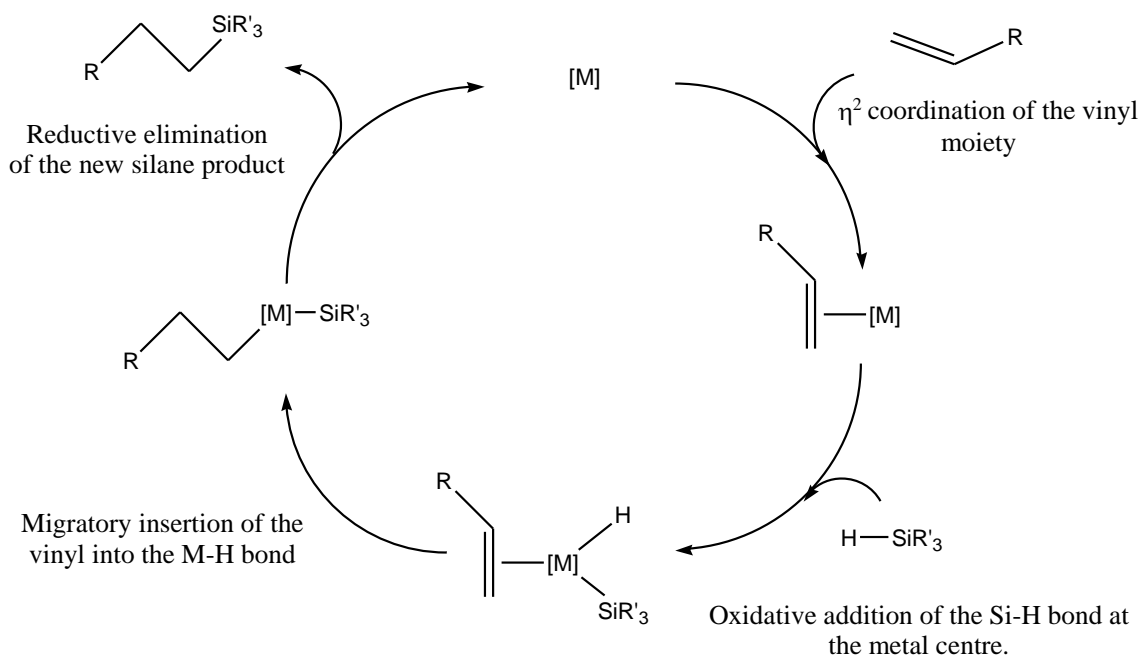
Studies to elucidate mechanistic details were described by Perutz and Sabo-Etienne in 2007,²⁵ who were the first to describe this mechanism in a generalised context. Prior to this description only reaction specific examples of the mechanism had been reported (including the observed hydrogen exchange for $TpRu(H)(\eta^2-E-H)(PPh_3)$ (Ng *et al.*)²⁶ and the borylation of alkenes (Hartwig *et al.*)^{27, 28} The studies required that NMR techniques were employed to demonstrate the interconversion of the hydride and σ ligands, by observing the exchange between the hydrogen atoms of the two ligands.

1.2.1.4 Hydrosilation

An important industrial application of Si-H oxidative addition is the hydrosilation process, whereby the Si-H adduct undergoes addition to a C-C double or triple bond. This process is widely used in the industry to crosslink silicon-based polymers.

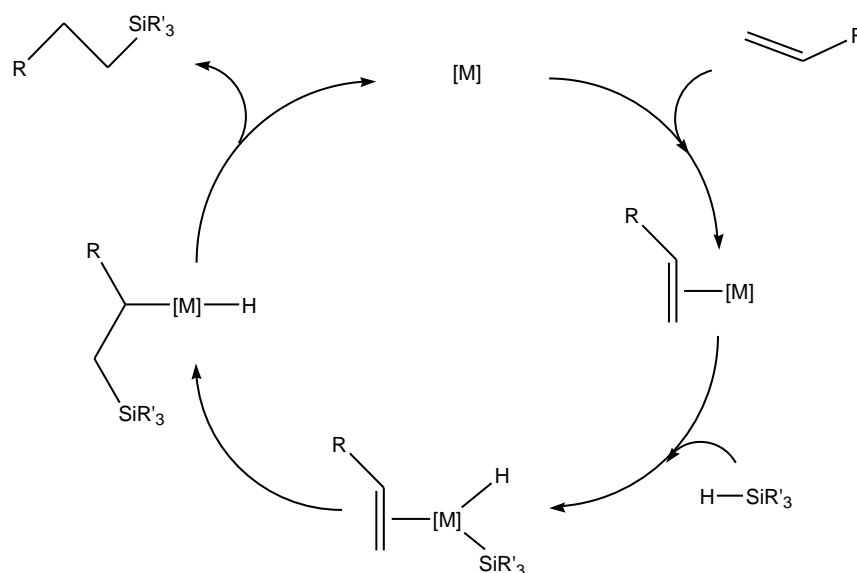
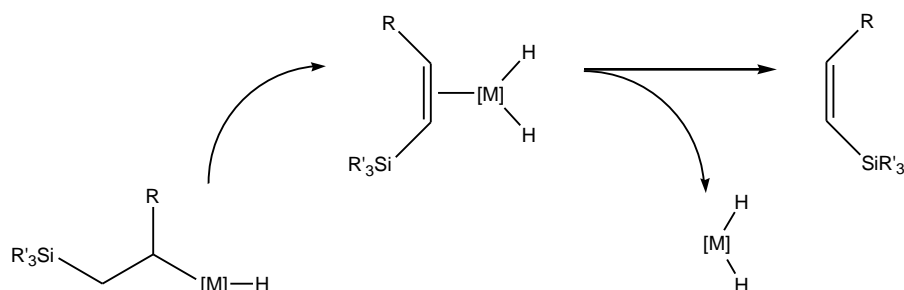
The Chalk and Harrod mechanism was first proposed in 1965 for the platinum catalysed hydrosilation of olefins, and was widely regarded as the general mechanism by which hydrosilation occurred for metal catalysts.^{29, 30} Figure 1.5 outlines the mechanistic steps for the Chalk-Harrod mechanism.

Figure 1.5 Generalised depiction of the Chalk-Harrod mechanism for hydrosilation



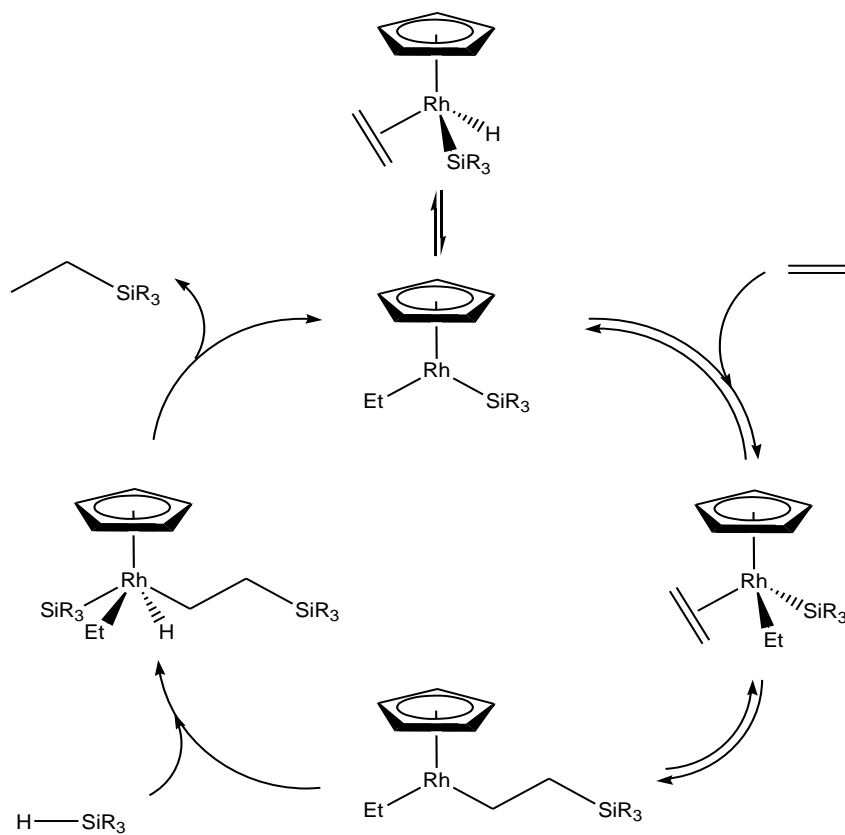
However, the Chalk-Harrod mechanism did not account for the formation of vinylsilanes,^{31, 32} which occurred as a by-product in reactions requiring catalysts containing metals other than platinum. This led Shroeder and Wrighton in 1977³³ to revise the mechanism to explain the formation of vinyl silanes. The revised cycle (Figure 1.6) deviates from the original in that the silyl moiety migrates as opposed to the hydride. Literature precedents favour the revised cycle,^{30, 34} as the Si-C reductive elimination step of the original mechanism is less commonly observed, compared with the reductive elimination of C-H (as suggested by the revised mechanism). This alternative mechanism is now the more commonly accepted of the two, and is seen as particularly relevant in the cases of cobalt, rhodium, iridium and iron containing catalysts.³² Figure 1.7 depicts the subsequent steps required to form vinylsilanes following the migration of the silyl moiety.

Figure 1.6 The silyl migration variant of the Chalk-Harrod mechanism

Figure 1.7 Formation of vinylsilane as a by-product of metal catalysed hydrosilation^{31, 34}

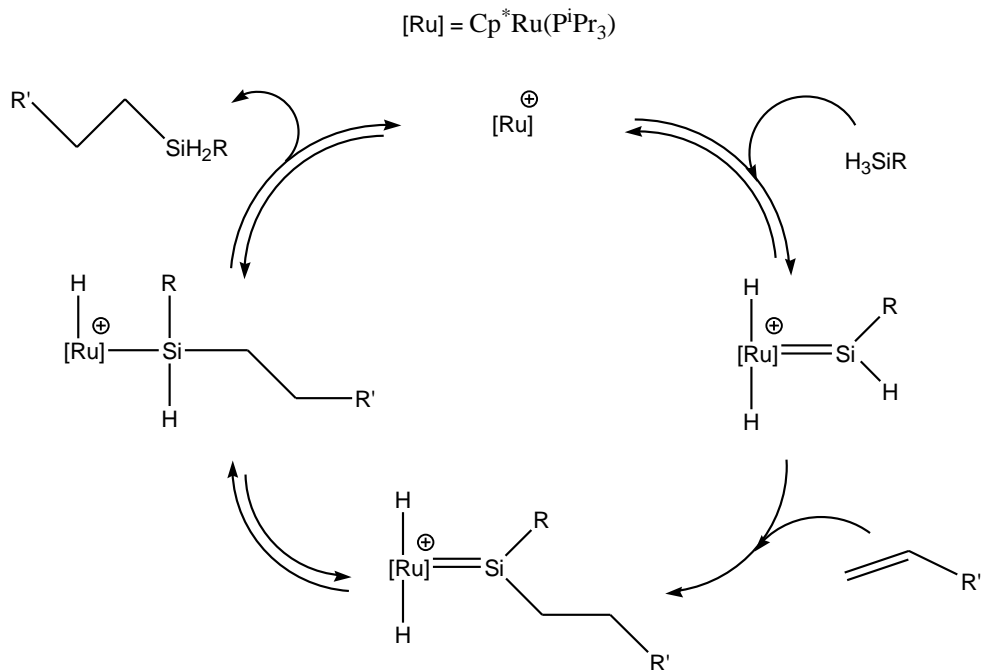
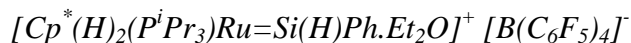
However, neither of these mechanisms apply to the complex $[\text{CpRh}(\text{C}_2\text{H}_4)\text{SiEt}_3(\text{H})]$, which was found by Duckett and Perutz³⁰ to form SiEt_4 and $\text{CH}_2=\text{CHSiEt}_3$, when photolysed with HSiEt_3 .⁸ $\text{CpRh}(\text{C}_2\text{H}_4)\text{SiEt}_3(\text{H})$ is formed when $\text{CpRh}(\text{C}_2\text{H}_4)_2$ is photolysed in the presence of short-chain tertiary alkyl silanes of the type SiR_3 (e.g. $\text{R} = \text{Me}$ or Et), re-association of the liberated ethene allows for hydrosilation. Isotope labelling studies elucidated the involvement of two silyl groups in the cycle (Figure 1.8). This work contrasts with that reported by Maitlis *et al.*, for the Cp^* analogues, which concluded that $\text{Cp}^*\text{Rh}(\text{C}_2\text{H}_4)_2$ and $\text{Cp}^*\text{Rh}(\text{SiEt}_3)_2(\text{H})_2$ were not involved in the catalytic process.³⁵ Similar cycles have since been proposed by Wrighton *et al.* for both $\text{Co}(\text{CO})_4(\text{SiR}_3)$ and $\text{Cp}^*\text{Fe}(\text{CO})_2(\text{SiR}_3)$.^{31, 36, 37}

Figure 1.8 Catalytic hydrosilation using $CpRh(C_2H_4)SiEt_3(H)$ – The Duckett-Pertutz mechanism



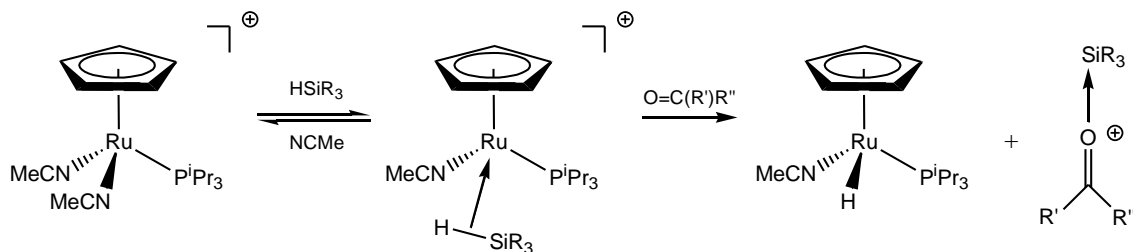
More recently, Tilley *et al.* have demonstrated another pathway using $[Cp^*(H)_2(P^iPr_3)Ru=Si(H)Ph.Et_2O]^+ [B(C_6F_5)_4]^-$ as a catalyst for the hydrosilation by primary silanes of alkenes.³⁸ The principle step in this process is the insertion of an alkene into a Si-H bond which acts as a spacer between the silyl moiety and the metal centre, following reductive elimination with the hydride, the functionalised silane is released (Figure 1.9). This is a departure from the original Chalk-Harrod mechanism (Figure 1.5) which undergoes reductive elimination of the silyl and alkyl groups to form a C-Si bond. The changes in the mechanistic character between these pathways are widely attributed to the differences in the metal centres and silanes used, in addition to the degree of steric crowding about the metal centre.³⁸ This attests to the tunability of the hydrosilylation process, when developing new silanes.

Figure 1.9 Proposed catalytic hydrosilation cycle for



More recent research by Nikonov *et al.* has determined the mechanisms for the hydrosilation of nitriles³⁹ and pyridines.⁴⁰ Nikonov *et al.* also note the hydrosilation of carbonyl by $[\text{CpRu}(\text{N}\equiv\text{CMe})_2(\text{P}^i\text{Pr}_3)]^+$, which proceeds via a sigma-bound silane intermediate. DFT studies of this cationic intermediate revealed the formation of a silylium cation (Figure 1.10).⁴¹

Figure 1.10 Hydrosilation of carbonyl compounds by $[\text{CpRu}(\text{N}\equiv\text{CMe})_2(\text{P}^i\text{Pr}_3)]^+$, and the subsequent formation of a σ -bound cationic silane complex, and silylium cation⁴¹

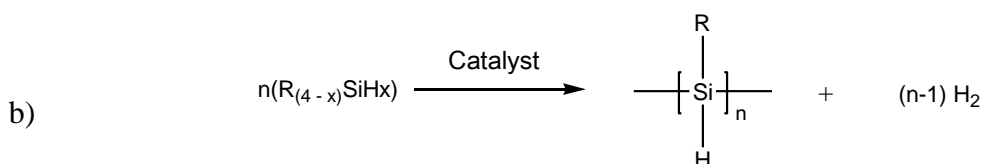
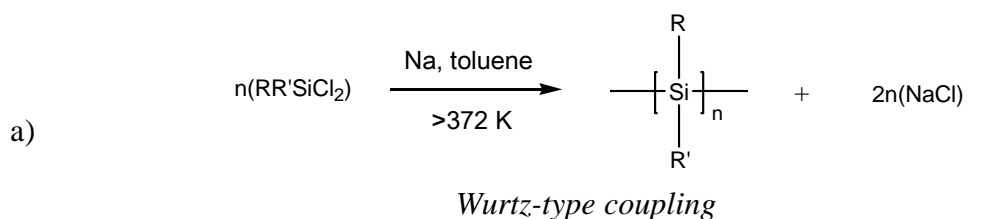


1.2.1.5 Polymerisation

Polymerisation of silanes is a known (and often considered an undesirable) side reaction of the hydrosilation process. However, over the past several decades the value of polysilanes in industry has increased,^{42, 43} as polysilanes are now frequently employed as photoinitiators, electroconductors and ceramic precursors.^{21, 44} The hydrosilation process however, is unreliable as a means to form polysilanes of varied chain length and in the quantities required. Therefore traditional synthesis methods of polysilane production are used, such as the Wurtz-type coupling reaction (Figure 1.11, a). Despite the ability of this reaction to produce polysilanes of sufficient lengths, the temperatures required for reaction are high (and often involving boiling toluene or xylene) which risks ignition and potentially the loss of functional groups on the silane (unless well protected⁴⁵⁻⁴⁸).

The use of metal complexes as catalysts for a dehydrogenative coupling reaction is of current interest (Figure 1.11, b), as they would provide an alternative to the traditional Wurtz-type reaction method.

Figure 1.11 Methods of polysilane synthesis

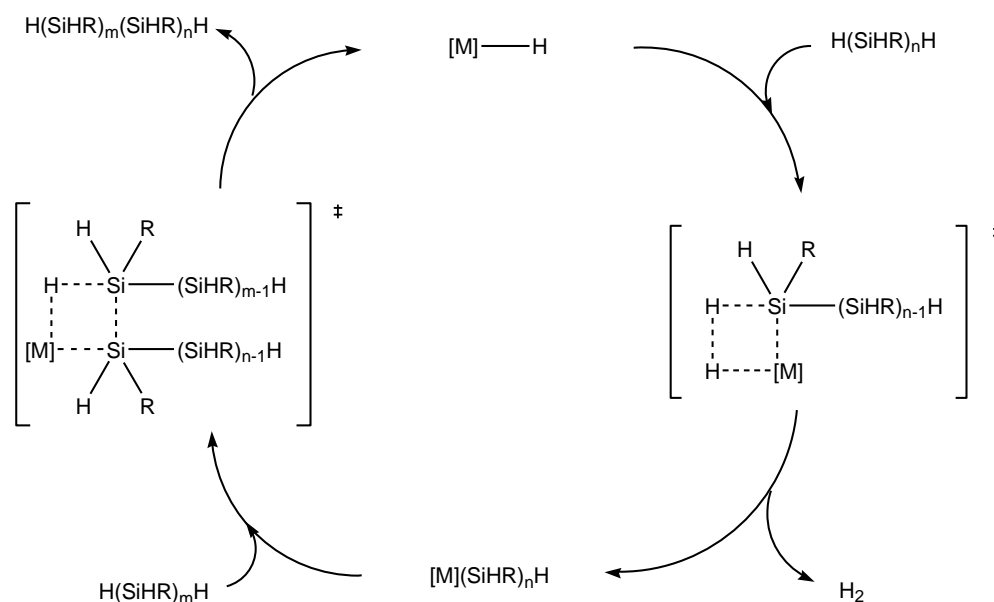


Transition metal catalysed dehydrogenative coupling

The challenge associated with the catalytic formation of polysilanes is producing chains of the same chain length as those produced using the Wurtz-type coupling method. For example, titanium and zirconium catalysts of the type $(\text{Cp})_2\text{M}(\text{R})_2$, developed by Harrod *et al.*, are capable of producing polysilane chains of 10 to 20 units in length.^{49, 50} Tilley *et al.* have considered other Group 4 metallocenes, including those of hafnium. Some of

these metallocene complexes have been demonstrated to produce chain length of 70-100 units in length.^{50, 51} Further investigation of the mechanistic pathway by Tilley has revealed that the formation of the Si-Si bond proceeds through a σ -bond metathesis step (Figure 1.12). This mechanism is widely considered to apply to other d^0 metallocene catalysts, such as titanocene.⁴³

Figure 1.12 Generalised mechanism for the transition metal catalysed formation of polysilanes

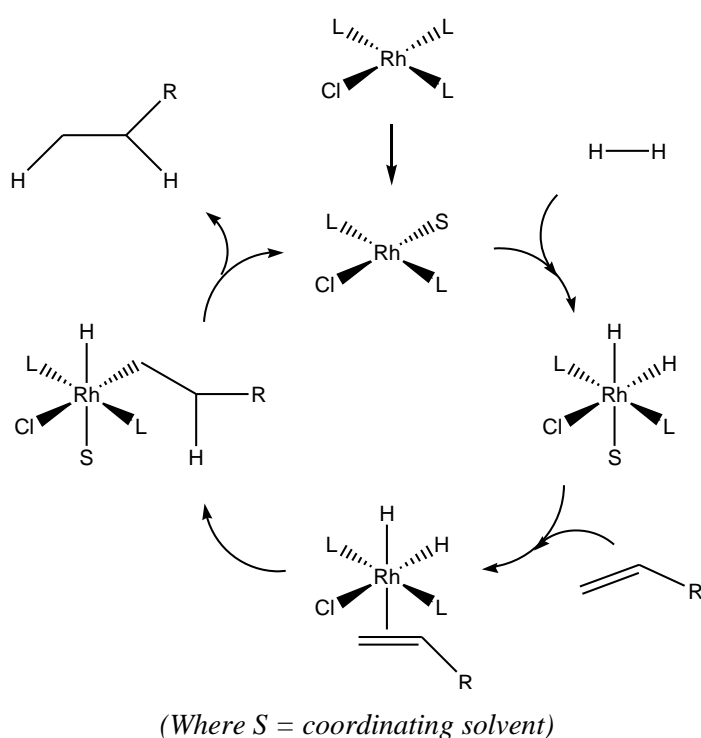


Rosenberg *et al.*⁵¹⁻⁵⁴ have demonstrated that late transition metal complexes, such as Wilkinson's catalyst, have the capacity to catalyze dehydrogenative coupling reactions. However, the resulting polymers are usually of short length (typically 5-6 units). Further studies involving Wilkinson's catalyst revealed that the system is sensitive towards hydrogen, and it has been considered that the removal of excess hydrogen may lead to an increase in chain length of the product polymers. Such character would enable the system to be tuned to favour the formation of custom length polymers, based on the concentration of hydrogen available. This catalyst has the additional advantage over the Wurtz-type reaction, of enabling the synthesis of di-silanes with different side-chains.^{51, 54} The use of such silanes in further polymerisation reactions would potentially form novel polysilane chains.

1.2.2 H-H activation

Activation of molecular hydrogen plays a key role in industrial catalytic hydrogenation processes. There are three principle methods by which molecular hydrogen can bind to a metal centre: oxidative addition, heterolytic cleavage, homolytic cleavage and by η^2 -coordination to the metal centre.⁵⁵⁻⁵⁷ The most widely reported of these in the literature is the oxidative addition pathway, which plays a key role in many industrial catalytic processes, for example, the hydrogenation of alkenes (Figure 1.13).

Figure 1.13 catalytic hydrogenation of alkenes using Wilkinson's catalyst

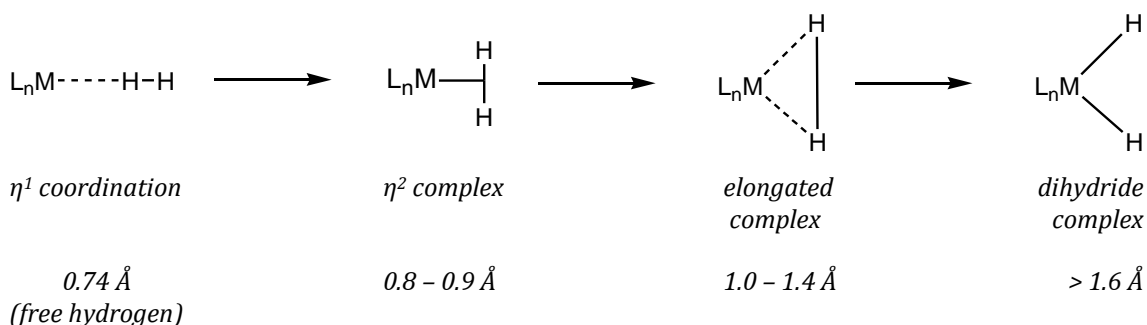


1.2.2.1 Oxidative addition pathway

Initially, the oxidative addition pathway for molecular hydrogen proceeds with the weak orientation of the molecule in an η^1 fashion with the metal centre. Rearrangement at the metal centre gives rise to a η^2 derivative, which also reduces the distance between the metal and the H-H adduct. Following elongation of the H-H bond, the dihydride species is formed.^{58, 59} This pathway has been well documented in the literature, to the extent

that average bond length may be used to identify the coordination mode for these complexes (as shown in Figure 1.14).²⁰

Figure 1.14 Depiction of the oxidative addition pathway for the H-H adduct and the average H-H bond length of the intervening complexes²⁰

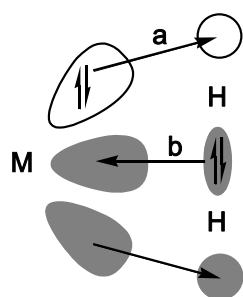


The initial step involving the η^1 interaction of dihydrogen with the metal centre was first proposed by Hoffman *et al.* in 1984, following modelling studies of the oxidative addition pathway for dihydrogen with rhodium centre of $Rh(Cl)(PPh_3)_3$.

The first example of an η^2 hydrogen complex was reported by Kubas *et al* in 1984,⁶⁰ for the complex $W(CO)_3(PiPr_3)_2(H_2)$. Subsequent characterisation of this stable η^2 complex led to the identification of other previously reported complexes as being η^2 hydrogen complexes.^{20, 60, 61} Over the last 25 years this area of research has rapidly expanded with hundreds of similar η^2 complexes reported in the literature.

The σ bonding of these η^2 complexes is markedly similar to the π bonding for olefins bound to metal centres. Therefore the bonding of these η^2 hydrogen complexes may be expressed in terms of the Dewar-Chatt-Duncanson model (Figure 1.15). Bonding proceeds through the donation from the highest occupied molecular orbital (HOMO) of hydrogen to the $d_{x^2-y^2}$ orbital of the metal. While back-donation occurs via the metal d_{xy} orbitals to the lowest unoccupied molecular orbital (LUMO) of hydrogen.^{17, 20, 61, 62, 58}

Figure 1.15 Metal-hydrogen bonding for dihydrogen complexes



- a) Back-donation from the metal d_{xy} orbitals to the σ^* orbitals of dihydrogen.
- b) Formation of a σ bond via donation from the σ orbital of dihydrogen to the $d_{x^2-y^2}$ orbital of the metal.

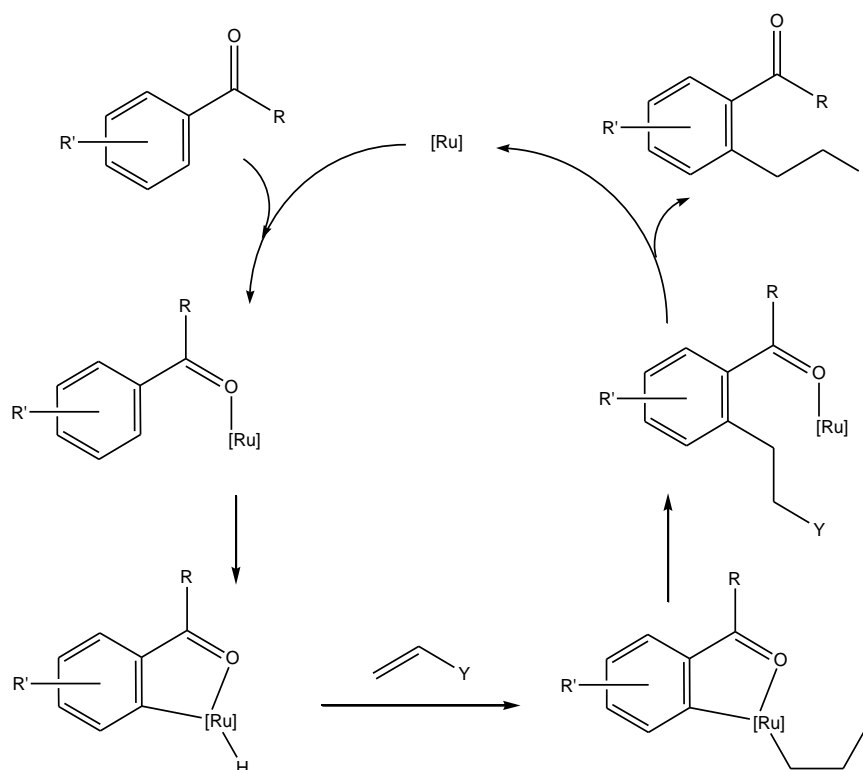
Donation from the H-H bond and subsequent back-donation to the σ^* (anti-bonding) orbitals leads to the elongation of the H-H bond (as shown in Figure 1.14) relative to the bond length of free hydrogen. Consequently the H-H bond lengths within a complex yield diagnostic information about the type of bonding interactions between the metal and hydrogen. NMR techniques may therefore be used to estimate bond lengths through the acquisition of J_{HD} coupling parameters or T_1 relaxation measurements.^{17, 62} Typically J_{HD} coupling values decrease along the complexes depicted in Figure 1.14, with free (gaseous) H-D possessing a J_{HD} coupling of 42.3 Hz and around 33.5 Hz for η^2 complexes (in the case of $W(CO)_3(PiPr_3)_2(H_2)$). Smaller J_{HD} couplings are expected for dihydride species.⁶²

It is clear that the degree of back-donation directly affects the whether a non-classical complex proceeds to full oxidative addition, thereby forming a classical complex. By varying the ligands on the metal centre, dihydrogen, elongated or dihydride species may be favoured as products. For example, a strong π acid such as CO would act as an electron withdrawing group, and would consequently favour a dihydrogen species. Alternatively, phosphines are generally weaker π acids (relative to CO) and would be more likely to be an electron donating ligand.²⁰ A probable increase in the degree of back-donation to the σ^* (anti-bonding) orbitals would favour the cleavage of the H-H bond, and result in the formation of a dihydride species.

1.2.3 C-H activation

The formation of C-C bonds is a fundamental step in many industrial synthetic processes. Traditional organic synthetic methods of carbon coupling include the Pinacol⁶³ reaction, the Gomberg–Bachmann⁶⁴ reaction, Gilman reagent⁶⁵ coupling and some Grignard-type⁶⁶ reactions. However, many industrial processes now use metal catalysed reactions to achieve the same result (Figure 1.16). A fundamental step in these cycles is the activation of a C-H bond on to a metal centre, from which the compound may be subsequently functionalised through a reductive elimination step. It is therefore clear that the conversion of readily available carbon compounds, such as alkanes, to functionalised organic compounds, such as alcohols, would prove highly desirable (and commercially profitable) for chemical industry.

Figure 1.16 The catalytic addition of an olefin to an aromatic compound using $Ru(H)_2(CO)(PPh_3)_3$ ^{67, 68}

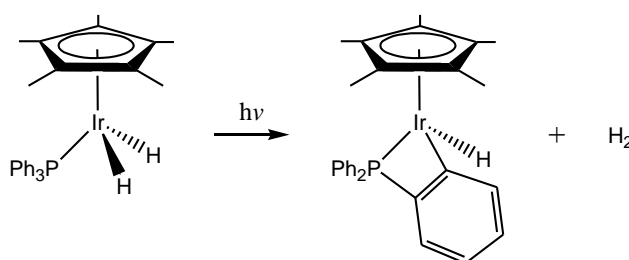


However, the C-H adduct for alkanes is difficult to activate on a metal centre, relative to the Si-H bond of silanes and the H-H bond of free hydrogen, due to the increased electronegativity⁶⁹ owing to strong localised C-H and C-C bonds (whereby the

electrons participating in the bond lie close to the connecting atoms, resulting in stronger bonding). Consequently, many of the examples for C-H activation in the literature focus on those of arene compounds and those lying adjacent to hydroxyl and vinyl groups, which are demonstrably more reactive.

A common example of C-H activation products are those which have undergone the processes of cyclometallation e.g. Figure 1.17.⁷⁰ This is an example of intramolecular C-H activation, which affords the resulting complexes greater thermal stability.

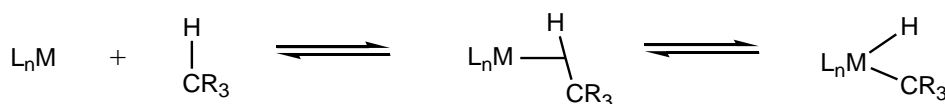
Figure 1.17 The photochemically induced cyclometallation of $Cp^*Ir(PPh_3)(H)_2$ ⁷¹



1.2.3.1 Oxidative addition pathway

The first reactions involving the activation of C-H alkane bonds were reported by Shilov *et al* in 1969.⁷² Shilov's work described the Pt(II) salt catalysed exchange of H-D between methane and D₂O at 283 K, and the Co(H)₃(PPh₃)₃ catalysed deuteration of methane at 298 K, using D₂. Figure 1.18, depicts the activation of C-H bonds suggested by Shilov's work.

Figure 1.18 The oxidative addition of a C-H adduct to a metal centre



As depicted in Figure 1.18, the alkane binds in an η^2 C-H bond interaction similar to that previously discussed for Si-H and H-H. The C-H bond approaches the metal centre in a side-on fashion η^2 (unlike the η^1 approach for H-H),⁵⁹ where upon binding the

hydrogen atom is orientated closer to the metal than the carbon atom, leading to an initial M-H-C bond angle of approximately 150° . This arises from the lack of full access by the metal to the C-H σ^* orbital, which is sterically hindered (relative to the H-H and Si-H adducts described previously).^{23, 73} The unreactivity of C-H is also attributed to the low-lying HOMO and high energy LUMO (σ^*) of the C-H bond, compared to high HOMO and low energy LUMO of H-H, which is more accessible to the metal centre.⁷⁴ The η^2 -CH complex then rearranges to form the oxidative addition product.⁵⁵

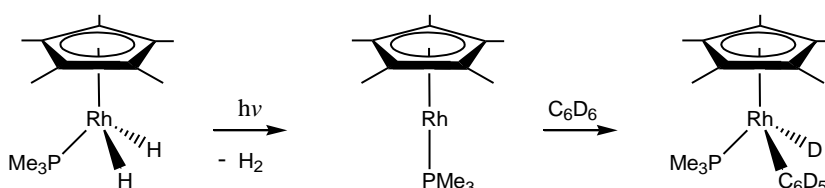
The gathering of evidence to support the existence of a sigma bonded intermediate in the oxidative addition of C-H bonds has been an active area of research over the past several decades. The first direct evidence for these alkane complexes was provided by Perutz and Turner *et al.*^{75, 76} based on the photochemical studies of chromium, molybdenum and tungsten pentacarbonyl fragments in alkane and alkane/rare gas matrices. Gould and Heinekey in 1989 provided further evidence for the existence of a σ alkane intermediate, based on studies of alkyl rhenium complexes of the type: $(\text{Cp})_2\text{Re}(\text{R})$.⁷⁷ In 1998 Geftakis and Ball conducted low temperature photochemical experiments which provided direct observation of a transition metal alkane complex, $\text{CpRe}(\text{CO})_2(\text{cyclopentane})$, by NMR spectroscopy.⁷⁸ However, it could not be distinguished from these results alone whether the geometry corresponded to η^2 C-H or an η^2 H-H alkane complex. Later, Jones *et al.* in 2001 provided the first set of indirect evidence to support the role of σ alkane intermediates in oxidative addition / reductive elimination pathways. The evidence consisted of scrambling of the deuterium label of the metal bound alkyl moiety for Tp^iRh (where Tp^i = tris-3,5-dimethylpyrazolylborate) complexes.⁷⁹

A greater number of sigma bonded arene complexes are reported in the literature compared to their alkyl counterparts, owing to increased ability of arenes to accept backdonation from the metal. This contrasts with alkanes which have increased electronegativity localised on the C-H bond (therefore the σ^* orbital is high in energy). For benzene and methane, bond energies for the first C-H bond are 473 kJ mol^{-1} and 439 kJ mol^{-1} (respectively),⁸⁰ suggesting that arene compounds are harder to activate at metal centres. However, owing to the readiness of arene to form sigma complexes, Templeton *et al.* found that the barrier to oxidative addition onto Pt centres for arenes

was lower (53.14 – 53.97 kJ mol⁻¹, for benzene⁸¹) than that found for alkanes (107.53 kJ mol⁻¹, for methane⁸²).

The complex, Cp^{*}Rh(PMe₃)(H)₂, has been the focus of many studies⁸³⁻⁸⁵ and has been used to demonstrate the difference in aromatic and aliphatic C-H bond activation (Figure 1.19). Studies using benzene and propane prompted Jones *et al.* to conclude that it is kinetically and thermodynamically favourable to cleave aromatic C-H bonds, over aliphatic C-H bonds.⁸⁶ This is due to increased strength of the rhodium-aryl bond, and the ability of the aromatic moiety and hydride to rearrange into a stable η² complex.

Figure 1.19 Photochemical C-D activation of benzene by Cp^{*}Rh(PMe₃)(H)₂



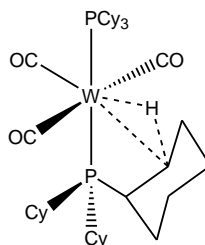
1.2.3.2 Agostic interactions

The majority of the examples of η² C-H coordination complexes reported in the literature are unstable, and the few which possess stability owe this to the presence of a chelate or agostic C-H bond interaction.^{69, 87-89} The notion of the existence of such agostic interactions was first proposed by Cotton *et al.* in 1974,^{90, 91} but it was not until 1988 that a fully characterised example of such a species was reported by Brookhart and Green.⁹²

The η² C-H interaction for agostic alkane complexes is primarily stabilised by the chelate effect, which is often facilitated when the alkyl moiety is part of a ligand with is coordinated to the metal centre through another site.⁶ This is clear for the complex W(CO)₃(PCy₃)₂ (Figure 1.20),⁹³ which possess an agostic interaction between the tungsten centre and the cyclohexyl moiety, which is tethered through the coordination of the phosphine ligand. The chelate effect acts to increase the entropy and disorder, which serves to stabilise the agostic complex over η² C-H alkane complexes.⁹⁴

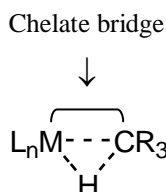
The inherent lability of the C-H adduct for such complexes has led to their use as precursors. For example, Kubas *et al.* used the agostic species $W(CO)_3(PCy_3)_2$ (Figure 1.20) as a precursor to the formation of numerous η^2 dihydrogen species.⁹³

Figure 1.20 The agostic interaction of $W(CO)_3(PCy_3)_2$



Unlike the oxidative addition route, the C-H adduct is already close in space to the metal centre due to the chelate link; the coordinated phosphine (Figure 1.21). The bond length is hardly affected, owing to the relatively weak interaction of the C-H adduct with the metal centre (e.g. a typical bond length for a C-H bond of an alkane complex is 1.1 Å, while a 1.13 to 1.19 Å length is more typical for agostic complexes).⁹⁵

Figure 1.21 The agostic interaction of a C-H adduct with a metal centre

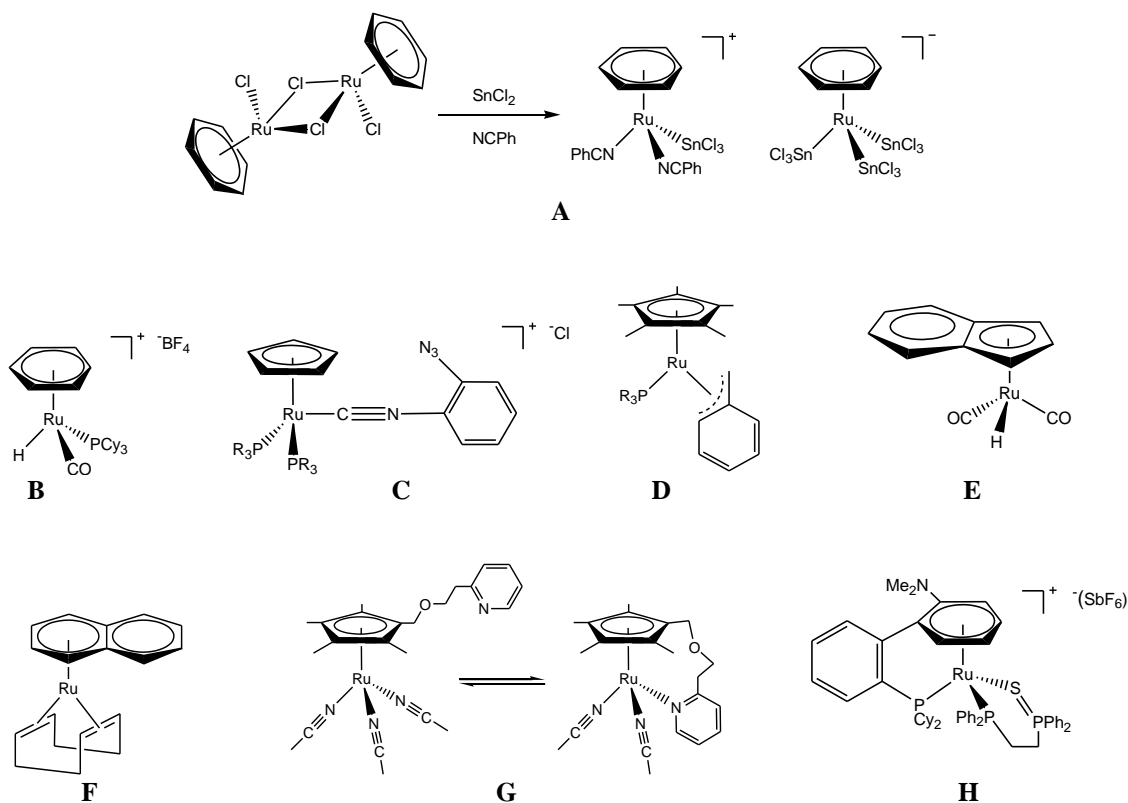


The presence of agostic interactions may be determined by x-ray or neutron crystal structure work. Alternatively, an agostic proton would be expected to experience a high-field shift, relative to the proton resonance for an analogous non-agostic complex, in a 1H NMR spectrum.⁵⁵

1.3 Reactions of cyclopentadienyl ruthenium complexes

The defining characteristic of a half-sandwich complex is the coordination of a single arene ligand, of structure C_nR_n , which is bound to a metal centre through haptic covalent bonds. Over the past half century, this class of complex has sparked much interest, particularly for their ability to activate small molecules and potentially facilitate catalytic transformations.⁹⁶⁻⁹⁹ Some examples of the types of arenes which comprise half-sandwich complexes include: C_6H_6 (Figure 1.22, **A**¹⁰⁰ and **B**¹⁰¹), C_5H_5 (Figure 1.22, **C**¹⁰²), C_5Me_5 (Figure 1.22, **D**¹⁰³), C_9H_9 (Figure 1.22, **E**¹⁰⁴) and $C_{10}H_{10}$ (Figure 1.22, **F**¹⁰⁵). Many derivatives exist for these coordinating arenes, which possess tethered functionalities (Figure 1.22, **G**¹⁰⁶ and **H**¹⁰⁷) capable of undergoing intramolecular coordination to the metal centre, which affords increased stabilisation for the complex. For the purposes of this introduction, cyclopentadienyl ligands are mainly considered; in particular those which exist as complexes coordinated to ruthenium centres.

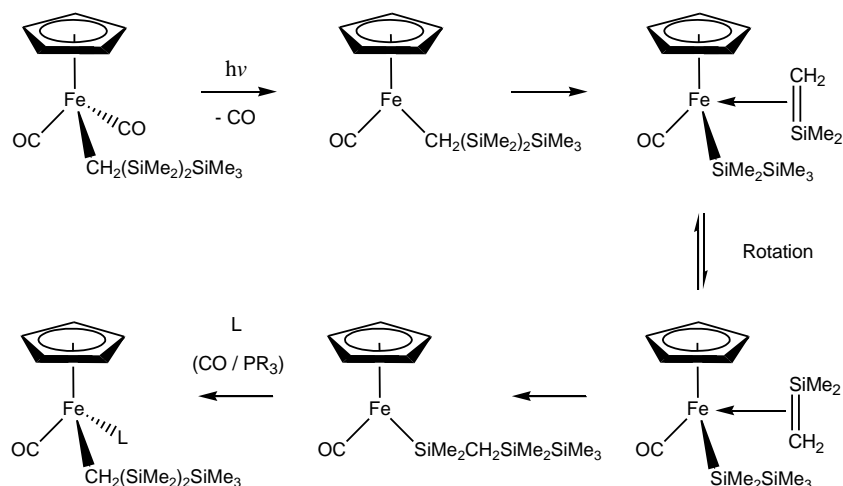
Figure 1.22 Examples of ruthenium half-sandwich complexes



The coordinated cyclopentadienyl ring of $\text{CpRu(L)}_2\text{R}$ type complexes affords increased stability, yet the presence of other coordinated ligands allow for a far wider spectrum of reactivity over their bis-cyclopentadienyl (sandwich complex) derivatives. The nature of the reactivity of these complexes can be adjusted by varying the ligands bound to the metal centre.

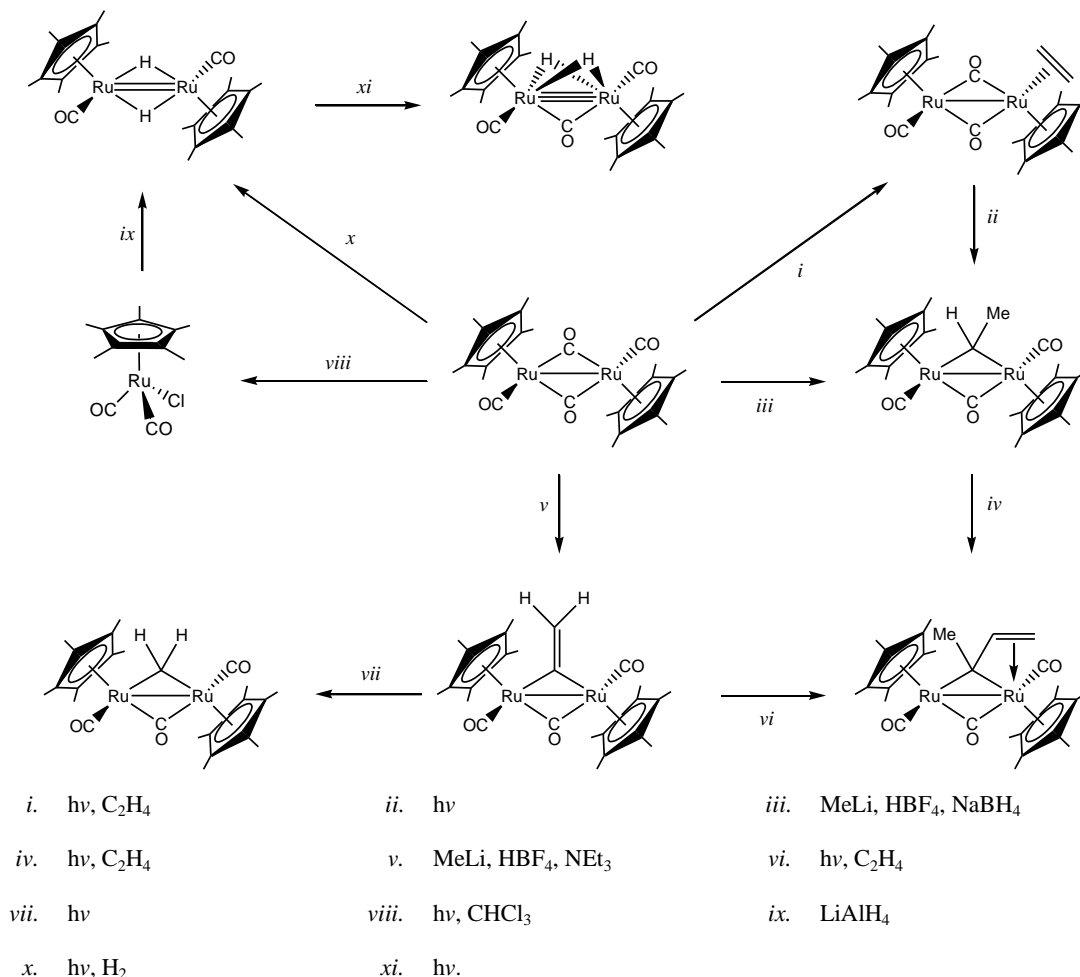
Iron complexes of this type have been widely studied in both their thermal and photochemical reaction pathways. Notable examples of such work include studies by Pannell *et al.*,¹⁰⁸ who over several decades have probed the photochemical reactivity of bis-carbonyl cyclopentadienyl iron complexes with silanes (Figure 1.23).

Figure 1.23 Photochemically initiated isomerisation of silane moieties of $\text{CpFe(CO)}_2\text{R}$ complexes¹⁰⁸



Though the thermal reactivity of the ruthenium analogues has been widely explored, examples of their photochemical reactivity are not prevalent in the literature. Most of the examples of photochemical activity focus on bimetallic carbonyl complexes, with contrasts made to their iron derivatives.^{109, 110} Studies of the photochemical reactivity of $(\text{CpRu(CO)}_2)_2$ have been reported by Farrow and Knox,¹¹¹ examples of these reactions are depicted in Figure 1.24.

Figure 1.24 Examples of photochemical reactions of the bimetallic complex

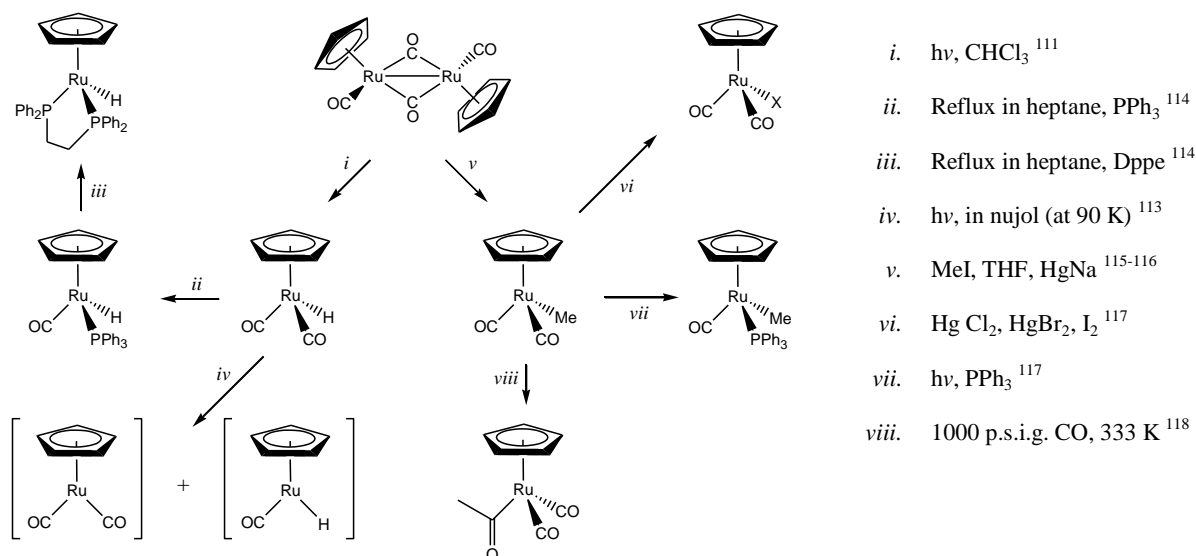


Bis-carbonyl and bis-phosphine complexes are the most widely studied ligand combinations for this type of complex, owing to their lability towards ligand exchange. The bis-carbonyl containing complex, $\text{CpRu}(\text{CO})_2\text{H}$ is readily synthesised from $\text{Ru}_3\text{CO}_{12}$ and cyclopentadiene,¹¹² and provides a convenient starting point towards to the synthesis of other more novel cyclopentadienyl ruthenium complexes.

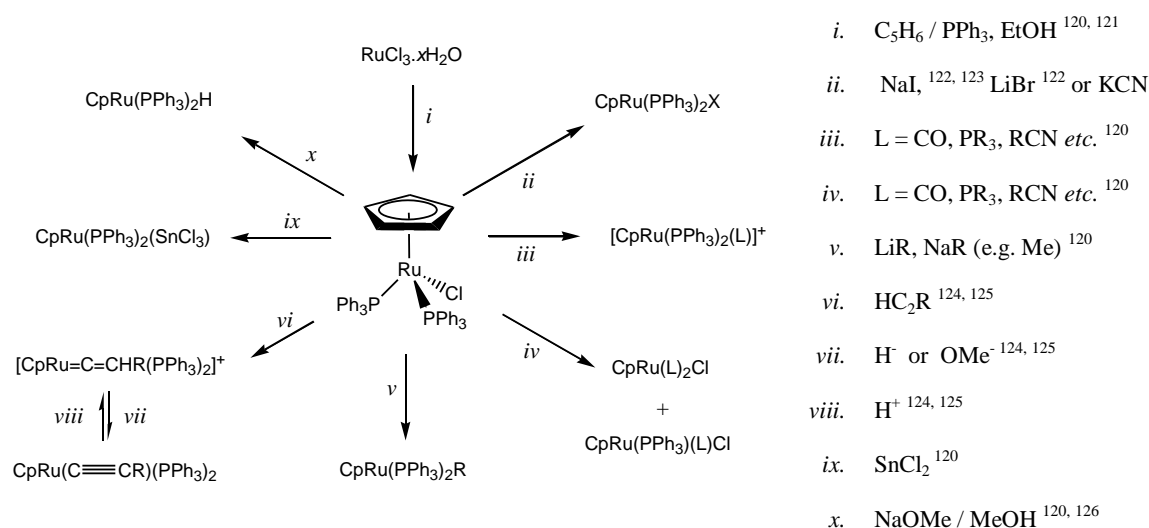
The photochemical and thermal chemistry of the bis-carbonyl complexes, $\text{CpRu}(\text{CO})_2\text{H}$ and $\text{CpRu}(\text{CO})_2\text{Me}$; Figure 1.25 depicts some of the reactions reported for these complexes in the literature. Reaction iv in Figure 1.25 demonstrates the low temperature observation of two coordinatively unsaturated species, which were obtained through the photochemical dissociation of one of the ligands.¹¹³ These structures are likely to be (or

similar, for the reactions of the methyl derivative) intermediary structures for the other reactions depicted in Figure 1.25.

Figure 1.25 The synthesis and reactions of $\text{CpRu}(\text{CO})_2\text{H}$ and $\text{CpRu}(\text{CO})_2\text{Me}$

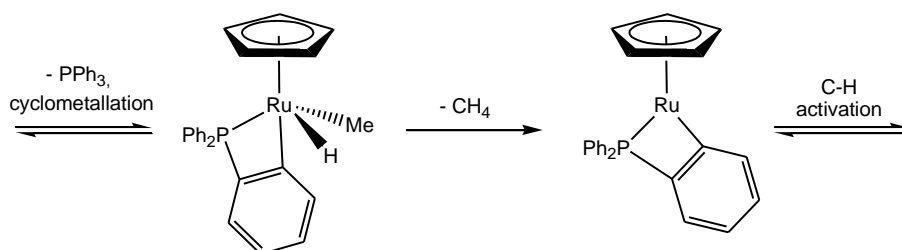


The bis-phosphine derivative, $\text{CpRu}(\text{PPh}_3)_2\text{Cl}$, was first discovered by Wilkinson ¹¹⁹ as a side product of the reaction $\text{RuCl}_2(\text{PPh}_3)_3$ and cyclopentadiene, the complex was subsequently identified and characterised by Stone *et al.* ¹²⁰ The method by which $\text{CpRu}(\text{PPh}_3)_2\text{Cl}$ can be synthesised has been revised numerous times over the past thirty years, ¹²¹ and can now be prepared more swiftly and reliably in high yields. The ready availability of $\text{CpRu}(\text{PPh}_3)_2\text{Cl}$ makes it an ideal starting point in the synthesis of other cyclopentadienyl ruthenium complexes (Figure 1.26 outlines some examples of the more common syntheses). As a general observation, the chloride may be readily substituted using ionic reagents in polar solvents, while (mono or bis) substitution of the phosphine ligands can generally be achieved thermally in hydrocarbon solvents. This variability can lead to the controlled formation of novel complexes.

Figure 1.26 The synthesis and reactions of $\text{CpRu}(\text{PPh}_3)_2\text{Cl}$ 

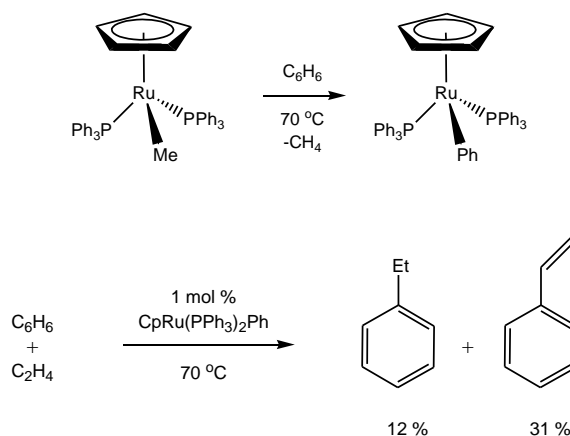
Bruce *et al.* ^{11, 127} (with further subsequent work by Lehmkuhl *et al.* ¹²⁸) detailed the mechanism by which methane is liberated from the complex, $\text{CpRu}(\text{PPh}_3)_2\text{Me}$, where C-H bond activations of arene compounds on the metal centre were observed. They determined that the methane was liberated, prior to the oxidative addition of the arene, via cyclometallated intermediates (Figure 1.27). Over the past several decades the cyclometallation reactions of half-sandwich ruthenium complexes (and other ruthenium complexes) have been of great interest. ¹²⁹ Further discussion of this orthometallation pathway and the role it serves in the reactions of $\text{CpRu}(\text{PPh}_3)_2\text{Me}$ thermally and photochemically, appears in Chapter 3.

Figure 1.27 Cyclometallated intermediates formed prior to arene C-H bond activation



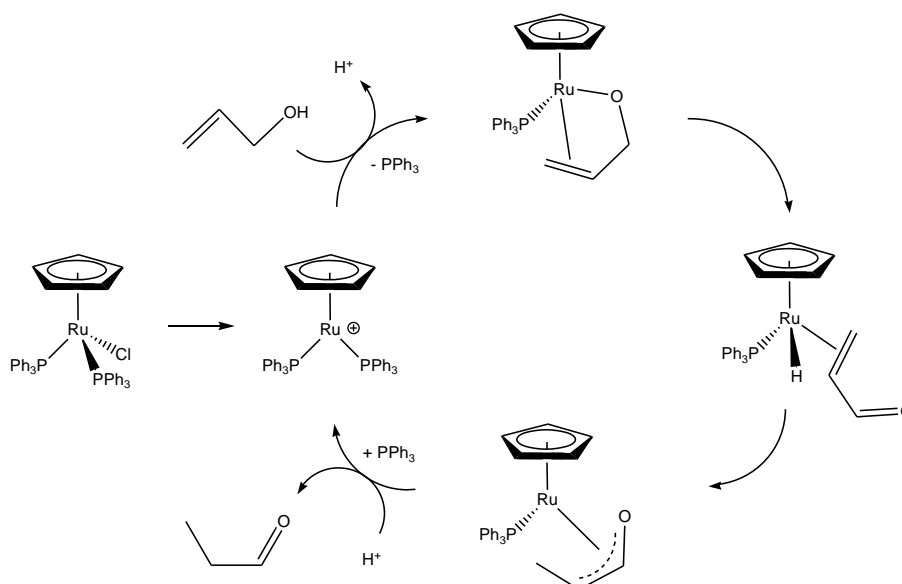
Interest has increased in studying the potential of these complexes as catalysts for industrial processes. Recently, Gunnoe *et al.* attempted to form ethyl benzene catalytically, using $\text{CpRu}(\text{PPh}_3)_2\text{Me}$ / $\text{CpRu}(\text{PPh}_3)_2\text{Ph}$ with ethene in benzene. However, the reaction was initiated thermally, and the catalyst was observed to decompose under these catalytic conditions.¹³⁰

Figure 1.28 Attempt to form ethylbenzene catalytically using $\text{CpRu}(\text{PPh}_3)_2\text{Me}$



Successful catalytic pathways have been established for $\text{CpRu}(\text{PPh}_3)_2\text{Cl}$.^{131, 132} For example, Figure 1.29 describes the role of $\text{CpRu}(\text{PPh}_3)_2\text{Cl}$ in the catalytic isomerisation of alkenyl alcohols to aldehydes and ketones.¹³³

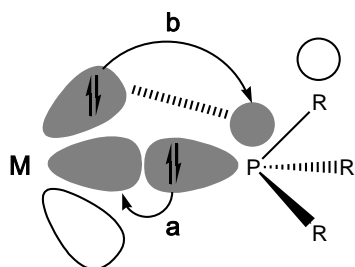
Figure 1.29 Catalytic isomerisation of alkenyl alcohols to aldehydes (and ketones) using $\text{CpRu}(\text{PPh}_3)_2\text{Cl}$



1.4 The role of phosphine ligands in organometallic complexes

Phosphines are good donor ligands, which are readily employed in organometallic chemistry to fine-tune the reactivity of late transition metal complexes. The bonding of phosphines to metal centres is similar to that of carbonyl and cyanide ligands, in that they are π acids; σ donors and π acceptors (Figure 1.30 describes the bonding of phosphines to metal centres). However, alkyl phosphines generally rank lower in the spectrochemical ligand series than CO or CN^- and are therefore not expected to bind as strongly to metal centres.^{55, 57} This allows for their remarkable versatility and role as spectator ligands in many chemical reactions.

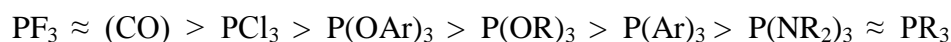
Figure 1.30 Metal-phosphorus bonding for phosphine bound complexes



- Donation of the phosphorus lone pair from the sp hybridised PR_3 orbital (HOMO) to the $d_{x^2-y^2}$ orbital of the metal.
- Back-donation from the d_{xy} metal orbital to the (LUMO) σ^* orbitals of the P-R bond. This also lengthens the P-R bonds, relative to those in free phosphine.

The greater the electronegativity of the R groups of the phosphine, the greater the stability of the σ^* orbital of the alkyl/aryl carbon (R) which bonds to the phosphorus atom. Consequentially, this also stabilises the σ^* orbital of the P-R bond,^{134, 135} by becoming lower in energy. This makes the empty σ^* orbital more accessible for back-donation, increasing the overall π acidity of the ligand (i.e. PF_3 , has a slightly greater π acidity than CO). Figure 1.31 provides an overview of the order of π acidity for phosphine ligands.

Figure 1.31 General order of π acidity for phosphine ligands (highest to lowest)

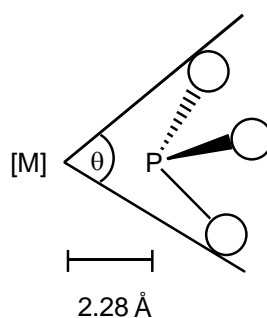


The electronic properties of phosphines have long been known to be partly responsible for their strong binding character to metal centres. In 1977 Tolman compiled IR $\nu(\text{CO})$ data for phosphine complexes of the type $\text{Ni}(\text{CO})_3(\text{PR}_3)$, in order to quantify the relative

binding strength of phosphines to metal centres.¹³⁶ The stronger donor phosphine ligands would increase the electron density on the Ni centre. Some of this increased density would be expected to flow to the bound carbonyl ligands, lowering the $\nu(\text{CO})$ frequency. The IR data demonstrated that phosphine ligand coordination at the Ni(0) centre was decreased, and could not be explained fully in terms of electronic effects. Tolman deduced that steric hindrance of the moieties bound to the phosphorus atom were responsible.

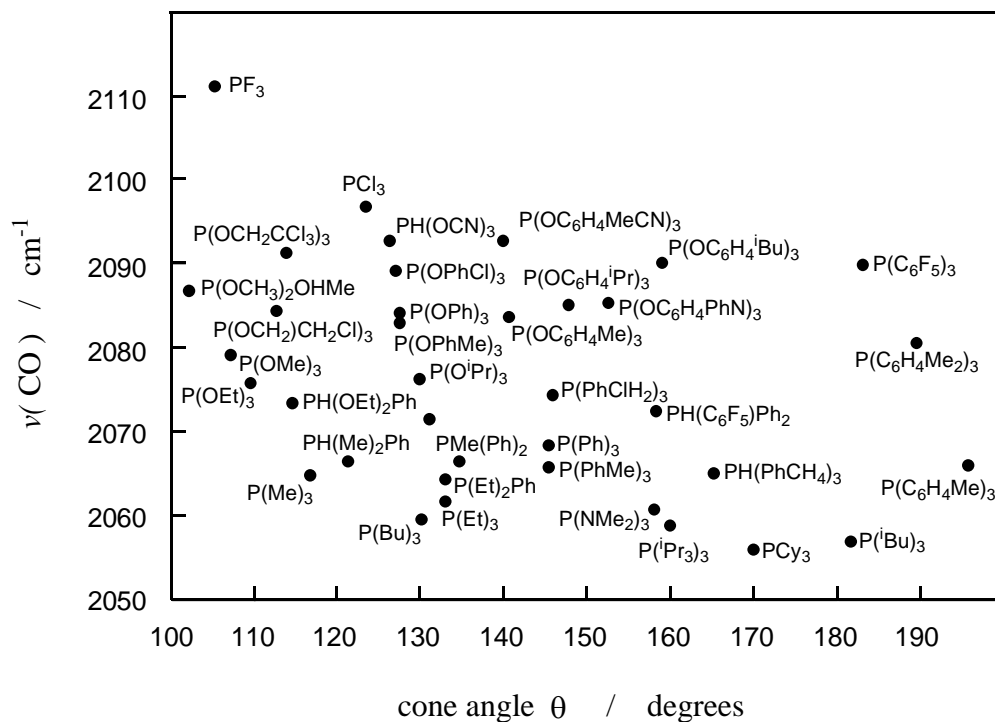
The steric properties of phosphines (and other ligands) may be determined by measuring the cone angle. Tolman described this concept by using crystallography data to calculate the cone angle (θ) for a variety of different phosphine ligands, with a broad range of steric properties. The cone angle data is standardised by taking measurements from a point 2.28 Å from the phosphorus atom, towards the metal centre, along the M-P bond. The cone extends to encompass the van der Waals radii of the outermost atoms of the phosphine ligand (Figure 1.32).

Figure 1.32 Depiction of the Tolman cone angle (θ) for sterically hindered phosphines



Tolman compiled this steric and electronic data into what has since become known as the Tolman map (Figure 1.33), which relates the electronic properties ($\nu(\text{CO})$) to the steric properties, to demonstrate relative binding strength of phosphine ligands.

Figure 1.33 Tolman map correlating the electronic and steric factors of phosphine ligands



The effect of the sterically hindered phosphine ligands on the formation of predominant isomeric forms of metal complexes, has been known since 1968.¹³⁷ The formation of the *trans* configuration of $\text{Mn}(\text{CO})_4(\text{COMe})(\text{PR}_3)_2$ was reported to be favoured over the *cis*-isomer, when the steric bulk of the coordinated phosphine ligand was increased.

Concerning catalytic activity, Grubbs *et al.* observed that when sterically hindered phosphine ligands were incorporated into the structure of the complexes $\text{Ru}(\text{X})_2(\text{C}=\text{CR}'\text{H})(\text{PR}_3)_2$ and $\text{Ru}(\text{X})_2(\text{C}=\text{CR}'\text{H})(\text{NHC})\text{PR}_3$, catalytic activity for olefin metathesis was increased.¹³⁸ This was deduced to be caused by the stabilising effect of the phosphine ligand on the Ru(IV) cyclometallated butyl intermediate, owing to the electron donating character of the phosphine. For the case of $\text{Ru}(\text{X})_2(\text{C}=\text{CR}'\text{H})(\text{PR}_3)_2$, the increased steric bulk of the phosphine facilitated the dissociation of one of the phosphine ligands, which was an initial step in the catalytic cycle. The complex $\text{Ru}(\text{X})_2(\text{C}=\text{CR}'\text{H})(\text{NHC})\text{PR}_3$, was observed to possess even greater activity owing to the presence of the N-heterocyclic carbene (NHC) ligand, which was more sterically encumbered and electron donating than the trialkylphosphine ligands. More recent investigations into phosphine design by Pringle *et al.* have led to the effective design of

ligands which enable the catalytic hydromethoxycarbonylation of ethane,¹³⁹ and tri / tetra-merisations of ethene,¹⁴⁰ when incorporated into metal complexes.

For complexes of the type $\text{CpRu}(\text{PR}_3)_2\text{X}$, the steric hinderance around the ruthenium centre is relieved by favouring ligand loss, therefore the M-P bond is increasingly sensitive to sterically hindered R groups. This was explained by Bruce *et al.*¹⁴¹ for the complex $\text{CpRu}(\text{PPh}_3)_2\text{Cl}$, which was observed to readily undergo thermal dissociation of one of the triphenylphosphine ligands, to relieve steric hindrance about the metal centre. However, the relief of the steric encumbrance led to strengthening of the M-P bond for the remaining phosphine ligand, as a result of the binding now relying more on electronic effects. This was demonstrated by the inability of CO (which processes greater π acidity) to displace the remaining triphenylphosphine ligand, for the mono-substituted complex $\text{CpRu}(\text{CO})(\text{PPh}_3)\text{Cl}$.¹²⁰

For $\text{CpRu}(\text{PMe}_3)_2\text{X}$ The barrier to the loss of PMe_3 is approximately lowered by the extent to which X acts as a π donor (relative to the case where X is a non- π donor, e.g. Me). This electronic effect coupled with the steric effect of phosphine ligands, means that no one set of bond dissociation energies will apply over the full spectrum of organometallic complexes. This is evidenced by the varying stability of M-CO bonds, where a range of bond dissociation energies have been found (between 22 and 84 kcal mol⁻¹), for a variety of metal carbonyl complexes.

1.5 Photochemically induced reactivity

Photochemistry provides an alternative to the thermal methods of initiating chemical reactions for organometallic complexes. The absorption of photons of light by metal containing complexes leads to the promotion of an electron from the ground state to a level of higher energy; an excited state. The higher energy of the excited species often allows for complexes to undergo reaction by fulfilling the energy requirement to overcome the activation barrier to reaction. In addition, the promotion of an electron to an orbital of different symmetry can lead to structural changes between the excited species and the ground state species. These two factors enable complexes to react by alternative pathways, which would have been inaccessible via thermal reaction of the

ground state species. For organometallic complexes, this generally involves the dissociation of coordinated ligands, allowing complexes to isomerise or react further by ligand substitution or oxidative addition.^{55, 57}

Consequently one of the major benefits of photochemically induced reactions over thermal reactions is the relatively mild reaction conditions required. Thermal processes often require high temperature and pressure to initiate reactions, which may prove to be impractical. For example, the thermal substitution of one of the carbonyl ligands of CpMn(CO)_3 , with THF, requires high temperature. However, the same reaction has been demonstrated to proceed photochemically at room temperature.⁵⁷ The product, $\text{CpMn(CO)}_2\text{THF}$, has since been used as a precursor to the formation of many $\text{CpMn(CO)}_2\text{L}$ type complexes, owing to the labile nature of the coordinated THF, which can undergo ligand substitution thermally.¹⁴²⁻¹⁴⁵

1.5.1 Low temperature photochemistry

Conducting photochemical reactions at low temperature allows for the stabilisation of products which would not be observable for thermal reactions. For instance, the previously discussed thermal instability of η^2 C-H alkane complexes may be overcome by the use of low temperature matrices, to stabilise volatile photoproducts. Geftakis and Ball demonstrated this technique with the stabilisation and subsequent NMR characterisation of $\text{CpRe(CO)}_2(\text{cyclopentane})$.⁷⁸

Low temperature photolysis may also be employed to generate and stabilise 16 electron intermediates, which subsequently undergo coordination with a new incoming ligand to form a coordinatively saturated 18 electron complex. The net effect of this process is ligand exchange at the metal centre, which is useful in cases where complexes do not readily undergo ligand dissociation. Haddleton and Perutz demonstrated this with the photochemical generation of the 16 electron fragment, $[\text{CpRh(C}_2\text{H}_4)]$, from the parent complex, $\text{CpRh(C}_2\text{H}_4)_2$, in an argon / methane matrix at 12 K with $\lambda > 200$ nm.^{7, 146, 147} An analogous experiment in a CO matrix led to the mono-substitution of one of the ethene ligands for a CO ligand, to form the complex, $\text{CpRh(C}_2\text{H}_4)(\text{CO})$. This method has since been used further to form a range of novel and previously inaccessible CpRh complexes.

One challenge associated with the study of low temperature stabilised complexes, is the reliable identification of their structure, as the characterisation process of some techniques will likely lead to the decomposition of the more volatile species. In this case, NMR spectroscopy is generally used as the primary means of characterisation, owing to the ability to lower the temperature of the probe, in order to record spectral data. However, in some cases even the brief transfer process of the sample to the probe leads to the decomposition of the unstable species.

Geftakis and Ball first demonstrated that unstable species can be generated photochemically within an NMR probe, using a fibre optic cable to direct broad-band UV / visible light into the probe, and successfully irradiate the sample *in situ*. This technique has the added advantage of allowing NMR to be recorded during photolysis reactions, in order to monitor the formation of new species.^{78, 148, 149} At York, a similar fibre optic system has been developed, in addition to a He-Cd laser set-up,¹² which both allow for the UV irradiation of NMR samples *in situ*, while at low temperature. The operation of this equipment is discussed further in Chapter 7, section 7.3.

1.6 The role of NMR spectroscopy in organometallic chemistry

The use of NMR spectroscopy as a non-destructive technique has enabled the study of many air sensitive, thermally unstable or moisture sensitive organometallic complexes.^{150, 151} The following sections discuss several techniques employed in NMR spectroscopy to report reliable structural data.

1.6.1 NOE

NOE (Nuclear Overhauser Effect) experiments are commonly employed to investigate the through space interactions of ^1H nuclei, which are spatially close, yet do not display mutual coupling. This technique can provide further information about the geometry and ligand orientations for organometallic complexes. The effect occurs via relaxation through the dipole interactions of two close nuclei. The energy associated with one nucleus is transferred to the other, to a degree directly related to their mutual proximity.

¹⁵²

Figure 1.34 Relaxation pathways for a two spin system

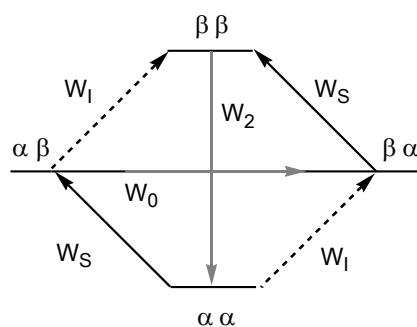
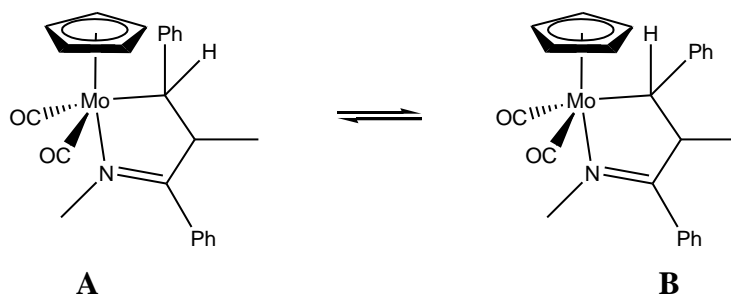


Figure 1.34, represents the energy levels for the two nuclei I and S, which display dipole-dipole interactions, yet lack any scalar couplings. If no NOE is present (i.e. a nucleus has not been saturated) the system will relax via spin lattice pathway (W_1 and W_S) and would lead to the observation of two singlets in a typical NMR experiment.

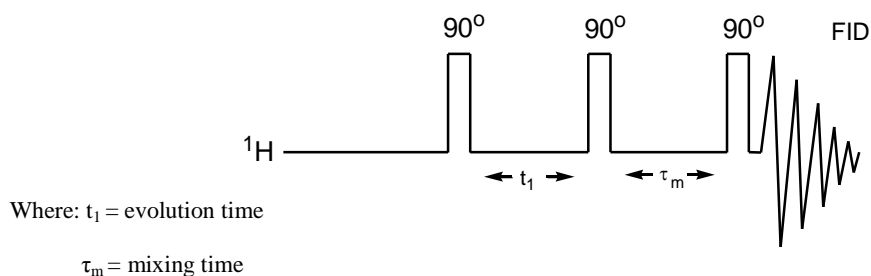
The initial step of an NOE measurement is the irradiation of one of the nuclei (in this case S, which corresponds to the W_S transition). This causes the equalisation (saturation) of the populations of the $\alpha\alpha$ and $\alpha\beta$ states, and also the $\beta\alpha$ and $\beta\beta$ states. The population difference is then restored through the cross relaxation pathways (W_0 and W_2). The resulting cross polarisation results in the transfer of magnetisation from the saturated spin to the dipole coupled spin.¹⁵³ For systems involving small molecule or non-viscous solutions, relaxation proceeds through the W_2 pathway, while large molecules and viscous solutions proceed via the W_0 pathway. The cross relaxation rate has been determined to be proportional to $1/r^6$, where 'r' represents the distance between nuclei.¹⁵⁴ This demonstrates dependence of the NOE interaction on the spatial distance between nuclei.

The technique has been widely used to differentiate between the resonances of two or more structural isomers. For example, Brunner et al used the technique to identify the orientations of the two isomers of $\text{CpMo}(\text{MeN}=\text{CPhNMeCHPh})(\text{CO})_2$ (Figure 1.35).¹⁵⁵ Isomer A was observed to demonstrate an NOE interaction between the Cp protons and the protons of the phenyl moiety. While for isomer B an interaction between the Cp protons and H was observed. However, no such interaction was found between the Cp protons and phenyl moiety protons.

Figure 1.35 The two isomers of $\text{CpMo}(\text{MeN}=\text{CPhNMeCHPh})(\text{CO})_2$ 

1.6.2 Dynamic NMR spectroscopy

NMR spectroscopy may be used to monitor environment changes seen by individual nuclei. Such changes may result as a consequence of chemical exchange within a complex, for example ligand rotation or isomerism.¹⁵⁶ Exchange spectroscopy (EXSY) experiments may be employed to monitor these changes, and determine the rates of interconversion / ligand rotation. The pulse sequences (Figure 1.36) of an EXSY and a 2D NOESY experiment are the same, and the two names are used to identify the application to which the pulse sequence is applied; EXSY for rotation / interconversion of resonances and NOESY for determining the extent of spatial interaction. A key component of EXSY experiments is magnetisation transfer associated with the interchange of position, which was first used by Forsen and Hoffman to describe the conformational flipping for [2,2]2,5-prolloparacyclophane.

Figure 1.36 Basic pulse sequence for EXSY / NOESY 2D NMR experiment¹⁵³

Magnetisation transfer is achieved by selective irradiation of an individual nucleus to establish a non-equilibrated Boltzmann distribution. Chemical exchanges transfer the magnetisation between the exchanging nuclei, consequently changing the intensity of their observed resonances. The rate of these processes can be determined using Equation 1.1.

$$\text{Equation 1.1} \quad k = \frac{1}{t_m} \ln \frac{I + 1}{I - 1}$$

k = rate constant
t_m = mixing time
I = integral ratio

Activation parameters may be found by applying Equation 1.2 (the Eyring equation), for rate constants obtained at varying temperatures. Details regarding the exchange mechanism can be elucidated from the values obtained for the activation parameters by comparison with similar values reported in the literature.

$$\text{Equation 1.2} \quad k = \frac{k_B T}{h} e^{-\Delta G^\ddagger / RT}$$

T = temperature
R = gas constant
k_B = Boltzmann constant
h = Planck's constant
ΔG[‡] = activation energy

The activation enthalpy (ΔH^\ddagger) of chemical exchange and activation entropy (ΔS^\ddagger) may be derived from a plot of $\ln(k/T)$ as a function of $1/T$, which relates to the activation energy (ΔG^\ddagger), as shown in Equation 1.3.

$$\text{Equation 1.3} \quad \Delta G^\ddagger = \Delta H^\ddagger - T\Delta S^\ddagger$$

ΔH[‡] = activation enthalpy
ΔS[‡] = activation entropy

1.7 Studies described in this thesis

This thesis reports on the thermal and photochemical activity of a series of cyclopentadienyl ruthenium complexes containing two electron phosphine and one electron Cl, Me and H ligands. The concept that was to be tested involved identifying whether this route could be used to generate reactive 16 electron fragments which upon binding an alkene could undergo transformations such as ligand migration. A related rhodium complex was prepared and studied with a view to identifying a new CH bond activation pathway. Advanced NMR spectroscopy methods including those facilitated by *in situ* photolysis are used as the primary means of complex characterisation.

Chapter 2 focuses on examining the thermal and photochemical reactions of $\text{CpRu}(\text{PPh}_3)_2\text{Cl}$ towards a range of different 2-electron donor substrates, and the characterisation of the subsequent products by NMR techniques. This chapter illustrates the concepts employed to characterise materials and follow the reactions described throughout the thesis.

Chapter 3 describes the thermal reactions of $\text{CpRu}(\text{PPh}_3)_2\text{Me}$ in addition to low temperature photolysis experiments carried out using an *in situ* setup. The reactivity of $\text{CpRu}(\text{PPh}_3)_2\text{Me}$ towards silanes is also considered. A range of highly unstable complexes are characterised and the complications associated with wide ranging CH bond activation identified.

Chapter 4 discusses an analogous study to that described for Chapter 2, for the complex $\text{CpRu}(\text{PPh}_3)_2\text{H}$, in which its reactivity towards substrates both thermally and photochemically is considered. This complex proved to be relatively inert under these conditions and hence surprisingly unsuitable as a reagent.

Chapter 5 contrasts the relative stability of the four complexes $\text{CpRu}(\text{PPh}_3)(\eta^3\text{-Si}(\text{Me}_2)\text{-CH=CH}_2)$, $\text{CpRu}(\text{PPh}_3)(\eta^3\text{-CH}_2\text{-CH=CH}_2)$, $\text{CpRu}(\text{PPh}_3)(\eta^3\text{-CH}_2\text{C}_6\text{H}_5)$, and $\text{CpRu}(\text{PPh}_3)_2(\text{CH}_2\text{C}_{10}\text{H}_7)$, which have ligands that have the capacity to bind to the ruthenium centre in either an η^1 or an η^3 mode. The thermal and photochemical reactivity of these complexes with substrates is explored. Additionally the

rearrangement from η^3 to η^1 complexes allows for the reaction of substrates with the metal centre without the liberation of phosphine.

Chapter 6 reports the photochemical reactions between $\text{CpRh}(\text{C}_2\text{H}_4)_2$ and amines (at low temperature) in order to form a complex capable of C-H activation of benzene and naphthalene. One of the key criteria was to find an amine labile enough to be selectively removed in favour of incoming ligands, yet still allow for C-H activation. Whilst a CH bond activation pathway was discovered, the stability of the resulting complex even at low temperature was very low due to the reversible nature of the reaction.

Chapter 7 details the experimental methods used in the previous chapters.

Chapter 2

Thermal and Photochemical Reactions of CpRu(PPh₃)₂Cl

2.1 Introduction

Since the complex, CpRu(PPh₃)₂Cl, was first reported by Wilkinson in 1969,¹⁵⁷ there has been much interest surrounding the reactivity of this complex with reagents. The thermal and air stability of this complex, in addition to the relative ease by which it may be synthesised,¹⁵⁸ affords the complex great potential towards catalysis. This complex has been widely studied over the past forty years, and the means by which neutral and anionic ligands may be exchanged at the ruthenium centre is well understood, allowing for this complex to be converted to other novel ruthenium half-sandwich complexes.¹⁵⁹⁻¹⁶⁴ This has led to the publication of studies which seek to address the chemical reactivity of CpRu(PPh₃)₂Cl in terms of its electronic structure.¹⁵⁹

More notably, CpRu(PPh₃)₂Cl has been shown to possess the scope for catalytic activity:

- Hydration of 1-alkynes to aldehydes^{165, 166}
- Isomerisation of allylic alcohols¹⁶⁷
- Heterocyclisation of aryl alkynols to benzoxepines¹⁶⁸

However, the photochemical activity of CpRu(PPh₃)₂Cl has been mainly overlooked, with the literature reporting on thermal reactions. Reports of UV / Vis spectroscopy data for this complex reveal major absorption peaks at 348 nm¹⁶⁹ in THF, and 355 nm in DCM.¹⁷⁰ This suggests that this complex could demonstrate photochemical reactivity upon UV irradiation. As discussed in the previous chapter, photochemistry allows for

access to alternative reaction pathways (by electron excitation and the subsequent change of the electronic structure), potentially leading to the formation of novel reaction products.^{171, 172}

2.2 Overview

In this chapter, the photochemical and thermal activity of the parent complex $\text{CpRu}(\text{PPh}_3)_2\text{Cl}$ is examined for a range of target substrates.

The sample preparation procedures and NMR techniques employed in the characterisation of these complexes will be discussed in greater depth in section 2.4.1. These techniques have been applied to the characterisation of all further complexes described in this thesis. Full characterisation tables for all of the complexes presented in this thesis are located at the end of each chapter. Each complex is numbered according to the order in which it appears in the whole volume. A list of abbreviations used in this work is presented on page 295.

2.3 Synthesis and characterisation of $\text{CpRu}(\text{PPh}_3)_2\text{Cl}$

2.3.1 Synthesis of $\text{CpRu}(\text{PPh}_3)_2\text{Cl}$

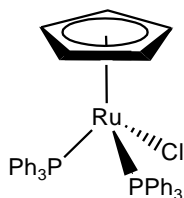
$\text{CpRu}(\text{PPh}_3)_2\text{Cl}$ was prepared according to a known literature method,¹⁵⁸ by heating cyclopentadiene with PPh_3 and $\text{RuCl}_3 \cdot n\text{H}_2\text{O}$ in ethanol (under N_2 , a reflux). The complex was isolated as an orange solid in 96% yield. Full experimental details for this preparation are described in Chapter 7.

2.3.2 NMR characterisation of $\text{CpRu}(\text{PPh}_3)_2\text{Cl}$

The $^3\text{1P}\{^1\text{H}\}$ NMR spectrum of $\text{CpRu}(\text{PPh}_3)_2\text{Cl}$ contains a single peak at δ 39.6, which was demonstrated to couple, via a $^1\text{H}/^3\text{1P}$ HMQC experiment, to proton signals at δ 7.74, 7.16 and 7.02. These three signals show mutual couplings, and are typical of the *ortho*, *meta* and *para* protons of an aryl moiety of a metal-bound PPh_3 ligand. They have intensity 12:12:6, relative to the Cp ^1H signal intensity of 5. The $^1\text{H}/^3\text{1P}$ HMQC

experiment also shows a coupling between the ^{31}P resonance at δ 39.6 and a signal at δ 4.27, which is consistent with a coordinated Cp ring. Based on these peaks, and comparison with literature values, the identity of the prepared complex is confirmed as $\text{CpRu}(\text{PPh}_3)_2\text{Cl}$ (Figure 1.2). Full NMR data for this complex is listed in table 2.1

Figure 2.1 Structure of $\text{CpRu}(\text{PPh}_3)_2\text{Cl}$



Figures 2.2 and 2.3 show the corresponding ^1H NMR and $^{31}\text{P}\{^1\text{H}\}$ NMR spectra (respectively) of $\text{CpRu}(\text{PPh}_3)_2\text{Cl}$ in d_6 -benzene, and serve to confirm the NMR purity of the synthesised complex.

Figure 2.2 ^{31}P NMR spectrum of $\text{CpRu}(\text{PPh}_3)_2\text{Cl}$ in d_6 -benzene

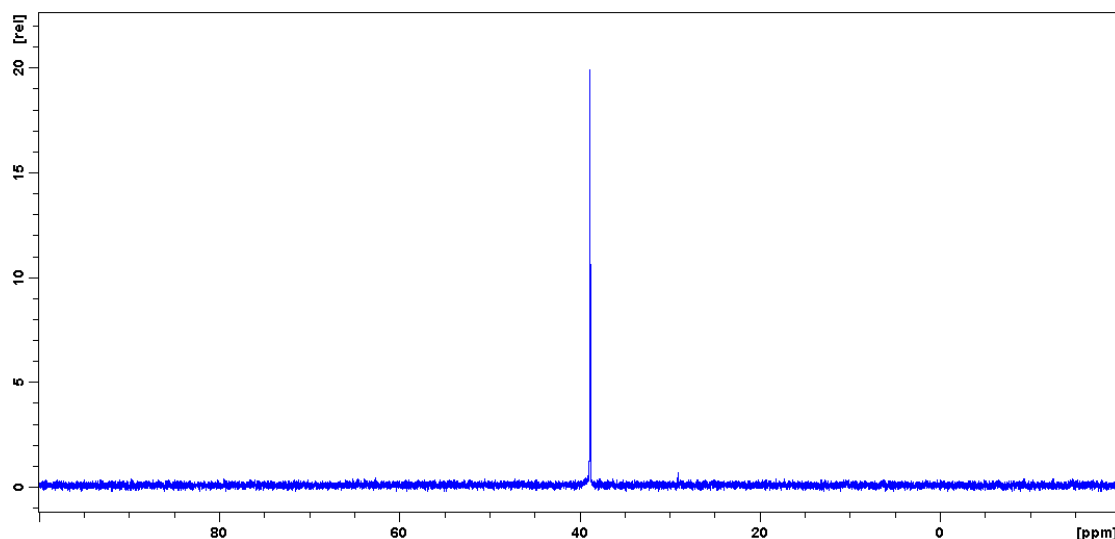
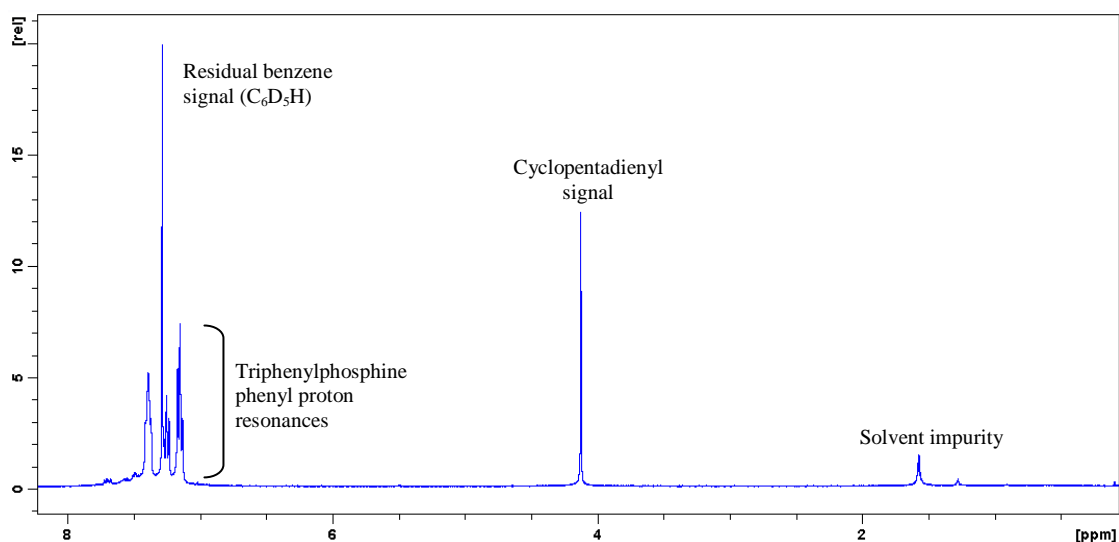
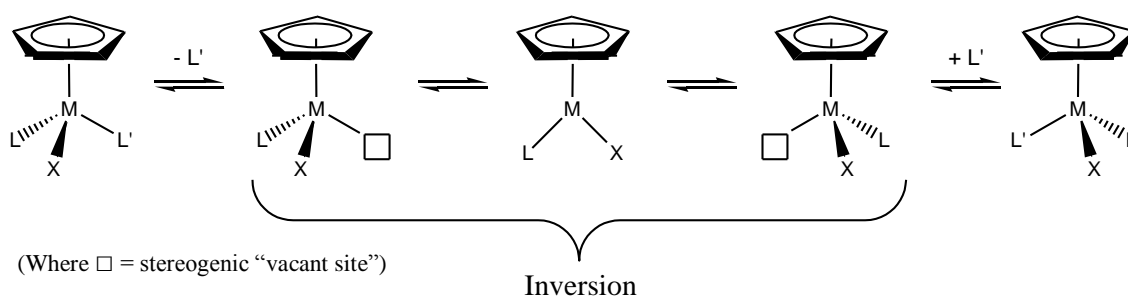


Figure 2.3 ^1H NMR spectrum of $\text{CpRu}(\text{PPh}_3)_2\text{Cl}$ in d_6 -benzene

$\text{CpRu}(\text{PPh}_3)_2\text{Cl}$ is pro-chiral about the ruthenium centre. Previous computational and experimental procedures on similar cyclopentadienyl iron complexes have determined that the liberation of a ligand (e.g. phosphine) yields a chiral and coordinatively unsaturated intermediate.^{173, 174} Figure 2.4 shows a generalised depiction of the interconversion between the two chiral forms of this intermediate, through inversion of the unsaturated pyramid, about the metal centre. A similar mechanism has been suggested to apply to interconversion of the enantiomers of $\text{CpRu}(\text{Prophos})\text{Cl}$ (where $\text{Prophos} = \text{PPh}_2\text{CH}(\text{CH}_3)\text{CH}_2\text{PPh}_2$), following the cleavage of the $\text{Ru}-\text{Cl}$ bond.¹⁷⁵

Figure 2.4 Interconversion of chiral structures, about the metal centre, via coordinatively unsaturated pyramidal intermediates



2.4 Thermal and photochemical reactions of $\text{CpRu}(\text{PPh}_3)_2\text{Cl}$ with substrates

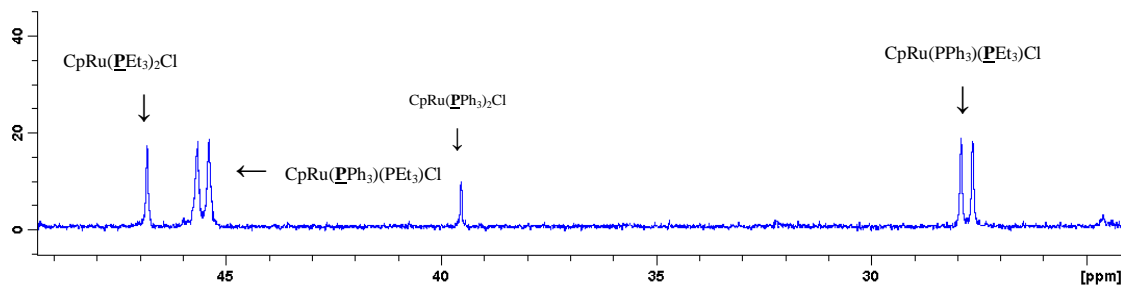
2.4.1 Reactions of $\text{CpRu}(\text{PPh}_3)_2\text{Cl}$ with PEt_3

2.4.1.1 Thermally initiated reaction of $\text{CpRu}(\text{PPh}_3)_2\text{Cl}$ with PEt_3

An NMR tube fitted with a J. Young's tap (henceforth abbreviated as J-Y NMR tube) was charged with $\text{CpRu}(\text{PPh}_3)_2\text{Cl}$ and dissolved in d_6 -benzene, to a depth of 4 cm, followed by the addition of PEt_3 to the sample. ^1H and $^{31}\text{P}\{^1\text{H}\}$ NMR spectra were recorded for the sample to demonstrate that no initial reaction had taken place when compared with the subsequently recorded NMR spectra. The sample tube was then heated to 323 K in a silicone oil bath for a period of 24 hours.

Subsequent ^1H and $^{31}\text{P}\{^1\text{H}\}$ NMR spectra indicated the presence of new products. The $^{31}\text{P}\{^1\text{H}\}$ NMR spectrum revealed the presence of four new peaks at δ 46.8, 45.5, 27.8 and -6.4 in addition to the ^{31}P resonance for the phosphine of $\text{CpRu}(\text{PPh}_3)_2\text{Cl}$ (in a ratio of 3:6:6:2 respectively). The signal at δ -6.4 appears as a singlet and is typical of the resonance expected for liberated PPh_3 . The two signals at δ 45.5 and 27.8 appear as doublets with common coupling values of 44 Hz. This implies that the phosphorus atoms of the corresponding resonances are bound to the same metal centre, resulting in the observed mutual splitting. Additionally, this splitting would arise only for ^{31}P nuclei of different magnetic environments, e.g. for the two phosphines PPh_3 and PEt_3 , which suggests these signals may be from the mono-substituted complex, $\text{CpRu}(\text{PPh}_3)(\text{PEt}_3)\text{Cl}$. An alternative explanation for the splitting pattern of the two signals would be that they belong to a cyclometallated complex, as described in Chapter 1. The remaining signal at δ 46.8 is also consistent with signals observed for phosphine bound metal complexes, suggesting that this is likely to be due to a bis-substituted complex.

Figure 2.5 $^{31}\text{P}\{^1\text{H}\}$ NMR spectrum obtained after the thermal reaction of $\text{CpRu}(\text{PPh}_3)_2\text{Cl}$ with PEt_3 at 323 K, after irradiation had proceeded for 24 hours



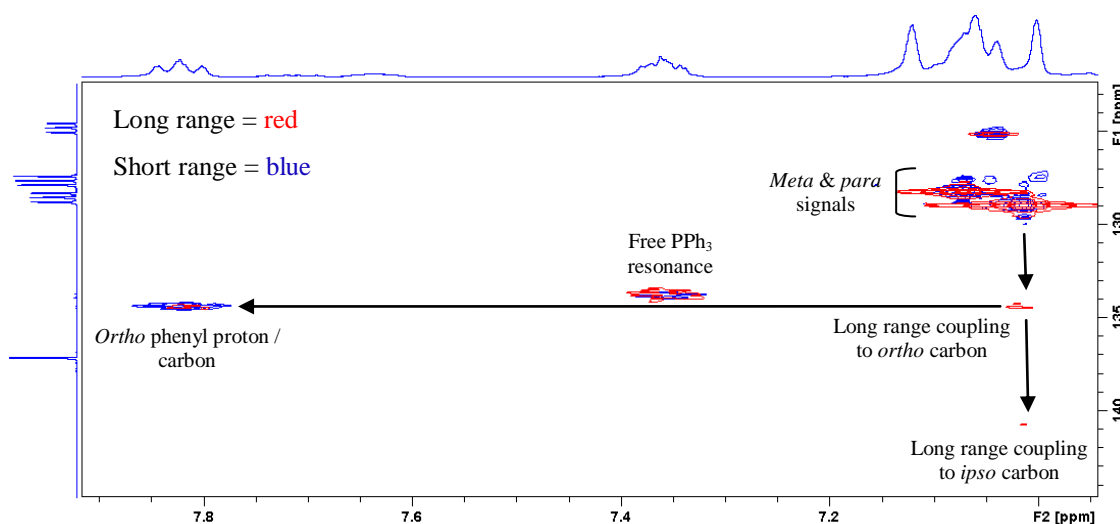
Comparison of a number of ^1H NMR spectra recorded to monitor this reaction revealed the presence of a number of new peaks, in particular two singlets at δ 4.17 and 4.21. These two peaks fall within the ^1H region δ 4 - 5 which is commonly referred to as the ‘Cp region’; the proton resonances for metal coordinated cyclopentadienyl ligands appear in this area of the ^1H NMR spectrum. This is useful, as this region can be used to estimate the number of products formed in these reactions, or indeed to determine whether a reaction has occurred, by simple comparison of the starting ^1H NMR spectrum with those recorded subsequently. The lack of any hydride resonances (signals between δ 0 and -30) suggests that a C-H activated product has not been formed in this reaction.

A $^1\text{H}/^{31}\text{P}$ HMQC experiment was employed to demonstrate the connectivity between these proton resonances to their respective, coupled, phosphorus atoms, in order to identify the complexes. The ^{31}P doublet resonance at δ 45.5 was observed to couple to three ^1H signals at δ 7.82, 7.08, 7.02, which are in the region consistent with the proton resonances associated with those of an aryl group. This confirms the signal at δ 45.5, is from a PPh_3 ligand, owing to its close association with the aryl protons. Coupling is also demonstrated from this ^{31}P signal to a ^1H signal at δ 4.21, which is suggested to be the metal-bound Cp proton resonance. This ^1H signal also couples to the doublet at 27.8, confirming that both of these ^{31}P signals correspond to phosphorus atoms in the same complex. Such strong coupling between the ^{31}P resonances, demonstrated by their mutual *cis* coupling, is typical of metal-bound phosphorus atoms, such as those found in phosphine complexes. Additionally, the ^{31}P signal at δ 27.8 couples to signals at δ 0.92,

1.15, and 1.83, which correspond to the expected proton resonances for the ethyl group of PEt_3 . A *trans* P-P coupling would be much larger, in the order of 200-300 Hz.^{176, 177} Integration of the three ^1H peaks at δ 0.92, 1.15, and 1.83 determined a ratio of 3:1:1, respectively. This ratio directly correlates to the number of protons responsible for the generation of the ^1H NMR signal (this applies only to protons within the same complex). It can therefore be determined that the signal at δ 0.92 is the CH_3 portion of the ethyl chain, while the signals at δ 1.15 and 1.83 correspond to the inequivalent protons of the phosphorus bound CH_2 group. This is confirmed by the existence of mutual couplings between these three proton resonances by ^1H COSY. The identity of the Cp resonance at δ 4.21 may also be confirmed, owing to the relative integration of this peak compared with those of the ethyl moiety, 5:3:3:9. Integration of the aryl proton signals for the PPh_3 ligands was not possible, owing to the overlap of the resonances for these protons.

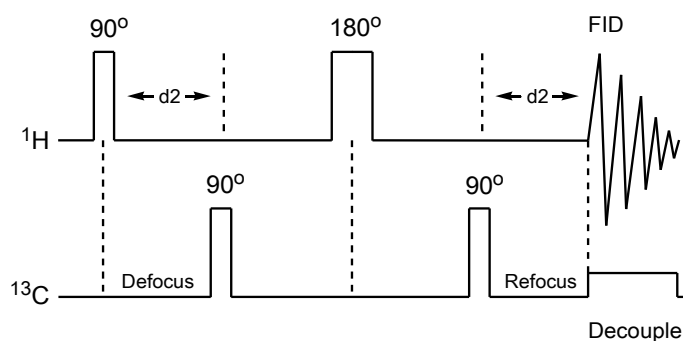
The ^{13}C signals within these products were located by exploiting coupling between protons and carbon using a $^1\text{H}/^{13}\text{C}$ HMQC experiment. The two proton signals at δ 1.15 and 1.83 were further confirmed as inequivalent protons owing to their mutual coupling to the same ^{13}C resonance at δ 19.9. Figure 2.6 shows two overlaid $^1\text{H}/^{13}\text{C}$ HMQC spectra recorded with different delay values. The $^1\text{H}/^{13}\text{C}$ HMQC experiment therefore proved to be a useful diagnostic tool in the identification of the aryl protons of PPh_3 .

Figure 2.6 Overlaid short and long range $^1\text{H}/^{13}\text{C}$ HMQC NMR spectra which depict the signals of the phenyl protons and carbons of the triphenylphosphine ligand (original appears in colour)



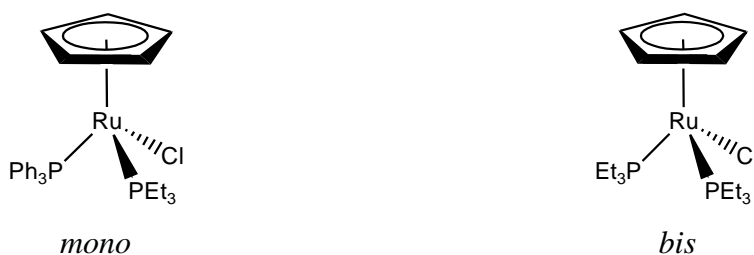
These delays allow for couplings of different magnitudes to be observed e.g. long / short range couplings. Figure 2.7 shows a basic HMQC NMR pulse sequence where the delay (d_2) is used in the defocusing and refocusing phases. This delay is related to the C-H coupling by the relationship $d_2 = 1/(2 \cdot \text{CNST}^2)$, where CNST2 is the value of the coupling in Hertz. The spectra shown in Figure 2.6 used CNST2 values of 5 and 145 Hz for collection, respectively. The same method was applied to the $^1\text{H}/^{31}\text{P}$ HMQC NMR experiments, where the majority of the protons coupling to the ^{31}P spin could be found using an experiment with a CNST2 value of 24 Hz. However, to locate corresponding ^1H Cp signal, CNST2 values between 2-5 Hz were more commonly employed.

Figure 2.7 Depiction of a basic $^1\text{H}/^{13}\text{C}$ HMQC NMR pulse sequence ¹⁷⁸



Based on these data, the complex that has been produced is readily identified as $\text{CpRu}(\text{PPh}_3)(\text{PEt}_3)\text{Cl}$ (Figure 2.8). The same method was employed to determine the identity of the fully substituted derivative, $\text{CpRu}(\text{PEt}_3)_2\text{Cl}$, which provides the previously mentioned ^{31}P signal at δ 46.8. The Cp protons were identified using $^1\text{H}/^{31}\text{P}$ HMQC data as the resonance at δ 4.17. Further connections from the proton signals at δ 0.91, 1.16 and 1.21 signals were made to this ^{31}P signal which, as discussed for the previous complex, corresponds to the ethyl protons of the PEt_3 ligand.

Figure 2.8 Depiction of the mono and bis-substituted phosphine complexes,
 $\text{CpRu}(\text{PPh}_3)(\text{PEt}_3)\text{Cl}$ and $\text{CpRu}(\text{PEt}_3)_2\text{Cl}$



Heating this sample to 353 K for a further 24 hours favoured the formation of the bis-substituted product. This bis- PEt_3 complex, $\text{CpRu}(\text{PEt}_3)_2\text{Cl}$, has been previously reported to be produced by the thermal reaction of $\text{CpRu}(\text{PPh}_3)_2\text{Cl}$ with PEt_3 in toluene.¹⁷⁹ This report made no mention of the existence of a mono-substituted product. The NMR data for $\text{CpRu}(\text{PPh}_3)(\text{PEt}_3)\text{Cl}$ and $\text{CpRu}(\text{PEt}_3)_2\text{Cl}$ are listed in Table 2.2 and 2.3.

2.4.1.2 Photochemical reaction of $\text{CpRu}(\text{PPh}_3)_2\text{Cl}$ with PEt_3

A sample of $\text{CpRu}(\text{PPh}_3)_2\text{Cl}$ was prepared in d_6 -benzene, as outlined for the previous thermal reaction. The sample was photolysed at room temperature using the *ex situ* photolysis set-up as a UV irradiation source (diagrams and further explanation of this photolysis method is detailed in Chapter 7). Irradiation was maintained for 18 hours, with frequent ^1H and $^{31}\text{P}\{^1\text{H}\}$ spectra being recorded to monitor the progress of the reaction. Comparison of these $^{31}\text{P}\{^1\text{H}\}$ NMR spectra reveal peaks consistent with those found previously for the mono and bis-substituted complexes, $\text{CpRu}(\text{PPh}_3)(\text{PEt}_3)\text{Cl}$ and $\text{CpRu}(\text{PEt}_3)_2\text{Cl}$.

In contrast, when a sample of $\text{CpRu}(\text{PPh}_3)_2\text{Cl}$ in d_8 -toluene with a 7 fold excess of PEt_3 , was irradiated using the *ex situ* photolysis setup (Chapter 7) at 198 K, only the mono substituted product, $\text{CpRu}(\text{PPh}_3)(\text{PEt}_3)\text{Cl}$ was formed. After 18 hours of UV irradiation at low temperature, the sample was checked by ^1H and $^{31}\text{P}\{^1\text{H}\}$ NMR, to confirm that full conversion to $\text{CpRu}(\text{PPh}_3)(\text{PEt}_3)\text{Cl}$ had been achieved. The sample was washed using ethanol to remove the excess PEt_3 and liberated PPh_3 . The sample was re-dissolved in d_8 -toluene, and an excess of PMe_3 (5 fold excess) was added. The sample was photolysed using the *in situ* NMR set-up (cooled to 233 K), and the products monitored by NMR.

^1H and ^{31}P NMR spectra revealed no change in either of the NMR spectra compared with those for $\text{CpRu}(\text{PPh}_3)(\text{PEt}_3)\text{Cl}$. This would indicate that the complex $\text{CpRu}(\text{PPh}_3)(\text{PEt}_3)\text{Cl}$ is not photosensitive under these conditions. It can therefore be concluded that the thermal effects produced by photolysis are responsible for the formation of $\text{CpRu}(\text{PEt}_3)_2\text{Cl}$ in the room temperature experiment. It should be noted that when $\text{CpRu}(\text{PPh}_3)(\text{PEt}_3)\text{Cl}$ is warmed with PMe_3 , $\text{CpRu}(\text{PMe}_3)_2\text{Cl}$ is formed. ^{163}MS revealed peaks consistent with m/z $\text{M}^+ = 438$ and $[\text{M}^+ - \text{PEt}_3] = 320$, for this complex, confirming the formation of the bis- PEt_3 product.

This provides information regarding the possible products which can be formed when using CO or $^t\text{BuNC}$ as potential ligands (which are discussed in turn in the following

sections). Based on this experiment, mono substituted product would be expected in each of these cases, with bis-substitution being unlikely.

2.4.2 Reactions of $\text{CpRu}(\text{PPh}_3)_2\text{Cl}$ with CO

2.4.2.1 Thermally initiated reaction of $\text{CpRu}(\text{PPh}_3)_2\text{Cl}$ with CO

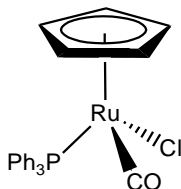
A J-Y NMR tube was charged with $\text{CpRu}(\text{PPh}_3)_2\text{Cl}$ in d_6 -benzene. The tube was degassed and pressurised with 1.5 bar CO. ^1H and $^{31}\text{P}\{^1\text{H}\}$ NMR spectra were recorded for the sample to demonstrate that no initial reaction had taken place when compared with the subsequently recorded NMR spectra. The sample was heated to 323 K for 24 hours to enable the complex to react thermally with the substrate.

Comparison of the ^{31}P spectra showed the presence of a single new product resonance, δ 49.1, and a resonance consistent with liberated PPh_3 , which demonstrates that mono phosphine substitution has taken place. A connection was made through the ^{31}P signal to a new resonance at δ 4.49 in the ^1H NMR spectrum, which is consistent with the protons of a Cp ring. The ^{31}P signal at 49.1 also connected to signals at δ 7.68, 7.05 and 6.99, which are again consistent with aryl protons, indicating that PPh_3 ligand is coordinated to the complex.

This left one coordination site unaccounted for owing to the liberation of one of the PPh_3 ligands. In order to determine whether this site was occupied by a CO ligand, a ^{13}C NMR spectrum was recorded. This spectrum was compared to the spectrum recorded previously for $\text{CpRu}(\text{PPh}_3)_2\text{Cl}$, to identify new product peaks. New peaks at δ 85.7, 133.7, 127.9, 129.8 and 201.3 were found and identified, using $^1\text{H}/^{13}\text{C}$ HMQC and ^1H COSY experiments, as resonances belonging to the Cp, and the *ipso*, *ortho*, *meta* and *para* carbons of the coordinated PPh_3 ligand. A doublet resonance was therefore left unaccounted for at δ 201.3 (22.9 Hz), which is the region typically associated with resonances belonging to metal-bound CO ligands.

This suggests that the complex is the mono-substituted carbonyl derivative, $\text{CpRu}(\text{PPh}_3)(\text{CO})\text{Cl}$, and as suggested by the literature¹⁶⁰ this complex does not undergo further substitution to the bis-carbonyl complex, $\text{CpRu}(\text{CO})_2\text{Cl}$.

Figure 2.9 Illustration of the mono carbonyl substituted product $\text{CpRu}(\text{CO})_2\text{Cl}$



The lack of a second singlet in the Cp region of the ^1H NMR spectrum or a singlet resonance $\delta \sim 200$ in the ^{13}C NMR spectrum, shows that the fully substituted CO complex, $\text{CpRu}(\text{CO})_2\text{Cl}$ has not been formed. Further confirmation of the identity of this structure was provided by comparison of the IR and MS values recorded for this complex, with those reported previously in the literature: MS, (calculated weight 491.91) m/z M^+ 492,¹⁸⁰ and IR, ν_{CO} 1961 cm^{-1} .^{181, 182} Full NMR data are reported in Table 2.4.

2.4.2.2 Photochemical reaction of $\text{CpRu}(\text{PPh}_3)_2\text{Cl}$ with CO

An NMR tube was charged with 5 mg of $\text{CpRu}(\text{PPh}_3)_2\text{Cl}$ in d_6 -benzene. The tube was degassed and pressurised with 1.5 bar CO. ^1H and $^{31}\text{P}\{^1\text{H}\}$ NMR spectra were recorded for the sample to demonstrate a reaction had taken place when compared with subsequently recorded NMR spectra.

The sample was first irradiated for 2 hours at room temperature using the broadband UV Lamp set-up. The respective ^1H and $^{31}\text{P}\{^1\text{H}\}$ NMR spectra showed resonances consistent with those reported previously for $\text{CpRu}(\text{PPh}_3)(\text{CO})\text{Cl}$ and $\text{CpRu}(\text{PPh}_3)_2\text{Cl}$ in the ratio of 5:2. No evidence for a bis-substituted carbonyl or carbonyl insertion product was observed in these NMR spectra.

Further irradiation of this sample, after CO replenishment, for 18 hours afforded no additional products. At this point these NMR spectra were consistent with the complete conversion of $\text{CpRu}(\text{PPh}_3)_2\text{Cl}$ to $\text{CpRu}(\text{PPh}_3)(\text{CO})\text{Cl}$. This reaction therefore appears to stop thermally and photochemically at the mono-substitution stage.

2.4.3 Reactions of $\text{CpRu}(\text{PPh}_3)_2\text{Cl}$ with ${}^t\text{BuNC}$

2.4.3.1 Thermally initiated reaction of $\text{CpRu}(\text{PPh}_3)_2\text{Cl}$ with ${}^t\text{BuNC}$

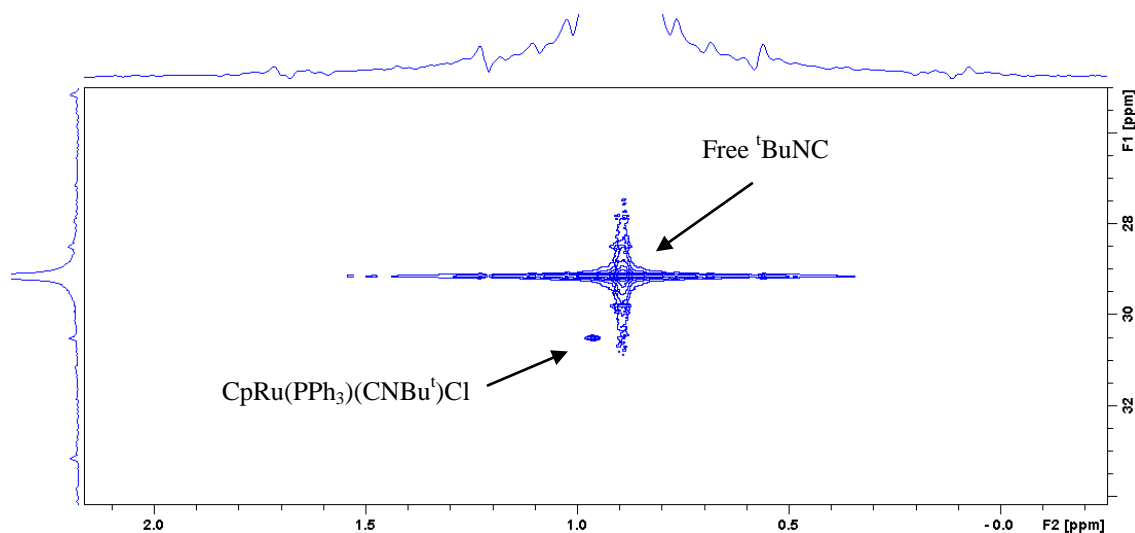
A J-Y NMR tube was charged with $\text{CpRu}(\text{PPh}_3)_2\text{Cl}$ in d_6 -benzene. The tube was degassed and ${}^t\text{BuNC}$ was added. ${}^1\text{H}$ and ${}^{31}\text{P}\{{}^1\text{H}\}$ NMR spectra were recorded for the sample to demonstrate that no initial reaction had taken place when compared with the subsequently recorded NMR spectra. The sample was heated to 323 K for 24 hours to enable the complex to react thermally with the substrate.

Comparison of the ${}^{31}\text{P}$ spectra shows the presence of two new resonances at δ -6.4 and 52.4, indicating the formation of new products. The emergence of a signal at δ -6.4 demonstrates that PPh_3 has been liberated from the parent complex, allowing the coordination of ${}^t\text{BuNC}$ to the metal centre. As for the previous reaction with CO, reactions with ${}^t\text{BuNC}$ may possibly undergo insertion into other bonds. For the peak at δ 52.4, a ${}^1\text{H}/{}^{31}\text{P}$ HMQC was used to observe the further connection to a resonance at δ 4.52 in the ${}^1\text{H}$ NMR spectrum, which is consistent with the protons of a Cp ring. The ${}^{31}\text{P}$ signal also connected to signals at δ 7.81, 7.08 and 7.01, which are again consistent with those of aryl protons, thereby indicating that PPh_3 is coordinated to the complex.

The presence of a bound ${}^t\text{BuNC}$ ligand was confirmed through the identification of a new singlet peak at δ 0.96 in the ${}^1\text{H}/{}^{13}\text{C}$ HMQC spectrum, which almost overlaps with the signal for free ${}^t\text{BuNC}$ (Figure 2.10). This singlet corresponds to the equivalent protons of the tertiary butyl moiety, for the bound ligand. Removing the excess ${}^t\text{BuNC}$ *in vacuo* allowed for the integration of the Cp and methyl protons in the complex, which were found to appear in a ratio of 5:9, thereby indicating that the ${}^t\text{BuNC}$ ligand is bound

to the ruthenium centre. These assignments agree with those described in the literature.¹⁸³ Furthermore, only mono-substitution is again observed.

Figure 2.10 $^1\text{H}/^{13}\text{C}$ HMQC spectrum showing the tertiary carbons for the free $^t\text{BuNC}$, and that of the complex, $\text{CpRu}(\text{PPh}_3)(\text{CNBu}^t)\text{Cl}$



2.4.3.2 Photochemical reaction of $\text{CpRu}(\text{PPh}_3)_2\text{Cl}$ with $^t\text{BuNC}$

Bruce and Wallis previously reported the apparent formation of the bis-substituted complex, $\text{CpRu}(\text{CNBu}^t)_2\text{Cl}$, by heating $\text{CpRu}(\text{PPh}_3)_2\text{Cl}$ to 453 K in an excess of $^t\text{BuNC}$.¹⁸³ The complex was reported as an unstable white solid, and minimal characterisation was provided, consisting of two ^1H NMR signals at δ 1.10 and 4.73. These resonances mutually integrated to a ratio of 18:5, and were consequently assigned to the methyl $^t\text{Butyl}$ and Cp protons, respectively. A review paper, written by Albers *et al.*, expressed uncertainty over this assignment based on the dissimilarity of the properties of Bruce's $\text{CpRu}(\text{CNBu}^t)_2\text{Cl}$, compared with those of other reported isonitrile complexes.¹⁸⁴ A similar Cp^* derivative has previously been reported in the literature, formed from the displacement of the 2,5-norbornadiene ligand from $\text{Cp}^*\text{Ru}(\eta^4\text{-2,5-norbornadiene})\text{Cl}$ by $^t\text{BuNC}$.¹⁸⁵

A J-Y NMR tube was charged with $\text{CpRu}(\text{PPh}_3)_2\text{Cl}$ in d_6 -benzene. The tube was degassed and $^t\text{BuNC}$ was added. The sample was irradiated for 2 hours at room

temperature using the broadband UV Lamp set-up. ^1H and $^{31}\text{P}\{^1\text{H}\}$ NMR spectra were recorded for the sample to demonstrate that a reaction had taken place when compared with subsequently recorded NMR spectra.

As for the case of the thermal reactions, photochemical irradiation of the sample led only to the formation of the mono-substituted product, $\text{CpRu}(\text{PPh}_3)(\text{CNBu}^t)\text{Cl}$, as shown in the ^1H and $^{31}\text{P}\{^1\text{H}\}$ NMR spectra. The ^1H peaks at δ 0.96, 4.52, 7.81 and a ^{31}P peak at δ 52.4 agree with the previous characterisation. Further photochemical irradiation of the sample for 18 hours only led to the increased conversion of $\text{CpRu}(\text{PPh}_3)_2\text{Cl}$ to $\text{CpRu}(\text{PPh}_3)(\text{CNBu}^t)\text{Cl}$, to the ratio of 5:6, as determined by integration of the ^1H NMR Cp proton resonances for each complex. No observation of a second cyclopentadienyl resonance belonging to $\text{CpRu}(\text{CNBu}^t)_2\text{Cl}$ (Figure 2.11) could be found. Full NMR data for this complex appear in Table 2.5.

The following section describes the method employed here to synthesise $\text{CpRu}(\text{CNBu}^t)_2\text{Cl}$ (Figure 2.11), and attain full characterisation of the complex by NMR.

Figure 2.11 Depiction of the mono and bis-substituted isocyanide complexes, $\text{CpRu}(\text{PPh}_3)(\text{CNBu}^t)\text{Cl}$ and $\text{CpRu}(\text{CNBu}^t)_2\text{Cl}$



2.4.3.3 Synthesis of $\text{CpRu}(\text{CNBu}^t)_2\text{Cl}$

A modified preparation of the one used to form $\text{CpRu}(\text{PPh}_3)_2\text{Cl}$ was used to form a bulk quantity of $\text{CpRu}(\text{CNBu}^t)_2\text{Cl}$. An excess of $^t\text{BuNC}$ was added to a refluxing mixture of ruthenium trichloride and cyclopentadiene in ethanol, which led to the formation of a light yellow solution following a day of stirring and heating.

Two singlet peaks were evident in the ^1H NMR spectrum at δ 4.85 and 0.92, in a ratio of 5:18. This ratio of peak intensities shows that there are two $^t\text{BuNC}$ ligands bound to the ruthenium centre. It should be noted that these resonances appear in a different position to those reported by Bruce.¹⁸³ The complete NMR characterisation for the complex $\text{CpRu}(\text{CNBu}^t)_2\text{Cl}$ is listed in Table 2.6. MS was also employed to confirm this assignment: (m/z) M^+ , 368 and $\text{M}^+ - ^t\text{BuNC}$, 285.

2.4.4 Reactions of $\text{CpRu}(\text{PPh}_3)_2\text{Cl}$ with HSiEt_3

2.4.4.1 Thermally initiated reaction of $\text{CpRu}(\text{PPh}_3)_2\text{Cl}$ with HSiEt_3

A J-Y NMR tube was charged with $\text{CpRu}(\text{PPh}_3)_2\text{Cl}$ in d_6 -benzene. The tube was degassed and HSiEt_3 was added. ^1H and $^{31}\text{P}\{^1\text{H}\}$ NMR spectra were recorded for the sample to demonstrate whether a reaction had taken place when compared with subsequently recorded spectra. The sample was heated to 323 K for 24 hours to enable the complex to react thermally with the substrate. No evidence of reaction was observed in these ^1H and $^{31}\text{P}\{^1\text{H}\}$ NMR spectra, which only indicated resonances belonging to the protons of $\text{CpRu}(\text{PPh}_3)_2\text{Cl}$. The sample was heated further to 353 K for 24 hours. No reaction was again evident.

2.4.4.2 Photochemical reaction of $\text{CpRu}(\text{PPh}_3)_2\text{Cl}$ with HSiEt_3

A J-Y NMR tube was charged with $\text{CpRu}(\text{PPh}_3)_2\text{Cl}$ in d_6 -benzene. The tube was degassed and HSiEt_3 was added. The sample was irradiated for 12 hours at room temperature using the broadband UV Lamp set-up.

Comparison of the 1D ^1H and $^{31}\text{P}\{^1\text{H}\}$ NMR spectra recorded for $\text{CpRu}(\text{PPh}_3)_2\text{Cl}$ with the spectra recorded for the present sample indicated no sign of reaction. As mentioned in Chapter 1, exchange of the chloride moiety is achieved readily in polar solvents,^{186, 187} this may possibly form HCl or chloride salts as a by-product of producing $\text{CpRu}(\text{PPh}_3)_2\text{SiEt}_3$. The reaction was subsequently repeated using acetone as a reaction solvent, in which the compound was observed to have modest solubility. Again, no reaction was evident by comparison of the NMR spectra, which is likely to be caused due to $\text{CpRu}(\text{PPh}_3)_2\text{Cl}$ displaying non-electrolytic behaviour in acetone.¹⁸⁸ However, previous research has noted the ionic character of $\text{CpRu}(\text{PPh}_3)_2\text{Cl}$ in methanol.^{189, 190}

A sample was prepared using methanol, but $\text{CpRu}(\text{PPh}_3)_2\text{Cl}$ proved to be only slightly soluble in methanol. Consequently, the sample was heated to encourage solubility, and therefore only a thermal reaction was attempted. As found previously, activation of silane by the ruthenium centre of $\text{CpRu}(\text{PPh}_3)_2\text{Cl}$ was not achieved under these conditions.

Investigation of the hydride region revealed no sign of resonances for $\text{CpRu}(\text{PPh}_3)_2\text{H}$ (characterised in Chapters 3 and 4), which could be potentially formed owing to the reductive elimination of Cl-SiEt_3 . This would be favoured owing to the increased bond strength of Si-Cl over Si-H ;¹⁹¹ this process is a known synthetic route for the production of chlorosilanes.¹⁹²

2.4.5 Reactions of $\text{CpRu}(\text{PPh}_3)_2\text{Cl}$ with H_2

2.4.5.1 Thermally initiated reaction of $\text{CpRu}(\text{PPh}_3)_2\text{Cl}$ with H_2

A J-Y NMR tube was charged with $\text{CpRu}(\text{PPh}_3)_2\text{Cl}$ in d_6 -benzene. The tube was degassed and pressurised with 1.5 bar of H_2 . ^1H and $^{31}\text{P}\{^1\text{H}\}$ NMR spectra were recorded for the sample to demonstrate a reaction had taken place when compared with subsequently recorded spectra. The sample was heated to 323 K for 24 hours to enable the complex to react thermally with the substrate.

As previously found for the reaction of $\text{CpRu}(\text{PPh}_3)_2\text{Cl}$ with HSiEt_3 , no reaction of H_2 and $\text{CpRu}(\text{PPh}_3)_2\text{Cl}$ was evident under thermal conditions, therefore photochemical methods were considered.

2.4.5.2 Photochemical reaction of $\text{CpRu}(\text{PPh}_3)_2\text{Cl}$ with H_2

An NMR tube was charged with $\text{CpRu}(\text{PPh}_3)_2\text{Cl}$ in d_6 -benzene. The tube was degassed and pressurised with 1.5 bar of H_2 . ^1H and $^{31}\text{P}\{^1\text{H}\}$ NMR spectra were recorded for the sample to demonstrate that no initial reaction had taken place when compared with the subsequently recorded NMR spectra. The sample was irradiated for 12 hours at room temperature using the broadband UV Lamp set-up. Similarly to the previous photochemical reaction of $\text{CpRu}(\text{PPh}_3)_2\text{Cl}$ with HSiEt_3 , no reaction was evident with H_2 . Analogous samples were prepared using acetone and methanol, but still no reaction was observed, by comparison of the NMR spectra.

2.4.6 Reactions of $\text{CpRu}(\text{PPh}_3)_2\text{Cl}$ with ethene

2.4.6.1 Thermally initiated reaction of $\text{CpRu}(\text{PPh}_3)_2\text{Cl}$ with ethene

An NMR tube was charged with $\text{CpRu}(\text{PPh}_3)_2\text{Cl}$ in d_6 -benzene. The tube was degassed and pressurised with 1.5 bar of ethene. ^1H and $^{31}\text{P}\{^1\text{H}\}$ NMR spectra were recorded for the sample to demonstrate that no initial reaction had taken place when compared with the subsequently recorded NMR spectra. The sample was heated to 323 K for 24 hours to enable the complex to react thermally with the substrate.

Comparison of the ^1H and $^{31}\text{P}\{^1\text{H}\}$ NMR spectra recorded prior to and following heating of the sample, showed that no new peaks were formed, indicating no new products were formed. Heating the sample to 353 K for a further 12 hours also did not show any evidence of reaction. The sample was subsequently irradiated with broadband UV, to attempt to initiate a reaction photochemically.

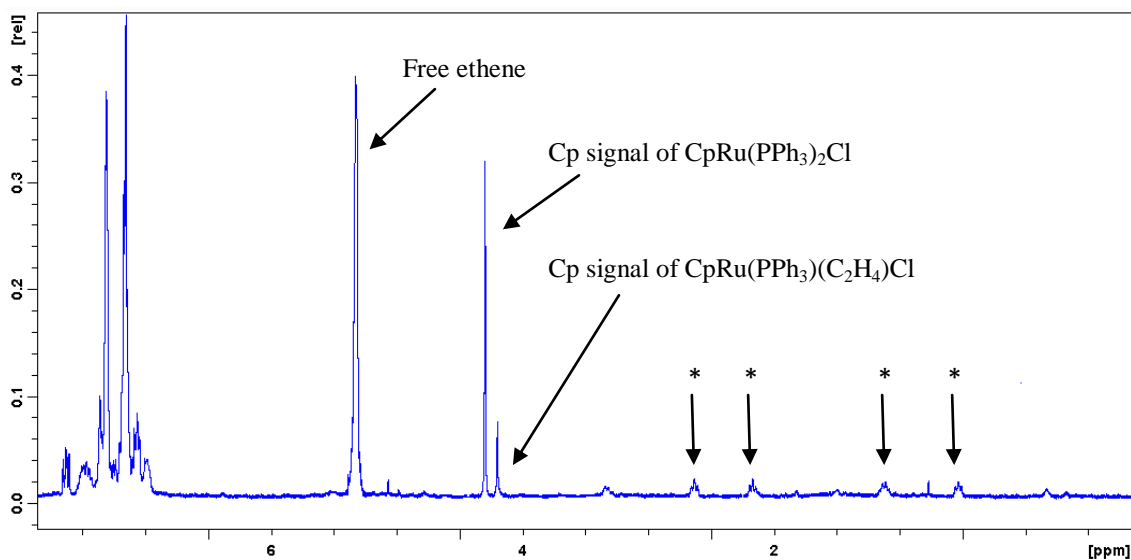
2.4.6.2 Photochemical reaction of $\text{CpRu}(\text{PPh}_3)_2\text{Cl}$ with ethene

An NMR tube was charged with $\text{CpRu}(\text{PPh}_3)_2\text{Cl}$ in d_6 -benzene. The tube was degassed and pressurised with 1.5 bar of ethene. ^1H and $^{31}\text{P}\{^1\text{H}\}$ NMR spectra were recorded for the sample to demonstrate that no initial reaction had taken place when compared with the subsequently recorded NMR spectra. The sample was irradiated for 12 hours at room temperature using the broadband UV Lamp set-up. No sign of reaction was found in the ^1H and ^{31}P NMR spectra, following photolysis at room temperature.

A second sample was prepared in the same way, and photolysed at low temperature (198 K), in order to stabilise any potential photoproducts. Following irradiation of the sample, the ^1H NMR spectrum recorded after 12 hours of photolysis at 198 K shows the formation of a new resonance at δ 4.23, consistent with a new Cp complex. Four new peaks at δ 0.56, 1.18, 2.23 and 2.64 (multiplets) were also found, these represent the

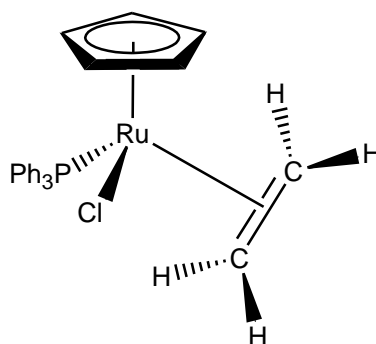
inequivalent protons of the η^2 -bound ethene ligand of $\text{CpRu}(\text{PPh}_3)(\eta^2\text{-C}_2\text{H}_4)\text{Cl}$. Figure 2.12 depicts the ^1H NMR resonances of the metal bound ethene protons.

Figure 2.12 ^1H NMR spectrum highlighting the low intensity peaks corresponding to the coordinated ethene protons.



(* = Protons of the ethene moiety)

A ^1H COSY experiment confirmed that these four ethene resonances were coupled. These five resonances are therefore consistent with those expected for $\text{CpRu}(\text{PPh}_3)(\eta^2\text{-C}_2\text{H}_4)\text{Cl}$, where alkene rotation is restricted at low temperature. A $^1\text{H}/^{31}\text{P}$ HMQC experiment connects the δ 56.2 ^{31}P NMR signal to these four ethene proton resonances, the Cp signal, and a new *ortho*-phenyl proton signal at δ 133.7. A $^1\text{H}/^{13}\text{C}$ HMQC experiment located the corresponding ^{13}C data while examination of the COSY located the phenyl group signals. These signals are all listed in Table 2.7. The structure of $\text{CpRu}(\text{PPh}_3)(\eta^2\text{-C}_2\text{H}_4)\text{Cl}$ is depicted in Figure 2.13.

Figure 2.13 $\text{CpRu}(\text{PPh}_3)(\eta^2\text{-C}_2\text{H}_4)\text{Cl}$ 

Following characterisation of the complex, the sample temperature was raised to room temperature, in order to appraise the thermal stability of the complex. The corresponding ^1H and $^{31}\text{P}\{^1\text{H}\}$ NMR spectra reveal a lack of signals corresponding to the ethene protons (in the ^1H spectrum) and the absence of the signal at δ 56.2 in the corresponding $^{31}\text{P}\{^1\text{H}\}$ NMR spectrum. The only observed signals in these spectra are now consistent with those of $\text{CpRu}(\text{PPh}_3)_2\text{Cl}$, which suggests that the thermal instability of $\text{CpRu}(\text{PPh}_3)(\eta^2\text{-C}_2\text{H}_4)\text{Cl}$ leads to the reformation of the starting material, $\text{CpRu}(\text{PPh}_3)_2\text{Cl}$.

2.4.7 Reactions of $\text{CpRu}(\text{PPh}_3)_2\text{Cl}$ with naphthalene

2.4.7.1 Thermally initiated reaction of $\text{CpRu}(\text{PPh}_3)_2\text{Cl}$ with naphthalene

An NMR tube was charged with $\text{CpRu}(\text{PPh}_3)_2\text{Cl}$ in d_6 -benzene. The tube was degassed and naphthalene was added. ^1H and $^{31}\text{P}\{^1\text{H}\}$ NMR spectra were then recorded to demonstrate that no reaction had taken place. The sample was then heated to 323 K for 24 hours to enable the complex to react thermally with the substrate.

Comparison of the ^1H and $^{31}\text{P}\{^1\text{H}\}$ NMR spectra recorded prior to and following heating of the sample, showed that no new peaks were formed, indicating no new products were formed. Heating the sample to 353 K for a further 48 hours still indicated the formation of no new products, in the NMR spectra for the sample.

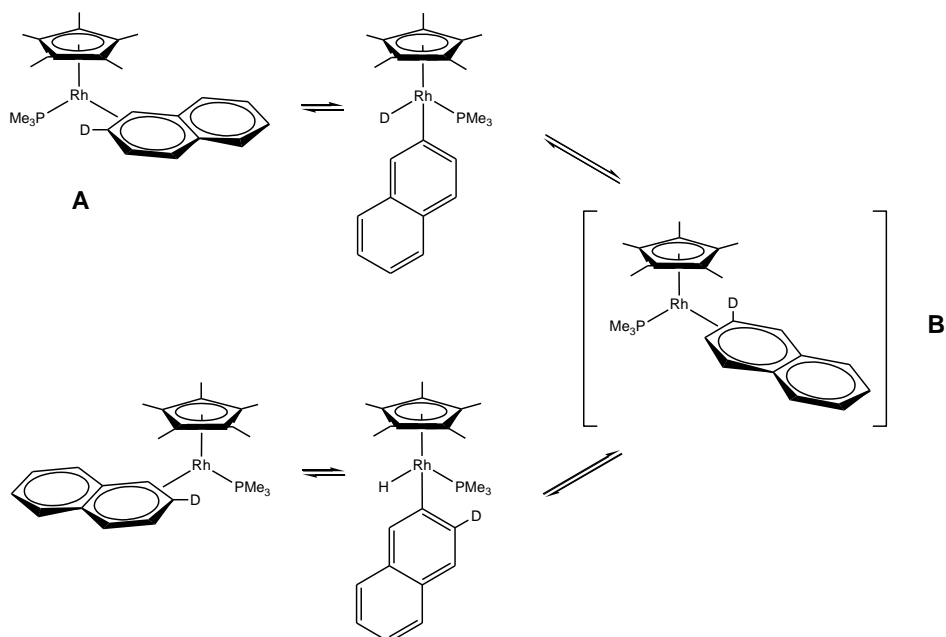
2.4.7.2 Photochemical reaction of $\text{CpRu}(\text{PPh}_3)_2\text{Cl}$ with naphthalene

An NMR tube was charged with $\text{CpRu}(\text{PPh}_3)_2\text{Cl}$ in d_6 -benzene. The tube was degassed and naphthalene was added. The sample was then irradiated for 12 hours at room temperature using the broadband UV Lamp set-up. No sign of a reaction was found in the ^1H and ^{31}P NMR spectra, following photolysis at room temperature. A second sample was then prepared and photolysed at low temperature (198 K), in order to stabilise any potential photoproducts.

This led to the observation of a new peak at δ 57.9 in the ^{31}P NMR spectrum. This new phosphorus peak was of low intensity (~5% conversion) and demonstrated to be connected to the ^1H signals at δ 4.34 due to a Cp ligand and at δ 7.71 and 7.10 due to a PPh_3 group using $^1\text{H}/^{31}\text{P}$ HMQC NMR spectra. Additional ^1H signals appear at δ 4.13 and 3.74 in these spectra which are coupled according to COSY spectroscopy. These signals are similar to those found for $\text{CpRu}(\text{PPh}_3)(\eta^2\text{-C}_{10}\text{H}_8)\text{Me}$ (see Chapter 3). However, owing to the low conversion, the characterisation as $\text{CpRu}(\text{PPh}_3)(\eta^2\text{-C}_{10}\text{H}_8)\text{Cl}$ cannot be fully confirmed. Prolonged photolysis and varying the temperature during photolysis, did not affect the amount of conversion.

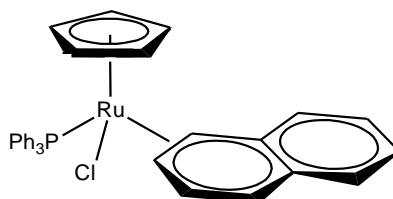
Examples of η^2 -naphthalene complexes are known in the literature, Figure 2.14 depicts such complexes characterised by Jones *et al.*,¹⁸⁹ and how the interconversion between these complexes can be monitored through deuterium labelling experiments. Complex **A** (in Figure 2.14) was observed to be stable, and subsequently characterised using NMR techniques, as was the activated naphthyl hydride complex. However, structure **B** is a high energy short-lived intermediate, and therefore too unstable to characterise by NMR.

Figure 2.14 The equilibrium between coordinated and activated complexes, $Cp^*Rh(PMe_3)(\eta^2-C_{10}H_8)$ and $Cp^*Rh(PMe_3)(C_{10}H_7)H$, as determined by Jones et al. using deuterium labelling experiments¹⁸⁹



This information from the literature can be used to inform the assignment of the present coordinated naphthalene structure. The 1H NMR signals found at δ 4.13 and 3.74 are consistent with the protons of the coordinated naphthalene, reported for structure **A**. Observation of the 1H NMR hydride region revealed the absence of any hydride resonances. Based on the lack of hydride signals (which suggests that there is no interconversion taking place) and the instability of structures corresponding to **B**, it is likely that the present structure adopts a structure similar to that of **A**. Figure 2.15 shows the possible structural form of this complex based on the limited characterisation data presented.

Figure 2.15 Possible structures for $CpRu(PPh_3)(\eta^2-C_{10}H_8)Cl$



2.5 Conclusions

The studies reported in this chapter confirm that the reaction between $\text{CpRu}(\text{PPh}_3)_2\text{Cl}$ and two electron donor ligands is possible both thermally and photochemically. The phosphine substitution studies show that the exchange when initiated photochemically will proceed to form the mono substituted products. Only in the case of PEt_3 double substitution achieved, although the second stage appeared to be thermal in nature.

For the reactions involving CO and $^t\text{BuNC}$, only the mono substitution products were obtained, and the same result was observed in the thermal experiments. However, reports have been made in the literature of full phosphine displacement by CO, when carried out under forcing conditions.

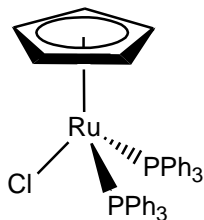
An alternative method was employed in order to prepare $\text{CpRu}(\text{CNBu}^t)_2\text{Cl}$ (detailed further in Chapter 7), so as to compare my NMR data with the minimal NMR characterisation obtained by Bruce *et al.* for the complex they speculated to be $\text{CpRu}(\text{CNBu}^t)_2\text{Cl}$. Both sets of NMR data are consistent, with characterisation for $\text{CpRu}(\text{CNBu}^t)_2\text{Cl}$ presented here in this chapter. The method employed here provides the product in higher yield than that reported for Bruce's preparation, and also requires less purification, owing to a 'one-pot' process.

Photochemical reactions of $\text{CpRu}(\text{PPh}_3)_2\text{Cl}$ at 198 K, involving ethene and naphthalene led to the successful formation of η^2 -containing complexes, similar to those found for the indenyl analogue. Full NMR data are reported for the coordinated ethene derivative, despite low conversion, compared with the previous reactions involving the two electron donor ligands. However, only partial characterisation could be achieved for the coordinated naphthalene derivative. Among the proton resonances found were those bonded to the metal-bound carbon atoms; this allowed for comparison with reported literature values for similar rhodium complexes, allowing the structure of the complex to be inferred. The migration of Cl onto the unsaturated carbon framework was not expected in these systems.

Attempts to activate Si-H and H-H bonds at the ruthenium centre proved unsuccessful, despite attempts to induce oxidative addition using UV photolysis and employing different reaction solvents. Presumably this reluctance is related to the inability of the complex to undergo orthometallation of one of the phenyl rings of one of the triphenylphosphine ligands. The reasons for this are not fully understood, and may arise as a consequence of a combination of steric and electronic effects, owing to the ability of the similar triphenylphosphite complex, $\text{CpRu}(\text{P}(\text{OPh})_3)_2\text{Cl}$, to orthometallate.

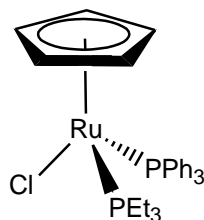
The next chapter examines the chemistry of $\text{CpRu}(\text{PPh}_3)_2\text{Me}$ (a complex known to readily undergo orthometallation). This system contains a highly reactive RuMe group which was expected to result in new chemistry. It should be noted that the Cp* analogue exists in the orthometalated form because of this reactivity.¹⁹³

2.6 Characterisation data

Table 2.1 NMR data for $\text{CpRu}(\text{PPh}_3)_2\text{Cl}$ 

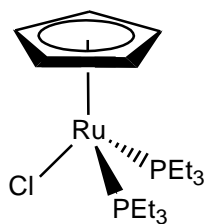
In d_8 -toluene at 298 K	δ / ppm (multiplicity, integration)	Assignment	Coupling constant / Hz	Assignment
^1H	4.27 (s, 5) 7.02 (m)* 7.16 (m)* 7.74 (m, 12)	$\eta^5\text{-C}_5\text{H}_5$ <i>Para</i> - $\text{P}(\text{C}_6\text{H}_5)_3$ <i>Meta</i> - $\text{P}(\text{C}_6\text{H}_5)_3$ <i>Ortho</i> - $\text{P}(\text{C}_6\text{H}_5)_3$	8.1	$ \text{}^3\text{J}_{\text{PH}} $
^{13}C	81.2 (s) 127.9 (t) 128.7 (s) 133.3 (t) 141.5 (dd)	$\eta^5\text{-C}_5\text{H}_5$ <i>Meta</i> - $\text{P}(\text{C}_6\text{H}_5)_3$ <i>Para</i> - $\text{P}(\text{C}_6\text{H}_5)_3$ <i>Ortho</i> - $\text{P}(\text{C}_6\text{H}_5)_3$ <i>Ips</i> o- $\text{P}(\text{C}_6\text{H}_5)_3$	9.4 10.9 13.5, 33.6	$ \text{}^3\text{J}_{\text{PC}} $ $ \text{}^2\text{J}_{\text{PC}} $ $ \text{}^3\text{J}_{\text{PC}} , \text{}^1\text{J}_{\text{PC}} $
^{31}P	39.6 (s)	<i>P</i> (C_6H_5) ₃		

* Resonances were overlapped in the ^1H NMR spectrum, and were therefore found using a $^1\text{H}/^{31}\text{P}$ HMQC NMR experiment.

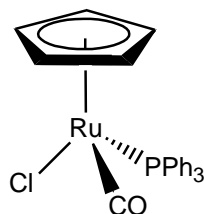
Table 2.2 NMR data for $CpRu(PPh_3)(PEt_3)Cl$ 

In d_8 -toluene at 298 K	δ / ppm (multiplicity, integration)	Assignment	Coupling constant / Hz	Assignment
1H	0.92 (m, 9) 1.15 & 1.83 (m, 6) 4.21 (s, 5) 7.02 (m)* 7.08 (m)* 7.82 (m, 6)	$P(CH_2-CH_3)_3$ $P(CH_2-CH_3)_3$ $\eta^5-C_5H_5$ <i>Para</i> - $P(C_6H_5)_3$ <i>Meta</i> - $P(C_6H_5)_3$ <i>Ortho</i> - $P(C_6H_5)_3$	8.4	$ ^3J_{PH} $
^{13}C	10.1 (t) 19.9 (t) 79.8 (s) 128.2 (d) 129.1 (s) 134.4 (d) 140.7 (d)	$P(CH_2-CH_3)_3$ $P(CH_2-CH_3)_3$ $\eta^5-C_5H_5$ <i>Meta</i> - $P(C_6H_5)_3$ <i>Para</i> - $P(C_6H_5)_3$ <i>Ortho</i> - $P(C_6H_5)_3$ <i>Ipsso</i> - $P(C_6H_5)_3$	4.3 15.7 9.3 10.9 12.0, 33.2	$ ^2J_{PC} $ $ ^1J_{PC} $ $ ^3J_{PC} $ $ ^2J_{PC} $ $ ^3J_{PC} , ^1J_{PC} $
^{31}P	27.8 (d) 45.5 (d)	$P(Et)_3$ $P(Ph)_3$	44 44	$ ^2J_{PC} $ $ ^2J_{PC} $

* Resonances were overlapped in the 1H NMR spectrum, and were therefore found using a $^1H/^{31}P$ HMQC NMR experiment.

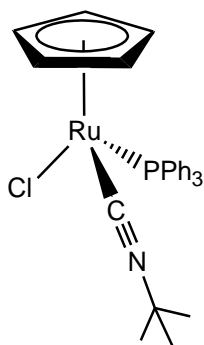
Table 2.3 NMR data for $CpRu(PEt_3)_2Cl$ 

In d_8 -toluene at 298 K	δ / ppm (multiplicity, integration)	Assignment	Coupling constant / Hz	Assignment
1H	0.91 (m, 18) 1.16 & 1.21 (m, 12) 4.17 (s, 5)	$P(CH_2-CH_3)_3$ $P(CH_2-CH_3)_3$ $\eta^5-C_5H_5$	4.1 15.9	$ ^3J_{PH} $ $ ^2J_{PH} $
^{13}C	9.7 (s) 20.4 (t) 79.3 (s)	$P(CH_2-CH_3)_3$ $P(CH_2-CH_3)_3$ $\eta^5-C_5H_5$	12.0	$ ^1J_{PC} $
^{31}P	46.8 (s)	$P(Et)_3$		

Table 2.4 NMR data for $CpRu(PPh_3)(CO)Cl$ 

In d_8 -toluene at 298 K	δ / ppm (multiplicity, integration)	Assignment	Coupling constant / Hz	Assignment
1H	4.49 (s, 5) 6.99 (m)* 7.05 (m)* 7.68 (m, 6)	$\eta^5-C_5H_5$ <i>Para</i> - $P(C_6H_5)_3$ <i>Meta</i> - $P(C_6H_5)_3$ <i>Ortho</i> - $P(C_6H_5)_3$	8.0	$ ^3J_{PH} $
^{13}C	85.7 (s) 127.9 (d) 129.8 (s) 133.7 (d) 141.2 (d) 201.3 (d)	$\eta^5-C_5H_5$ <i>Meta</i> - $P(C_6H_5)_3$ <i>Para</i> - $P(C_6H_5)_3$ <i>Ortho</i> - $P(C_6H_5)_3$ <i>Ipsa</i> - $P(C_6H_5)_3$ $C\equiv O$	9.6 10.8 43.1 22.9	$ ^3J_{PC} $ $ ^2J_{PC} $ $ ^1J_{PC} $ $ ^2J_{PC} $
^{31}P	49.1 (s)	$P(Ph)_3$		

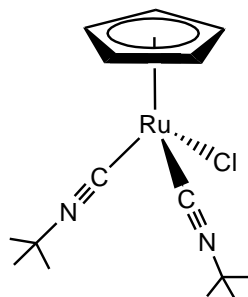
* Resonances were overlapped in the 1H NMR spectrum, and were therefore found using a $^1H/^{31}P$ HMQC NMR experiment.

Table 2.5 NMR data for $\text{CpRu}(\text{PPh}_3)(\text{CNBu}^t)\text{Cl}$ 

In d_8 -toluene at 298 K	δ / ppm (multiplicity, integration)	Assignment	Coupling constant / Hz	Assignment
^1H	0.96 (s, 9) 4.52 (s, 5) 7.01 (m)* 7.08 (m)* 7.81 (m, 6)	$\text{C}(\text{CH}_3)_3$ $\eta^5\text{-C}_5\text{H}_5$ <i>Para</i> - $\text{P}(\text{C}_6\text{H}_5)_3$ <i>Meta</i> - $\text{P}(\text{C}_6\text{H}_5)_3$ <i>Ortho</i> - $\text{P}(\text{C}_6\text{H}_5)_3$	8.5	$ \text{}^3\text{J}_{\text{PH}} $
^{13}C	30.5 (s) 53.1 (s) 81.7 (s) 128.0 (d) 129.1 (s) 134.1 (d) 140.8 (d) 156.4 (t)**	$\text{C}(\text{CH}_3)_3$ $\text{C}(\text{CH}_3)_3$ $\eta^5\text{-C}_5\text{H}_5$ <i>Meta</i> - $\text{P}(\text{C}_6\text{H}_5)_3$ <i>Para</i> - $\text{P}(\text{C}_6\text{H}_5)_3$ <i>Ortho</i> - $\text{P}(\text{C}_6\text{H}_5)_3$ <i>Ips</i> o- $\text{P}(\text{C}_6\text{H}_5)_3$ $\text{C}\equiv\text{N}$	9.2 10.4 44.2 19.6	$ \text{}^3\text{J}_{\text{PC}} $ $ \text{}^2\text{J}_{\text{PC}} $ $ \text{}^1\text{J}_{\text{PC}} $ $ \text{}^1\text{J}_{\text{CN}} $
^{31}P	52.4 (s)	$\text{P}(\text{Ph})_3$		

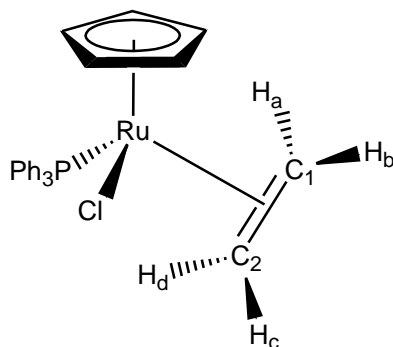
* Resonances were overlapped in the ^1H NMR spectrum, and were therefore found using a $^1\text{H}/^{31}\text{P}$ HMQC NMR experiment.

** Appears as a broad triplet in the $^{13}\text{C}\{^1\text{H}\}$ NMR spectrum.

Table 2.6 NMR data for $\text{CpRu}(\text{CNBu}^t)_2\text{Cl}$ 

In d_8 -toluene at 298 K	δ / ppm (multiplicity, integration)	Assignment	Coupling constant / Hz	Assignment
^1H	0.92 (s, 18) 4.85 (s, 5)	$\text{C}(\text{CH}_3)_3$ $\eta^5\text{-C}_5\text{H}_5$		
^{13}C	27.6 (s) 51.7 (s) 84.0 (s) 137.6 (t)*	$\text{C}(\text{CH}_3)_3$ $\text{C}(\text{CH}_3)_3$ $\eta^5\text{-C}_5\text{H}_5$ $\text{C}\equiv\text{N}$	19.3	$ ^1J_{\text{CN}} $

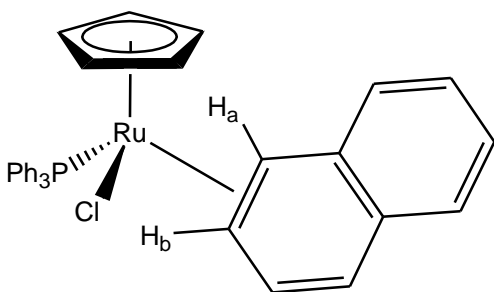
* Appears as a broad triplet in the $^{13}\text{C}\{^1\text{H}\}$ NMR spectrum.

Table 2.7 NMR data for $\text{CpRu}(\text{PPh}_3)(\eta^2\text{-C}_2\text{H}_4)\text{Cl}$ 

In d_8 -toluene at 198 K	δ / ppm (multiplicity, integration)	Assignment	Coupling constant / Hz	Assignment
^1H	0.56 (br, 1) 1.18 (br, 1) 2.23 (br, 1) 2.64 (br, 1) 4.23 (s, 5) 7.07 (m)* 7.19 (m)* 7.62 (m)*	H_c H_b H_a H_d $\eta^5\text{-C}_5\text{H}_5$ <i>Para</i> - $\text{P}(\text{C}_6\text{H}_5)_3$ <i>Meta</i> - $\text{P}(\text{C}_6\text{H}_5)_3$ <i>Ortho</i> - $\text{P}(\text{C}_6\text{H}_5)_3$		
^{13}C	38.3 (t) 41.9 (t) 80.6 (s) 127.5 (d) 128.4 (s) 133.7 (d) 140.3 (d)	C_1 C_2 $\eta^5\text{-C}_5\text{H}_5$ <i>Meta</i> - $\text{P}(\text{C}_6\text{H}_5)_3$ <i>Para</i> - $\text{P}(\text{C}_6\text{H}_5)_3$ <i>Ortho</i> - $\text{P}(\text{C}_6\text{H}_5)_3$ <i>Ips</i> o- $\text{P}(\text{C}_6\text{H}_5)_3$	8.4 8.4 8.9 10.6 42.3	$ ^2J_{\text{PC}} $ $ ^2J_{\text{PC}} $ $ ^3J_{\text{PC}} $ $ ^2J_{\text{PC}} $ $ ^1J_{\text{PC}} $
^{31}P	56.2 (s)	$\text{P}(\text{Ph})_3$		

* Resonances were overlapped in the ^1H NMR spectrum, and were therefore found using a $^1\text{H}/^{31}\text{P}$ HMQC NMR experiment.

Table 2.8 NMR data for $CpRu(PPh_3)(\eta^2-C_{10}H_8)Cl$

				
In d_8 -toluene at 198 K	δ / ppm (multiplicity, integration)	Assignment	Coupling constant / Hz	Assignment
1H	3.74 (m, 1) 4.13 (m, 1) 4.34 (s, 5) 7.10 (m)* 7.71 (m)*	H_b H_a $\eta^5-C_5H_5$ <i>Meta</i> - $P(C_6H_5)_3$ <i>Ortho</i> - $P(C_6H_5)_3$	14.7 14.7	$ ^3J_{PH} $ $ ^3J_{PH} $
^{31}P	57.9 (s)	$P(Ph)_3$		

* Resonances were overlapped in the 1H NMR spectrum, and were therefore found using a $^1H/^{31}P$ HMQC NMR experiment.

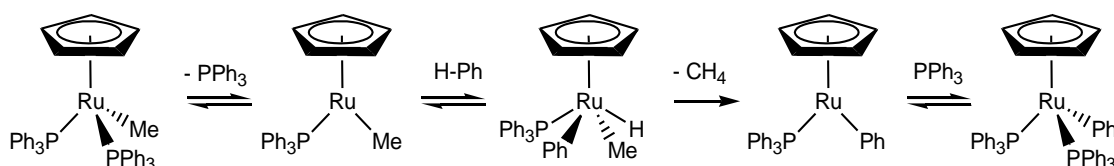
Chapter 3

Thermal and Low Temperature Photochemical Reactions of $\text{CpRu}(\text{PPh}_3)_2\text{Me}$

3.1 Introduction

The complex $\text{CpRu}(\text{PPh}_3)_2\text{Me}$ represents one of the most widely explored half-sandwich ruthenium bis-phosphine species. The thermal reactivity of this complex has been extensively probed and instances of its ability to activate C-H bonds are widely known (for example, heating the complex at reflux in the presence of benzene readily leads to the formation of the phenyl derivative, $\text{CpRu}(\text{PPh}_3)_2\text{Ph}$).^{194, 195} The activation of the C-H bond in benzene by the ruthenium centre was thought to occur directly following the dissociation of triphenylphosphine (Figure 3.1). The hydride product of this activation step is proposed to be highly unstable, and readily eliminate methane from the metal centre. The vacant site of the resulting 16 electron species allows for the re-association of a triphenylphosphine ligand, to form the final stable 18 electron product.

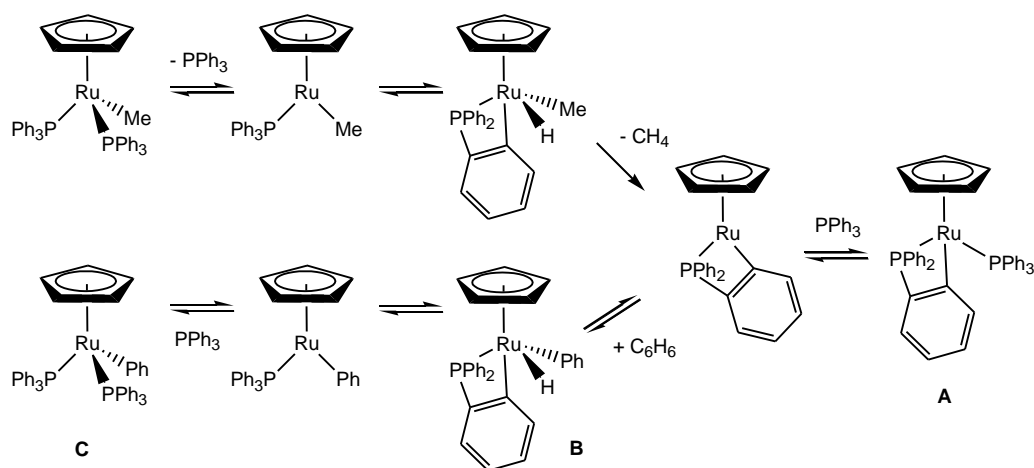
Figure 3.1 Proposed mechanism for the replacement of alkyl moieties at $\text{CpRu}(\text{PPh}_3)_2\text{Me}$ by benzene



Following work conducted by Bruce *et al.*^{196, 197} and Lehmkuhl *et al.*,¹⁹⁴ the mechanism shown in Figure 3.1 is now thought to be inaccurate. Bruce proposed that following the dissociation of the first triphenylphosphine ligand, the remaining coordinated triphenylphosphine ligand undergoes cyclometallation at the *ortho* position

as shown in Figure 3.2. The cyclometallated (orthometallated) hydride product formed in this way is thermally unstable, and rapidly eliminates methane. The newly formed 16-electron orthometallated species has been trapped by re-association of triphenylphosphine to form the thermally stable complex $\text{CpRu}(\kappa^2\text{-2-C}_6\text{H}_4\text{PPh}_2)(\text{PPh}_3)$ (Figure 3.2, **A**). Alternatively, if this species is formed in the presence of a large excess of an aromatic compound, such as benzene, C-H (or C-D) bond activation occurs to give a short-lived orthometallated-phenyl-hydride complex (Figure 3.2, **B**). In the case of benzene, this complex rapidly interconverts to $\text{CpRu}(\text{PPh}_3)\text{Ph}$ by loss of the cyclometallated ring. Following re-association of the phosphine ligand, a stable 18 electron complex is formed (Figure 3.2, **C**). The evidence for these suggestions is based on product studies and the isolation of $\text{CpRu}(\kappa^2\text{-2-C}_6\text{H}_4\text{PPh}_2)(\text{PPh}_3)$.

Figure 3.2 The replacement of the alkyl moiety of $\text{CpRu}(\text{PPh}_3)_2\text{Me}$ by benzene via an orthometallation mechanism (illustrated for benzene, proposed to be general)



Attempts have been made to exploit this behaviour in catalytic transformations. Gunnoe *et al.* recently demonstrated an attempt to form ethylbenzene catalytically using $\text{CpRu}(\text{PPh}_3)_2\text{Me}$ under ethene. Only stoichiometric conversion was achieved, owing to the decomposition of $\text{CpRu}(\text{PPh}_3)_2\text{Me}$.¹⁹⁵ In contrast, the η^5 -indenyl analogue ($(\eta^5\text{-C}_9\text{H}_7)\text{Ru}(\text{PPh}_3)_2\text{C}\equiv\text{CPh}$) has been shown to catalytically dimerize terminal alkynes.^{198.}

3.1.1 Context

The previous chapter demonstrated the ability of $\text{CpRu}(\text{PPh}_3)_2\text{Cl}$ to undergo photochemical dissociation of one of the triphenylphosphine ligands, allowing for the formation of mono and some bis-substituted products. The reluctance of $\text{CpRu}(\text{PPh}_3)_2\text{Cl}$ to undergo oxidative addition of H-H, Si-H and C-H bonds can be attributed to electronic differences between the ruthenium centres in the 16-electron chloride and methyl complexes (see intro). This change in character prevents the orthometallation of the triphenyl phosphine. As discussed earlier in this chapter, the orthometallation of $\text{CpRu}(\text{PPh}_3)_2\text{Me}$, is believed now to be pivotal to its reaction chemistry.

This chapter presents a series of studies designed to explore the thermal and photochemical reactions of $\text{CpRu}(\text{PPh}_3)_2\text{Me}$ to detect the proposed intermediates and widen the scope of this reaction.

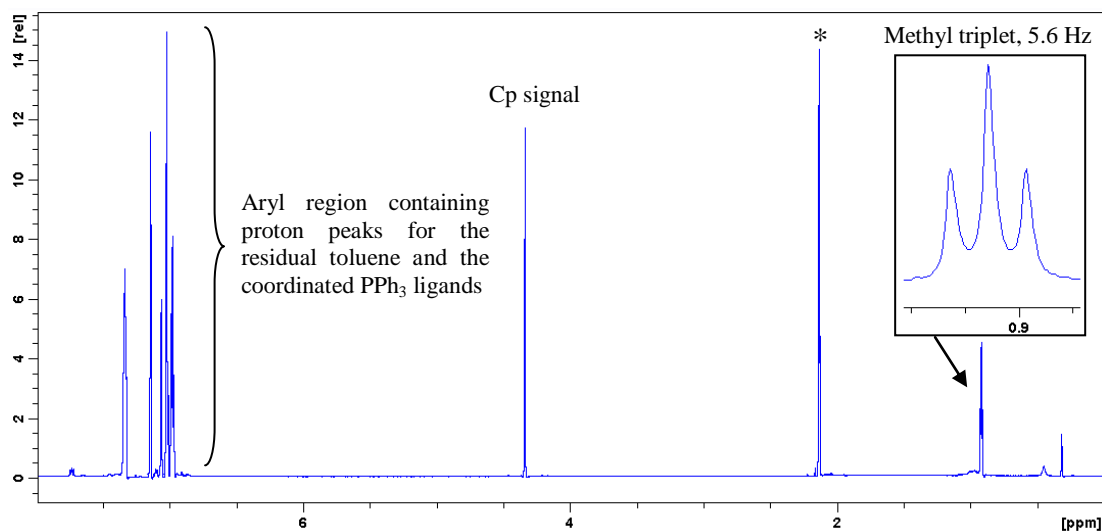
3.2 Synthesis and characterisation of $\text{CpRu}(\text{PPh}_3)_2\text{Me}$

3.2.1 Synthesis of $\text{CpRu}(\text{PPh}_3)_2\text{Me}$

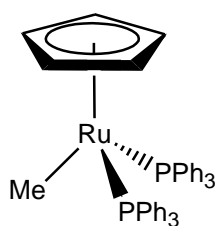
$\text{CpRu}(\text{PPh}_3)_2\text{Me}$ was prepared by treating $\text{CpRu}(\text{PPh}_3)_2\text{Cl}$ with methyl lithium in dried and degassed toluene, according to literature methods (see experimental Section for details). A typical yield of such a reaction was 96 %.²⁰⁰

3.2.2 NMR characterisation of $\text{CpRu}(\text{PPh}_3)_2\text{Me}$

Characterisation of the parent complex $\text{CpRu}(\text{PPh}_3)_2\text{Me}$ was achieved in d_8 -toluene by ^1H , ^{13}C and ^{31}P NMR experiments. A singlet resonance is observed in the 1D ^1H NMR spectrum at δ 4.35, which is indicative of the cyclopentadienyl (Cp) ring of the complex (Figure 3.3). An additional triplet resonance was clearly visible at δ 0.97 (5.7 Hz), which is characteristic of the protons of the methyl (Me) group. It is split into a triplet by the ^{31}P nuclei of the two triphenylphosphine ligands. The lack of a splitting in the Cp resonance suggests that such an interaction cannot be used to count the number of phosphine ligands in these complexes.

Figure 3.3 ^1H NMR spectrum of $\text{CpRu}(\text{PPh}_3)_2\text{Me}$ with Cp and Me resonances indicated(* = the residual CHD_2 resonances of the $\text{C}_6\text{D}_5\text{CD}_3$ solvent)

A 1D $^{31}\text{P}\{^1\text{H}\}$ NMR spectrum revealed a single peak at δ 55.3, which is typical of the ^{31}P resonance for the bound triphenylphosphine ligands. A $^1\text{H}/^{31}\text{P}$ HMQC experiment showed coupling between the phosphine peak at δ 55.3 and the ^1H Cp and methyl resonances. The Cp proton resonance can therefore be used to locate the corresponding ^{31}P signals in such complexes. In addition, three other proton resonances are clearly visible (which had previously been obscured by the solvent peaks) at δ 7.34, 6.95 and 6.91 which correspond to the *ortho*, *meta* and *para* protons of the phenyl rings of the triphenylphosphine ligand. Complete NMR data for this species (Figure 3.4) is listed in Table 3.1. The corresponding ESI mass spectrum produced a signal for the M^+ at m/z 706, while further selective fragmentation of this peak led to the observation of peaks m/z peaks of 691 and 444, which are indicative of $[\text{M}^+ - \text{Me}]$ and $[\text{M}^+ - \text{PPh}_3]$, respectively.

Figure 3.4 Structure of $\text{CpRu}(\text{PPh}_3)_2\text{Me}$ 

3.3 Synthesis and characterisation of $\text{CpRu}(\kappa^2\text{-2-C}_6\text{H}_4\text{PPh}_2)(\text{PPh}_3)$

3.3.1 Synthesis of $\text{CpRu}(\kappa^2\text{-2-C}_6\text{H}_4\text{PPh}_2)(\text{PPh}_3)$

The complex, $\text{CpRu}(\kappa^2\text{-2-C}_6\text{H}_4\text{PPh}_2)(\text{PPh}_3)$, was prepared in bulk according to the method reported by Bruce *et al.*¹⁹⁷ This complex may also be prepared by irradiation of $\text{CpRu}(\text{PPh}_3)_2\text{Me}$ at room temperature in cyclohexane using a broadband UV light source such as that provided by a 200 w Hg/Xe arc lamp. This procedure was developed as part of this work. It should also be noted that in analogous thermal experiments (at 354 K) of $\text{CpRu}(\text{PPh}_3)_2\text{Me}$ in cyclohexane no $\text{CpRu}(\kappa^2\text{-2-C}_6\text{H}_4\text{PPh}_2)(\text{PPh}_3)$ was formed upon reflux of the solution even after three days. Bruce used decalin as the solvent where the reflux temperature is 463 K. This reaction is described further in the experimental Section (Chapter 7, Section 7.2.2.2). The photochemical synthesis is therefore achieved at much lower temperatures.

3.3.2 NMR characterisation of $\text{CpRu}(\kappa^2\text{-2-C}_6\text{H}_4\text{PPh}_2)(\text{PPh}_3)$

Characterisation of this complex was achieved (in d_{12} -cyclohexane) using ^1H , ^{13}C and ^{31}P NMR experiments. A peak at δ 4.27 was indicative of the proton resonances of the Cp ring in this complex. A $^{31}\text{P}\{^1\text{H}\}$ NMR spectrum displayed a pair of doublets of 33.8 Hz splitting at δ -16.9 and 63.5 respectively, which represent the bound triphenylphosphine ligand (**A**) and the orthometallated phosphine ligand (**B**). A $^1\text{H}/^{31}\text{P}$ HMQC experiment reported coupling between the ^{31}P resonance at 63.5 and the ^1H resonances at δ 7.73, 7.09 and 7.05, which represent the *ortho*, *meta* and *para* protons of this triphenylphosphine ligand. The second ^{31}P signal at δ -16.9 connects to ^1H resonances at δ 7.53, 7.11, 7.33 and 6.98 which correspond to the protons of the orthometallated phenyl ring of the triphenylphosphine ligand (Figure 3.5). Three additional proton resonances are observed to couple to this signal at δ 7.64, 7.14 and 6.93 (by varying the CNST2 delay) which are representative of the *ortho*, *meta* and *para* protons of the remaining two phenyl rings of the orthometallated phosphine ligand. The resonances of these phenyl rings ^1H NMR signals therefore overlap and cannot be distinguished from one another at 400 MHz.

Figure 3.5 A $^1\text{H}/^{31}\text{P}$ HMQC NMR spectrum showing the coupling between the ^{31}P signal at δ -16.9 and the corresponding phenyl protons

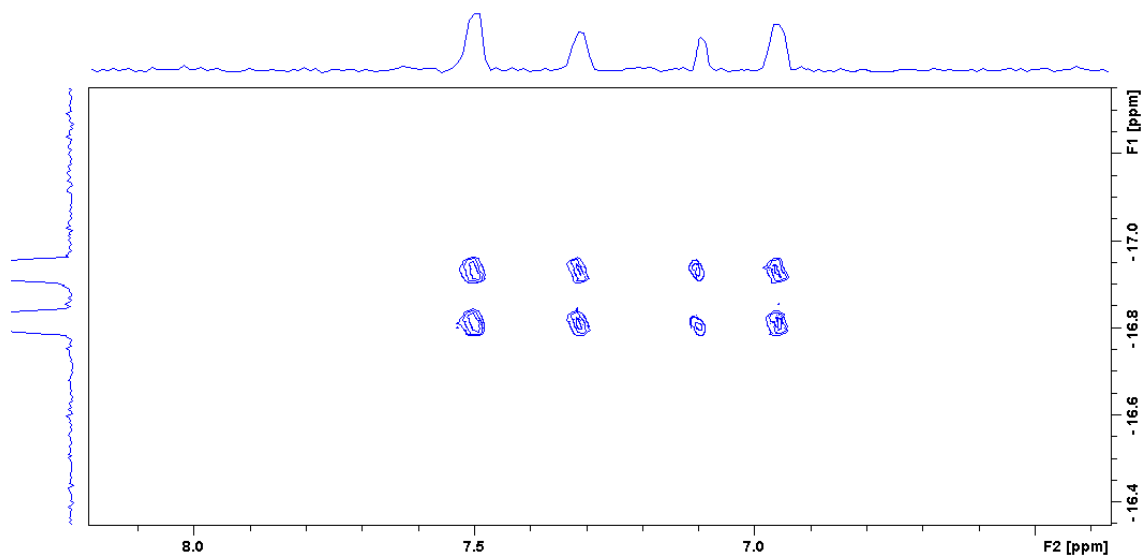
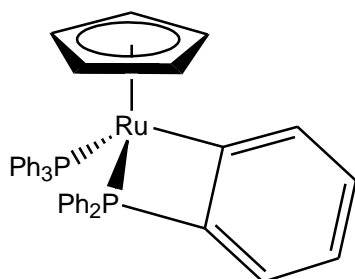


Figure 3.6 Structure of $\text{CpRu}(\text{PPh}_3)(\kappa^2\text{-}2\text{-C}_6\text{H}_4\text{PPh}_2)$



3.3.3 The role $\text{CpRu}(\kappa^2\text{-}2\text{-C}_6\text{H}_4\text{PPh}_2)(\text{PPh}_3)$

The preparation of $\text{CpRu}(\kappa^2\text{-}2\text{-C}_6\text{H}_4\text{PPh}_2)(\text{PPh}_3)$ from $\text{CpRu}(\text{PPh}_3)_2\text{Me}$ proceeds initially via the loss of triphenylphosphine, which is known to occur thermally¹⁹⁶ and has also been shown through our own work to occur via UV photolysis in cyclohexane. From this point onwards, the thermal and photochemical activity of $\text{CpRu}(\text{PPh}_3)_2\text{Me}$ is explored.

3.4 Thermal and photochemical reactions of $\text{CpRu}(\text{PPh}_3)_2\text{Me}$

3.4.1 Reactions with PEt_3

In order to demonstrate phosphine loss and the formation of the 16 electron fragment, $[\text{CpRu}(\text{PPh}_3)\text{Me}]$ upon UV irradiation, a reaction was undertaken in the presence of an excess of triethylphosphine. The triethylphosphine ligand should efficiently “trap” the intermediate, $[\text{CpRu}(\text{PPh}_3)\text{Me}]$, as it is formed, and therefore allow characterisation of the new mono-substituted phosphine complex, $\text{CpRu}(\text{PPh}_3)(\text{PEt}_3)\text{Me}$. This approach was described in Chapter 2 for $\text{CpRu}(\text{PPh}_3)_2\text{Cl}$.

3.4.1.1 Thermal reactions of $\text{CpRu}(\text{PPh}_3)_2\text{Me}$ with PEt_3

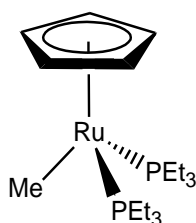
A J-Y NMR tube was charged with 5 mg of $\text{CpRu}(\text{PPh}_3)_2\text{Me}$ and dissolved in d_6 -benzene, to a depth of 4 cm. Using a micro syringe 9 μl of PEt_3 was added to the sample. Initial ^1H and $^{31}\text{P}\{^1\text{H}\}$ NMR spectra were recorded prior to the thermal reaction. The sample tube was heated to 323 K in a silicone oil bath for 24 hours.

Comparison of the $^{31}\text{P}\{^1\text{H}\}$ NMR recorded prior to thermal reaction and after, reveal the presence of four new peaks, with the ^{31}P resonance for $\text{CpRu}(\text{PPh}_3)_2\text{Me}$ (δ 55.3) being absent. These signals appeared at δ -6.4, 35.2, 62.9 and 40.5. The peak at δ -6.4 corresponds to the resonance of liberated triphenylphosphine, suggesting that one or more of the new complexes has exchanged phosphine ligands. The peaks at δ 35.2 and 62.9 possess a mutual coupling of 39.3 Hz suggesting that two distinct phosphine ligands are coordinated to the metal centre in this complex. Owing to the small intensity of the signal, full characterisation of this complex was not possible at this point (see the subsequent reaction for full characterisation of this product). The following experiments employing photochemical irradiation at low temperature, led to greater conversion to this species, $\text{CpRu}(\text{PPh}_3)(\text{PEt}_3)\text{Me}$, and allowed its full NMR characterisation.

The dominant product of the thermal reaction yields the ^{31}P signal at δ 40.5. This signal appears as a singlet, which indicates that the complex either contains only one phosphine ligand, or if two, both are the same. A $^1\text{H}/^{31}\text{P}$ HMQC experiment connected this phosphine resonance with signals in the ^1H NMR spectrum at δ 0.15 (t, 5.8), 1.48,

1.90, 0.92 and 4.54. The lack of any connections to signals corresponding to aryl protons clearly demonstrates that triphenylphosphine is not present in this complex. The signal at δ 4.54 is consistent with the protons of a ruthenium bound η^5 -cyclopentadienyl moiety. The resonance at δ 0.15 appears as a triplet with a 5.8 Hz splitting. Integration of this signal with the cyclopentadienyl proton resonance at δ 4.54 reveals a ratio of 3:5 (respectively), confirming that this signal belongs to a ruthenium-bound methyl group. The triplet splitting is characteristic of a bis-phosphine complex (as discussed earlier in this chapter for $\text{CpRu}(\text{PPh}_3)_2\text{Me}$), suggesting that the identity of this complex as $\text{CpRu}(\text{PEt}_3)_2\text{Me}$. Confirmation of this identity was made through the investigation of the remaining signals at δ 1.48, 1.90 and 0.92, which were found to mutually couple through a ^1H COSY NMR experiment. The signals at δ 1.48 and 1.90 were observed to mutually couple to the same carbon resonance at δ 31.8 in a $^1\text{H}/^{13}\text{C}$ HMQC experiment. This result clearly shows that these proton resonances correspond to the diastereotopic protons on the methylene carbon of the ruthenium-bound PEt_3 ligand. The resonance at δ 0.92 may similarly be assigned as belonging to the protons of the terminal methyl of the ethyl chain of the PEt_3 ligand. In the corresponding ESI spectrum obtained after reaction, peaks at m/z M^+ 418 and $[\text{M}^+ - \text{PEt}_3]$ 299, were found, which also confirms the identity as $\text{CpRu}(\text{PEt}_3)_2\text{Me}$. This suggests that $\text{CpRu}(\text{PPh}_3)(\text{PEt}_3)\text{Me}$ reacts readily thermally to form $\text{CpRu}(\text{PEt}_3)_2\text{Me}$ at 323 K.

Figure 3.7 Structure of $\text{CpRu}(\text{PEt}_3)_2\text{Me}$

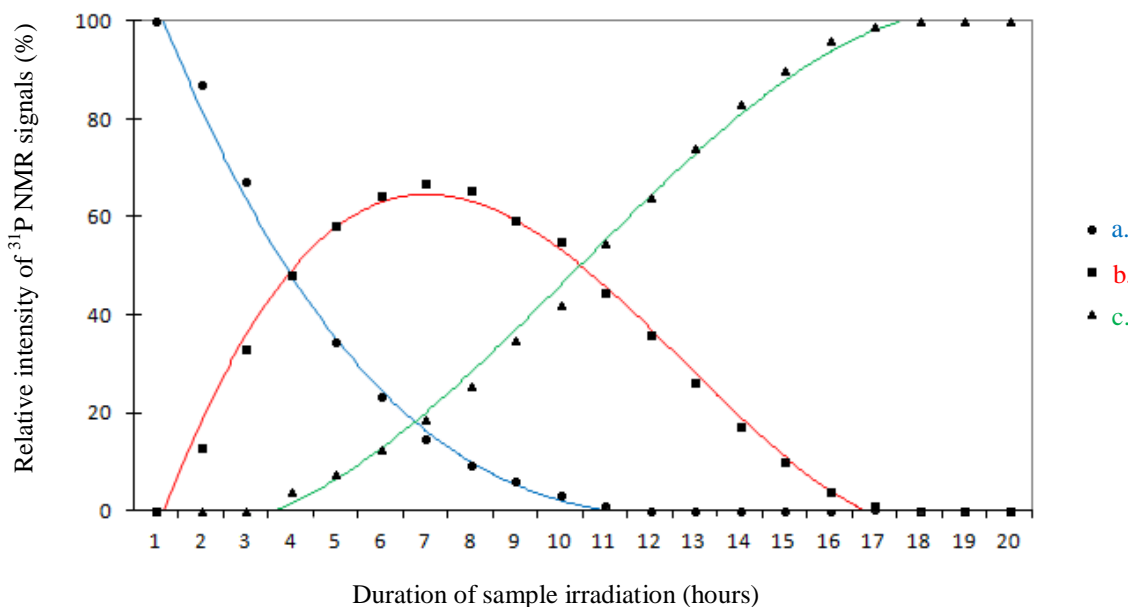


3.4.1.2 Photolysis of $\text{CpRu}(\text{PPh}_3)_2\text{Me}$ with PEt_3

In order to plot the formation of the mono and bis products, the *in situ*-laser setup was employed to monitor the progress of the reaction at room temperature (Figure 3.8). The plot demonstrates that after an irradiation time of 18 hours full conversion of the complex $\text{CpRu}(\text{PPh}_3)_2\text{Me}$ to $\text{CpRu}(\text{PEt}_3)_2\text{Me}$ can be achieved. The intermediate

complex, $\text{CpRu}(\text{PPh}_3)(\text{PEt}_3)\text{Me}$, achieves a maximum intensity of $\sim 70\%$ after 7.5 hours, prior to the total conversion to $\text{CpRu}(\text{PEt}_3)_2\text{Me}$.

Figure 3.8 A plot of the relative ^{31}P resonances over time, for the photochemically formed products of the reaction between $\text{CpRu}(\text{PPh}_3)_2\text{Me}$ and PEt_3 , at 298 K (original illustration appears in colour)



a. $\text{CpRu}(\text{PPh}_3)_2\text{Me}$

b. $\text{CpRu}(\text{PPh}_3)(\text{PEt}_3)\text{Me}$

c. $\text{CpRu}(\text{PEt}_3)_2\text{Me}$

Simulation of these data using a kinetic model that allows $\text{CpRu}(\text{PPh}_3)_2\text{Me}$ to form $\text{CpRu}(\text{PPh}_3)(\text{PEt}_3)\text{Me}$, $\text{CpRu}(\text{PPh}_3)_2\text{Me}$ to form $\text{CpRu}(\text{PEt}_3)_2\text{Me}$ and $\text{CpRu}(\text{PPh}_3)(\text{PEt}_3)\text{Me}$ to form $\text{CpRu}(\text{PEt}_3)_2\text{Me}$. This produced effective photochemical rates of formation (which shall now be referred to as k_{obs}) of 0.311, 0.079 and 0.154 s^{-1} for each process respectively. This confirms that the pathway involves the stepwise conversion from $\text{CpRu}(\text{PPh}_3)_2\text{Me}$ to $\text{CpRu}(\text{PPh}_3)(\text{PEt}_3)\text{Me}$ to $\text{CpRu}(\text{PEt}_3)_2\text{Me}$. The activity of $\text{CpRu}(\text{PPh}_3)(\text{PEt}_3)\text{Me}$ relative to $\text{CpRu}(\text{PPh}_3)_2\text{Me}$ is 2:1. This shows that $\text{CpRu}(\text{PPh}_3)_2\text{Me}$ is more photoactive than $\text{CpRu}(\text{PPh}_3)(\text{PEt}_3)\text{Me}$.

3.4.1.3 Photolysis of $\text{CpRu}(\text{PPh}_3)_2\text{Me}$ with PEt_3 at 198 K

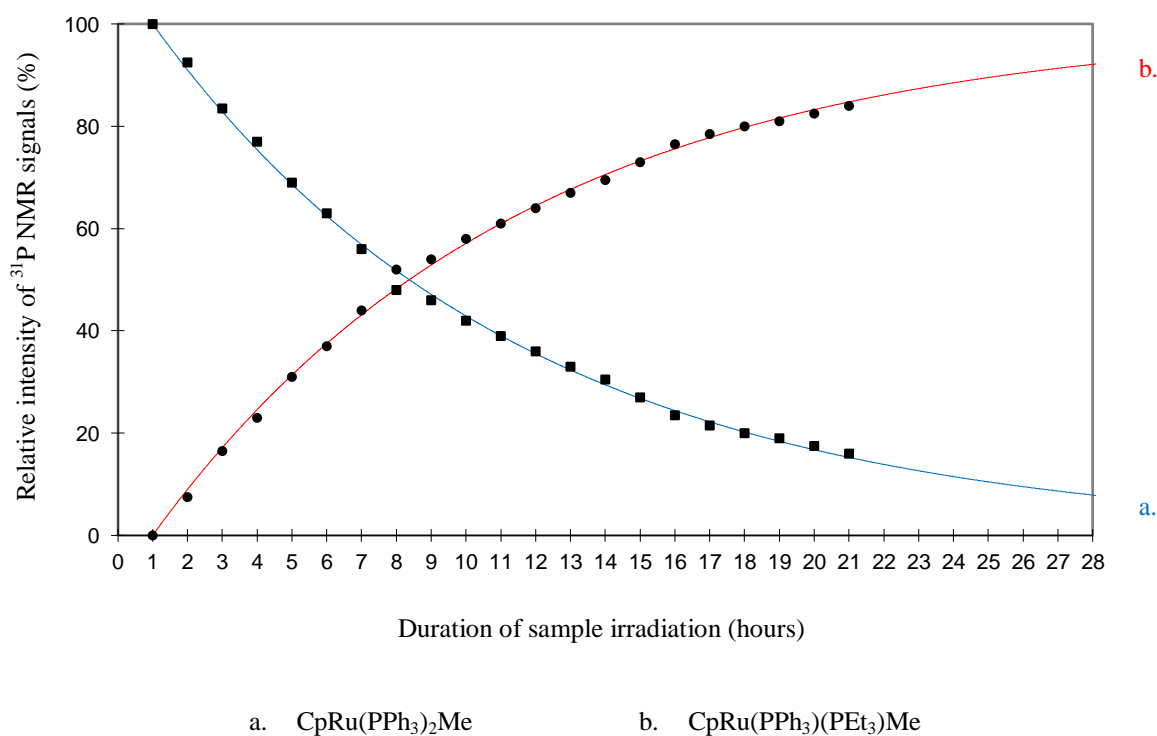
In a second reaction, PEt_3 was added to a Young's tap capped NMR tube containing $\text{CpRu}(\text{PPh}_3)_2\text{Me}$ in $\text{d}_8\text{-THF}$. The sample was degassed prior to *in situ* irradiation using a UV laser for 18 hours at 198 K. The progress of the reaction was tracked during this period by 1D ^1H and $^{31}\text{P}\{^1\text{H}\}$ NMR methods. A comparison of the ^1H NMR spectrum recorded prior to UV irradiation with one that was recorded after 4 hours of irradiation, showed new proton resonances at δ 0.39, 0.83, 1.39, 1.50 and 4.49. The peak at δ 4.49 is consistent with the expected position of the proton resonances of the cyclopentadienyl ring in $\text{CpRu}(\text{PPh}_3)(\text{PEt}_3)\text{Me}$. A new triplet (5.6 Hz) peak at δ 0.39 is consistent with the proton resonances of a ruthenium-bound methyl group, the apparent triplet splitting indicates that two phosphine ligands couple to this group and are hence bound to the complex.

There are no signals in the high field region (δ 0 to -20 range) of the ^1H NMR spectrum where hydride resonances are commonly observed. The lack of a hydride signal and the observed methyl resonance suggest that no cyclometallated phosphine ligands are present within the complex. Nor has cyclometallation been involved in the route to the formation of this complex because as demonstrated later such products should be stable. This is due to the presence of the methyl group within the present complex. Were CH activation to have occurred, rapid elimination of methane would be expected.

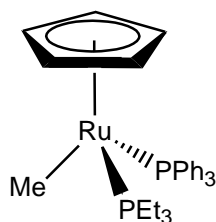
The corresponding $^{31}\text{P}\{^1\text{H}\}$ NMR spectrum, recorded after 4 hours clearly showed the appearance of several new resonances. A large singlet resonance at δ -6.4 is characteristic of free triphenylphosphine, which shows that PPh_3 had been lost from the parent complex thereby indicating that phosphine exchange had occurred. The lack of any other resonances with negative chemical shifts means that cyclometallation of either of the phosphine ligands to the ruthenium centre had not occurred. There were two doublet peaks of equal intensity that share a common splitting of 39.3 Hz at δ 35.2 and 62.9 in the $^{31}\text{P}\{^1\text{H}\}$ NMR spectrum. These doublet resonances represent the two ^{31}P nuclei in the distinct environments of the two phosphine ligands for the complex $\text{CpRu}(\text{PPh}_3)(\text{PEt}_3)\text{Me}$. The mutual coupling between the two ^{31}P nuclei results in the 39.3 Hz splitting of these resonances. The chart shown in Figure 3.9 presents the change in relative intensities of these ^{31}P signals as a function of the irradiation time. The

corresponding ^1H spectra contained characteristic C_5H_5 resonances which also vary in a similar way. The k_{obs} for the process $\text{CpRu}(\text{PPh}_3)_2\text{Me} \rightarrow \text{CpRu}(\text{PPh}_3)(\text{PEt}_3)\text{Me}$ is 0.094 s^{-1} , with no evidence in the NMR spectra for the formation of C-H activation products. The corresponding $T_{1/2}$ is 510 minutes.

Figure 3.9 A plot of the relative ^{31}P resonances over time, for the photochemically formed products of the reaction between $\text{CpRu}(\text{PPh}_3)_2\text{Me}$ and PEt_3 , at 193 K (original illustration appears in colour)



A $^1\text{H}/^{31}\text{P}$ HMQC of the sample showed that these two ^{31}P resonances connected to common ^1H resonances at δ 0.39, 1.39, 1.50, 4.49 and 7.61. The resonance at ^{31}P δ 62.9 couples strongly to ^1H resonances at δ 7.61, 7.06 and 6.97, which comprise the *ortho*, *meta* and *para* phenyl protons of the bound triphenylphosphine ligand. Signals at ^1H δ 0.83, 1.39 and 1.50 were found to couple strongly to the ^{31}P resonance at δ 35.2. These peaks represent the proton resonances of the ethyl chains of the triethylphosphine. The proton resonances at δ 1.39 and 1.50 correspond to the inequivalent CH_2 protons of the triethylphosphine ligand (confirmed by their mutual coupling to a common carbon at δ 23.4 in the corresponding $^1\text{H}/^{13}\text{C}$ HMQC experiment).

Figure 3.10 Structure of $\text{CpRu}(\text{PPh}_3)(\text{PEt}_3)\text{Me}$ 

The observation of this complex as a product of the irradiation of $\text{CpRu}(\text{PPh}_3)_2\text{Me}$ with triethylphosphine, confirms that the reaction intermediate $[\text{CpRu}(\text{PPh}_3)\text{Me}]$ is formed under photolysis, although PEt_3 is so reactive no other products are formed. Under thermal conditions, the dominance of $\text{CpRu}(\text{PEt}_3)_2\text{Me}$ (Figure 3.10) suggests that complete phosphine exchange is possible. Under irradiation however, the selective formation of $\text{CpRu}(\text{PPh}_3)(\text{PEt}_3)\text{Me}$ is achieved even after 30 hours of photolysis with the 325 nm source.

It can therefore be concluded that the reaction of $\text{CpRu}(\text{PPh}_3)_2\text{Me}$ with PEt_3 reacts both thermally and photochemically to form $\text{CpRu}(\text{PPh}_3)(\text{PEt}_3)\text{Me}$. Subsequent reactivity to form $\text{CpRu}(\text{PEt}_3)_2\text{Me}$ occurs thermally, but was also observed in photochemical reactions as a consequence of warming effects of the UV lamp. At low temperature, selective photochemistry allowed for the conversion to $\text{CpRu}(\text{PPh}_3)(\text{PEt}_3)\text{Me}$ only. These results are consistent with those found for the analogous reactions conducted with $\text{CpRu}(\text{PPh}_3)_2\text{Cl}$ in Chapter 2.

The chloride derivative described in the previous chapter reacts to form similar complexes. Neither of these complexes undergo C-H activation with the alkyl chains of PEt_3 , or the *ortho* phenyl protons of PPh_3 , suggesting that association of the phosphine occurs faster than the orthometallation process. The corresponding ^{31}P resonances for the chloride derivative appear to be shifted significantly upfield compared with those observed for the methyl derivative. This is likely attributed to the electron withdrawing effect of the chloride moiety, which may also be responsible for its lack of ability to orthometallate (as discussed in Chapter 1, electron-rich metal centres tend to readily activate C-H bonds). In both cases the J_{PP} coupling constants for the mono substituted product appear similar, and are indicative of a *cis*-type phosphine arrangement.

3.4.2 Photochemical reactivity of $\text{CpRu}(\text{PPh}_3)_2\text{Me}$ with solvents

3.4.2.1 Low temperature photolysis with THF

The previous experiment demonstrated that the 16 electron complex, $\text{CpRu}(\text{PPh}_3)_2\text{Me}$, can be trapped by coordination of the two electron donor PET_3 prior to orthometallation. This further demonstrated that $\text{CpRu}(\text{PPh}_3)_2\text{Me}$ is photosensitive on a reasonable timescale at 198 K, where $T_{1/2}$ is achieved upon 240 minutes of irradiation.

The preparation of $\text{CpRu}(\kappa^2\text{-}2\text{-C}_6\text{H}_4\text{PPh}_2)(\text{PPh}_3)$ from $\text{CpRu}(\text{PPh}_3)_2\text{Me}$ proceeds initially also via the loss of triphenylphosphine, which is known to occur thermally¹⁹⁶ and has also been shown through our own work to occur via UV photolysis in cyclohexane (described in Chapter 7).

A series of photolysis experiments were therefore undertaken with $\text{CpRu}(\text{PPh}_3)_2\text{Me}$ at low temperature (198 K) in order to generate, stabilise and ultimately characterise the observable reaction intermediates that are formed in such a reaction in the absence of a strongly ligating species such as PET_3 . Four reaction outcomes might be envisaged:

- Detection of $\text{CpRu}(\kappa^2\text{-}2\text{-C}_6\text{H}_4\text{PPh}_2)(\text{PPh}_3)$ as a single product
- Loss of PPh_3 and detection of $\text{CpRu}(\text{PPh}_3)\text{Me}$ which may be solvated
- Detection of $\text{CpRu}(\kappa^2\text{-}2\text{-C}_6\text{H}_4\text{PPh}_2)\text{HMe}$
- Detection of $\text{CpRu}(\kappa^2\text{-}2\text{-C}_6\text{H}_4\text{PPh}_2)$ which may be solvated or undergo CH bond activation

Based on literature precedent, stabilisation of the sixteen-electron intermediate, $[\text{CpRu}(\text{PPh}_3)\text{Me}]$, by phosphine loss, would require a coordinating solvent such as THF (coordination through oxygen) or toluene (η^2 -arene coordination).²⁰¹ Through previous photolysis experiments, THF was found to be less likely to undergo CH activation when compared to toluene, which is consistent with the use of THF as a solvent for many C-H activation reactions.²⁰² Using THF would therefore provide an increased chance of forming a solvent “trapped” derivative of $[\text{CpRu}(\text{PPh}_3)\text{Me}]$. Additionally, THF can act as a σ -donor thereby stabilising the ruthenium centre. For these reasons, it was decided to use THF (deuterated) initially in the low temperature photolysis experiments with

CpRu(PPh₃)₂Me.

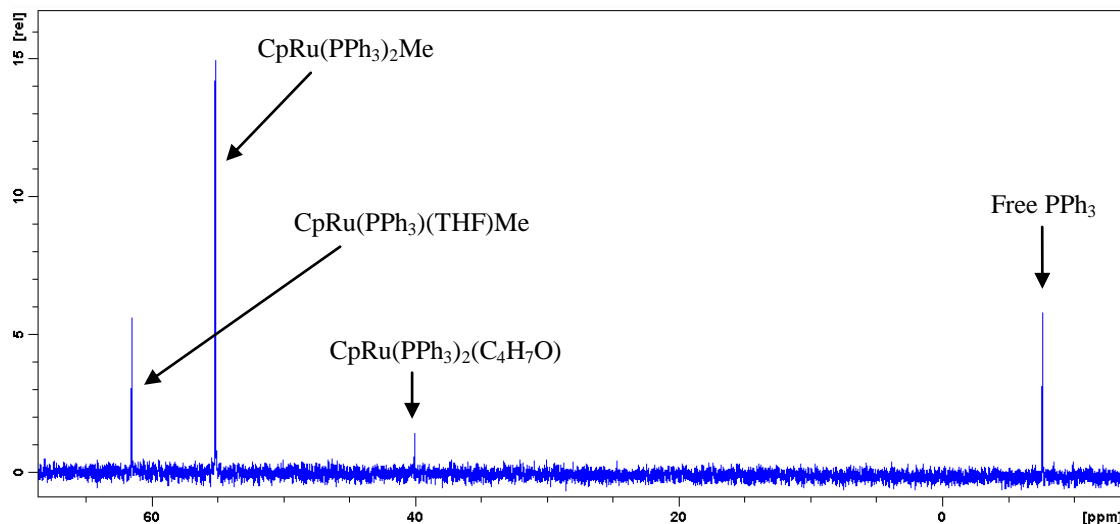
A J-Y NMR tube was therefore charged with CpRu(PPh₃)₂Me, and dry degassed d₈-THF alone. The photolysis of this sample was conducted to see if any new products would form without any other reagents being present. The sample was irradiated for 18 hours using the *in situ* 325 nm laser at 198 K.

Four possible outcomes, indicated below, were identified as being possible in THF:

- Detection of CpRu(κ^2 -2-C₆H₄PPh₂)(PPh₃) as a single product
- Loss of PPh₃ and detection of either CpRu(PPh₃)(THF)Me or the THF C-D bond activation product CpRu(PPh₃)Me(D)(OC₄D₇)
- Detection of CpRu(κ^2 -2-C₆H₄PPh₂)HMe
- Detection of CpRu(κ^2 -2-C₆H₄PPh₂) which again might be solvated or have undergone THF C-D bond activation

After four hours irradiation, a ¹H NMR peak at δ 4.59 corresponding to the cyclopentadienyl ring of a new complex was observed. This resonance coupled to a ³¹P signal at δ 61.3 in a ¹H/³¹P HMQC experiment. Further coupling to a ¹H peak at δ 0.16 due to a set of methyl protons was evident. This signal showed a doublet splitting of 5.91 Hz thereby confirming the formation of a mono phosphine based product. In agreement with this suggestion, a singlet was observed in the ³¹P NMR spectrum at δ -6.4 due to free triphenylphosphine (Figure 3.11). The product giving rise to this signal decomposed when the temperature was raised above 218 K. A second minor product CpRu(PPh₃)₂(C₄H₇O) (which is discussed in more detail later in this Section) was also produced.

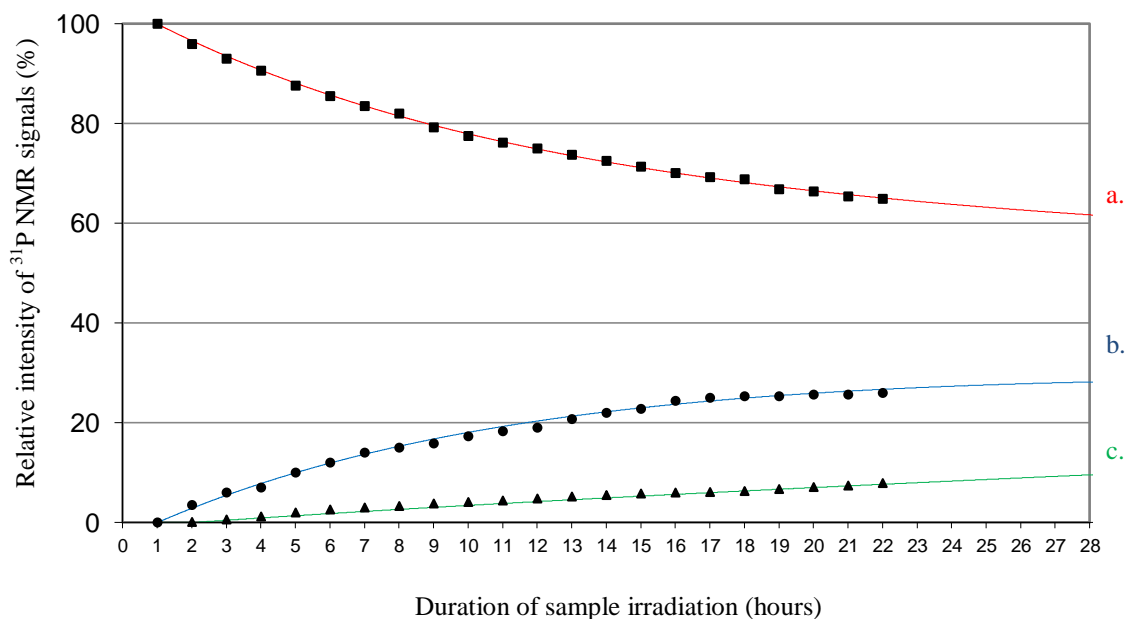
Figure 3.11 $^{31}\text{P}\{^1\text{H}\}$ NMR spectrum showing the ^{31}P signals corresponding to $\text{CpRu}(\text{PPh}_3)(\text{THF})\text{Me}$ and $\text{CpRu}(\text{PPh}_3)_2(\text{C}_4\text{H}_7\text{O})$, following 5 hours of photolysis



A 16-electron complex would be far too unstable to be observed at 193 K (typically these observations are made using IR techniques, while low temperature matrices are employed to stabilise the products).²⁰³ The lack of a hydride resonance confirms that orthometallation of the phosphine has not occurred. There are therefore two possible reaction outcomes that need to be considered, the first being that THF has coordinated to the ruthenium centre via the oxygen lone pair. The second situation corresponds to where an interaction with the C-D bond occurs which could either break it or weakly interact with it. It should be noted that there are two types of C-D bond in d_8 -THF.

Similar half-sandwich rhodium complexes which possess a σ coordinated THF moiety have been previously reported in the literature.^{204, 205} Such complexes have also been shown to be stable at temperatures approaching 223 K. Peaks belonging to coordinated THF cannot be seen in this ^1H NMR spectrum, since d_8 -THF is used.

Figure 3.12 A plot of the relative ^{31}P resonances over time, for the photochemically formed products of the reaction between $\text{CpRu}(\text{PPh}_3)_2\text{Me}$ and THF, at 193 K (original illustration appears in colour)



a. $\text{CpRu}(\text{PPh}_3)_2\text{Me}$

b. $\text{CpRu}(\text{PPh}_3)(\text{THF})\text{Me}$

c. $\text{CpRu}(\text{PPh}_3)_2(\text{C}_4\text{H}_7\text{O})$

Figure 3.12 illustrates the time course of this reaction, simulation of these data suggest that $\text{CpRu}(\text{PPh}_3)_2\text{Me}$ reacts photochemically to form $\text{CpRu}(\text{PPh}_3)(\text{THF})\text{Me}$ (Figure 3.13, **A**) and $\text{CpRu}(\text{PPh}_3)_2(\text{C}_4\text{H}_7\text{O})$ (Figure 3.13, **B**) in two competing pathways. The k_{obs} for these processes are 0.050 s^{-1} (for $\text{CpRu}(\text{PPh}_3)_2\text{Me} \rightarrow \text{CpRu}(\text{PPh}_3)(\text{THF})\text{Me}$) and 0.030 s^{-1} (for $\text{CpRu}(\text{PPh}_3)_2\text{Me} \rightarrow \text{CpRu}(\text{PPh}_3)_2(\text{C}_4\text{H}_7\text{O})$), with no evidence of interconversion between $\text{CpRu}(\text{PPh}_3)(\text{THF})\text{Me}$ and $\text{CpRu}(\text{PPh}_3)_2(\text{C}_4\text{H}_7\text{O})$. The presence of both of these complexes shows that THF is a weakly coordinating ligand, as THF can coordinate to the metal centre prior to orthometallation, but also associates after orthometallation, to form the C-H activation product, $\text{CpRu}(\text{PPh}_3)_2(\text{C}_4\text{H}_7\text{O})$. No evidence was obtained in these spectra for $\text{CpRu}(\text{PPh}_3)(\text{C}_4\text{H}_7\text{O})(\text{H})(\text{Me})$ which must be unstable and rapidly eliminate MeH.

Figure 3.13 Structure of $\text{CpRu}(\text{PPh}_3)(\text{C}_4\text{H}_8\text{O})\text{Me}$ and $\text{CpRu}(\text{PPh}_3)_2(\text{C}_4\text{H}_7\text{O})$ 

These products were identified through the use of a second sample containing a 2:1 mixture of protio THF and d_8 -THF. This allows $^1\text{H}/^{13}\text{C}$ HMQC data to be recorded, and hence the detection of key ^1H resonances. The sample was irradiated for a total time of 18 hours at 198 K (to ensure maximum conversion to any potentially new products given the limited liquid N_2 source used for cooling) and tracked during the irradiation by recording 1D ^1H and $^{31}\text{P}\{^1\text{H}\}$ NMR experiments every 12 minutes.

Examination of the NMR spectra after 4 hours revealed the lack of any signals that could be associated with a ruthenium-hydride or a $\text{Ru}-\eta^2\text{-CH}$ signal.²⁰⁶⁻²¹⁰ The δ 61.3 ^{31}P resonance is clearly visible but no protio THF signals could be located. We therefore conclude that this highly unstable product is fluxional even at 198 K and a σ coordinated THF moiety is likely.

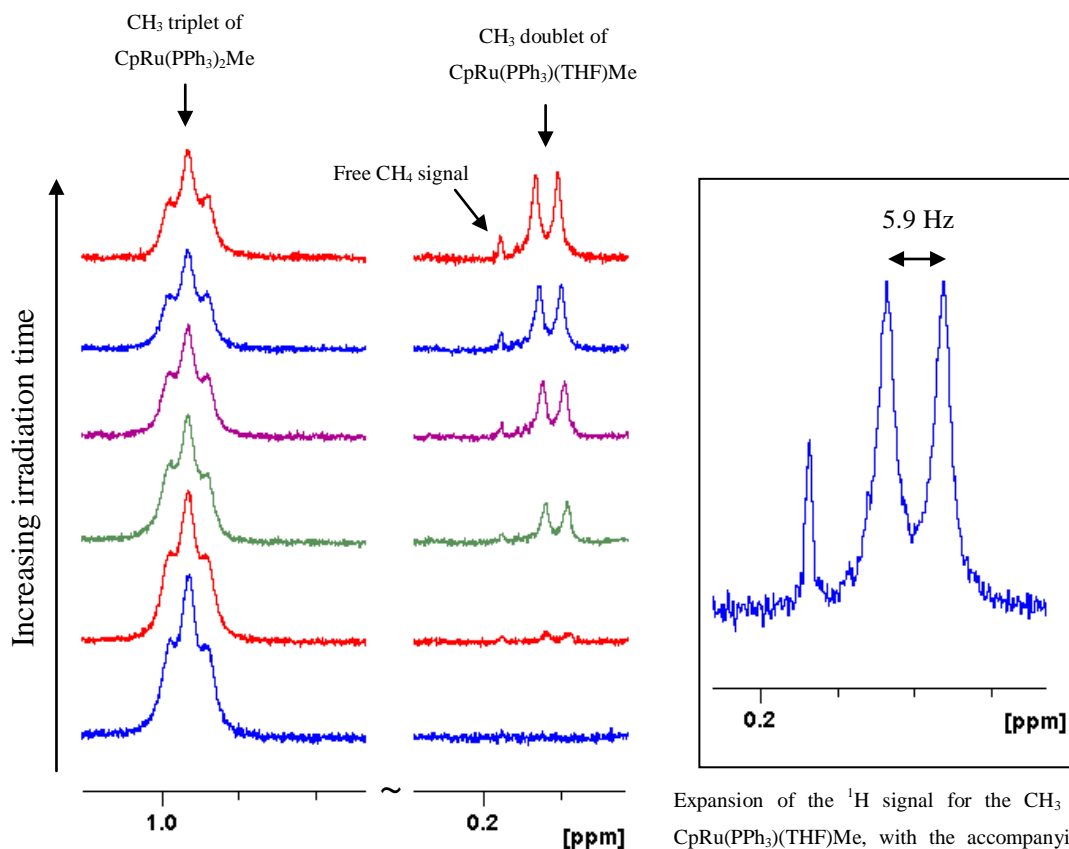
As mentioned, this species converted into a new product, $\text{CpRu}(\text{PPh}_3)_2(\text{C}_4\text{H}_7\text{O})$ (Figure 3.13, **B**), which was stable at room temperature and yields a resonance at δ 41.9 in the ^{31}P NMR spectrum. The ^{31}P resonance of $\text{CpRu}(\text{PPh}_3)_2(\text{C}_4\text{H}_7\text{O})$ appears at δ 41.9 and connects, using a $^1\text{H}/^{31}\text{P}$ HMQC experiment, to a Cp resonance at δ 4.23 and to other peaks at δ 5.37, 3.86, 3.70, 1.75, 1.94, 2.41 and 2.19 which were subsequently identified as proton resonances of a tetrahydrofuryl group. Significantly, there was no methyl proton resonance in this product. Bound *ortho*, *meta* and *para* PPh_3 resonances were located at δ 7.38, 7.16 and 7.09, using $^1\text{H}/^{31}\text{P}$ HMQC and ^1H COSY NMR experiments. The ^1H signal at δ 5.37 was identified as the α -proton of a ruthenium-bound tetrahydrofuryl group, which was determined by the coupling observed by this proton signal to a carbon signal at δ 145.7 (t, 17.8 Hz), found using a $^1\text{H}/^{13}\text{C}$ HMQC

NMR experiment. The triplet splitting indicated the presence of two triphenylphosphine within the structure, and the coupling constant of 17.8 Hz, is typical of a $|^2J_{CP}|$ splitting, consistent with a ruthenium-bound carbon in this complex. A 1H COSY experiment was employed to show the coupling between the signal at δ 5.37 and the remaining pairs of inequivalent protons, for the tetrahydrofuryl moiety; δ 3.86, 3.70, 1.75, 1.94, 2.41 and 2.19. Complete characterisation data for this complex appears in Table 3.9.

Integration of 1H NMR signals described above confirmed that a complex of the type $CpRu(PPh_3)_2(C_4H_7O)$ was formed and the chemical shift data would suggest that the Ru-C bond involves the carbon adjacent to oxygen. This site of activation is consistent with the known acidity of these C-H bonds²¹¹ and studies of similar complexes.^{212, 213}

Upon re-examination of these 1H NMR spectra, a peak consistent with formation of protio-methane (singlet at δ 0.19)²¹⁴ was evident (Figure 3.14). If this were formed from the d_8 -THF, it would be CH_3D . This suggests that the orthometallation product $CpRu(\kappa^2\text{-}2\text{-}C_6H_4PPh_2)(H)(Me)$ is formed but not detected.

Figure 3.14 ^1H spectra depicting the increasing intensity of the signal corresponding to liberated methane (original in colour)



To determine whether $\text{CpRu}(\text{PPh}_3)_2(\text{C}_4\text{H}_7\text{O})$ can indeed be formed via the orthometallated intermediate $[\text{CpRu}(\kappa^2\text{-}2\text{-C}_6\text{H}_4\text{PPh}_2)]$, a sample of $\text{CpRu}(\kappa^2\text{-}2\text{-C}_6\text{H}_4\text{PPh}_2)(\text{PPh}_3)$ was prepared by the UV irradiation of $\text{CpRu}(\text{PPh}_3)_2\text{Me}$ in cyclohexane within the NMR tube. Following the full conversion to $\text{CpRu}(\kappa^2\text{-}2\text{-C}_6\text{H}_4\text{PPh}_2)(\text{PPh}_3)$, the cyclohexane solvent was replaced with $d_8\text{-THF}$. Further photolysis of the sample for 16 hours resulted in 70% conversion to $\text{CpRu}(\text{PPh}_3)_2(\text{C}_4\text{H}_7\text{O})$. Evidence for partial deuteration of the PPh_3 ligand in the *ortho* position was now evident in the ^1H NMR spectrum (this is further described in Section 3.4.12). This is consistent with the low temperature photochemical formation of $\text{CpRu}(\text{PPh}_3)_2(\text{C}_4\text{H}_7\text{O})$.

3.4.2.2 Low temperature photolysis with acetone

In order to test whether $\text{CpRu}(\text{PPh}_3)(\text{acetone})\text{Me}$ was more stable than $\text{CpRu}(\text{PPh}_3)(\text{THF})\text{Me}$ the following reaction was examined. A sample of $\text{CpRu}(\text{PPh}_3)_2\text{Me}$ in $\text{d}_8\text{-THF}$ with 10 fold excess of acetone was cooled to 198 K and irradiated using the *in situ* set-up (He-Cd laser) for a total time of 18 hours. ^1H and $^{31}\text{P}\{^1\text{H}\}$ NMR spectra were recorded at intervals of 12 minutes, as the sample was irradiated.

Comparison of all of the recorded $^{31}\text{P}\{^1\text{H}\}$ spectra showed clearly the presence of a peak at δ 61.9 due to $\text{CpRu}(\text{C}_4\text{D}_8\text{O})(\text{PPh}_3)\text{Me}$ at early reaction times. A second peak found at δ -6.4 indicated that triphenylphosphine had been liberated. Further resonances were present at δ 4.59 and 0.16 in the ^1H NMR spectrum of this species. These resonances are consistent with the previously characterised THF coordination complex and not a new acetone solvent complex. This demonstrates that acetone is too weakly coordinating to displace the oxygen bound THF ligand of the solvent. $\text{CpRu}(\text{PPh}_3)_2(\text{C}_4\text{H}_7\text{O})$ was also formed in this reaction.

3.4.2.3 Low temperature photolysis with methanol

A sample of $\text{CpRu}(\text{PPh}_3)_2\text{Me}$ in $\text{d}_8\text{-THF}$ was then photolysed with a 10 fold excess of methanol at 198 K for 18 hours. ^1H and $^{31}\text{P}\{^1\text{H}\}$ NMR spectra were recorded as the sample was irradiated at 12 minute intervals. Comparison of all of the recorded $^{31}\text{P}\{^1\text{H}\}$ spectra again revealed peaks at δ 61.9 and δ -6.4. No reaction with the methanol was therefore indicated. $\text{CpRu}(\text{PPh}_3)_2(\text{C}_4\text{H}_7\text{O})$ was also formed in this reaction.

3.4.3 Reactions with CO

The reaction between $\text{CpRu}(\text{PPh}_3)_2\text{Cl}$ and CO, described in the previous chapter, led to the formation of the mono-substituted product $\text{CpRu}(\text{PPh}_3)(\text{CO})\text{Cl}$, even when photochemical methods are employed as a means to initiate the reaction. Previous studies have also shown that the same product is formed when the complex, $\text{CpRu}(\text{CO})_2\text{Cl}$, reacts thermally with PPh_3 over 2-3 weeks.²¹⁵ However, for the reaction of $\text{CpRu}(\text{CO})_2\text{Me}$ with PPh_3 , Baird *et al.* found that prolonged photochemical

irradiation of a sample led to conversion to both $\text{CpRu}(\text{PPh}_3)_2\text{Me}$ (10%)²¹⁶ and $\text{CpRu}(\text{PPh}_3)(\text{CO})\text{Me}$ (40%).²¹⁷ The following Section describes the thermal and photochemical reactions of $\text{CpRu}(\text{PPh}_3)_2\text{Me}$ with CO.

3.4.3.1 Thermal reaction with CO

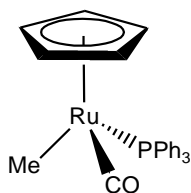
An NMR tube was charged with 5 mg of $\text{CpRu}(\text{PPh}_3)_2\text{Me}$ in d_8 -toluene. The tube was degassed and pressurised with 1.5 bar CO. ^1H and $^{31}\text{P}\{^1\text{H}\}$ NMR spectra were recorded for the sample to demonstrate a reaction had taken place when compared with subsequently recorded spectra. The sample was heated to 323 K for 24 hours to enable the complex to react thermally with the substrate.

Comparison of the $^{31}\text{P}\{^1\text{H}\}$ NMR spectra showed the presence of a single new product resonance, δ 63.9, and a resonance consistent with liberated PPh_3 , demonstrating that mono phosphine substitution has taken place. A connection was made through the ^{31}P signal to a new resonances at δ 0.79 (d, 5.3), 4.91 and 7.78 in the ^1H NMR spectrum, which is consistent with the protons of a methyl group, Cp ring, and *ortho*-phenyl protons, respectively. The integrals of methyl and Cp signals correlate in a ratio of 3:5, confirming the location of these resonances in the same complex. The doublet splitting of the methyl resonance indicates that a single phosphine ligand is coordinated to the ruthenium centre. The δ 4.91 signal also connected to signals at δ 7.78, 7.33 and 7.31, which are again consistent with aryl protons, indicating that PPh_3 ligand is coordinated to the complex. This left one coordination site unaccounted for, owing to the liberation of one of the PPh_3 ligands.

In order to determine whether this site was occupied by a coordinated CO ligand, a ^{13}C NMR spectrum was recorded. This spectrum was compared to the spectrum recorded previously for $\text{CpRu}(\text{PPh}_3)_2\text{Me}$, to identify new product peaks. New peaks at δ 140.3, 133.9, 128.0, 129.5 and 201.4 were found and identified, using $^1\text{H}/^{13}\text{C}$ HMQC and ^1H COSY experiments, as resonance belonging to the Cp, and the *ipso*, *ortho*, *meta* and *para* carbons of the coordinated PPh_3 ligand. A doublet resonance was therefore left unaccounted for at δ 201.4 (Figure 3.15), which is the region typically associated with resonances belonging to metal-bound CO ligands. Figure 3.15 shows the connection between the methyl ^{13}C peak and the corresponding proton signal, via a $^1\text{H}/^{13}\text{C}$ HMQC.

This suggests that the complex is the mono-substituted carbonyl derivative, $\text{CpRu}(\text{PPh}_3)(\text{CO})\text{Me}$ (Figure 3.15).

Figure 3.15 Structure of $\text{CpRu}(\text{PPh}_3)(\text{CO})\text{Me}$



The lack of a second singlet in the Cp region of the ^1H NMR spectrum or a singlet resonance $\delta \sim 200$ in the ^{13}C NMR spectrum, suggests that the fully substituted CO complex, $\text{CpRu}(\text{CO})_2\text{Cl}$ has not been formed.

Figure 3.16 $^{13}\text{C}\{^1\text{H}\}$ NMR focusing on the doublet carbonyl signal

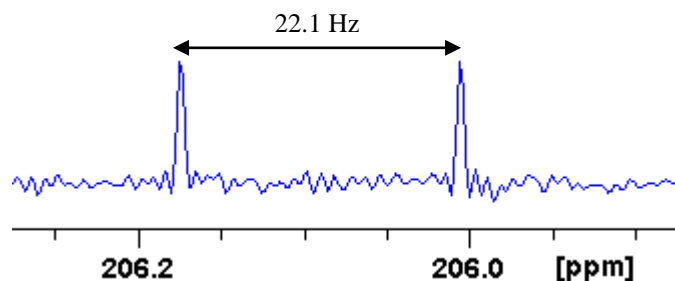
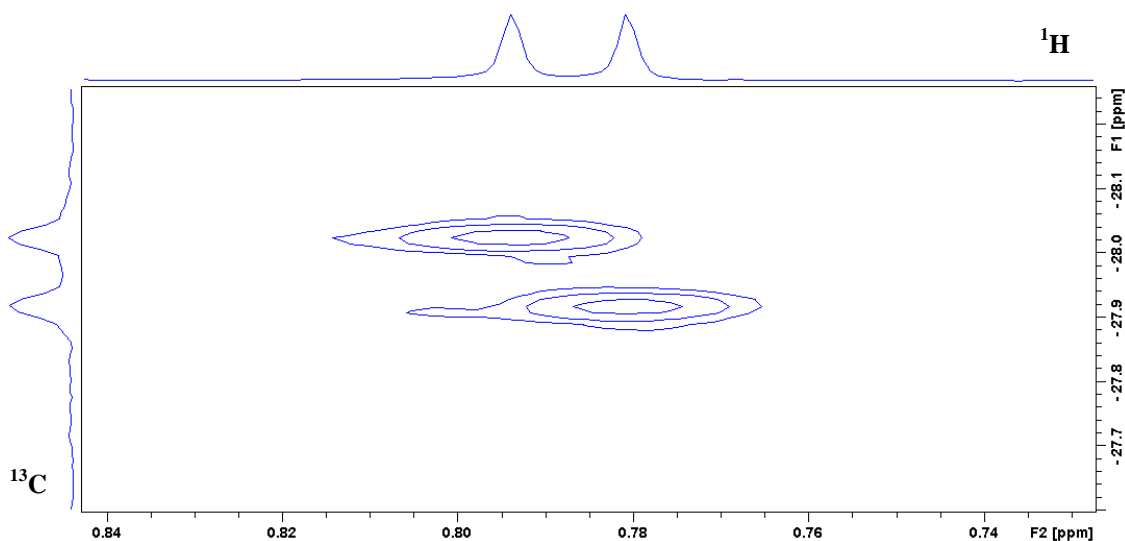


Figure 3.17 $^1\text{H}/^{13}\text{C}$ HMQC of Methyl moiety of $\text{CpRu}(\text{PPh}_3)(\text{CO})\text{Me}$



Consequently it was concluded that only mono substitution is possible under these conditions.

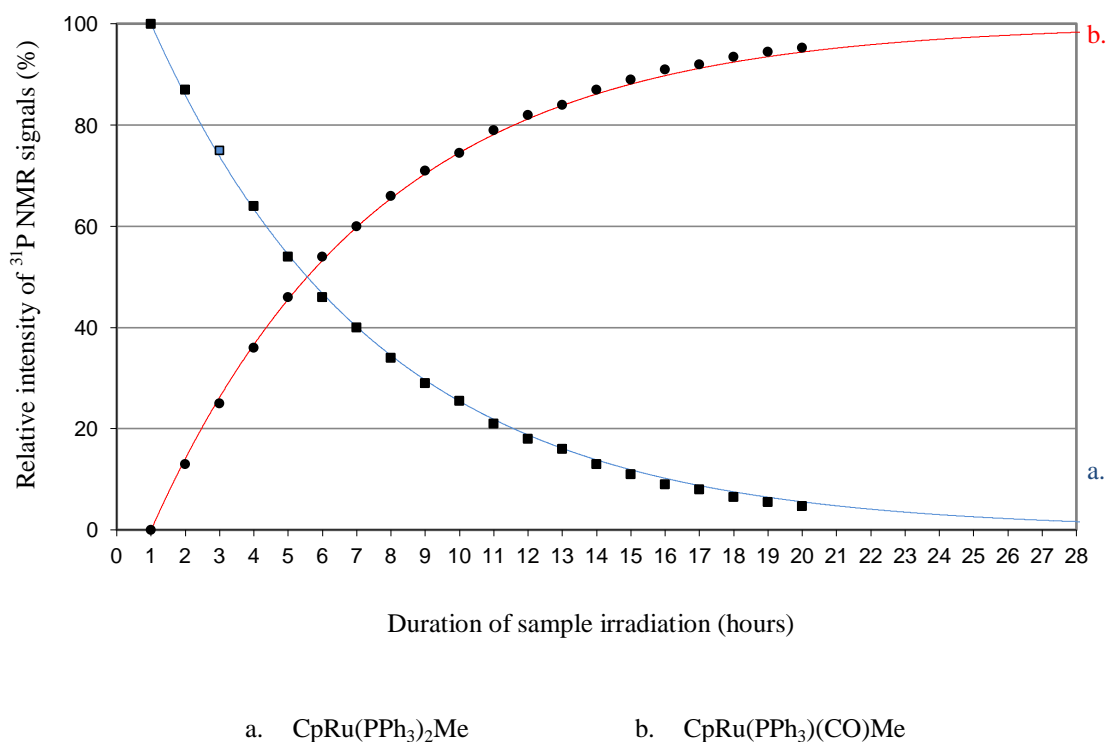
3.4.3.2 Photochemical reaction with CO

An NMR tube was charged with $\text{CpRu}(\text{PPh}_3)_2\text{Me}$ in d_8 -toluene. The tube was degassed and pressurised with 1.5 bar CO. ^1H and $^{31}\text{P}\{^1\text{H}\}$ NMR spectra were recorded of the sample to demonstrate a reaction had taken place when compared with subsequently recorded spectra. The sample was irradiated for 12 hours at room temperature using the broadband UV Lamp set-up.

A single new resonance was found in the subsequent $^{31}\text{P}\{^1\text{H}\}$ NMR spectrum at δ 63.9, which is consistent with the previously-characterised complex, $\text{CpRu}(\text{PPh}_3)(\text{CO})\text{Me}$. This is further supported by the presence of free phosphine, indicated by the peak at δ -6.4, which matches the intensity expected for the loss of a single triphenylphosphine ligand from the parent complex.

No evidence was again found for the formation of $\text{CpRu}(\text{CO})_2\text{Me}$. Upon extended photolysis 100 % conversion could be achieved with no evidence for further reaction. When the same reaction was undertaken at 198 K, $\text{CpRu}(\text{PPh}_3)(\text{CO})\text{Me}$ was still the only product detected. Figure 3.18 depicts the time plot for this reaction, which has a $T_{1/2}$ of 320 minutes. For this process no insertion product was observed, suggesting that CO coordination occurs on a faster timescale than the orthometallation process, following loss of phosphine. The lack of any signals corresponding to $\text{CpRu}(\text{PPh}_3)(\text{THF})\text{Me}$ demonstrates that CO binds more strongly than THF. The k_{obs} constant for this process ($\text{CpRu}(\text{PPh}_3)_2\text{Me} \rightarrow \text{CpRu}(\text{PPh}_3)(\text{CO})\text{Me}$) was found to be 0.152 s^{-1} .

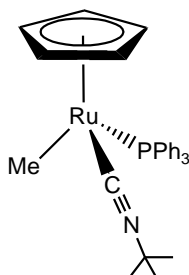
Figure 3.18 A plot of the relative ^{31}P resonances over time, for the photochemically formed products of the reaction between $\text{CpRu}(\text{PPh}_3)_2\text{Me}$ and CO , at 193 K (original illustration appears in colour)



3.4.4 Reactions with $^t\text{BuNC}$

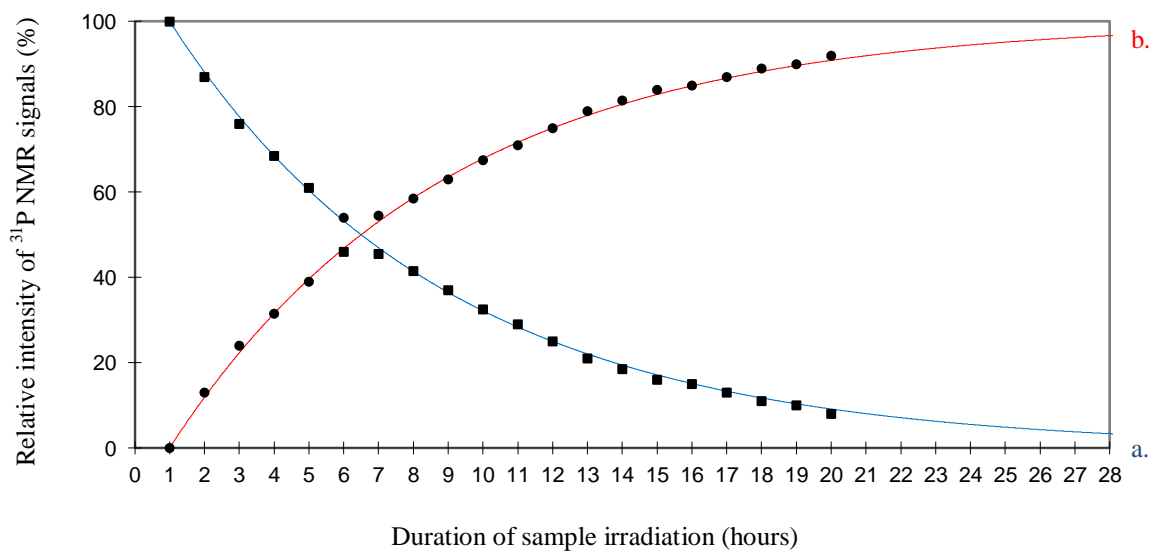
A related two electron donor to CO for which the concentration in solution can be increased is $^t\text{BuNC}$.

An NMR tube was therefore charged with $\text{CpRu}(\text{PPh}_3)_2\text{Me}$ in d_8 -toluene. The tube was degassed and $^t\text{BuNC}$ was added. The sample was heated to 323 K for 24 hours and the reaction monitored by NMR spectroscopy. The selective formation of $\text{CpRu}(\text{CN}^t\text{Bu})(\text{PPh}_3)\text{Me}$ was again found. NMR data for this species is presented in Table 3.11. Similar selectivity was obtained in both 298 K and 198 K irradiation studies.

Figure 3.19 Structure of $\text{CpRu}(\text{PPh}_3)(\text{CNBu}^t)\text{Me}$ 

The photochemical conversion of $\text{CpRu}(\text{PPh}_3)_2\text{Me} \rightarrow \text{CpRu}(\text{PPh}_3)(\text{CNBu}^t)\text{Me}$, is similar to the previous experiment with CO, as coordination of $^t\text{BuNC}$ occurs prior to orthometallation, hence no C-H bond activation or insertion products were observed. The process was found to have a k_{obs} of 0.126 s^{-1} and a $T_{1/2}$ of 390 minutes.

Figure 3.20 A plot of the relative ^{31}P resonances over time, for the photochemically formed products of the reaction between $\text{CpRu}(\text{PPh}_3)_2\text{Me}$ and $^t\text{BuNC}$, at 193 K (original illustration appears in colour)



a. $\text{CpRu}(\text{PPh}_3)_2\text{Me}$

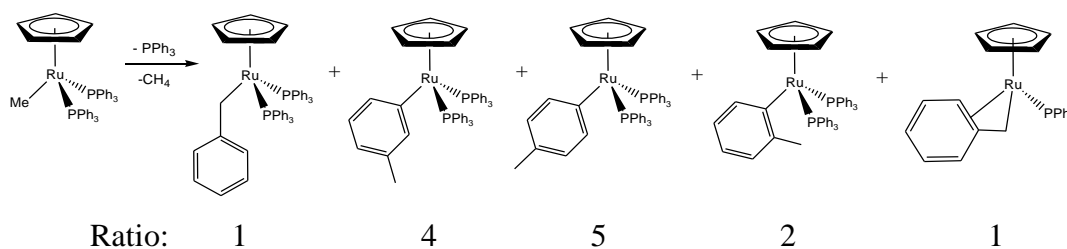
b. $\text{CpRu}(\text{PPh}_3)(\text{CNBu}^t)\text{Me}$

3.4.5 Photolysis with arenes

The activation of the CH bond of an arene is now a relatively common reaction in inorganic chemistry. The products are not always stable due to reductive elimination. Section 3.4.2.3 demonstrates that C-H bond activation by the $\text{CpRu}(\text{PPh}_3)_2\text{Me}$ fragment is feasible.

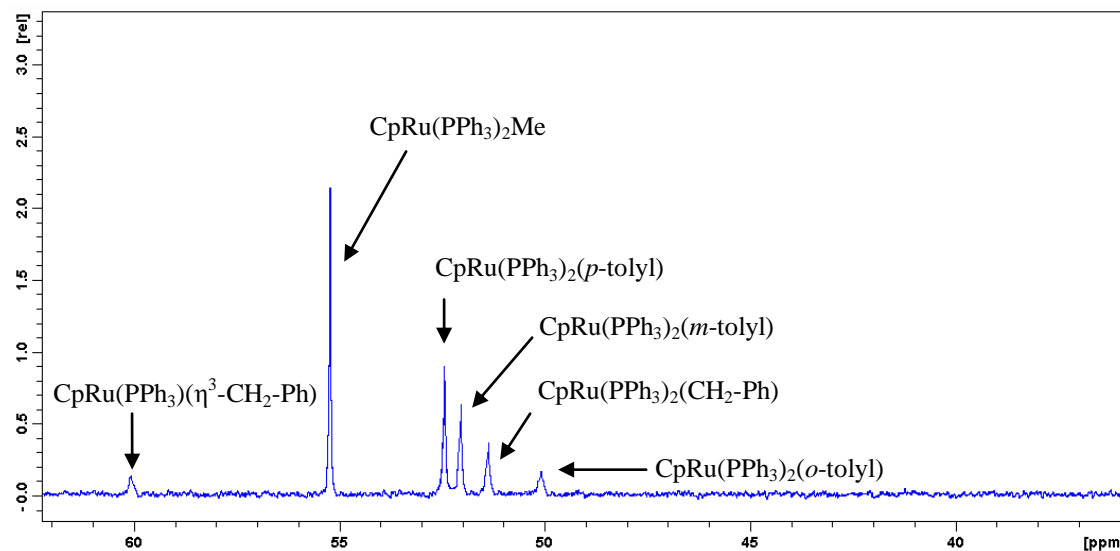
UV Irradiation of a sample of $\text{CpRu}(\text{PPh}_3)_2\text{Me}$ in protio toluene for 6 hours led to the formation of five products as determined by the formation of new ^{31}P resonances at δ 51.6, 52.0, 52.3, 52.6 and 60.3, in a $^{31}\text{P}\{^1\text{H}\}$ NMR experiment. In order to fully characterise these products, the sample was irradiated for a further 20 hours to improve the conversion ratio of the starting material to the products. Following irradiation, the protio toluene was removed *in vacuo*, and the sample was redissolved in d_8 -toluene. The ^{31}P signals at δ 52.0, 52.3, 52.6 were determined by NMR techniques to correspond to the *ortho*, *meta* and *para* activated toluene complexes respectively (Figure 3.22). Full NMR characterisation of these complexes appears in Tables 3.12, 3.13 and 3.14. Illustrations and the corresponding product ratios of these complexes are found in Figure 3.20.

Figure 3.21 Photochemical products of reaction of $\text{CpRu}(\text{PPh}_3)_2\text{Me}$ with toluene



The ^{31}P peaks at δ 51.6 and 60.3 correspond to the complexes $\text{CpRu}(\text{PPh}_3)_2(\text{CH}_2\text{Ph})$ and $\text{CpRu}(\text{PPh}_3)(\eta^3\text{-CH}_2\text{Ph})$, the former of these complexes has been previously described in the literature,²¹⁸ with partial NMR characterisation. Both of these complexes have been characterised fully, and are discussed in further detail in Chapter 5. No trace of peaks corresponding to the orthometallated complex, $\text{CpRu}(\kappa^2\text{-2-C}_6\text{H}_4\text{PPh}_2)(\text{PPh}_3)$, was found in the NMR spectra.

Figure 3.22 $^{31}\text{P}\{^1\text{H}\}$ NMR spectrum showing the ^{31}P signals of the activated toluene products



Previously the thermal reactivity of $\text{CpRu}(\text{PPh}_3)_2\text{Me}$ with toluene has been explored by Lehmkuhl *et al.*²¹⁸ He observed a series of tolyl C-H activation products: *meta*, *para* and benzyl, which can be seen in Figure 3.21, though the *ortho* and η^3 products have not been observed. In such reactions η^2 -arene intermediates have been indicated, however these are less stable for benzene than naphthalene.

3.4.5.1 Reactions with naphthalene

Owing to the inability of benzene to coordinate to the 16 electron ruthenium centre of $\text{CpRu}(\text{PPh}_3)_2\text{Me}$ (when a sample containing benzene was prepared and irradiated using an analogous method to the toluene reaction), and produce a stable complex at 198 K, naphthalene was considered as a replacement. Naphthalene has been shown by others to coordinate in an η^2 fashion^{13, 189} to several metal centres in an analogous way to benzene. However, the additional aromatic ring increases the thermal stability of the η^2 coordination product by offsetting the loss in resonance stabilisation energy. It might therefore be expected that such a product would be observable by NMR spectroscopy.

3.4.5.2 Thermal reactions with naphthalene

A sample of containing $\text{CpRu}(\text{PPh}_3)_2\text{Me}$ was prepared in d_8 -toluene, to which naphthalene was added. The resulting NMR tube, fitted with a Young's tap, was degassed and placed under N_2 . ^1H and $^{31}\text{P}\{^1\text{H}\}$ NMR spectra were recorded prior to heating this sample. These revealed diagnostic peaks for $\text{CpRu}(\text{PPh}_3)_2\text{Me}$ at δ 0.97 and 4.35 in the ^1H NMR spectrum and δ 55.3 in the $^{31}\text{P}\{^1\text{H}\}$ NMR spectrum. The fact the $^{31}\text{P}\{^1\text{H}\}$ NMR spectrum contained only a singlet peak confirms the purity of the starting compound. This sample was heated to 323 K and left to react over the next 24 hours. Further ^1H and $^{31}\text{P}\{^1\text{H}\}$ NMR spectra were recorded at this stage and compared with those previously obtained. No change in the NMR spectra was found.

The sample was then heated to the higher temperature of 353 K for a further 24 hours. The resulting NMR spectra again confirmed that no reaction had taken place. The previous experiments with PET_3 (Section 3.4.1) reveal that phosphine dissociation from $\text{CpRu}(\text{PPh}_3)_2\text{Me}$ occurs at this temperature. This suggests therefore that the coordination of naphthalene may lead to a thermally unstable product. In order to explore this hypothesis, the reaction of $\text{CpRu}(\text{PPh}_3)_2\text{Me}$ with naphthalene was then re-examined at low temperature using UV irradiation to drive the initial PPh_3 loss step, and stabilise any formed products.

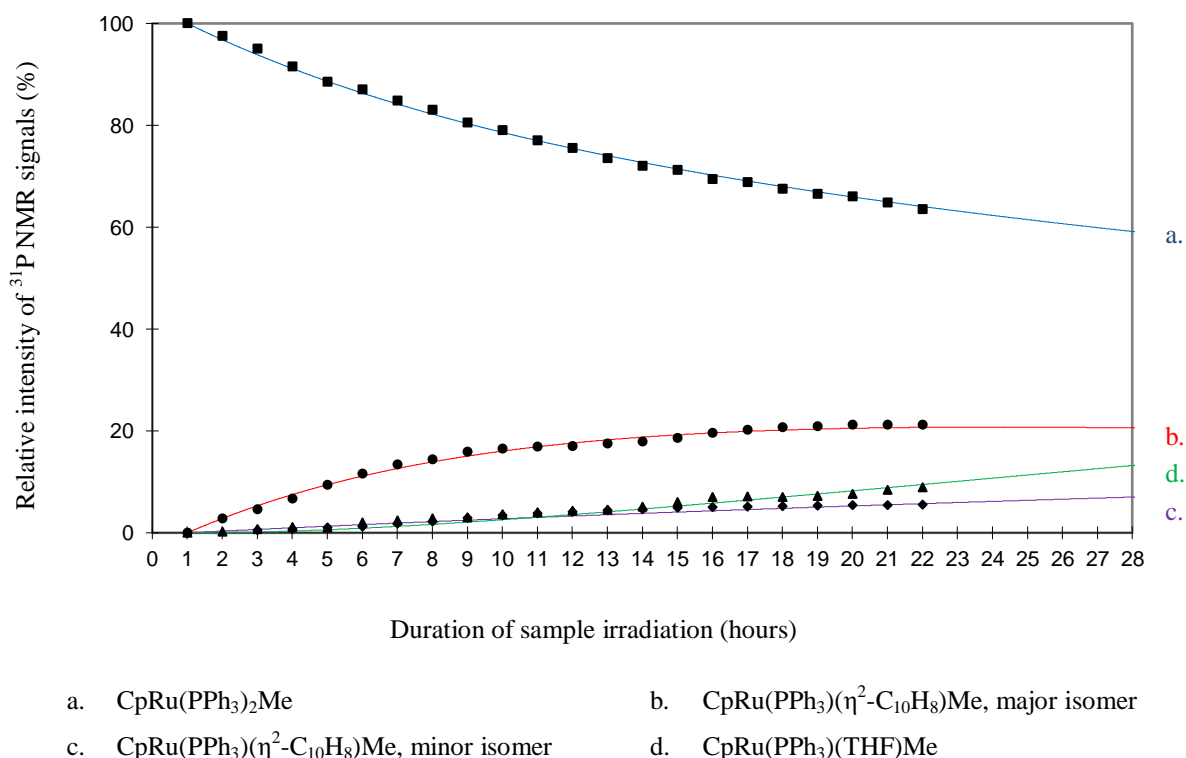
3.4.5.3 Photochemical reaction with naphthalene

An analogous sample of $\text{CpRu}(\text{PPh}_3)_2\text{Me}$ and naphthalene to that described in Section 3.4.5.2 was prepared and cooled to 198 K. Naphthalene was found to precipitate from this d_8 -toluene solution at temperatures below 243 K. As a consequence the solvent was changed to d_8 -THF, which while costing far more, is superior to toluene because it cannot coordinate through an aromatic ring in an η^2 fashion. The corresponding control reaction with $\text{CpRu}(\text{PPh}_3)_2\text{Me}$ and d_8 -THF alone is described in Section 3.4.2.1. The sample contained a 3 fold excess of naphthalene relative to $\text{CpRu}(\text{PPh}_3)_2\text{Me}$ and was irradiated using a He-Cd laser *in situ* at 198 K. The irradiation period was 18 hours, the limit of the cold N_2 source, which aimed to ensure maximum conversion to products. During this process, the progress of the photochemical reaction was monitored using both ^1H and $^{31}\text{P}\{^1\text{H}\}$ NMR experiments which were recorded every 12 minutes. In the

^{31}P NMR spectra, the singlet at δ 55.3 for $\text{CpRu}(\text{PPh}_3)_2\text{Me}$ reduced in intensity while three new singlet peaks grew in at δ 63.2, 62.8 and 61.3 (in a ratio of 4:2:1). The latter of these resonance was attributed to the THF adduct $\text{CpRu}(\text{PPh}_3)(\text{THF})\text{Me}$ described in Section 3.4.2.1.

The chart shown in Figure 3.23 presents the change in relative intensities of these peaks as a function of the irradiation time. The corresponding ^1H NMR spectra contained characteristic C_5H_5 resonances which also vary in a similar way. The plot suggests that naphthalene is a weakly coordinating ligand, yet more stable in one of its isomers compared with the complex, $\text{CpRu}(\text{PPh}_3)(\text{THF})\text{Me}$, which is formed during this reaction. The products are formed directly from $\text{CpRu}(\text{PPh}_3)_2\text{Me}$, and show no interconversion between the formed species. The k_{obs} for these three processes are 0.091 s^{-1} ($\text{CpRu}(\text{PPh}_3)_2\text{Me} \rightarrow \text{CpRu}(\text{PPh}_3)(\eta^2\text{-C}_{10}\text{H}_8)\text{Me}$ – major isomer), 0.059 s^{-1} ($\text{CpRu}(\text{PPh}_3)_2\text{Me} \rightarrow \text{CpRu}(\text{PPh}_3)(\eta^2\text{-C}_{10}\text{H}_8)\text{Me}$ – minor isomer) and 0.035 s^{-1} ($\text{CpRu}(\text{PPh}_3)_2\text{Me} \rightarrow \text{CpRu}(\text{PPh}_3)(\text{THF})\text{Me}$).

Figure 3.23 A plot of the relative ^{31}P resonances over time, for the photochemically formed products of the reaction between $\text{CpRu}(\text{PPh}_3)_2\text{Me}$ and C_{10}H_8 , at 193 K (original illustration appears in colour)

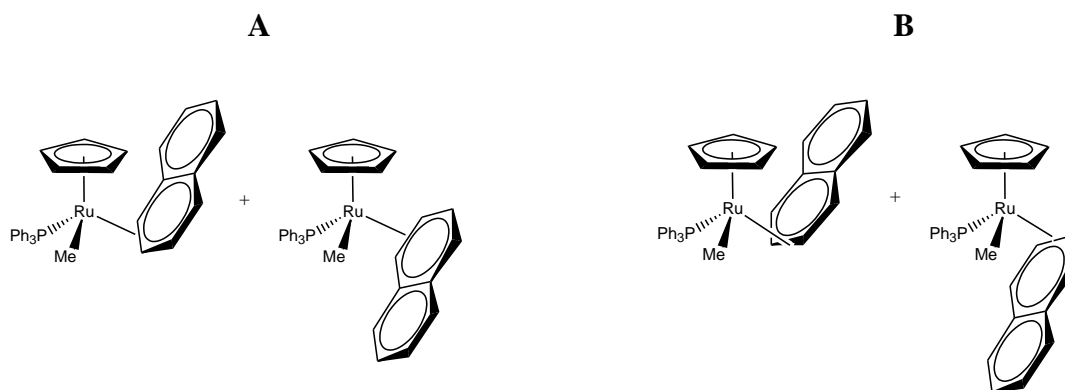


A $^1\text{H}/^{31}\text{P}$ HMQC experiment was then recorded to connect these ^{31}P signals to their proton coupling partners. The δ 63.2 resonance connected to ^1H signals at δ 4.55 and 0.95 (d, 5.8 Hz) which are consistent with the resonances expected for protons of a coordinated cyclopentadienyl ring and a ruthenium bound methyl group (respectively). The ^{31}P resonance at δ 62.8 was also observed to couple to two proton signals at δ 4.51 and 0.89 (d, 5.8 Hz). These four proton signals split into pairs of resonances with a 20:8 ratio, which is in accordance with the recorded ^{31}P data. The nature of the doublet splitting for the methyl resonance in each instance reveals that each of these complexes possess only one coordinated triphenylphosphine ligand, which is responsible for the $|^3J_{\text{PH}}|$ coupling.

Analysis of the recorded ^1H NMR spectra during the photochemical reaction also revealed the growth of a series of new peaks in the range δ 6.4 and δ 6.9 that are also diagnostic of a bound naphthalene ring. However, the overlap of these signals with those of the triphenylphosphine and free naphthalene resonances made the characterisation of these complexes using ^1H COSY and 2D NOE experiments difficult.

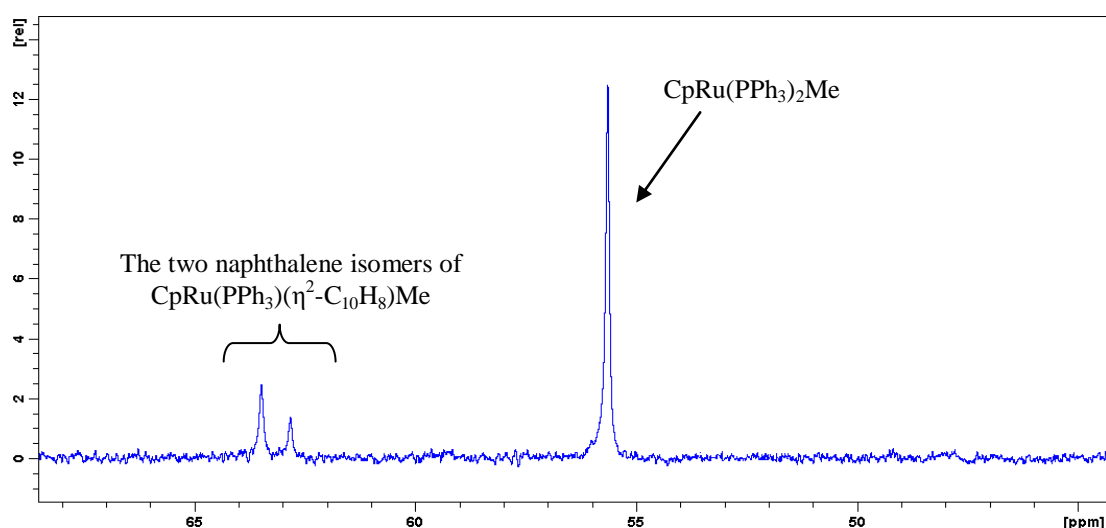
The 2D NOE spectra did, however, reveal two small, connected, signals between the δ 4.13 and δ 4.55 resonances which would be consistent with an interaction between the Cp ring and naphthalene proton. This is consistent with structure **A** (Figure 3.24), based on the NMR characterisation of similar $\text{Cp}^*\text{Rh}(\eta^2\text{-C}_{10}\text{H}_7)\text{PMe}_3$ complexes.²¹⁹ The yield of the second isomer (**B**) was insufficient to allow a similar measurement to be made. There was no evidence for isomer interconversion in the EXSY data.

Figure 3.24 Feasible binding modes of the naphthalene ligand to the ruthenium centre



Surveys of the literature show that coordination of naphthalene occurs predominantly at the 1,2 positions (Figure 3.24, **A**),²²⁰⁻²²² with the 2,3 coordination mode being far less common (Figure 3.24, **B**), with only one reported stable example.²²³ It is far more likely that both of the isomers for this complex coordinate through the 1,2 positions, with the naphthalene moiety orientated in different directions, relative to the metal centre, to produce resonances for the two isomers in the ^1H and $^{31}\text{P}\{^1\text{H}\}$ NMR spectra. Jones *et al.* have previously considered the possible orientations of the naphthalene moiety for the complex.²²⁴ More recent studies by Duckett *et al.* have shown using NMR techniques that $\text{Cp}^*\text{Rh}(\eta^2\text{-C}_2\text{H}_4)(\eta^2\text{-naphthalene})$ adopts two isomeric forms, through coordination of the naphthalene by the 1,2 positions to the rhodium centre.²²⁵ The results obtained by Duckett *et al.* likely mirror those obtained here (the formation of two distinct isomers) for $\text{CpRu}(\text{PPh}_3)(\eta^2\text{-naphthalene})\text{Me}$. However, owing to the relatively low conversion to the second naphthalene product, all of the resonances associated with the non-coordinating ring cannot be found. This prevents the collection of information regarding the position of the coordinated naphthalene using NOE NMR techniques. There were no signals indicative of the formation of $\text{CpRu}(\text{PPh}_3)_2(\text{C}_{10}\text{H}_7)$ in these low temperature experiments. The formation of $\text{CpRu}(\text{PPh}_3)(\eta^2\text{-C}_{10}\text{H}_8)\text{Me}$ however indicates that trapping of the 16-electron fragment $\text{CpRu}(\text{PPh}_3)\text{Me}$ by naphthalene prior to orthometallation is feasible. It has already been shown that PEt_3 fulfils the same role.

Figure 3.25 $^{31}\text{P}\{^1\text{H}\}$ NMR spectrum showing the relative conversion of $\text{CpRu}(\text{PPh}_3)_2\text{Me}$ to the two isomeric forms of $\text{CpRu}(\text{PPh}_3)(\eta^2\text{-C}_{10}\text{H}_8)\text{Me}$



3.4.6 Reactions with ethene

When $\text{CpRu}(\text{PPh}_3)_2\text{Me}$ was photolysed in d_8 -THF, with ethene a new product was formed. This complex was readily characterized using NMR techniques. It can be inferred from the literature that the product $\text{CpRu}(\text{PPh}_3)\text{Me}(\eta^2\text{-C}_2\text{H}_4)$ is stable at room temperature. However, low temperature photolysis will be employed here to ensure that only substitution of one of the triphenylphosphine ligand occurs, to produce $\text{CpRu}(\text{PPh}_3)\text{Me}(\eta^2\text{-C}_2\text{H}_4)$ in maximum abundance. This also minimises the possibility of forming the C-H activated side-product, $\text{CpRu}(\text{PPh}_3)(\text{C}_2\text{H}_4)\text{C}(\text{H})=\text{CH}_2$, which would be analogous to the Cp^* derivative, previously reported in the literature by Lehmkuhl.¹⁹⁴ Low temperature characterisation of the complex by a variety of NMR techniques will secure the detailed structural characterization of this product. Normally, bound ethene ligands are detected as highly fluxional and give broad resonances in the corresponding ^1H NMR spectra, which lack structural information. Low temperature studies using selective NOE experiments were therefore planned to determine both the rate of rotation of ethene ligand and its orientation.

The expected product of the reaction, $\text{CpRu}(\text{PPh}_3)\text{Me}(\eta^2\text{-C}_2\text{H}_4)$ has previously been reported as a partially characterized reaction product in the literature.²²⁶ However the method described here uses forcing conditions (50-150 bar of ethene at 373 K), whereas our proposed alternative procedure, using UV irradiation of the sample to initiate a reaction, would produce the same products under milder conditions.

3.4.6.1 Thermal reactions with ethene

A 5 mm J-Y NMR tube containing 5 mg of $\text{CpRu}(\text{PPh}_3)_2\text{Me}$ in d_8 -THF was pressurized with 1.5 bar of ethene. Initial ^1H and $^{31}\text{P}\{^1\text{H}\}$ NMR spectra were recorded prior to warming the sample at 323 K. These spectra were compared with those which were subsequently recorded after 24 hours, and show no new resonances. This indicates that no reaction has taken place under these thermal conditions.

Further warming of the sample to 353 K for 24 hours also lacks the formation of any new product peaks in the NMR spectra. This lack of thermal reactivity is similar to the

previously discussed reaction of $\text{CpRu}(\text{PPh}_3)_2\text{Cl}$ with ethene (Chapter 2, Section), and so attempts to induce reactivity by photochemical means was attempted.

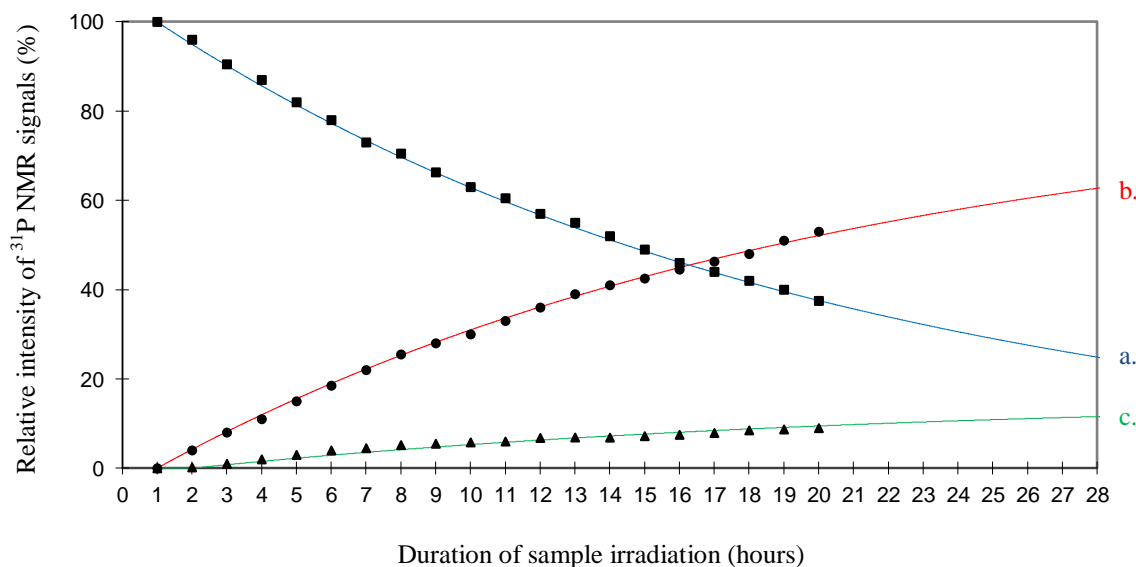
3.4.6.2 Photochemical reactions with ethene

A 5 mm J-Y NMR tube containing 5 mg of $\text{CpRu}(\text{PPh}_3)_2\text{Me}$ in d_8 -THF was pressurized with 1.5 bar of ethene. Initial ^1H and $^{31}\text{P}\{^1\text{H}\}$ NMR spectra were recorded prior to photolysis, which revealed diagnostic peaks for $\text{CpRu}(\text{PPh}_3)_2\text{Me}$ at δ 55.3 in the ^1H NMR spectrum and δ 55.3 in the $^{31}\text{P}\{^1\text{H}\}$ NMR spectrum. The sample was then irradiated at 325 nm using the He-Cd laser source for 18 hours, using the *in situ* NMR laser set-up at 198 K. The progress of the reaction was monitored by recording ^1H and $^{31}\text{P}\{^1\text{H}\}$ NMR spectra every 12 minutes.

In these ^{31}P NMR spectra, the singlet at δ 55.3 for $\text{CpRu}(\text{PPh}_3)_2\text{Me}$ reduced in intensity while three new peaks grew in at δ -6.4, δ 67.7 and δ 61.3. The latter of these resonance was attributed to the THF adduct $\text{CpRu}(\text{PPh}_3)(\text{THF})\text{Me}$ described in Section 3.4.2.3 and referred to in the introduction to this reaction while the former is due to free PPh_3 .

The chart showed in Figure 3.26 presents the change in relative intensities of these peaks as a function of the irradiation time. Those ^{31}P signals of free PPh_3 and $\text{CpRu}(\text{PPh}_3)(\text{THF})\text{Me}$ grow in at the same time. The corresponding ^1H NMR spectra contained characteristic C_5H_5 and Me resonances for $\text{CpRu}(\text{PPh}_3)(\text{THF})\text{Me}$. The k_{obs} for the two processes were determined: 0.429 s^{-1} ($\text{CpRu}(\text{PPh}_3)_2\text{Me} \rightarrow \text{CpRu}(\text{PPh}_3)(\text{C}_2\text{H}_4)\text{Me}$) and 0.009 s^{-1} ($\text{CpRu}(\text{PPh}_3)_2\text{Me} \rightarrow \text{CpRu}(\text{PPh}_3)(\text{THF})\text{Me}$), with a $T_{1/2}$ of 960 minutes for ($\text{CpRu}(\text{PPh}_3)_2\text{Me} \rightarrow \text{CpRu}(\text{PPh}_3)(\text{C}_2\text{H}_4)\text{Me}$). This shows again, as for the previous experiment with naphthalene, that ethene is a better ligand than THF, for which only a relatively small quantity of the corresponding THF coordination product, $\text{CpRu}(\text{PPh}_3)(\text{THF})\text{Me}$, for this experiment is formed.

Figure 3.26 A plot of the relative ^{31}P resonances over time, for the photochemically formed products of the reaction between $\text{CpRu}(\text{PPh}_3)_2\text{Me}$ and C_2H_4 , at 193 K (original illustration appears in colour)

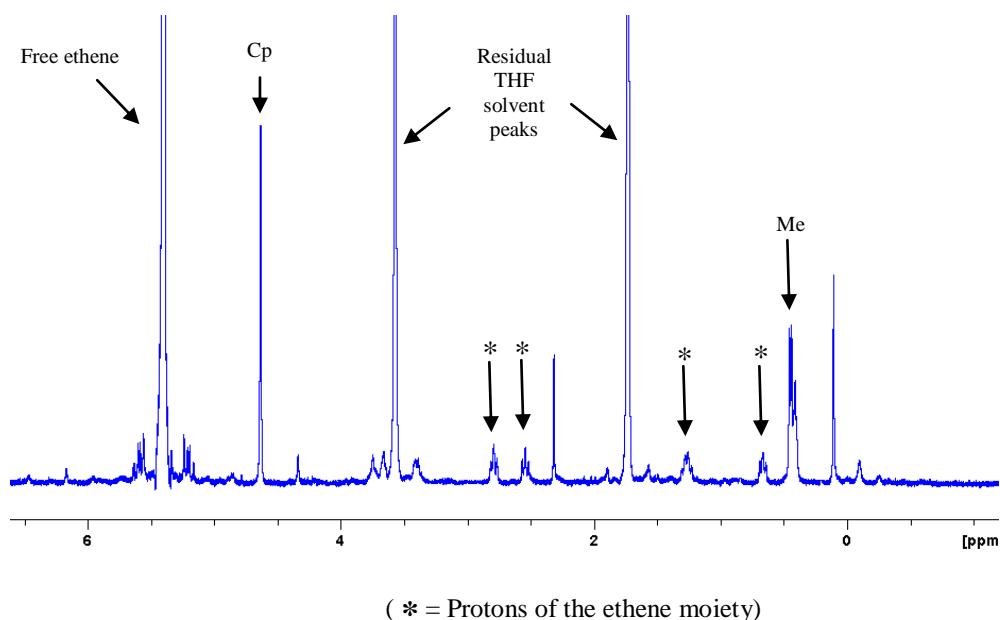


a. $\text{CpRu}(\text{PPh}_3)_2\text{Me}$

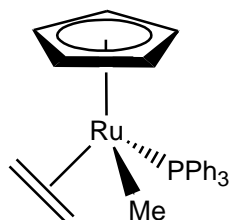
b. $\text{CpRu}(\text{PPh}_3)(\text{C}_2\text{H}_4)\text{Me}$

c. $\text{CpRu}(\text{PPh}_3)(\text{THF})\text{Me}$

Comparison of the initial ^1H NMR spectrum with that recorded after 4 hours of photolysis shows the formation of a new resonance at δ 4.63 in the “Cp region”. Four new peaks at δ 0.67, 1.28, 2.54 and 2.81 (multiplets) were also found, these were likely to represent the inequivalent protons of the η^2 bound ethene in $\text{CpRu}(\text{PPh}_3)\text{Me}(\eta^2\text{-C}_2\text{H}_4)$. A ^1H COSY experiment was employed to show coupling between these four proton resonances. A final proton resonance was found at δ 0.43 (d, 6.7 Hz due to the methyl protons of $\text{CpRu}(\text{PPh}_3)(\eta^2\text{-C}_2\text{H}_4)\text{Me}$ (Figure 3.28). These six resonances are consistent with those expected for $\text{CpRu}(\text{PPh}_3)(\eta^2\text{-C}_2\text{H}_4)\text{Me}$ where alkene rotation is restricted by the low temperature (Figure 3.26).

Figure 3.27 ^1H NMR spectrum for $\text{CpRu}(\text{PPh}_3)(\text{C}_2\text{H}_4)\text{Me}$ at 198K

A $^1\text{H}/^{31}\text{P}$ HMQC experiment connected the δ 67.7 ^{31}P signal to the four ethene proton resonances, the methyl, the Cp signal, and a new *ortho* phenyl proton signal at δ 133.2. A $^1\text{H}/^{13}\text{C}$ HMQC experiment located the corresponding ^{13}C data while examination of the COSY located the phenyl group signals. These signals are listed in Table 3.18.

Figure 3.28 Structure of $\text{CpRu}(\text{PPh}_3)(\eta^2\text{-C}_2\text{H}_4)\text{Me}$ 

A ^1H NMR recorded at 233 K shows broadened resonances for the ethene protons, indicating that the *trans* pairs of ethene protons may undergo exchange of their magnetic environment, at this temperature, as the η^2 -ethene ligand rotates. To confirm this, a selective NOE experiment was employed. Selective irradiation of the signal at δ 0.67 showed transfer of magnetisation to the signal at 2.54 ppm. This shows that the protons belonging to these resonances are positioned *trans* to each other. No link was observed to the Cp resonance, while a link to the methyl protons was observed. This

suggests that this proton lies away from the Cp ring and is orientated closer to the methyl protons. No evidence for products resulting from methyl migration was found.

3.4.6.3 Determination of the rate of rotation for the η^2 -ethene moiety

The ethene moiety of $\text{CpRu}(\text{PPh}_3)(\eta^2\text{-C}_2\text{H}_4)\text{Me}$ is also labile to rotation, even at low temperatures. This rotation was evidenced by an NOESY NMR experiment which showed the exchange of magnetisation between the proton signals of the bound ethene group (this rotation is depicted in Figure 3.29). The delay, d_8 – the mixing time, in the NOESY NMR pulse sequence (Chapter 1, Figure 1.36) may be varied in order to allow more transfer of magnetisation between the peaks. The data obtained for the mixing time vs the intensity of the exchanging ethene protons, may be plotted and the rate of rotation at that temperature may be calculated. Therefore, by varying the temperature and the mixing time of the experiment, the activation energy to the rotation of this ligand may be calculated. Table 3.1 Summarises the data obtained for the temperatures between 203 K and 235 K and their corresponding rate constants.

Figure 3.29 Ethene rotation in $\text{CpRu}(\text{PPh}_3)(\eta^2\text{-C}_2\text{H}_4)\text{Me}$ (original in colour)

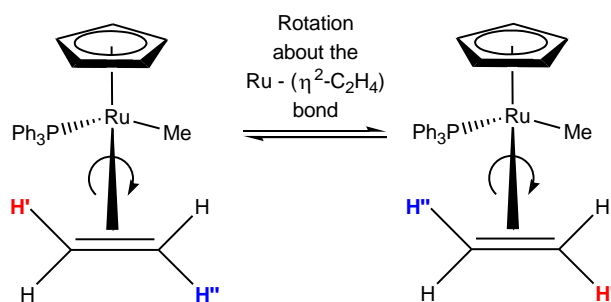


Table 3.1 The exchange rates for the ethene rotation at varying temperatures

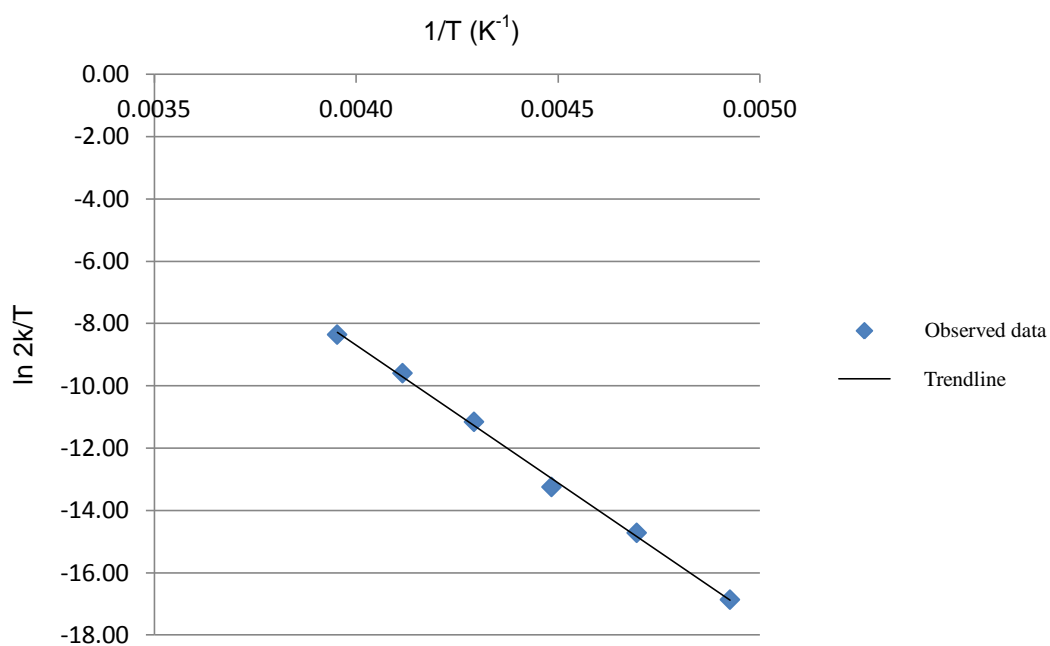
T / K	1/T / K ⁻¹	k / s ⁻¹	ln2k/T
253	3.95 × 10 ⁻³	2.96 × 10 ⁻²	-8.36
243	4.12 × 10 ⁻³	8.24 × 10 ⁻³	-9.60
233	4.29 × 10 ⁻³	1.66 × 10 ⁻³	-11.16
223	4.48 × 10 ⁻³	1.96 × 10 ⁻⁴	-13.25
213	4.70 × 10 ⁻³	4.30 × 10 ⁻⁵	-14.72
203	4.93 × 10 ⁻³	4.80 × 10 ⁻⁶	-16.87

Based on the data obtained, the inverse of the temperature and the natural log of the rate divided by the temperature can be determined for each of the temperatures employed (Table 3.1). These values can be used to determine the activation enthalpy (ΔH^\ddagger) and activation entropy (ΔS^\ddagger) of the exchange process, using the Eyring equation (Equation 3.1). Pictorially, this is shown in the Eyring plot (Figure 3.30). It should be noted that $\ln 2k/T$ was used in place of $\ln k/T$ owing to the equal chance of a reverse or forward progression of the rotation, from the transition state.

$$\text{Equation 3.1} \quad \ln \frac{k}{T} = \frac{-\Delta H^\ddagger}{R} \cdot \frac{1}{T} + \ln \frac{k_B}{h} + \frac{\Delta S^\ddagger}{R}$$

T = temperature
R = gas constant
k_B = Boltzmann constant
h = Planck's constant
 ΔH^\ddagger = activation enthalpy
 ΔS^\ddagger = activation entropy

Figure 3.30 Eyring plot for the rate of rotation of for the ethene moiety $\text{CpRu}(\text{PPh}_3)(\eta^2\text{-C}_2\text{H}_4)\text{Me}$



Equation 3.2

$$\Delta G^\ddagger = \Delta H^\ddagger - T\Delta S^\ddagger$$

ΔH^\ddagger = activation enthalpy

ΔS^\ddagger = activation entropy

ΔG^\ddagger = activation entropy

Table 3.2 summarises the parameters obtained for the rotation of the ethene moiety in this present complex.

Table 3.2 Parameters for the rotation of the ruthenium-bound ethene

$\Delta H^\ddagger / \text{kJ mol}^{-1}$	$\Delta S^\ddagger / \text{kJ mol}^{-1}$	$\Delta G^\ddagger_{300} / \text{kJ mol}^{-1}$
72.9 ± 3.0	21.7 ± 4.0	66.4 ± 0.8

3.4.7 Reactions with DMSO

Based on the sigma coordination of THF with the [CpRu(PPh₃)Me] fragment, a similar low temperature reaction with DMSO was carried out, to determine whether coordination through the oxygen was possible. DMSO has been shown to coordinate to metal centres through either the oxygen or sulfur of the molecule. This experiment should also show whether one or the other coordination modes is preferred in this system.^{227, 228}

3.4.7.1 Photochemical reaction with DMSO

The potential for DMSO to act as a ligand was explored through low temperature *in situ* UV photolysis, within a 400 MHz NMR spectrometer. A sample of CpRu(PPh₃)₂Me in d₈-THF with DMSO, was irradiated using a He-Cd laser for 18 hours. The temperature of the sample was maintained at 198 K and ¹H and ³¹P{¹H} NMR spectra were recorded at 12 minute intervals as the sample was irradiated.

After 4 hours of irradiation a single new resonance was observed in the ³¹P{¹H} NMR spectrum at δ 59.0, which is consistent with the formation of a single new product. New peaks were observed in the ¹H NMR spectrum at δ 4.43, and -0.02 (d, 5.8 Hz) in addition to two singlet peaks at δ 2.37 and 2.56. A ¹H/³¹P HMQC experiment showed a connection from the ³¹P signal at δ 59.0 to the resonance at δ 4.43 and the two peaks at δ 2.37 and 2.56, which represent the resonances belonging to protons of the cyclopentadienyl ring and those of the DMSO methyl groups, respectively. The methyl resonance clearly appears as a doublet, which indicates that only one triphenylphosphine ligand is present within the complex, which is responsible for the coupling observed to this proton resonance. The presence of a free phosphine resonance (δ -6.4) in the ³¹P{¹H} NMR spectrum also supports that this complex possesses a single phosphine ligand.

A connection was seen from the ³¹P signal δ 59.0 to peaks at δ 7.56, 7.34 and 7.32 in the ¹H/³¹P HMQC, which are characteristic resonances of the *ortho*, *meta* and *para* protons of the triphenylphosphine rings of the bound triphenylphosphine ligand. These three phenyl protons were observed to mutually couple to each other through the use of a ¹H COSY experiment.

Selective NOE interrogation of the resonances at δ 4.43 and -0.02 (Cp and methyl protons), showed a mutual coupling in both cases to the two previously mentioned proton resonances at δ 2.37 and 2.56. Integration of these peaks reveals that they have the intensity of three protons, when compared with the five proton intensity of the cyclopentadienyl resonance. These peaks represent the methyl protons of the two magnetically inequivalent methyl protons of a coordinated dimethylsulphoxide (DMSO) ligand. Individual NOE interrogation of the methyl proton resonances showed that the resonance at δ 2.37 had a stronger connection to the protons of the ruthenium bound methyl group, suggesting that these two methyl groups are orientated close to each other, within the structure. Both of the methyl resonances couple strongly to the cyclopentadienyl proton resonances, suggesting that the orientation of the bound DMSO ligand lies with the methyl groups positioned 'upward' towards that cyclopentadienyl ring.

DMSO is known to bind in two coordination modes, and it has been previously demonstrated²²⁹ that NMR techniques may be employed to determine whether coordination proceeds through the sulfur or oxygen moieties of the ligand. A $^1\text{H}/^{13}\text{C}$ HMQC was used to connect the methyl resonances at δ 2.37 and 2.56 to two carbon signals at δ 46.5 and 48.2. The literature states that the ^{13}C chemical shifts of the methyl carbons of the bound ligand will change relative to the ^{13}C resonances for the methyl carbons of the free DMSO (observed to be δ 40.1 in d_8 -THF). This relative downfield field shift in the chemical shift indicates that the DMSO ligand is coordinated to the ruthenium centre through the sulfur atom (Figure 3.31). No evidence for a bis-substituted product was found. The time plot for this reaction is shown in Figure 3.31, and has a corresponding $T_{1/2}$ value of 960 minutes. The absence of a C-H bond activation product shows that DMSO coordinates to the metal centre faster than the orthometallation process. The absence of $\text{CpRu}(\text{PPh}_3)(\text{THF})\text{Me}$ shows that DMSO is a better coordination ligand than THF.

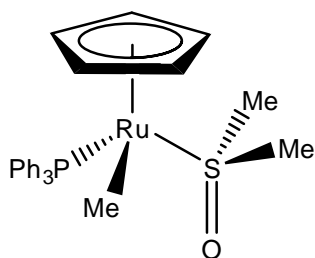
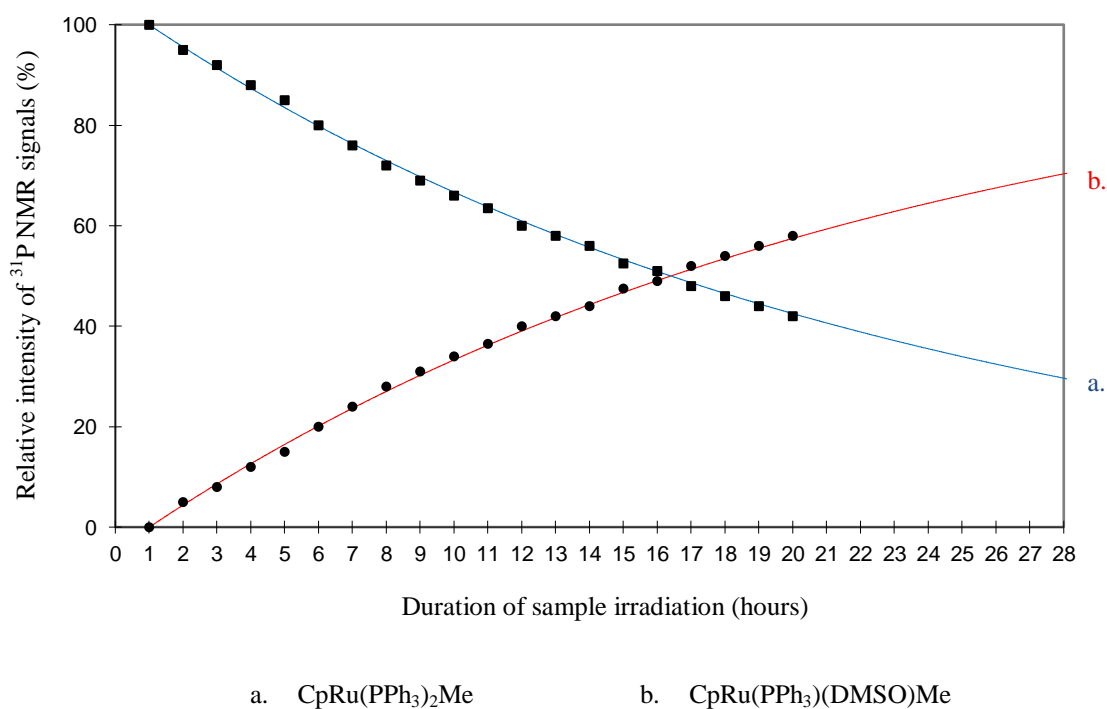
Figure 3.31 Structure of $\text{CpRu}(\text{PPh}_3)(\text{S}(\text{O})\text{Me}_2)\text{Me}$ 

Figure 3.32 A plot of the relative ^{31}P resonances over time, for the photochemically formed products of the reaction between $\text{CpRu}(\text{PPh}_3)_2\text{Me}$ and DMSO, at 193 K (original illustration appears in colour)



3.4.8 Reactions with pyridine

3.4.8.1 Thermal reactions with pyridine

A J-Y tap NMR tube was charged with $\text{CpRu}(\text{PPh}_3)_2\text{Me}$ and dissolved in $d_8\text{-THF}$, to a depth of 4 cm, pyridine was then added to the sample. Initial ^1H and $^{31}\text{P}\{^1\text{H}\}$ NMR spectra were recorded prior to beginning the thermal reaction. The sample tube was heated to 323 K in a silicone oil bath for 24 hours.

A new singlet resonance was found in the recorded $^{31}\text{P}\{^1\text{H}\}$ NMR spectrum at δ 54.7. This ^{31}P signal was found to couple to ^1H NMR signals at δ 4.64, 7.00 and 7.51, through a $^1\text{H}/^{31}\text{P}$ HMQC NMR experiment. The signals at δ 4.64 and 7.51 have relative integrations in a ratio of 5:12, which indicates that these signals belong to the cyclopentadienyl protons and the *ortho*-phenyl protons of this new complex. The relative integration of 12 for the *ortho*-phenyl signal indicates that two triphenylphosphine ligands are coordinated to the ruthenium centre. The remaining resonance at δ 7.00 connects through a ^1H COSY experiment to three additional signals at δ 6.89, 7.21 and 8.48, which are consistent with the signals expected for an activated pyridine ring. The complex is therefore identified as $\text{CpRu}(\text{PPh}_3)_2(\text{pyridyl})$, and full characterisation of this complex by NMR is presented in Table 3.21.

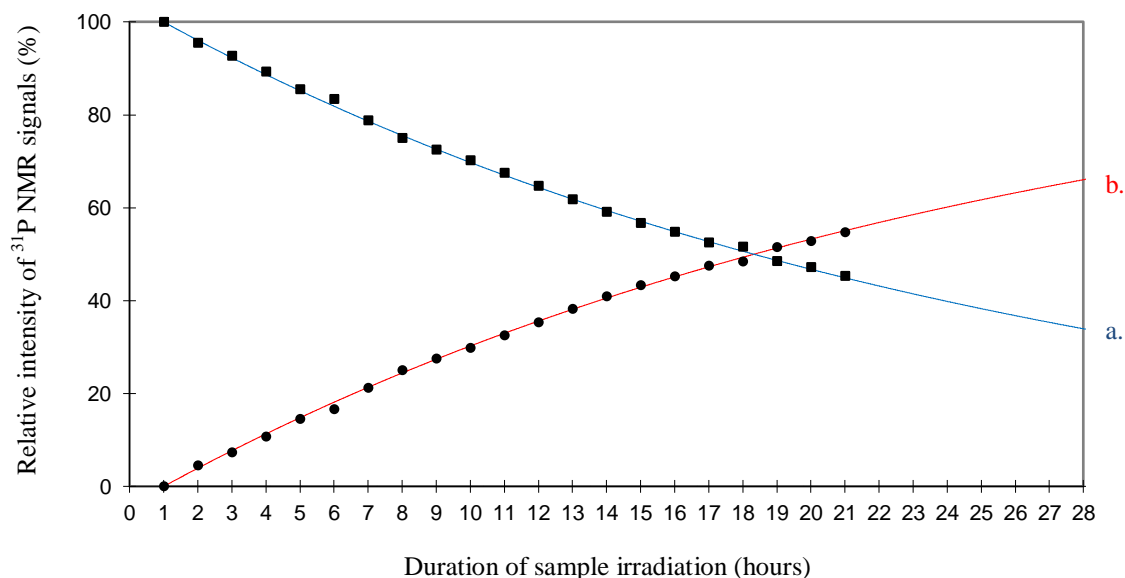
3.4.8.2 Photochemical reactions with pyridine

To a sample of $\text{CpRu}(\text{PPh}_3)_2\text{Me}$ in $d_8\text{-THF}$, an equimolar quantity of pyridine was added. The sample was then irradiated at 198 K using a He-Cd laser for a total duration of 18 hours. ^1H and $^{31}\text{P}\{^1\text{H}\}$ NMR spectra were recorded at intervals of every 12 minutes.

After 4 hours of sample irradiation a single new peak was visible in the recorded $^{31}\text{P}\{^1\text{H}\}$ spectrum at δ 68.3 with a matching amount of free phosphine being formed. Several new peaks were clearly visible in the corresponding ^1H NMR spectrum, including those at δ 4.16 and 0.30 (d, 6.1 Hz). These peaks are consistent with the resonances of the protons of the cyclopentadienyl ring and methyl protons (respectively) of a new complex. These ^1H proton signals were observed to couple to the ^{31}P

resonance, through the use of a $^1\text{H}/^{31}\text{P}$ HMQC experiment. The methyl proton resonance appears as a doublet, indicating that only one triphenylphosphine ligand is present within this new complex, which is responsible for splitting this proton resonance.

Figure 3.33 A plot of the relative ^{31}P resonances over time, for the photochemically formed products of the reaction between $\text{CpRu}(\text{PPh}_3)_2\text{Me}$ and $\text{C}_5\text{H}_5\text{N}$, at 193 K (original illustration appears in colour)



a. $\text{CpRu}(\text{PPh}_3)_2\text{Me}$

b. $\text{CpRu}(\text{PPh}_3)(\text{Py})\text{Me}$

In the ^{31}P NMR spectra, the singlet at δ 55.3 for $\text{CpRu}(\text{PPh}_3)_2\text{Me}$ reduced in intensity while a new peak grew in at δ 68.3. The lack of a signal at δ 61.3 (attributed to the THF adduct $\text{CpRu}(\text{PPh}_3)(\text{THF})\text{Me}$) shows that the coordination strength of the pyridine is greater than that of the surrounding THF. The chart showed in Figure 3.33 presents the change in relative intensities of these peaks as a function of the irradiation time, with a $T_{1/2}$ value of 360 minutes. The corresponding ^1H spectra contained characteristic C_5H_5 resonances which also vary in a similar way. Despite the thermal instability of the complex $\text{CpRu}(\text{PPh}_3)(\text{Py})\text{Me}$, which is similar to $\text{CpRu}(\text{PPh}_3)(\text{THF})\text{Me}$, no evidence for the formation of the latter complex was found in this reaction. This suggests that pyridine is a better coordination ligand than THF.

The $^1\text{H}/^{31}\text{P}$ HMQC also shows coupling to a proton signal at δ 7.25 which are characteristic of a phenyl proton within a ruthenium bound triphenylphosphine ligand. A ^1H COSY experiment revealed mutual coupling between this peak and two other peaks at δ 7.16 and 7.09. These peaks are consistent with those of protons of a triphenylphosphine's phenyl rings and may therefore be identified as *ortho* (δ 7.25), *meta* (δ 7.16), and *para* (δ 7.09) phenyl protons.

Additional comparisons of the ^1H spectrum obtained prior to low temperature photolysis and those acquired during, show the growth of a new peak at δ 6.80. This peak mutually coupled to two other peaks at δ 7.45 and 8.59, via a ^1H COSY experiment. The later of these peaks is overlapped by the proton resonances for free pyridine.

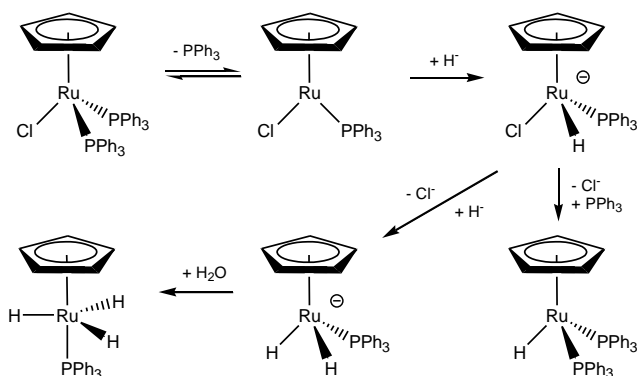
The close proximity of the chemical shifts of the bound pyridine protons lead to the overlap of some peaks. This suggests that the pyridine is bound through the nitrogen, rather than coordination the ruthenium centre through a double bond.²³⁰ Double bond coordination would lead to further differentiation of the proton signals from each other, resulting in five clearly distinct proton signals. The similarity of the proton signals for the bound pyridine ligand are similar to those observed for those of free pyridine, further demonstrating that the pyridine is bound to the ruthenium centre through nitrogen.

As shown in Figure 3.33, a peak corresponding to $\text{CpRu}(\text{PPh}_3)(\text{THF})\text{Me}$ is absent, to determine where this complex acts as a precursor to the coordinated pyridine complex, $\text{CpRu}(\text{PPh}_3)(\text{Py})\text{Me}$, a sample of $\text{CpRu}(\text{PPh}_3)(\text{THF})\text{Me}$ was prepared as described in Section 3.4.2.1. This sample was removed from the *in situ* photolysis set-up, with the low temperature maintained by submerging the base of the tube in a dry ice / acetone bath. An excess of pyridine was added to this sample, which was then thoroughly degassed and placed back into the NMR spectrometer at 193 K. Photolysis of this sample showed the decrease in the ^{31}P peak at δ 61.3 ($\text{CpRu}(\text{PPh}_3)(\text{THF})\text{Me}$) with the gradual increase of peak at δ 68.3 ($\text{CpRu}(\text{PPh}_3)(\text{Py})\text{Me}$).

3.4.9 Reactions with H₂

Following the ability of the [CpRu(κ^2 -2-C₆H₄PPh₂)] fragment to activate aromatic compounds and THF, oxidative addition reactions of hydrogen with the fragment were considered. The expected products of reaction are CpRu(PPh₃)₂H and CpRu(PPh₃)(H)₃, which have both been previously reported, with partial characterisation by NMR. Davies *et al.* have previously described CpRu(PPh₃)₂H does not readily react thermally with hydrogen to form CpRu(PPh₃)(H)₃ by phosphine loss, but proceeds through the mechanism described in Figure 3.34. This has been generally attributed to the unreactive nature of CpRu(PPh₃)₂H compared with the methyl and chloride derivatives, and requires long periods of time and / or forcing conditions in order to undergo substitution reactions.

Figure 3.34 Formation of CpRu(PPh₃)₂H and CpRu(PPh₃)(H)₃, proposed by Davies *et al.*



CpRu(PPh₃)(H)₃ has been speculated to possess two distinct possible geometries C_s and C_{3v}, for which only the latter has been confirmed to be present, using IR techniques.²³¹ Davies *et al.* also noted that exposure of a sample containing CpRu(PPh₃)(H)₃ to sunlight led to a colour change of the solution from pale yellow to dark green. However, this photochemical reaction was not further explored nor was the subsequently formed complex characterised.²³²⁻²³⁴

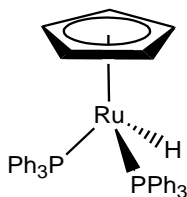
3.4.9.1 Thermal reaction with H₂

A J-Y tap containing NMR tube was charged with CpRu(PPh₃)₂Me and dissolved in d₈-THF, to a depth of 4 cm. The sample tube was pressurised to 1.5 bar with H₂. Initial ¹H and ³¹P{¹H} NMR spectra were recorded. The sample tube was heated to 323 K in a silicone oil bath for 24 hours.

Following the thermal reaction, ¹H and ³¹P{¹H} NMR experiments were recorded. A major feature of the ¹H NMR spectrum was the triplet hydride signal at δ -11.59 (t, 33.8 Hz). The ³¹P{¹H} NMR experiment clearly showed a single new phosphorus resonance at δ 68.3. Connections were made from the ³¹P signal at δ 68.3, to ¹H resonances at δ 4.49 and 7.52, using a ¹H/³¹P HMQC NMR experiment. These signals typically correspond to the proton resonances associated with a coordinated cyclopentadienyl ring and an *ortho*-phenyl proton of a coordinated triphenylphosphine ligand. For the case of the protons of the cyclopentadienyl ring, this assignment was confirmed by comparing the integrals of its associated signal with that of the hydride resonance at δ -11.59, which gave a ratio of 5:1. This ratio confirms that the signal at is produced by five protons, i.e. a cyclopentadienyl ring, and also provides information of the triplet hydride signal which by comparison is found to have an intensity of one proton. For the triplet splitting of the hydride resonance to occur, there must be two phosphine ligands coordinated to the ruthenium centre. This complex can be readily assigned as CpRu(PPh₃)₂H, which fulfils the 18 electron requirement (Figure 3.35). This characterisation agrees with the previous data obtained for this complex, when prepared synthetically (Chapter 4) and with the partial characterisation reported in the literature.

231

Figure 3.35 Structure of CpRu(PPh₃)₂H



3.4.9.2 Photochemical reaction with H₂

A 5 mm NMR tube containing CpRu(PPh₃)₂Me in d₈-THF was pressurized with 1.5 bar of H₂. Initial ¹H and ³¹P{¹H} NMR spectra were recorded prior to photolysis, which revealed diagnostic peaks for CpRu(PPh₃)₂Me at δ 55.3 in the ¹H NMR spectrum and δ 55.3 in the ³¹P{¹H} NMR spectrum. The sample was then irradiated at 325 nm using the He-Cd laser source for 18 hours, using the *in situ* NMR laser set-up at 198 K. The progress of the reaction was monitored by recording ¹H and ³¹P{¹H} NMR spectra every 12 minutes.

The subsequently recorded ³¹P{¹H} NMR spectrum show the presence of two new product peaks at δ 68.3 and 73.1. An abundance of liberated triphenylphosphine is indicated by the modest peak at δ -6.4, which suggests that one of the triphenylphosphine ligands has been liberated from the ruthenium centre to allow the coordination of hydrogen and subsequently form the product complexes.

The presence of three prominent new resonances in the hydride region of a ¹H NMR spectrum was detected: δ -9.64 (d, 19.6 Hz), -11.59 (t, 33.8 Hz) and δ -9.66 (dt, 12.8 Hz). These hydride signals were found to couple to individual ³¹P resonances via a ¹H/³¹P HMQC NMR experiment; this establishes that the signals belong to three separate products. The ¹H signals at δ -9.64 and -11.94 coupled to the ³¹P signals at δ 73.1 and 68.3, respectively, via a ¹H/³¹P HMQC experiment.

For the complex corresponding to the hydride signal at δ -9.64 and the ³¹P resonance at 73.1, a ¹H/³¹P HMQC revealed a connection to peaks at δ 4.81 and 7.73, which are consistent with the signals for protons of a cyclopentadienyl ring and the *ortho*-phenyl proton of a phenyl ring of a coordinated triphenylphosphine ligand. No connection was made to a methyl resonance in the ¹H/³¹P HMQC experiment, which suggests that the coordinated methyl moiety is absent from this complex. The doublet splitting of the hydride signal suggests that a single phosphine ligand is coordinated to the ruthenium centre. In order to determine the number of hydride protons that were present in the structure, the integrals of the cyclopentadienyl proton resonance at δ 4.81 was compared with the integral of the hydride signal at δ -9.64. This comparison gave an integral ratio of 5:3, which suggests the presence of three hydrides coordinated to the ruthenium

centre. Based on this information, the identity of the complex is likely to be $\text{CpRu}(\text{PPh}_3)(\text{H})_3$, as this assignment agrees with the partial characterisation encountered in the literature. The structure, having changed from a Ru(II) to an Ru(IV) oxidation state may adopt different geometries, as shown in Figure 3.36.

Figure 3.36 Depiction of the two possible geometries for $\text{CpRu}(\text{PPh}_3)(\text{H})_3$



Previous characterisations based on IR techniques conclude that the structure adopts a C_{3v} symmetry (as evidenced by the presence of the two peaks in the IR spectrum), which agrees with this assignment.²³¹ To confirm the identity of this complex, an IR spectrum was run on a second sample of $\text{CpRu}(\text{PPh}_3)_2\text{Me}$ and H_2 , which had been irradiated for 4 hours to ensure that $\text{CpRu}(\text{PPh}_3)(\text{H})_3$ had formed as the major product relative to the other product complexes. The IR spectrum revealed two peaks at 1998 and 2041 cm^{-1} which are consistent with those found for the C_{3v} geometry of the complex $\text{CpRu}(\text{PPh}_3)(\text{H})_3$. Full NMR characterisation of this complex is reported in Table 3.22.

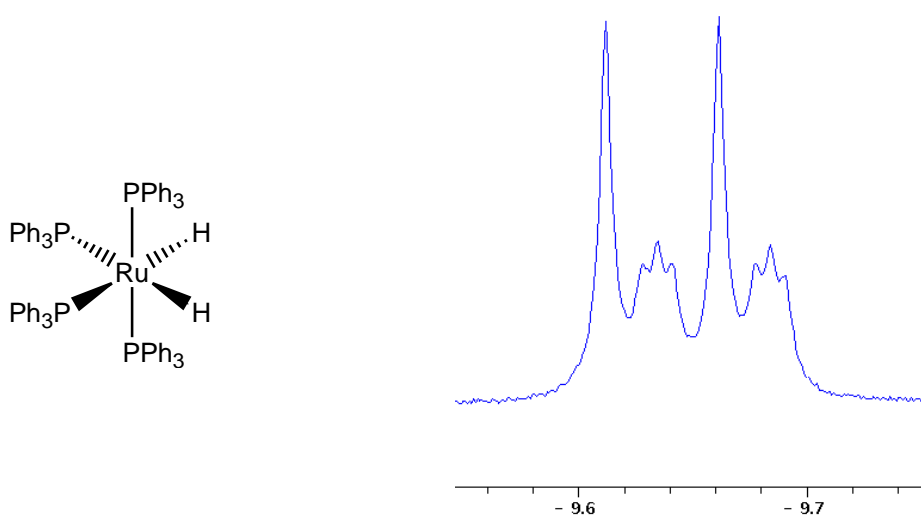
The final hydride at δ -9.66 showed no connection using $^1\text{H}/^{31}\text{P}$ HMQC NMR experiment to a ^1H signal within the cyclopentadienyl region of the NMR spectrum. Additionally, the hydride signal diminished over the time taken to characterise by NMR the other products within the sample. The loss of this product was consistent with the colour change of the sample from a deep green to pale yellow. This observation is consistent with the report made by Davies *et al.*,²³¹ however the full characterisation of this complex by NMR was not made.

Attempts to stabilise this product using low temperature for subsequent NMR characterisation proved unsuccessful, and the complex subsequently decomposed even at 198 K. Repeated UV irradiation of samples formerly containing this hydride complex

do not show the reformation of these hydride signals, indicating that neither $\text{CpRu}(\text{PPh}_3)_2\text{H}$ nor $\text{CpRu}(\text{PPh}_3)(\text{H})_3$ react with hydrogen to form this complex. Based on the minimal characterisation obtained, the presence of phosphine and hydride ligands about the metal centre can be confirmed, with a lack of a cyclopentadienyl ring.

Repeating the photochemical reaction of H_2 with $\text{CpRu}(\text{PPh}_3)_2\text{Me}$ numerous times led to the increased accumulation of NMR data for this complex. This meant that the identification of the complex could be achieved. Based on the doublet of triplets splitting for the hydride signal (Figure 3.37), the possible configurations for the complex were narrowed. The complex, *trans*- $\text{Ru}(\text{PPh}_3)_4(\text{H})_2$ (with the hydride ligands orientated in axial positions) was considered as a likely identity for the complex. However, the NMR data reported for this complex do not match with the data obtained for the present complex.^{235, 236} The *cis* derivative has not been reported in the literature, but a few similar derivatives incorporating different phosphine ligands have.²³⁷ These sources report the observation of similar hydride signals observed here in the ^1H NMR spectrum. This hydride at δ -9.66 is split into a doublet of triplets, and is consistent with that expected for *cis*- $\text{Ru}(\text{PPh}_3)_4(\text{H})_2$, based on the symmetry of this complex.

Figure 3.37 Structure of *cis*- $\text{Ru}(\text{PPh}_3)_3(\text{H})_2$, and the accompanying doublet of triplets hydride resonance (overlapped by the doublet hydride signal of $\text{CpRu}(\text{PPh}_3)(\text{H})_3$)



3.4.10 Reactions with HSiEt₃

The previous Section demonstrated that the [CpRu(κ^2 -2-C₆H₄PPh₂)] fragment photochemically forms unique H-H activated complexes compared to those formed under thermal conditions. As described in Chapter 1, H-H and H-Si bonds are readily activated by transition metal complexes, compared to the relatively more difficult C-H bond activations. Consequently, it is expected that the reaction between CpRu(PPh₃)₂Me and HSiEt₃ will form novel products under photochemical conditions.

3.4.10.1 Thermal reaction with HSiEt₃

A Young's tap capped NMR tube was charged with CpRu(PPh₃)₂Me and dissolved in d₆-benzene. Using a micro syringe an equimolar quantity of HSiEt₃ was added to the sample. Initial ¹H and ³¹P{¹H} NMR spectra were recorded prior to the thermal reaction. The sample tube was heated to 323 K in a silicone oil bath for 24 hours.

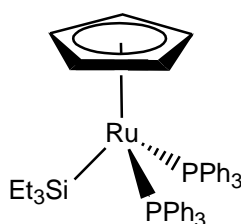
Comparison of the ³¹P{¹H} NMR recorded prior to thermal reaction and after, reveal the presence of an intense signal at δ -6.4 corresponding to free phosphine and two new signals at δ 54.4 and 58.0 (4:6). The peak at δ 55.3 corresponding to the starting material CpRu(PPh₃)₂Me was absent, indicating complete conversion to the products.

A ¹H/³¹P HMQC experiment was employed to detect coupling between the ³¹P resonance at δ 54.4 with ¹H signals. Connections were made to signals at δ 4.53 and 7.26, which correspond to the resonances of the protons of a cyclopentadienyl ring and ortho-phenyl proton of the triphenylphosphine. The resonance corresponding to the methyl moiety is absent. A ¹H-COSY experiment showed mutual coupling between the three signals at δ 7.26, 6.97 and 6.88, which are indicative of *ortho*, *meta* and *para* protons of the coordinated phosphine phenyl ring.

Proton signals at δ 1.31 and 1.19 were also found to mutually couple. Integrations of these signals were found by removing the volatiles *in vacuo* and redissolving the sample in benzene, to remove the overlapping signals present, due to free silane. The integral ratio of these peaks is 6:9 indicating that these signals belong to protons of the ethyl chains of a bound silyl moiety (CH₂ and CH₃, respectively). The CH₂ protons appear

equivalent at this temperature, owing to the single (triplet) resonance found. Confirmation of the presence of a silane ligand was found using a $^1\text{H}/^{29}\text{Si}$ HMQC experiment, which showed a connection between a ^{29}Si resonance at δ 16.0 with the two ethyl proton signals. Confirmation of the coordination of silane to the ruthenium centre was found owing to the triplet splitting (25.6 Hz) of the ^{29}Si signal, this also reveals that two phosphine ligands are coordinated to the metal centre. Based on these data, the identity of the complex is $\text{CpRu}(\text{PPh}_3)_2\text{SiEt}_3$ (Figure 3.38).

Figure 3.38 Structure of $\text{CpRu}(\text{PPh}_3)_2\text{SiEt}_3$



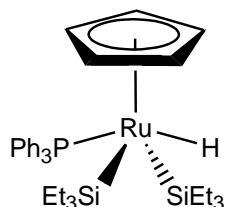
This characterisation agrees with the partial NMR characterisation reported previously by Lemke and Chaitheerapakul.²³⁸

The second ^{31}P signal at δ 58.0 was found using a $^1\text{H} / ^{31}\text{P}$ HMQC experiment to connect to three proton signals at δ -11.89, 4.76 and 7.41. The latter two signals correspond to the proton signals of a cyclopentadienyl ring and the *ortho*-phenyl protons of a coordinated phosphine ligand. The former signal is typical of a ruthenium bound hydride, which appears as a doublet (9.7 Hz). This doublet splitting indicates that only a single phosphine ligand is coordinated to the ruthenium centre which is responsible for the ^{31}P coupling.

In order to determine whether the remaining positions were filled by silyl ligands, a $^1\text{H} / ^{29}\text{Si}$ HMQC experiment was used to determine that a doublet ^{29}Si resonance (14.4 Hz) connected with two distinct proton signals at δ 0.97 and 1.15 (CH_3 and CH_2 proton signals). To conclude whether two silyl ligands were present, comparisons of the integral ratios of the cyclopentadienyl and hydride peaks were made with the peaks of the ethyl chains. The overlapping signals of the free silane were removed following the removal of the excess silane *in vacuo*. The ratio of these signals was found to confirm the presence of two coordinated silane ligands (18:5 of CH_2 to Cp). This indicates that

the proton signals of the two silanes overlap. The structure of this material is therefore assigned $\text{CpRu}(\text{PPh}_3)(\text{SiEt}_3)_2\text{H}$ (Figure 3.39), which was not previously reported by Lemke and Chaitheerapakul, for similar thermal reactions of $\text{CpRu}(\text{PPh}_3)_2\text{Me}$ with HSiEt_3 .

Figure 3.39 Structure of $\text{CpRu}(\text{PPh}_3)(\text{SiEt}_3)_2\text{H}$



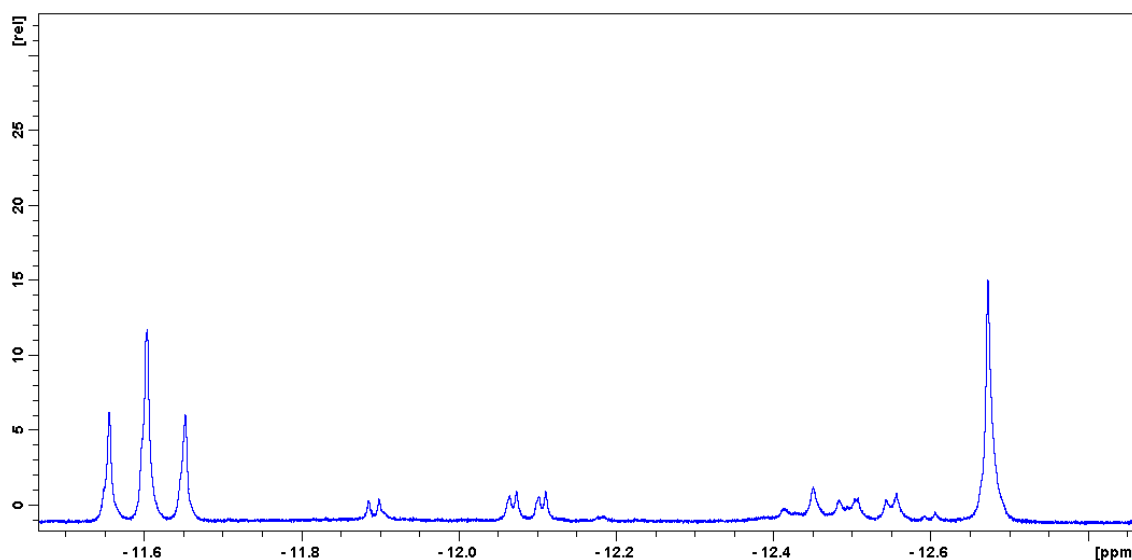
3.4.10.2 Photochemical reaction with HSiEt_3

Until now the reagents tested with $\text{CpRu}(\text{PPh}_3)_2\text{Me}$ in this thesis have bound to the ruthenium centre mainly by η^2 coordination, prior to C-H activation either by thermal decomposition or excess UV, irradiation. Thermal reactions of $\text{CpRu}(\text{PPh}_3)_2\text{Me}$ with HSiEt_3 have been described in the thesis that lead to the clean formation of $\text{CpRu}(\text{PPh}_3)_2\text{SiEt}_3$ and $\text{CpRu}(\text{PPh}_3)(\text{SiEt}_3)_2\text{H}$. UV irradiation of $\text{CpRu}(\text{PPh}_3)_2\text{Me}$ with an excess of HSiEt_3 at room temperature leads to the formation of these two previously mentioned complexes as the dominant products of reaction, but many additional minor products indicated by numerous other peaks in the ‘Cp’ region (and more notably in the ‘hydride’ region) are clearly visible in the ^1H NMR spectrum. Photolysis at low temperatures provides additional complexity to this situation. Based on the previously described results, the identity of these extra species is critical because solvent C-D bond activation is possible, as is activation of the C-H and Si-C bonds of the silane. These have precedent in the literature²³⁹ and are now described in detail.

3.4.10.3 Photolysis of $\text{CpRu}(\text{PPh}_3)_2\text{Me}$ with HSiEt_3 at 298 K

A sample of $\text{CpRu}(\text{PPh}_3)_2\text{Me}$ was dissolved in $\text{d}_8\text{-THF}$ and HSiEt_3 added. ^1H NMR integrations revealed that the ratio of $\text{CpRu}(\text{PPh}_3)_2\text{Me}$ to HSiEt_3 was 1:7 respectively. This sample was then subject to UV irradiation using the *in situ* approach for 18 hours at 294 K. The resulting ^1H NMR spectrum recorded after 36 minutes revealed the formation of two resonances in the hydride region δ -12.09 (major) and δ -12.07 (minor). These appeared as two sets of overlapping doublets that shared a common ^{31}P splitting of 24 Hz, which confirms that they each contain a single ruthenium-bound phosphorus centre (Figure 3.40).

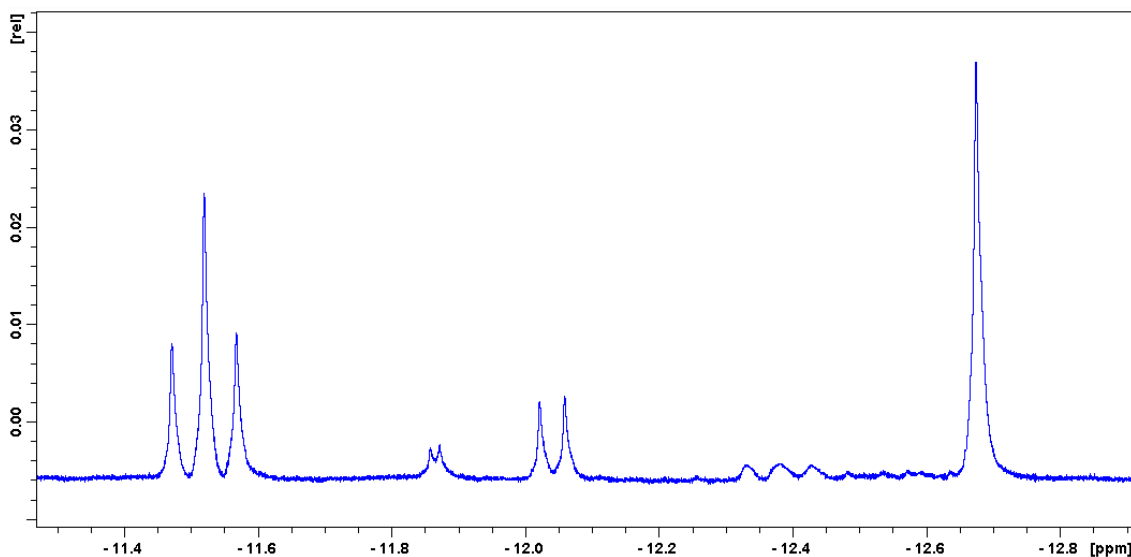
Figure 3.40 Hydride ^1H resonances for the products of the photochemical reaction of $\text{CpRu}(\text{PPh}_3)_2\text{Me}$ with HSiEt_3 in THF



When the corresponding $^1\text{H}/^{31}\text{P}$ HMQC experiment was completed the phosphorus centres providing these couplings were located as resonating at δ 72.4 and 72.9 respectively. No connection to the expected Ru-Me resonance was observed in either case. The presence of hydride signals suggests that these products are not simply formed through the activation of the deuterated solvent. It is therefore likely that the hydride comes from the silane or by orthometallation of the phenyl ring of the triphenylphosphine. Consequently products of the type $\text{CpRu}(\kappa^2\text{-}2\text{-C}_6\text{H}_4\text{PPh}_2)(\text{SiEt}_3)\text{H}$, $\text{CpRu}(\text{PPh}_3)(\text{SiEt}_3)(\text{tetrahydrofuryl})\text{H}$ and $\text{CpRu}(\text{PPh}_3)(\text{SiEt}_3)(\text{CH}_2\text{CH}_2\text{SiEt}_2)\text{H}$ (or $\text{CpRu}(\text{PPh}_3)(\text{SiEt}_3)(\text{CH}(\text{CH}_3)\text{SiEt}_2)\text{H}$) are possible. Both would provide the two isomers

necessary to account for very similar signals upon changing the solvent to d_8 -toluene and d_{12} -cyclohexane (Figure 3.41).

Figure 3.41 Hydride ^1H resonances for the products of the photochemical reaction of $\text{CpRu}(\text{PPh}_3)_2\text{Me}$ with HSiEt_3 in cyclohexane



The suggestion that solvent activation leads to the formation of the various isomers is further supported by the formation of three overlapping hydride resonances at δ -12.08, -12.09, -12.13, which possess doublet splitting of 24.5 Hz when d_8 -toluene is used as the solvent in place of d_8 -THF. The three peaks correspond to three isomers of $\text{CpRu}(\text{PPh}_3)(\text{SiEt}_3)(\text{tolyl})\text{H}$, whose tolyl moieties are bound to the metal centre through the *ortho*, *meta* and *para* positions. This assignment is consistent with other similar tolyl derivatives, such as $\text{Cp}^*\text{Rh}(\text{PMe}_3)(\text{tolyl})\text{H}$, which is formed photochemically from $\text{Cp}^*\text{Rh}(\text{PMe}_3)(\text{H})_2$ in toluene²⁴⁰ and $\text{Rh}(\text{PMe}_3)_2(\text{CO})(\text{tolyl})$ which are similarly formed from the photochemical reaction of $\text{Rh}(\text{PMe}_3)_2(\text{CO})\text{Cl}$ with toluene.^{241, 242} In each of these instances the ^{31}P NMR resonances corresponding to the separate isomers show that the formation of the *meta* bound tolyl isomer is favoured over the *ortho* and *para* variants.

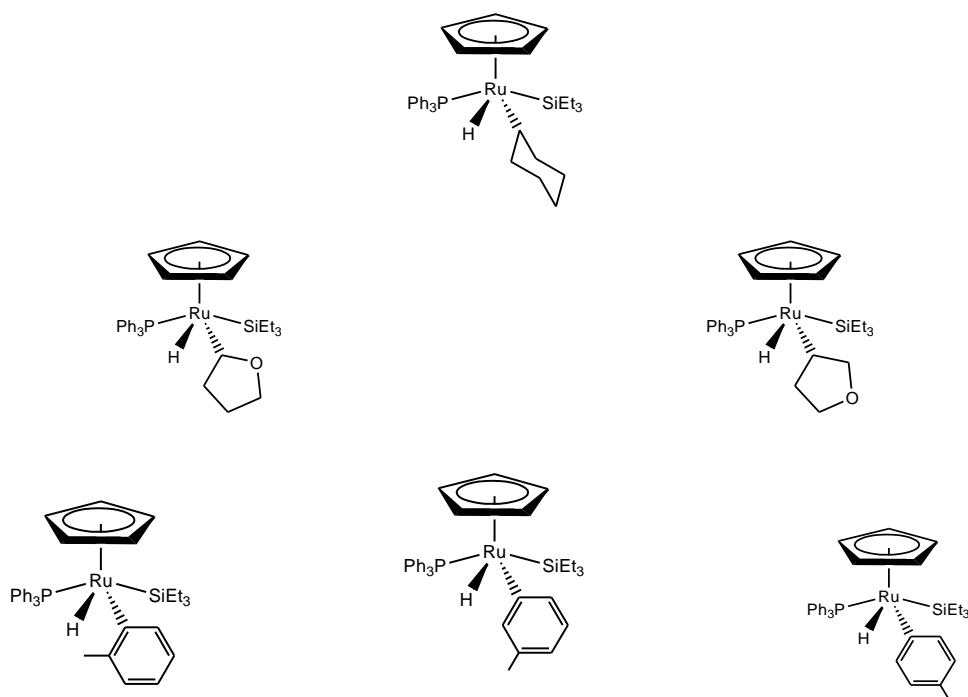
However, unlike the similar photochemical reaction of $\text{CpRu}(\text{PPh}_3)_2\text{Me}$ in toluene (discussed previously in Section 3.4.5) there is no evidence to suggest that a product formed from the C-H activation of the tolyl-methyl moiety exists. Additionally, the ^1H and $^{31}\text{P}\{^1\text{H}\}$ NMR spectra lack signs of any resonances corresponding to a ruthenium-

bound η^3 tolyl group. This suggests that $\text{CpRu}(\text{PPh}_3)\text{R}$ (where $\text{R} = \text{toluene or THF}$) the precursor complex to $\text{CpRu}(\text{PPh}_3)(\text{SiEt}_3)(\text{tolyl})\text{H}$, possess different selectivities towards the activation of the four distinct types of C-H bond in the toluene molecule, as indicated by the inherent differences in the C-H activation energies for the C-H bonds of toluene.^{243, 244} The reasons for this difference in selectivity are not yet fully understood, but may be attributed to steric effects and difference in oxidation state (Ru(II) and Ru(IV), respectively). The C-H BDE of the α -methyl protons of toluene should not cause a barrier to activation in this instance, as $\text{CpRu}(\text{PPh}_3)(\text{SiEt}_3)_2\text{H}$ is capable of activating cyclohexane (see below), which has a similar BDE to the α -methyl protons of toluene.^{245, 246} An alternative explanation lies with the M-C bond strength order, determined by Jones and Feher, which shows the increased bond stability of M-Ph over M-CH₂Ph (Figure 3.42).^{247, 248} This would imply that the $[\text{CpRu}(\text{PPh}_3)_2]$ possesses greater stability of bonds with CH₂Ph moieties than $[\text{CpRu}(\text{PPh}_3)(\text{SiEt}_3)\text{H}]$.

Figure 3.42 Relative order of M-C bond stability for metal alkane complexes, determined by Jones and Feher²⁴⁷



In order to confirm this proposal and simplify the resulting spectra, the same experiment was repeated in d₁₂-cyclohexane; fewer isomers were expected.

Figure 3.43 Structure for $CpRu(PPh_3)(SiEt_3)(R)H$ (Where $R = C_6D_{11}, C_4D_7O$ or C_7D_7)

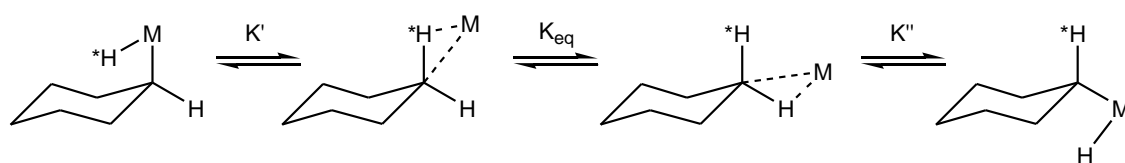
Using d_{12} -cyclohexane as a reaction solvent in place of d_8 -toluene and d_8 -THF led to the formation of only a single doublet resonance at δ 26.3. Based upon the two possible positions in which a cyclohexyl moiety may bind to the ruthenium centre (Figure 3.44), two signals were expected. It is unlikely that the cyclohexyl moiety adopts only a single orientation at the ruthenium centre, to produce a single isomer based on steric reasons. This is due to the ability of the ruthenium centre to accommodate other sterically demanding ligands, as demonstrated previously for the coordination of naphthalene. For this reason, even a small intensity signal corresponding to a second isomer would be expected. However this is not observed in any of the recorded NMR spectra for the complex. A probable explanation is that the resonances for the two isomeric forms overlap in the recorded NMR spectra.

Figure 3.44 Two possible cyclohexyl binding modes for $CpRu(PPh_3)(SiEt_3)(Cy)H$ 

The majority of the research conducted for metal-bound cyclohexyl complexes, was done by Bergman *et al.* during the 1980's for half-sandwich iridium²⁴⁹⁻²⁵¹ and rhodium²⁵² complexes. Their research lacks any mention of isomeric forms for their proposed cyclohexyl complexes. More recent work carried out by Perutz *et al.*²⁵³ describes the NMR characterisation of iridium cyclohexyl complexes, which again lack information concerning isomers, despite employing more sophisticated NMR techniques for the characterisation of the complexes. Our attempts to observe the two possible isomers of CpRu(PPh₃)(SiEt₃)(Cy)H in ³¹P{¹H} and ¹H NMR spectra, have relied on the use of progressively higher field NMR spectrometers (400 MHz, 500 MHz and 700 MHz), which would allow for a greater separation between the overlapping resonances. However, even at 700 MHz, no separation of the resonances could be made, suggesting that fluxional effects are likely to be responsible.

These fluxional effects have been recently described by Ball *et al.* in reference to the complex CpRe(PF₃)(CO)Cy.²⁵⁴ Ball suggests that the axial and equatorial protons of the bound cyclohexyl moiety (in the 'chair' configuration) produce inequivalent proton signals in a ¹H NMR spectrum, at temperatures around 190 K. This yields two separate isomers of CpRe(PF₃)(CO)Cy based on the binding position of the metal centre to the cyclohexane ring (Figure 3.45). This inherent fluxionality explains why only one set of complex signals are observed in the NMR spectra for the present activated cyclohexyl complexes. This matches the observation found in this present study, where only one set of ¹H and ³¹P{¹H} NMR resonances could be obtained for CpRu(PPh₃)(SiEt₃)(Cy)H, at 198 K.

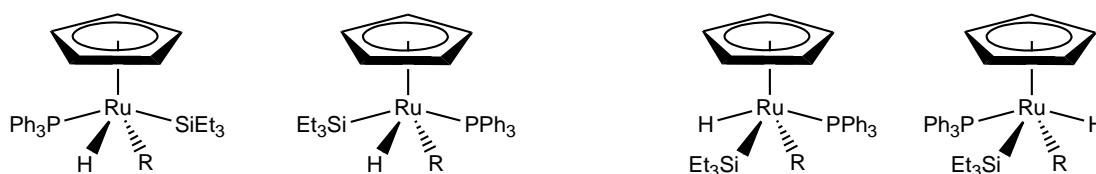
Figure 3.45 Possible equilibrium between isomers of cyclohexyl complexes, suggested by Ball *et al.*²⁵⁴



The chiral nature of the fragment [CpRu(PPh₃)Cl] was briefly described in Chapter 2, and similarly the present CpRu(PPh₃)₂Me derived complexes also display chirality. This is of particular importance for the Ru(IV) solvent activated species, for which two main

enantiomers exist with respect to the hydride and silyl moieties (Figure 3.46)

Figure 3.46 Some of the possible isomers for the stereogenic Ru(IV) centre



Were the R group and the hydride to be positioned at adjacent sites, the reductive elimination of the two ligands would be facilitated. Owing to the stability of these complexes at room temperature, the groups must be positioned opposite to each other. To confirm this, selective NOE NMR experiments were recorded. For CpRu(PPh₃)(SiEt₃)(tetrahydrofuryl)H the irradiation was targeted on the signal of the methylene protons of the coordinated silyl group. Transfer of the magnetisation, via the NOE pulse sequence to the protons of the adjacent groups, led to the observation of peaks (which are consistent with the hydride and α -tetrahydrofuryl proton signals. The irradiation centre was changed to centre on each of the other respective ligands, and their mutual neighbouring ligands were determined from the excited peaks. Centring irradiation on the hydride showed the hydride showed connections to silyl and PPh₃ *ortho*-phenyl signals, while irradiation of the *ortho*-phenyl proton led linked to the hydride and α -tetrahydrofuryl proton. Based on this assignment, the structure of the can be determined as either of the two structures denoted by an asterisk in Figure 3.46, where the hydride lies opposed to the R group. This method of structural assignment was applied to the other Ru(IV) complexes involving cyclohexyl and tolyl moieties.

3.4.10.4 Attempted synthesis of CpRu(PPh₃)₂SiEt₃

In order to access greater concentrations of these photolysis products attempts have also been made to synthesise CpRu(PPh₃)₂SiEt₃ (to provide a starting point for further photochemical reactions) by reacting ClSiEt₃ with [CpRu(PPh₃)₂]⁻ (formed by treating CpRu(PPh₃)₂Cl with a Na/Hg amalgam, see synthesis Section). However, attempts to synthesise the complex by this method have so far proved unsuccessful (the procedure was analogous to that described in Chapter 7, Section 7.2.4.8).

3.4.10.5 Photolysis of $\text{CpRu}(\text{PPh}_3)_2\text{Me}$ with HSiEt_3 at low temperature

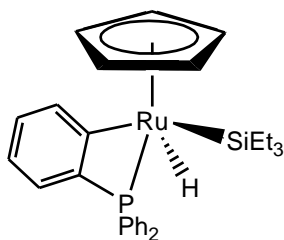
To stabilise the reaction intermediates that lead to the formation of these two hydride species, the previous reaction of $\text{CpRu}(\text{PPh}_3)_2\text{Me}$ with HSiEt_3 was repeated in d_8 -THF at 198 K. The sample was irradiated *in situ* over 18 hours using a 325 nm He/Cd laser. The sample was tracked by 1D ^1H and $^{31}\text{P}\{^1\text{H}\}$ NMR, with spectra recorded at intervals of 12 minutes.

The $^{31}\text{P}\{^1\text{H}\}$ NMR spectrum recorded after 4 hours of irradiation clearly showed the presence of a new major singlet peak at δ -16.2 which is a new species. A $^1\text{H} / ^{31}\text{P}$ HMQC experiment determined that the proton resonances at δ 7.07, 7.37, 7.74, 7.55, 7.62, 7.74, 8.09 and 4.82 connected to the ^{31}P signal at δ -16.2. The signal at δ 4.78 is characteristic of the resonance for the protons of a cyclopentadienyl ring bound to the ruthenium centre. The resonances at δ 7.09, 7.07 and 7.01 are characteristic of the *ortho*, *meta* and *para* protons of the phenyl rings of a triphenylphosphine ligand, each of these resonances were shown to couple through a ^1H COSY experiment. The resonance of these phenyl protons overlap and individual assignments for each phenyl ring could not be made at 400 MHz. The remaining four signals δ 7.55, 7.62, 7.74, 7.18 were observed to mutually couple in a ^1H COSY experiment. These signals are characteristic of the protons of an orthometallated phenyl ring of a triphenylphosphine ligand to a metal centre. The $^{31}\text{P}\{^1\text{H}\}$ NMR signal at δ -16.2 is similar to the up-field ^{31}P resonance encountered for $\text{CpRu}(\kappa^2\text{-}2\text{-C}_6\text{H}_4\text{PPh}_2)(\text{PPh}_3)$ at δ -16.9, which denotes the presence of an orthometallated triphenylphosphine ligand.

A second recorded $^1\text{H}/^{31}\text{P}$ HMQC experiment with an expanded window showed a connection between the ^{31}P δ -16.2 signal and a hydride resonance at δ -9.13 (d, 23.0 Hz). Further connections between the previously found cyclopentadienyl resonance at δ 4.82 and signals at δ 0.38, 0.54 and 0.81 were made through the use of a 2D NOE experiment. These new peaks mutually couple through a ^1H COSY experiment, and represent the CH_2 (δ 0.38 and 0.54) and CH_3 (δ 0.81) protons of the ethyl chains from a ruthenium-bound triethylsilane ligand. The CH_2 protons of the ethyl chains can be readily be distinguished from each other at sufficiently low temperatures. Hence two signals are reported for the inequivalent CH_2 protons – this was confirmed using a $^1\text{H}/^{13}\text{C}$ HMQC experiment, which demonstrated that these two signals coupled to a

single carbon resonance at δ 13.8. Following the characterisation of the sample by NMR, the new complex is identified as $\text{CpRu}(\kappa^2\text{-}2\text{-C}_6\text{H}_4\text{PPh}_2)(\text{SiEt}_3)\text{H}$.

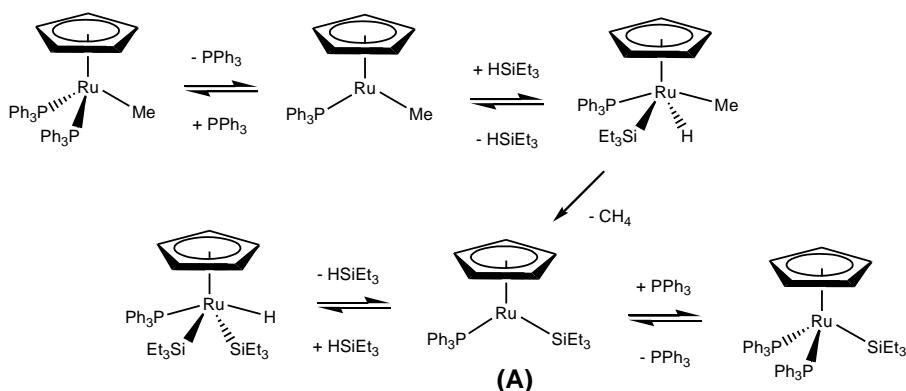
Figure 3.47 Structure of $\text{CpRu}(\kappa^2\text{-}2\text{-C}_6\text{H}_4\text{PPh}_2)(\text{SiEt}_3)\text{H}$



Warming of a sample of $\text{CpRu}(\kappa^2\text{-}2\text{-C}_6\text{H}_4\text{PPh}_2)(\text{SiEt}_3)\text{H}$ (in $d_8\text{-THF}$) from 198 K to room temperature led to the formation of the solvent-activated products, which were now deuterated.

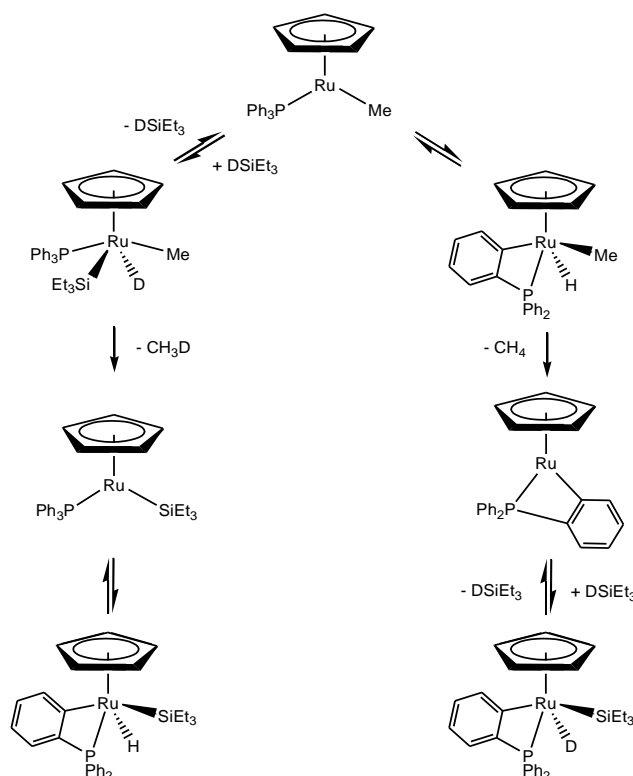
This experiment confirms that orthometallation occurs in a precursor step prior to the formation of these silane products. However, the question remains as to whether the orthometallation of the phosphine occurs prior to the Si-H activation of the silane to the ruthenium centre or vice versa. This is important as the existence of the intermediate (A) depends on the route taken; the lack of the intermediate would mean that the proposed route described previously in the literature²³⁸ (Figure 3.48), would be unlikely.

Figure 3.48 The reaction pathway proposed by Lemke et al.



The use of deuteriotriethylsilane (DSiEt₃) can be employed to confirm the order of reaction (as illustrated in Figure 3.49). A sample was prepared of CpRu(PPh₃)₂Me in d₈-THF with an excess of DSiEt₃. Irradiation of the sample for 18 hours at 198 K led to new signals in the recorded ¹H NMR spectrum of the sample, which correspond to those of the previously characterised complex, CpRu(κ²-2-C₆H₄PPh₂)(SiEt₃)H and couple to the ³¹P signal at δ -16.4 in a ¹H/³¹P HMQC experiment. The lack of a hydride signal at δ -9.13 suggests that the complex processes a Ru-D bond. Following the proposed route of Figure 3.49, the orthometallation of the phosphine must occur after the initial phosphine dissociation, prior to activation of the silane.

Figure 3.49 The two possible mechanistic routes towards the formation of the observed complex, CpRu(κ²-2-C₆H₄PPh₂)(SiEt₃)D, using DSiEt₃ as a reporter ligand

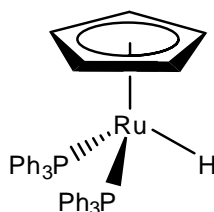


Decomposition of CpRu(κ²-2-C₆H₄PPh₂)(SiEt₃)D would lead to the reductive elimination of the phosphine phenyl ring with the deuteride from the ruthenium centre. This results in a partially deuterated phosphine which would lead to a change in the magnetic environment of the surrounding protons, compared with the protio ligands. This would consequently lead to a reduction in the integral for the associated proton resonance.

3.4.10.6 Formation of $\text{CpRu}(\text{PPh}_3)_2\text{H}$

With prolonged irradiation of the sample of $\text{CpRu}(\text{PPh}_3)_2\text{Me}$ with HSiEt_3 at room temperature, this complex is observed to increase in concentration via NMR, becoming the major product of reaction after 4 hours. The triplet signal at ^1H δ -11.59 (33.8 Hz) corresponds to the hydride resonance of $\text{CpRu}(\text{PPh}_3)_2\text{H}$, a $^1\text{H}/^{31}\text{P}$ HMQC NMR experiment links this proton signal to a ^{31}P resonance at δ 68.3. This ^{31}P resonance was shown to couple to further signals at δ 4.49 and 7.52, which are diagnostic of the protons of a cyclopentadienyl ring and the *ortho*-phenyl protons of a triphenylphosphine ligand. The hydride proton, cyclopentadienyl and *ortho*-phenyl protons have integrals in a ratio of 1:5:12, which suggests that the complex possesses two phosphine ligands, which matches with the characterisation previously attained for $\text{CpRu}(\text{PPh}_3)_2\text{H}$. The complex $\text{CpRu}(\text{PPh}_3)_2\text{H}$ has been found in previous experiments (Chapter 4) to be unreceptive to photochemical reaction using the conditions provided by the laser set-up. This accounts for the build-up of the complex during the course of the irradiation.

Figure 3.50 Structure of $\text{CpRu}(\text{PPh}_3)_2\text{H}$



In addition, a second triplet resonance δ -11.51 of lesser intensity is observed to overlap the proton resonance of $\text{CpRu}(\text{PPh}_3)_2\text{H}$. This triplet has a splitting of 34 Hz, which matches the splitting observed for $\text{CpRu}(\text{PPh}_3)_2\text{H}$. The only product complex able to produce these resonances is one which has two phosphine ligands in addition to the hydride signal. Since no additional phosphine has been added to the sample and the Cp resonance at δ 4.49 (identified through the mutually coupling of this Cp resonance and the hydride proton resonance to a common ^{31}P signal at δ 68.3, using a $^1\text{H}/^{31}\text{P}$ HMQC experiment) remains a singlet, the only option is that one of the triphenylphosphine ligands has been altered during the course of the irradiation.

This is consistent with the observation made earlier, when the hydride of $\text{CpRu}(\kappa^2\text{-C}_6\text{H}_4\text{PPh}_2)(\text{SiEt}_3)\text{H}$ was clearly visible in the recorded 1D ^1H spectrum. Reductive elimination of the orthometalated phenyl ring of the bound triphenylphosphine ligand with the deuteride would lead to an altered triphenylphosphine ligands having a deuterated *ortho* position on one the three phenyl rings. As depicted in Figure 3.51, a ring slip of the cyclopentadienyl ring ($\eta^5 \rightarrow \eta^3$) for the complex $\text{CpRu}(\kappa^2\text{-C}_6\text{H}_4\text{PPh}_2)(\text{SiEt}_3)\text{H}$, would lead to the formation of a 16 electron intermediate capable of activating the surrounding d_{12} -cyclohexane solvent, giving the short-lived complex **A** (Figure 3.51). Reductive elimination of the deuteride with the orthometalated phenyl ring would result in an isotopomer of the triphenylphosphine ligand, giving rise to the second hydride signal of $\text{CpRu}(\text{PPh}_3)_2\text{H}$, as a result of the change in the proton environment. The η^5 binding mode to the ruthenium centre may then be restored, yielding the complex $\text{CpRu}(\text{PPh}_3)(\text{SiEt}_3)(\text{C}_6\text{D}_{11})\text{H}$.

Figure 3.51 Possible Cp ring-slip mechanism

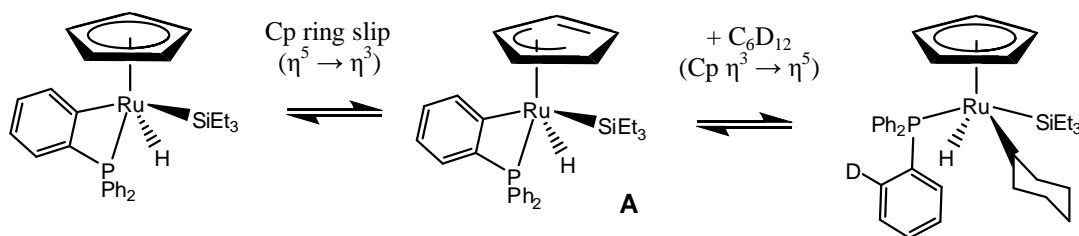
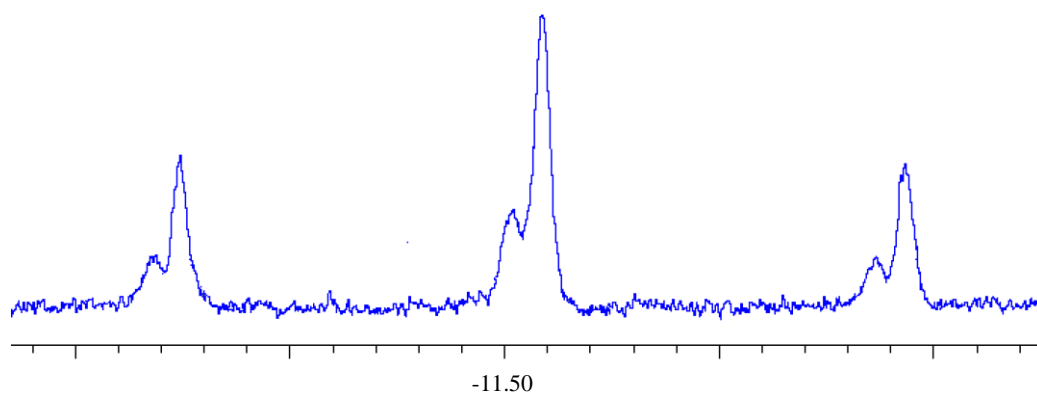


Figure 3.52 Magnified region of the ^1H NMR spectrum showing the triplet signal associated with $\text{CpRu}(\text{PPh}_3)_2\text{H}$ (major resonance) and a second overlapping minor triplet signal.



An alternative mode of the substitution at the *ortho* position of the phenyl ring of the triphenylphosphine ligand, may be a result of the formation of new a C-Si bond. Figure 3.53 illustrates two separate pathways by which the silyl substituent could be incorporated into the structure of the phosphine. Though only the left-hand route has merit, as this leads to a hydride product whose resonance is shown in Figure 3.51. The deuteride moiety would be silent in a recorded ^1H NMR experiment for the sample, and it is therefore unlikely that the reaction proceeds by this route.

Figure 3.53 Possible reaction pathways for bond activation

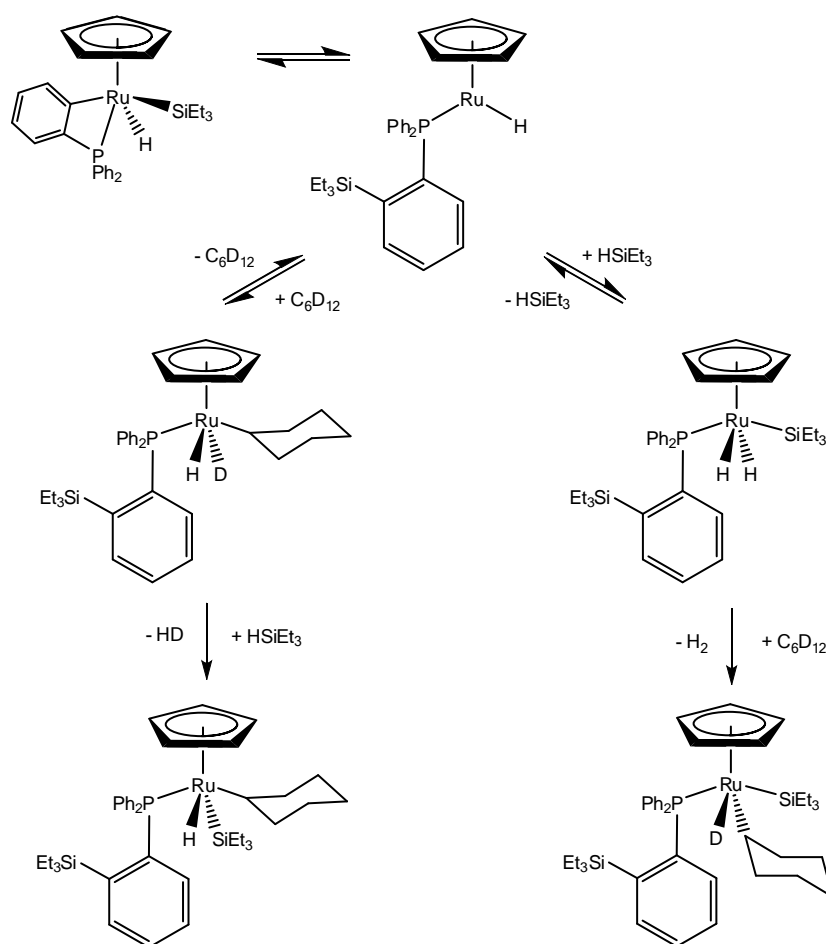
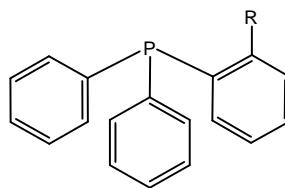


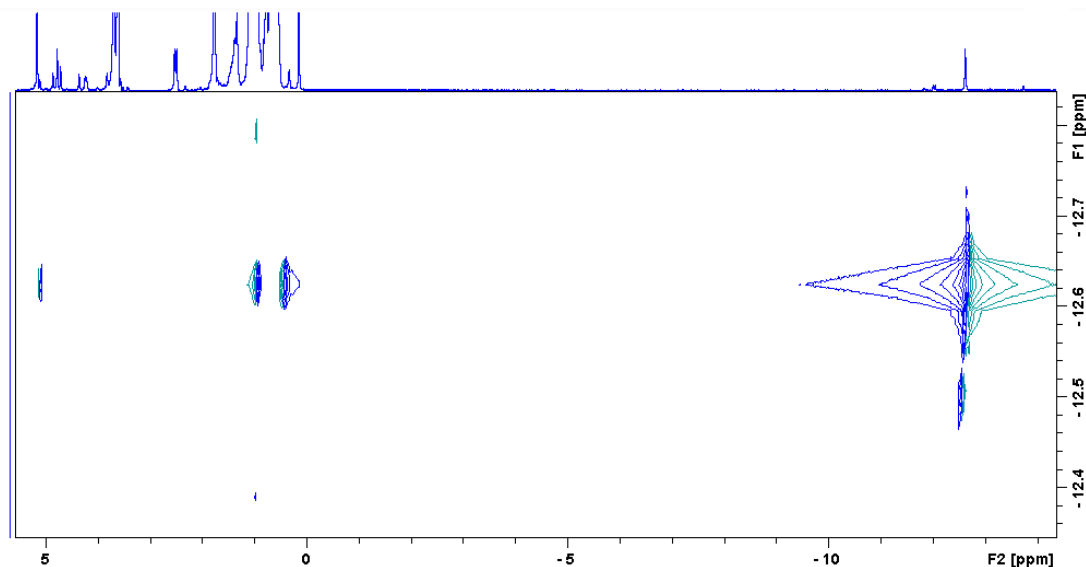
Figure 3.54 A depiction of the general structure of the substituted phosphine ligand
(where $R = {}^2\text{H}$ or SiEt_3)



To discern whether the aryl group of the triphenylphosphine ligand was deuterated or functionalisation by the silyl group, GC-MS techniques were employed. An NMR sample tube containing the formed products $\text{CpRu}(\text{PPh}_3)_2\text{H}$ and $\text{CpRu}(\text{PPh}_3)(\text{SiEt}_3)(\text{Cy})\text{H}$ was left to decompose under air for one week, in order to remove the organic ligands from the ruthenium metal centres. The decomposed precipitate was washed with ethanol, to ensure full removal of the organic components. GC-MS of this solution, with separation focused on the elution time of the compounds within the 200-450 range, gave only a signal at m/z value of 262 corresponding to PPh_3 and a larger signal at m/z 278, which is indicative of $\text{O}=\text{PPh}_3$. Signals at m/z 377 and 393 would be expected for the silyl containing phosphine / phosphine oxide compound. Though ${}^2\text{D}$ or ${}^{29}\text{Si}$ NMR experiments may in principle have been used to confirm this result, the residual silane / silyl-containing fragments and the residual deuterium solvent within the sample, meant that these methods could not conclusively be relied on to determine which of the two possible phosphine structures (Figure 3.54) was correct.

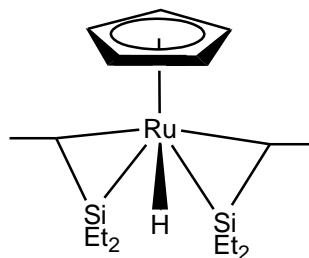
3.4.10.7 Formation of the metallated complex, $\text{CpRu}(\text{SiEt}_2\{\text{CHCH}_3\})_2\text{H}$

By using the methods to trap the excess phosphine described in Section 3.4.11, the singlet peak at δ -12.67 (observed in the ${}^1\text{H}$ NMR spectrum for the photochemical reaction of $\text{CpRu}(\text{PPh}_3)_2\text{Me}$ with HSiEt_3) was increased to a sufficient quantity to characterise by NMR methods. As determined in previous ${}^1\text{H}/{}^{31}\text{P}$ HMQC experiments, there is no coupling between this peak and a ${}^{31}\text{P}$ phosphine resonance. This is also evident from the lack of a doublet or triplet splitting for this peak. In order to determine the identity of this hydride complex, a 2D NOESY experiment was recorded, which displayed coupling between this peak and signals at δ 0.94, 0.48, 5.09, -12.67 (Figure 3.55) which are the CH_3 and CH_2 protons of a silyl chain, a Cp resonance and a hydride.

Figure 3.55 2D NOESY NMR experiment recorded for $\text{CpRu}(\text{SiEt}_2\{\text{CHCH}_3\})_2\text{H}$ 

Removal of the excess silane from the solution allowed for the peaks between δ 0-3 in the ^1H spectrum to be seen more clearly. A subsequently recorded $^1\text{H}/^{29}\text{Si}$ HMQC NMR experiment showed a connection between a ^{29}Si signal at 29.8 and the silyl alkyl protons and the hydride, in addition to a new signal at δ 0.75. A ^1H COSY experiment showed a coupling between this resonance and another at δ 0.26. Integration of the intensity of these peaks showed a ratio of 3:1. The corresponding ^{13}C signals for these resonances were found through the use of a $^1\text{H}/^{13}\text{C}$ HMQC experiment to be δ 9.4 and -11.5, respectively. This shows that the identities of these signals are CH_3 and CH (which is bound to ruthenium, owing to the upfield shift of the ^{13}C signal). The lack of any ^{31}P coupling to ^1H , ^{29}Si or ^{13}C observed in these spectra indicates that phosphine has been eliminated from this complex.

Integration of the signal at δ 0.75 with the hydride resonance, in the ^1H NMR spectrum, found a ratio of 6:1 between the two signals. It can therefore be concluded that the complex has a plane of symmetry, and that there are two of these coordinated ligands. Based on the 2D NOE shown in Figure 3.55, the hydride is shown to lie in close proximity to the silyl alkyl chains, thus describing further the orientation of the complex. Based on this data, the identity of the complex may be assigned as $\text{CpRu}(\text{SiEt}_2\{\text{CHCH}_3\})_2\text{H}$ (Figure 3.56), which is formed from the C-H activation of two coordinated silyl moieties.

Figure 3.56 The structure of $\text{CpRu}(\text{SiEt}_2\{\text{CHCH}_3\})_2\text{H}$ 

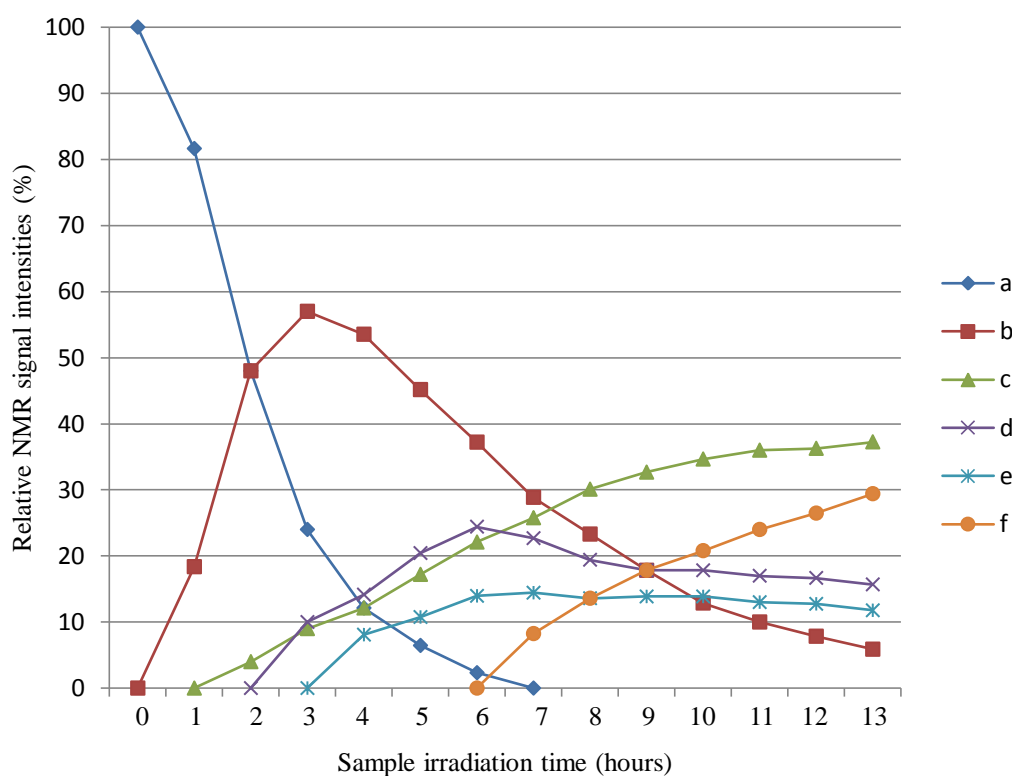
This complex is similar to previously reported Cp^* and Pt Silene complexes.²⁵⁵

3.4.10.8 Summary of the silane reactions

To summarise the processes described in this Section, a time-plot was recorded (Figure 3.57) to show the formation of the major products of the photochemical reaction of $\text{CpRu}(\text{PPh}_3)_2\text{Me}$ with HSiEt_3 . The formation of such a relatively large number of products in addition to the uncharacterised minor products indicates the complexity of this reaction, and for the characterisation of these individual complexes by NMR.

The plot shows that the starting material converts to form the bis-silyl product $\text{CpRu}(\text{PPh}_3)(\text{SiEt}_3)_2\text{H}$, which is photochemically active. This activity is not as great as the starting material, owing to the build up in the concentration of this complex. The decrease in the concentration of $\text{CpRu}(\text{PPh}_3)(\text{SiEt}_3)_2\text{H}$ leads to the formation of the solvent activated complex (e.g. $\text{CpRu}(\text{PPh}_3)(\text{SiEt}_3)(\text{Cy})\text{H}$), which continues to increase with prolonged photolysis. The complexes $\text{CpRu}(\text{PPh}_3)_2\text{SiEt}_3$ and $\text{CpRu}(\text{SiEt}_2\{\text{CHCH}_3\})_2\text{H}$ form following the decrease of the formation of the solvent activated complex, which begins to level to ~35%. This suggests that these products form from further photochemical reactions of this solvent activated complex. Following the decline of these two products, $\text{CpRu}(\text{PPh}_3)_2\text{H}$ is formed, which has been shown in previous experiments to become the dominant product if photolysis is prolonged.

Figure 3.57 A plot of the relative ^1H NMR Cp resonances over time, for the photochemically formed silane product complexes (original illustration appears in colour)



- | | | | |
|----|---|----|--|
| a. | $\text{CpRu}(\text{PPh}_3)_2\text{Me}$ | b. | $\text{CpRu}(\text{PPh}_3)(\text{SiEt}_3)_2\text{H}$ |
| c. | $\text{CpRu}(\text{PPh}_3)(\text{SiEt}_3)(\text{Cy})\text{H}$ | d. | $\text{CpRu}(\text{PPh}_3)_2\text{SiEt}_3$ |
| e. | $\text{CpRu}(\text{SiEt}_2\{\text{CHCH}_3\})_2\text{H}$ | f. | $\text{CpRu}(\text{PPh}_3)_2\text{H}$ |

3.4.11 Attempts to selectively sequester PPh_3 using sulfur and oxygen

In the previously described reactions, the initial step towards reaction involved the dissociation of a triphenylphosphine ligand from $\text{CpRu}(\text{PPh}_3)_2\text{Me}$. The liberation of phosphine allows for the formation of novel ruthenium complexes. However, the free phosphine may re-associate to the ruthenium centre (in a back reaction), which leads to a reduced yield of the new products. This was evident in the reactions involving HSiEt_3 and $\text{CpRu}(\text{PPh}_3)_2\text{Me}$, where many products formed, partly owing to the re-association of phosphine at key stages during the reaction. The ability to remove the excess phosphine from the sample would be useful in this instance to prevent further reaction, and maximise the quantities of certain complexes, for NMR interpretation.

On a larger scale, separation of a complex with ethanol would allow the excess phosphine to be removed. However, many of the generated species are thermally unstable and prepared on an NMR tube scale, which would provide considerable challenges for using this method. An alternative would be to ‘destroy’ the phosphine by converting it to its oxide or sulphide forms, which would effectively remove it from further reactions with the ruthenium centre. This is particularly relevant as triphenylphosphine is commonly used as an ‘oxygen scavenger’ in photopolymerisation processes²⁵⁶ and in oxo-transfer reactions.^{257, 258}

The challenge associated with using oxygen and sulfur to ‘trap’ the phosphine lies in the ability of these substances also to react with the ruthenium complex, leading to decomposition. The following Section discusses the attempt to overcome this challenge.

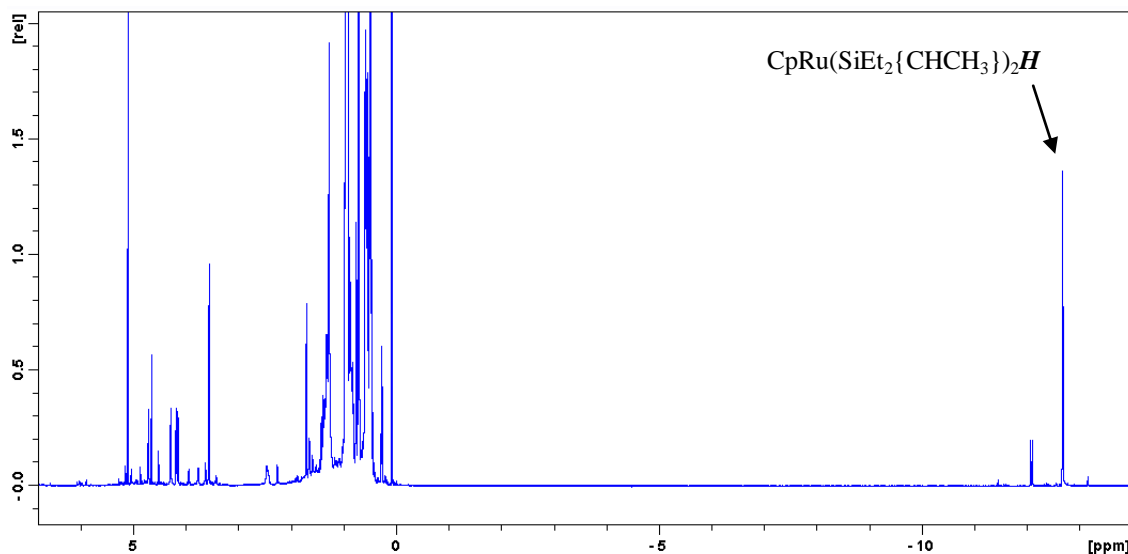
3.4.11.1 Reactions involving sulfur and oxygen

NMR samples of $\text{CpRu}(\text{PPh}_3)_2\text{Me}$ containing CO and HSiEt_3 were prepared as described in Sections 3.4.31 and 3.4.10 respectively, in d_8 -toluene. The sample containing CO was photolysed for two hours using the *ex situ* NMR set-up. Inspection of ^1H and $^{31}\text{P}\{^1\text{H}\}$ NMR spectra recorded after photolysis revealed signals characteristic of $\text{CpRu}(\text{PPh}_3)(\text{CO})\text{Me}$ and of free triphenylphosphine. The sample tube was then transferred a glovebox where a small quantity of ground elemental sulfur was added to the J-Y NMR tube. Measurement of the sulfur was impractical owing to the small quantity required, and dilution methods were unsuccessful owing to the lack of solubility of sulfur in the solvent. Based on the approximation of the sulfur added to the tube and the estimation of the quantity of phosphine liberated, samples often possessed an excess of sulfur required to trap the phosphine. This resulted in the swift decomposition of the ruthenium complex when further irradiation was applied. However when similar equivalents of sulfur and phosphine were added, the method was successful with greater conversion of the complex and an increase in the signal at δ 26.3 which corresponds to the resonance of $\text{S}=\text{PPh}_3$ in the $^{31}\text{P}\{^1\text{H}\}$ NMR spectrum. It should be noted that despite trapping the released phosphine in this manner and replenishing the CO supply following each addition of sulfur, the only product found was $\text{CpRu}(\text{PPh}_3)(\text{CO})\text{Me}$ and resonances associated with the bis-substituted carbonyl product were not observed.

To summarise, the method of using sulfur to quench the free phosphine is impractical on an NMR tube scale, owing to the difficulty in measuring the amount of sulfur required. This method is successful on larger scale synthesis, and has been employed in Chapter 5, where the addition of sulfur followed by heating was used to convert the η^1 complex $\text{CpRu}(\text{PPh}_3)_2(\text{CH}_2\text{Ph})$ to the η^3 derivative, $\text{CpRu}(\text{PPh}_3)(\eta^3\text{-CH}_2\text{Ph})$.

The use of oxygen also used to trap the liberated phosphine as O=PPh_3 . This method proved to be easier to control than the previous involving sulfur, and was successful when used to increase the amount of $\text{CpRu}(\text{SiEt}_2\{\text{CHCH}_3\})_2\text{H}$ formed in the previous silane experiments (Section 3.4.10.7). Following irradiation of the sample containing silane for 1.5 hours, the presence of the hydride consistent with $\text{CpRu}(\text{SiEt}_2\{\text{CHCH}_3\})_2\text{H}$ was observed in the ^1H NMR spectrum. The sample tube was briefly opened and exposed to air and shaken vigorously for about a minute. Following a degas of the sample using a high-vacuum line, a $^{31}\text{P}\{^1\text{H}\}$ NMR spectrum was recorded and the ratio between the two peaks at δ 21.4 and -6.4 (O=PPh_3 and PPh_3) was calculated. The process of exposing the sample to air was repeated until the free phosphine signal was almost removed. Further irradiation of the sample was then performed, and the process repeated until the concentration of product of interest (monitored using ^1H NMR) was great enough to be fully characterised by NMR techniques (Figure 3.58).

Figure 3.58 ^1H NMR spectrum showing the magnitude of the previously low intensity hydride signal for $\text{CpRu}(\text{SiEt}_2\{\text{CHCH}_3\})_2\text{H}$, compared with the other product resonances within the sample



The success of these methods to trap phosphine relies heavily on the susceptibility of these complexes to both oxygen and sulfur. However, they are both impractical when dealing with temperature and highly air sensitive complexes. Providing that the sample is moderately air-stable in solution for brief periods, that air “trap” method is more suitable for NMR-scale experiments, than the sulfur “trap” method.

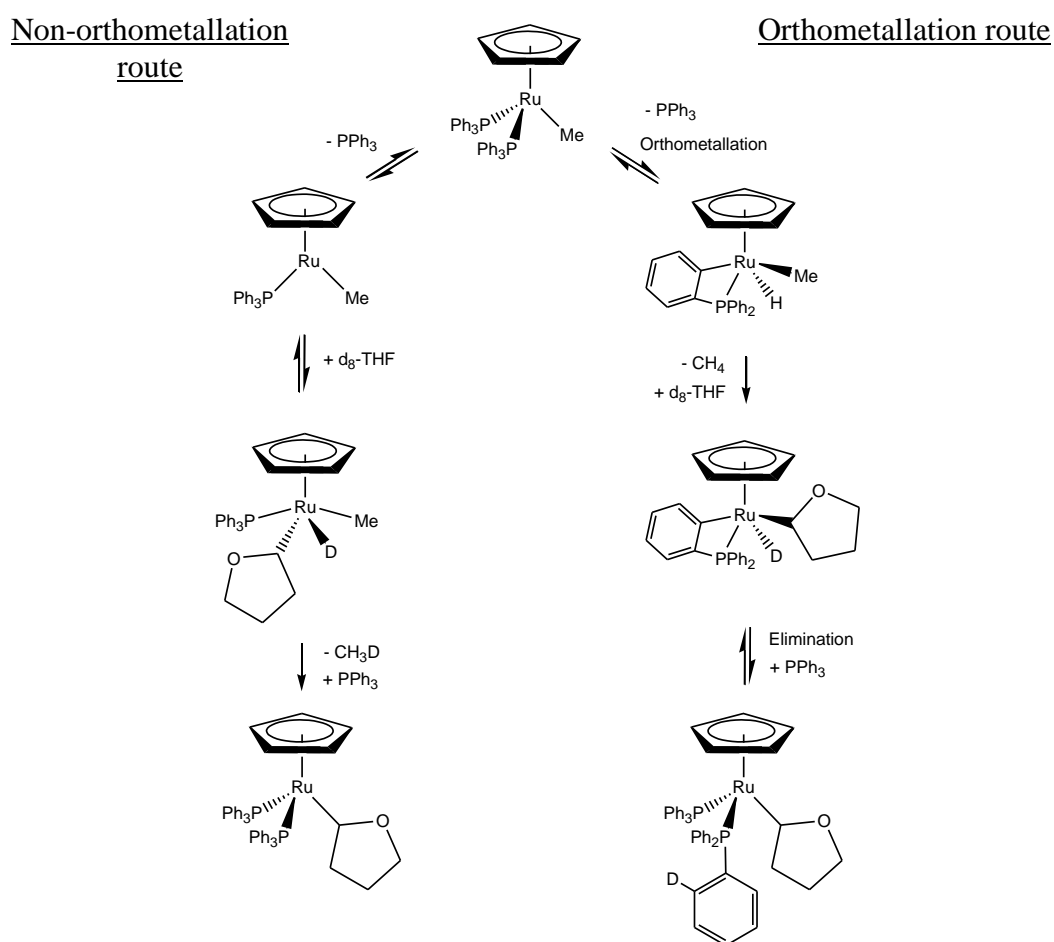
3.4.12 Determination of Orthometallation pathway

As outlined in the introduction, two pathways are possible for the activation of bonds by the Ru centre (Figure 3.59). In Section 3.4.10 it was clearly demonstrated that both Si-H bond activation and C-H bond activation by the $[(\text{CpRu}(\kappa^2\text{-}2\text{-C}_6\text{H}_4\text{PPh}_2)]$ fragment, is attainable. The formation of the silyl solvent activated complexes shows a structure which would be expected to be very similar to that of $\text{CpRu}(\text{PPh}_3)(\text{sol})(\text{H})\text{Me}$ (where sol = activated solvent fragment e.g. Ph), which is a proposed intermediate for the non-orthometallation activation C-H activation pathway. Sections 3.4.2.1, 3.4.5 and 3.4.8.2, present examples of C-H activated complexes. However, the speculated intermediate is unobserved, which is consistent with the prediction that $\text{CpRu}(\text{PPh}_3)(\text{sol})(\text{H})\text{Me}$ would be relatively unstable compared with $\text{CpRu}(\text{PPh}_3)(\text{sol})(\text{H})\text{SiEt}_3$, which is observable at

room temperature.

Since direct detection of $[(\text{CpRu}(\kappa^2\text{-}2\text{-C}_6\text{H}_4\text{PPh}_2)]$ is impractical, another method was employed to discern whether the C-H activation pathway occurs by an orthometallation route, like the silyl analogue. For this purpose, the experiment involving the photolysis of $\text{CpRu}(\text{PPh}_3)_2\text{Me}$ in $d_8\text{-THF}$ was re-examined. Figure 3.14 shows the ^1H NMR signal associated with methane liberated from the system. The signal appears as a singlet, as opposed to a triplet (which would occur if the methane contained deuterium – CH_3D). The triplet peak would only be present if the reaction progressed via the non-orthometallation route (Figure 3.59), otherwise, the singlet peak indicates that an orthometallation step has taken place.

Figure 3.59 Orthometallation and non-orthometallation routes to lead to C-H activation



To further support the case for the orthometallation pathway, further information can be obtained by comparison of the integrals for the Cp and *ortho*-phenyl ^1H signals for the

activated THF complex, $\text{CpRu}(\text{PPh}_3)_2(\text{OC}_4\text{D}_7)$. If deuterated THF is used as a reaction solvent, then deuteration of one of the *ortho*-phenyl proton positions of one of the triphenylphosphine ligands would occur. An integral ratio of 16:5 would be expected to account for this effect.

Based on this integration it can be confirmed that C-H activation takes place via the $[(\text{CpRu}(\kappa^2\text{-}2\text{-C}_6\text{H}_4\text{PPh}_2)]$ fragment, in an analogous way to the Si-H adduct activations.

For the cases involving two electron donor ligands (e.g. PEt_3 , CO, ${}^t\text{BuNC}$), the rate at which the ligand binds to the metal centre must be faster than the rate of orthometallation, and so the ligand acts to stabilise the coordinatively unsaturated complex before orthometallation of the phenyl ring of the phosphine can occur. This is evidenced by the lack of any of the following orthometallated products in the NMR spectra: $\text{CpRu}(\kappa^2\text{-}2\text{-C}_6\text{H}_4\text{PPh}_2)(\text{L})$ (where $\text{L} = \text{PEt}_3$, CO or ${}^t\text{BuNC}$).

Table 3.3 contains rate data acquired by Perutz *et al.*²³⁶ for the association of ligands to a metal centre following flash photolysis of $\text{cis-Ru}(\text{PMe}_3)_4(\text{H})_2$ (determined by TRIR methods). This data reveals some insight into the timescale by which these processes occur.

*Table 3.3 Second order rate constants for the reaction of substrates with a transient intermediate formed from the flash photolysis of $\text{cis-Ru}(\text{PMe}_3)_4(\text{H})_2$ in cyclohexane*²³⁶

Substrate	Second order rate / $\text{dm}^{-3} \text{mol}^{-1} \text{s}^{-1}$
$k(\text{CO})$	$(8.9 \pm 0.4) \times 10^8$
$k(\text{H}_2)$	$(5.6 \pm 0.4) \times 10^8$
$k(\text{H}_2\text{SiEt}_2)$	$(2.2 \pm 0.1) \times 10^7$
$k(\text{PMe}_3)$	$(1.1 \pm 0.1) \times 10^6$
$k(\text{HSiEt}_3)$	$(2.8 \pm 0.1) \times 10^5$
$k(\text{PEt}_3)$	$(2.7 \pm 0.8) \times 10^5$
$k(\text{C}_2\text{H}_4)$	$(1.8 \pm 0.1) \times 10^5$

Because the system is now known to proceed by an orthometallation step, the following question regarding the silane experiment (Section 3.4.10) may now be answered: why is $\text{CpRu}(\text{PPh}_3)(\text{H})(\text{SiEt}_3)(\text{Cy})$ (Figure 3.43) observable by NMR, whereas $\text{CpRu}(\text{PPh}_3)(\text{H})(\text{SiEt}_3)(\text{Me})$ is not? Based on the work of Jones and Feher,²⁴⁷ the Ru-Me adduct should be more stable than the Ru-Cy adduct, and therefore be observed in the recorded NMR spectra. However, it can now be determined that the complex $\text{CpRu}(\text{PPh}_3)(\text{H})(\text{SiEt}_3)(\text{Me})$ does not exist for this system, owing to the orthometallation step. The complex $\text{CpRu}(\kappa^2\text{-2-C}_6\text{H}_4\text{PPh}_2)(\text{Me})\text{H}$ rapidly eliminate methane and hence the methane signal at δ 0.19 in the ^1H NMR spectrum, leading to the formation of $[\text{CpRu}(\kappa^2\text{-2-C}_6\text{H}_4\text{PPh}_2)]$.

3.5 Conclusions

Like the previous reactions of $\text{CpRu}(\text{PPh}_3)_2\text{Cl}$ with two electron donors (PEt_3 , CO, $^t\text{BuNC}$), $\text{CpRu}(\text{PPh}_3)_2\text{Me}$ is capable of undergoing substitution of one (in the case of PEt_3 , CO, $^t\text{BuNC}$) or bis-substitution (for PEt_3). $\text{CpRu}(\text{PPh}_3)_2\text{Me}$ in this respect is shown to be more reactive than the chloride derivative, requiring shortened reaction times in order to undergo substitution. Further similarities include the ability to form η^2 structures through low temperature photolysis in the presence of an excess of either ethene or naphthalene. Both instances led to improved conversion over the chloride derivatives, subsequently allowing for the activation energy for the rotation of the coordinated ethene to be calculated, in addition to observing peaks belonging to the two expected isomers for the naphthalene coordination complexes.

For the 2-electron donor ligands CO and $^t\text{BuNC}$, mono substitution of these ligands was found to occur at a faster rate than the orthometallation process, following the dissociation of phosphine. The same observation was made for ethene and naphthalene, but the THF coordinated complex was found to form in small quantities, indicating that though these ligands were shown to be more strongly coordinating than THF, this effect is not as strong as the binding of CO. In the presence of DMSO and pyridine, no evidence of THF coordination was found. The relative binding of pyridine (which coordinates in a similar manner to that of THF) is much stronger than THF, taking into consideration the large excess of THF compared with the quantity of pyridine. None of these time-plots showed any evidence for the formation of C-H bond activation

products. However, the reaction involving THF did lead to the formation of both the coordination product and C-H activation product. Therefore it can be concluded that THF coordinates weakly to the metal centre and at a rate similar to that of the orthometallation process. These results are consistent with those reported in the literature for *cis*-Ru(PMe₃)₄(H)₂ (Table 3.3) which shows that CO binds at a faster rate than PEt₃ and that of ethene. PEt₃ was the only ligand that led to bis-substitution, which was shown through the rate plot to occur through a step wise pathway. This route led to the appreciable build up of the mono substituted product, CpRu(PPh₃)(PEt₃)Me, indicating that the photochemical activity of CpRu(PPh₃)₂Me is greater than that of the mono substitution product.

The major difference between the two starting materials (CpRu(PPh₃)₂Cl and CpRu(PPh₃)₂Me) lies with the ability of the methyl complex to undergo orthometallation of the aryl rings of the triphenylphosphine ligand. This generates the fragment, [CpRu(κ^2 -2-C₆H₄PPh₂)], which is capable of activating H-H, Si-H and C-C bonds. The work presented in this chapter demonstrates that this appears to be the only pathway by which CpRu(PPh₃)₂Me activates bonds, as the alternative pathway would involve [CpRu(PPh₃)Me], for which no evidence was found in these experiments.

The reactions with silane provided a convenient means of forming complexes of the type CpRu(PPh₃)(sol)(R)H and CpRu(κ^2 -2-C₆H₄PPh₂)(R)H (Where: sol = activated solvent and R = silyl), for which the C-H derived analogues are too unstable to observe by NMR at low temperature. This set of reactions allows the reaction mechanism to be probed, by using the more stable silane analogues. Though the product of C-H bond activation, the orthometallated fragment, could not be stabilised for characterisation by NMR, it was determined that this orthometallation pathway was followed exclusively by the C-H analogues. This was elucidated by the observation of the protio methane signal in the ¹H NMR spectrum, as opposed to a partially deuterated analogue.

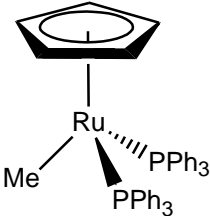
The challenge associated with recording these results lies equally with dealing with these samples at low temperature (owing to their high thermal instability), and with the numerous products formed by the photochemical irradiation, which leads to complicated NMR spectra. This meant that most experiments were repeated many times in attempts to enhance the formation of one product over the others (e.g. changing the

quantities of substrate, varying the sample temperature, lengthening / shortening the irradiation duration, the addition of sulfur etc.), in order to attain more complete NMR data.

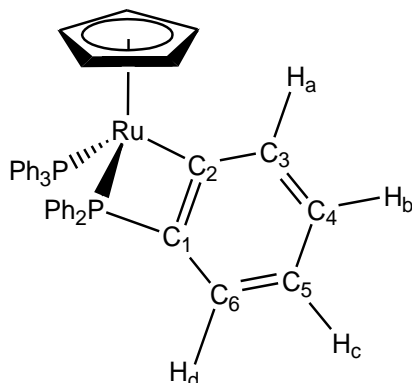
In summary, the orthometallation pathway allows for a wider range of reactivity to be accessed for the $\text{CpRu}(\text{PPh}_3)_2\text{Me}$ complex over the chloride derivative. Additionally, novel products may be accessed (as demonstrated for the silane reactions) when UV radiation is used to drive the reaction along normally inaccessible routes.

The following chapter focuses of the thermal and photochemical reactivity of $\text{CpRu}(\text{PPh}_3)_2\text{H}$, a product formed in several of these reactions. The intention is to find the conditions under which $\text{CpRu}(\text{PPh}_3)_2\text{H}$ will react, and whether the same orthometallation pathway is adhered to.

3.6 Characterisation data

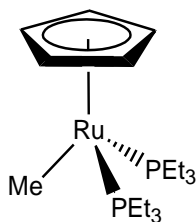
Table 3.4 NMR data for $CpRu(PPh_3)_2Me$				
				
In d_8 -toluene at 298 K	δ / ppm (multiplicity, integration)	Assignment	Coupling constant / Hz	Assignment
1H	0.97 (t, 3) 4.35 (s, 5) 6.91 (m)* 6.95 (m)* 7.34 (m, 12)	Ru- CH_3 C_5H_5 <i>Para</i> - $P(C_6H_5)_3$ <i>Meta</i> - $P(C_6H_5)_3$ <i>Ortho</i> - $P(C_6H_5)_3$	5.7	$ ^3J_{PH} $
^{13}C	-30.1 (t) 84.2 (s) 126.8 (d) 127.4 (s) 133.7 (t) 141.2 (dd)	Ru- CH_3 C_5H_5 <i>Meta</i> - $P(C_6H_5)_3$ <i>Para</i> - $P(C_6H_5)_3$ <i>Ortho</i> - $P(C_6H_5)_3$ <i>Ipsa</i> - $P(C_6H_5)_3$	10.8 10.3 16.2 13.6, 34.9	$ ^2J_{PC} $ $ ^4J_{PC} $ $ ^2J_{PC} $ $ ^3J_{PC} , ^1J_{PC} $
^{31}P	55.3 (s)	$P(Ph)_3$		

* Resonances were overlapped in the 1H NMR spectrum, and were therefore found using a $^1H/^{31}P$ HMQC NMR experiment.

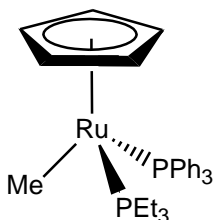
Table 3.5 NMR data for $CpRu(PPh_3)(\kappa^2\text{-}2\text{-}C_6H_4PPh_2)$ 

In d_{12} -cyclohexane at 298 K	δ / ppm (multiplicity, integration)	Assignment	Coupling constant / Hz	Assignment
1H	4.27 (s, 5) 6.72 (m)* 6.82 (m)* 6.98 (m)* 7.11 (m)* 7.33 (m)* 7.33 (m)* 7.53 (m, 1)	C_5H_5 <i>Para</i> - $P(C_6H_5)_3$ <i>Meta</i> - $P(C_6H_5)_3$ H_b H_c H_d <i>Ortho</i> - $P(C_6H_5)_3$ H_a	7.6	$ ^1J_{PH} $
^{13}C	80.4 (s) 125.9 (d) 127.3 (s) 128.7 (s) 129.7 (d) 134.2 (t) 139.8 (d) 142.7 (d) 143.6 (dd) 144.5 (d) 155.3 (d)	C_5H_5 C_1 <i>Meta</i> - $P(C_6H_5)_3$ C_5 <i>Para</i> - $P(C_6H_5)_3$ C_4 C_6 <i>Ortho</i> - $P(C_6H_5)_3$ <i>Ipsa</i> - $P(C_6H_5)_3$ C_2 C_3	10.7 4.4 10.6 15.6 44.8 17.2, 11.9 10.2 45.1	$ ^3J_{PC} $ $ ^4J_{PC} $ $ ^2J_{PC} $ $ ^2J_{PC} $ $ ^1J_{PC} $ $ ^2J_{PC} , ^2J_{PC} $ $ ^3J_{PC} $ $ ^1J_{PC} $
^{31}P	-16.9 (d) 63.5, (d)	$P(Ph)_2(\kappa^2\text{-}2\text{-}C_6H_4)$ $P(Ph)_3$	33.8 33.8	$ ^2J_{PP} $ $ ^2J_{PP} $

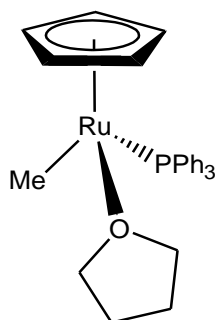
* Resonances were overlapped in the 1H NMR spectrum, and were therefore found using a $^1H/^{31}P$ HMQC NMR experiment.

Table 3.6 NMR data for $\text{CpRu}(\text{PEt}_3)_2\text{Me}$ 

In d_8 - THF at 298 K	δ / ppm (multiplicity, integration)	Assignment	Coupling constant / Hz	Assignment
^1H	0.15 (t, 3) 0.92 (br) 1.48 & 1.90 (m) 4.54 (s, 5)	CH_3 $\text{P}(\text{CH}_2\text{CH}_3)_3$ $\text{P}(\text{CH}_2\text{CH}_3)_3$ C_5H_5	5.8 7.5 7.4	$ \text{}^3\text{J}_{\text{PH}} $ $ \text{}^3\text{J}_{\text{HH}} $ $ \text{}^3\text{J}_{\text{HH}} $
^{13}C	-25.2 (t) 28.0 (t) 31.8 (t) 79.9 (s)	CH_3 $\text{P}(\text{CH}_2\text{CH}_3)_3$ $\text{P}(\text{CH}_2\text{CH}_3)_3$ C_5H_5	9.7 4.2 16.2	$ \text{}^2\text{J}_{\text{PC}} $ $ \text{}^2\text{J}_{\text{PC}} $ $ \text{}^1\text{J}_{\text{PC}} $
^{31}P	40.5 (s)	$\text{P}(\text{Et})_3$		

Table 3.7 NMR data for $CpRu(PPh_3)(PEt_3)Me$ 

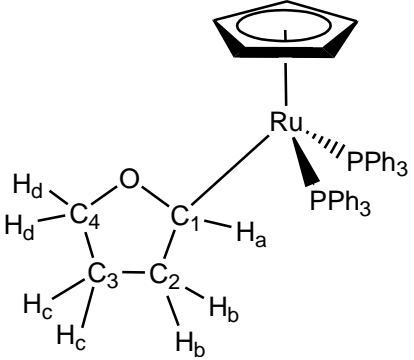
In d_8 - THF at 198 K	δ / ppm (multiplicity, integration)	Assignment	Coupling constant / Hz	Assignment
1H	0.39 (t, 3) 0.83 (br, 9) 1.39 & 1.50 (m) 4.49 (s, 5) 6.89 (m) 7.09 (m) 7.61 (m)	Ru- CH_3 $P(CH_2CH_3)_3$ $P(CH_2CH_3)_3$ C_5H_5 <i>Para</i> - $P(C_6H_5)_3$ <i>Meta</i> - $P(C_6H_5)_3$ <i>Ortho</i> - $P(C_6H_5)_3$	5.6 7.5 7.3	$ ^3J_{PH} $ $ ^3J_{HH} $ $ ^3J_{HH} $
^{13}C	-26.7 (t) 13.5 (t) 26.2 (t) 81.8 (s) 127.8 (t) 128.5 (s) 133.4 (t) 141.5 (dd)	Ru- CH_3 $P(CH_2-CH_3)_3$ $P(CH_2-CH_3)_3$ C_5H_5 <i>Meta</i> - $P(C_6H_5)_3$ <i>Para</i> - $P(C_6H_5)_3$ <i>Ortho</i> - $P(C_6H_5)_3$ <i>Ipsa</i> - $P(C_6H_5)_3$	10.1 4.3 16.1 10.5 15.7 12.4, 34.7	$ ^2J_{PC} $ $ ^1J_{PC} $ $ ^3J_{PC} $ $ ^2J_{PC} $ $ ^3J_{PC} , ^1J_{PC} $
^{31}P	35.2 (d) 62.9 (d)	$P(Et)_3$ $P(Ph)_3$	39.3 39.3	$ ^2J_{PP} $ $ ^2J_{PP} $

Table 3.8 NMR data for $\text{CpRu}(\text{PPh}_3)(\text{OC}_4\text{H}_8)\text{Me}$ 

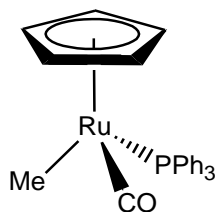
In d_8 - THF at 198 K	δ / ppm (multiplicity, integration)	Assignment	Coupling constant / Hz	Assignment
^1H	0.16 (d, 3) 4.59 (s, 5) 7.08 (m) 7.12 (m) 7.53 (m)	Ru- CH_3 C_5H_5 <i>Para</i> - $\text{P}(\text{C}_6\text{H}_5)_3$ <i>Meta</i> - $\text{P}(\text{C}_6\text{H}_5)_3$ <i>Ortho</i> - $\text{P}(\text{C}_6\text{H}_5)_3$	5.9	$ \text{}^3\text{J}_{\text{PH}} $
^{13}C	-28.7 (d) 84.4 (s) 126.5 (d) 127.6 (s) 133.8 (d) 141.1 (d)	Ru- CH_3 C_5H_5 <i>Meta</i> - $\text{P}(\text{C}_6\text{H}_5)_3$ <i>Para</i> - $\text{P}(\text{C}_6\text{H}_5)_3$ <i>Ortho</i> - $\text{P}(\text{C}_6\text{H}_5)_3$ <i>Ipsa</i> - $\text{P}(\text{C}_6\text{H}_5)_3$	10.8 10.4 16.0 45.3	$ \text{}^2\text{J}_{\text{PC}} $ $ \text{}^3\text{J}_{\text{PC}} $ $ \text{}^2\text{J}_{\text{PC}} $ $ \text{}^1\text{J}_{\text{PC}} $
^{31}P	61.3 (s)	$\text{P}(\text{Ph})_3$		

NMR data for the labile coordinated THF ligand could not be obtained.

Table 3.9 NMR data for $CpRu(PPh_3)(OC_4H_7)H$

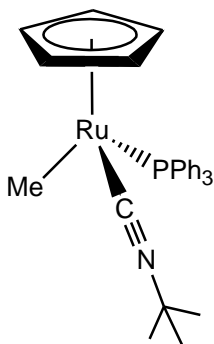
				
In d_8 - THF at 198 K	δ / ppm (multiplicity, integration)	Assignment	Coupling constant / Hz	Assignment
1H	1.75 & 1.94 (t) 2.19 & 2.41 (q, 2) 3.70 (q) & 3.86 (q) 4.23 (s, 5) 5.37 (m, dt, 1) 7.09 (m)* 7.16 (m)* 7.38 (m, 12)	H_c H_b H_d C_5H_5 H_a <i>Para</i> - $P(C_6H_5)_3$ <i>Meta</i> - $P(C_6H_5)_3$ <i>Ortho</i> - $P(C_6H_5)_3$	6.2 5.4 5.4 1.7, 16.3	$ ^3J_{HH} $ $ ^3J_{HH} $ $ ^3J_{HH} $ $ ^3J_{HH} , ^3J_{PH} $
^{13}C	50.9 (s) 61.4 (t) 82.7 (s) 84.3 (s) 127.3 (t) 128.1 (s) 133.5 (t) 140.4 (t) 145.7 (t)	C_3 C_2 C_5H_5 C_4 <i>Meta</i> - $P(C_6H_5)_3$ <i>Para</i> - $P(C_6H_5)_3$ <i>Ortho</i> - $P(C_6H_5)_3$ <i>Ipsa</i> - $P(C_6H_5)_3$	3.2 10.6 16.5 13.3, 35.0 17.8	$ ^3J_{PC} $ $ ^3J_{PC} $ $ ^2J_{PC} $ $ ^3J_{PC} , ^1J_{PC} $ $ ^2J_{PC} $
^{31}P	41.9 (s)	$P(Ph)_3$		

* Resonances were overlapped in the 1H NMR spectrum, and were therefore found using a $^1H/^{31}P$ HMQC NMR experiment.

Table 3.10 NMR data for $CpRu(PPh_3)(CO)Me$ 

In d_8 - THF at 298 K	δ / ppm (multiplicity, integration)	Assignment	Coupling constant / Hz	Assignment
1H	0.79 (d, 3) 4.91 (s, 5) 7.31 (m)* 7.33 (m)* 7.78 (m, 6)	Ru-CH ₃ C ₅ H ₅ Para - P(C ₆ H ₅) ₃ Meta - P(C ₆ H ₅) ₃ Ortho - P(C ₆ H ₅) ₃	5.3	$ ^2J_{PH} $
^{13}C	-28.0 (d) 82.4 (s) 128.0 (d) 129.5 (s) 133.9 (d) 140.3 (d) 201.4 (d)	Ru-CH ₃ C ₅ H ₅ Meta - P(C ₆ H ₅) ₃ Para - P(C ₆ H ₅) ₃ Ortho - P(C ₆ H ₅) ₃ Ipso - P(C ₆ H ₅) ₃ CO	10.8 10.7 16.3 45.2 22.1	$ ^2J_{PC} $ $ ^3J_{PC} $ $ ^2J_{PC} $ $ ^1J_{PC} $ $ ^2J_{PC} $
^{31}P	63.9 (s)	P(Ph) ₃		

* Resonances were overlapped in the 1H NMR spectrum, and were therefore found using a $^1H/^{31}P$ HMQC NMR experiment.

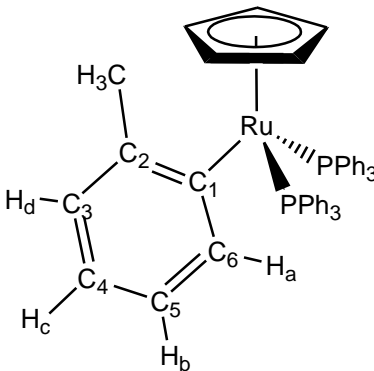
Table 3.11 NMR data for $CpRu(PPh_3)(NCBu^t)Me$ 

In d_8 - THF at 298 K	δ / ppm (multiplicity, integration)	Assignment	Coupling constant / Hz	Assignment
1H	0.77 (d, 3) 1.31 (s, 9) 5.00 (s, 5) 7.33 (m)* 7.37 (m)* 7.87 (m, 6)	CH_3 (CH_3) $CN\equiv C$ C_5H_5 <i>Para</i> - $P(C_6H_5)_3$ <i>Meta</i> - $P(C_6H_5)_3$ <i>Ortho</i> - $P(C_6H_5)_3$	5.4	$ ^2J_{PH} $
^{13}C	-27.7 (d) 31.4 (s) 53.4 (s) 85.19 (d) 127.6 (d) 128.7 (s) 133.9 (d) 138.8 (t)** 140.4 (d)	CH_3 (CH_3) $CN\equiv C$ (CH_3) $CN\equiv C$ C_5H_5 <i>Meta</i> - $P(C_6H_5)_3$ <i>Para</i> - $P(C_6H_5)_3$ <i>Ortho</i> - $P(C_6H_5)_3$ (CH_3) $CN\equiv C$ <i>Ipsso</i> - $P(C_6H_5)_3$	10.3 10.5 16.7 19.4 45.3	$ ^2J_{PC} $ $ ^3J_{PC} $ $ ^2J_{PC} $ $ ^1J_{CN} $ $ ^1J_{PC} $
^{31}P	67.2 (s)	$P(Ph)_3$		

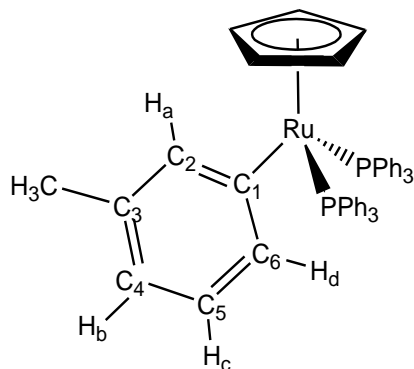
* Resonances were overlapped in the 1H NMR spectrum, and were therefore found using a $^1H/^{31}P$ HMQC NMR experiment.

** Appears as a broad triplet in the $^{13}C\{^1H\}$ NMR spectrum.

Table 3.12 NMR data for $CpRu(PPh_3)_2(o\text{-tolyl})$

				
In d_8 -toluene at 198 K	δ / ppm (multiplicity, integration)	Assignment	Coupling constant / Hz	Assignment
^1H	2.31 (s)* 4.37 (s) 6.97 (br)* 7.01 (m)* 7.10 (m)* 7.13 (br)* 7.37 (m)* 7.41 (br, 1) 7.54 (br, 1)	CH_3 C_5H_5 H_d <i>Para</i> - $\text{P}(\text{C}_6\text{H}_5)_3$ <i>Meta</i> - $\text{P}(\text{C}_6\text{H}_5)_3$ H_c <i>Ortho</i> - $\text{P}(\text{C}_6\text{H}_5)_3$ H_b H_a		
^{13}C	21.7 (s) 85.9 (s) 112.1 (d) 121.3 (t) 127.4 (s) 127.5 (d) 128.1 (s) 133.4 (d) 136.5 (d) 140.8 (d) 142.8 (t) 149.7 (t)	CH_3 C_5H_5 C_5 C_6 C_4 <i>Meta</i> - $\text{P}(\text{C}_6\text{H}_5)_3$ <i>Para</i> - $\text{P}(\text{C}_6\text{H}_5)_3$ <i>Ortho</i> - $\text{P}(\text{C}_6\text{H}_5)_3$ C_3 <i>Ipsa</i> - $\text{P}(\text{C}_6\text{H}_5)_3$ C_2 C_1	3.3 17.8 10.3 16.4 4.7 14.3, 34.7 14.6 21.2	$ ^4J_{\text{PC}} $ $ ^3J_{\text{PC}} $ $ ^3J_{\text{PC}} $ $ ^2J_{\text{PC}} $ $ ^4J_{\text{PC}} $ $ ^3J_{\text{PC}} , ^1J_{\text{PC}} $ $ ^3J_{\text{PC}} $ $ ^2J_{\text{PC}} $
^{31}P	50.2 (s)	$\text{P}(\text{Ph})_3$		

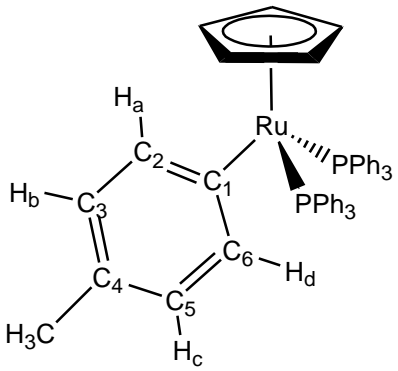
* Resonances were overlapped in the ^1H NMR spectrum, and were therefore found using a $^1\text{H}/^{31}\text{P}$ HMQC NMR experiment.

Table 3.13 NMR data for $CpRu(PPh_3)_2(m\text{-tolyl})$ 

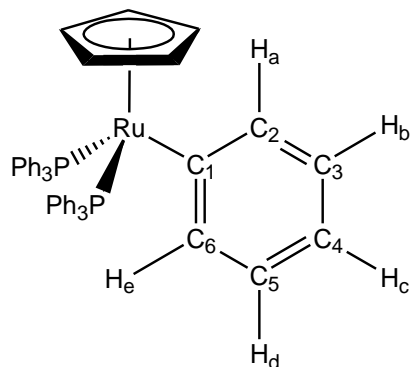
In d_8 -toluene at 198 K	δ / ppm (multiplicity, integration)	Assignment	Coupling constant / Hz	Assignment
^1H	2.36 (s) [*] 4.34 (s) 6.94 (br) [*] 7.01 (m) [*] 7.07 (br) [*] 7.10 (m) [*] 7.12 (br) [*] 7.15 (br) [*] 7.35 (m) [*]	CH_3 C_5H_5 H_c <i>Para</i> - $\text{P}(\text{C}_6\text{H}_5)_3$ H_b <i>Meta</i> - $\text{P}(\text{C}_6\text{H}_5)_3$ H_a H_d <i>Ortho</i> - $\text{P}(\text{C}_6\text{H}_5)_3$		
^{13}C	21.2 (s) 85.6 (s) 112.5 (d) 119.2 (s) 127.4 (d) 128.1 (s) 133.2 (t) 133.9 (t) 140.6 (dd) 141.3 (t) 146.4 (t) 151.6 (t)	CH_3 C_5H_5 C_5 C_4 <i>Meta</i> - $\text{P}(\text{C}_6\text{H}_5)_3$ <i>Para</i> - $\text{P}(\text{C}_6\text{H}_5)_3$ <i>Ortho</i> - $\text{P}(\text{C}_6\text{H}_5)_3$ C_3 <i>Ipsa</i> - $\text{P}(\text{C}_6\text{H}_5)_3$ C_6 C_2 C_1	2.7 10.3 16.4 4.4 14.3, 37.7 19.6 14.3 21.6	$ \text{}^4\text{J}_{\text{PC}} $ $ \text{}^3\text{J}_{\text{PC}} $ $ \text{}^2\text{J}_{\text{PC}} $ $ \text{}^4\text{J}_{\text{PC}} $ $ \text{}^3\text{J}_{\text{PC}} , \text{}^1\text{J}_{\text{PC}} $ $ \text{}^3\text{J}_{\text{PC}} $ $ \text{}^3\text{J}_{\text{PC}} $ $ \text{}^2\text{J}_{\text{PC}} $
^{31}P	52.3 (s)	$\text{P}(\text{Ph})_3$		

* Resonances were overlapped in the ^1H NMR spectrum, and were therefore found using a $^1\text{H}/^{31}\text{P}$ HMQC NMR experiment.

Table 3.14 NMR data for $CpRu(PPh_3)_2(p\text{-tolyl})$

				
In d_8 -toluene at 198 K	δ / ppm (multiplicity, integration)	Assignment	Coupling constant / Hz	Assignment
^1H	2.38 (s)* 4.30 (s) 6.94 (m)* 7.01 (m)* 7.11 (m)* 7.21 (m)* 7.34 (m)*	CH_3 C_5H_5 H_a & H_d <i>Para</i> - $\text{P}(\text{C}_6\text{H}_5)_3$ <i>Meta</i> - $\text{P}(\text{C}_6\text{H}_5)_3$ H_b & H_c <i>Ortho</i> - $\text{P}(\text{C}_6\text{H}_5)_3$		
^{13}C	20.6 (s) 85.2 (s) 112.3 (s) 124.8 (s) 127.4 (d) 128.1 (s) 133.7 (t) 140.5 (dd) 144.7 (t) 149.8 (t)	CH_3 C_5H_5 C_4 C_3 & C_5 <i>Meta</i> - $\text{P}(\text{C}_6\text{H}_5)_3$ <i>Para</i> - $\text{P}(\text{C}_6\text{H}_5)_3$ <i>Ortho</i> - $\text{P}(\text{C}_6\text{H}_5)_3$ <i>Ipsa</i> - $\text{P}(\text{C}_6\text{H}_5)_3$ C_2 & C_6 C_1	4.5 10.3 16.4 14.2, 37.7 14.3 21.6	$ ^4\text{J}_{\text{PC}} $ $ ^3\text{J}_{\text{PC}} $ $ ^2\text{J}_{\text{PC}} $ $ ^3\text{J}_{\text{PC}} , ^1\text{J}_{\text{PC}} $ $ ^3\text{J}_{\text{PC}} $ $ ^2\text{J}_{\text{PC}} $
^{31}P	52.6 (s)	$\text{P}(\text{Ph})_3$		

* Resonances were overlapped in the ^1H NMR spectrum, and were therefore found using a $^1\text{H}/^{31}\text{P}$ HMQC NMR experiment.

Table 3.15 NMR data for $CpRu(PPh_3)_2Ph$ 

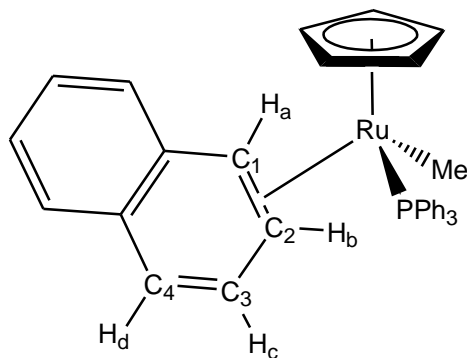
In d_6 -benzene at 298 K	δ / ppm (multiplicity, integration)	Assignment	Coupling constant / Hz	Assignment
1H	4.41 (s, 5) 7.04 (m)* 7.04 (m)* 7.15 (m)* 7.32 (m)* 7.36 (m)* 7.61 (m, 2)	C_5H_5 H_c <i>Para</i> - $P(C_6H_5)_3$ <i>Meta</i> - $P(C_6H_5)_3$ H_b & H_d <i>Ortho</i> - $P(C_6H_5)_3$ H_a & H_e		
^{13}C	84.9 (s) 118.6 (s) 122.5 (t) 127.6 (t) 128.7 (s) 133.7 (t) 141.1 (dd) 143.4 (t) 152.4 (t)	C_5H_5 C_4 C_3 & C_5 <i>Meta</i> - $P(C_6H_5)_3$ <i>Para</i> - $P(C_6H_5)_3$ <i>Ortho</i> - $P(C_6H_5)_3$ <i>Ips</i> o - $P(C_6H_5)_3$ C_2 & C_6 C_1	5.4 10.8 16.6 14.3, 37.9 18.0 15.2	$ ^4J_{PC} $ $ ^3J_{PC} $ $ ^2J_{PC} $ $ ^3J_{PC} , ^1J_{PC} $ $ ^3J_{PC} $ $ ^2J_{PC} $
^{31}P	52.2 (s)	$P(Ph)_3$		

* Resonances were overlapped in the 1H NMR spectrum, and were therefore found using a $^1H/^{31}P$ HMQC NMR experiment.

Table 3.16 NMR data for $CpRu(PPh_3)(C_{10}H_7)Me$ - Major isomer

In d_8 - THF at 198 K	δ / ppm (multiplicity, integration)	Assignment	Coupling constant / Hz	Assignment
1H	0.95 (d, 3)	Ru-CH ₃	6.7	$ ^2J_{PH} $
	3.72 (br,)*	H _b		
	4.13 (br,)*	H _a		
	4.55 (s, 5)	C ₅ H ₅		
	6.61 (br)*	H _d		
	6.74 (br)*	H _c		
	7.05 (m)*	Para - P(C ₆ H ₅) ₃		
	7.15 (m)*	Meta - P(C ₆ H ₅) ₃		
	7.49 (m, 6)	Ortho - P(C ₆ H ₅) ₃		
^{13}C	-27.3 (d)	Ru-CH ₃	9.9	$ ^2J_{PC} $
	82.4 (s)	C ₅ H ₅	10.3	$ ^3J_{PC} $
	124.8 (m)	C ₄		
	127.5 (d)	Meta - P(C ₆ H ₅) ₃		
	128.8 (s)	Para - P(C ₆ H ₅) ₃	16.2	$ ^2J_{PC} $
	130.3 (m)	C ₃		
	134.2 (d)	Ortho - P(C ₆ H ₅) ₃	44.8	$ ^1J_{PC} $
	142.5 (d)	Ipsa - P(C ₆ H ₅) ₃		
	156.4 (m)	C ₁		
158.1 (m)	C ₂			
^{31}P	63.2 (s)	P(Ph) ₃		

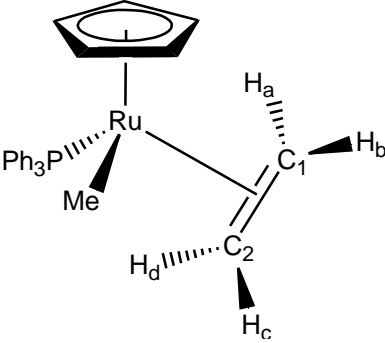
* Resonances were overlapped in the 1H NMR spectrum, and were therefore found using a $^1H/^{31}P$ HMQC NMR experiment.

Table 3.17 NMR data for $\text{CpRu}(\text{PPh}_3)(\text{C}_{10}\text{H}_7)\text{Me}$ – Minor isomer

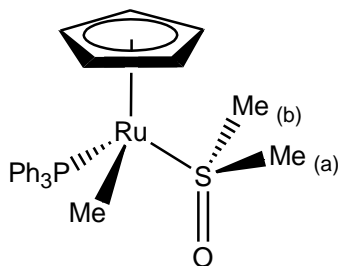
In d_8 - THF at 198 K	δ / ppm (multiplicity, integration)	Assignment	Coupling constant / Hz	Assignment
^1H	0.89 (d, 3) 3.67 (br)* 4.06 (br)* 4.51 (s, 5)	Ru- CH_3 \mathbf{H}_b \mathbf{H}_a $\text{C}_5\mathbf{H}_5$	6.6	$ \text{}^2\text{J}_{\text{PH}} $
^{13}C	-26.5 (d) 81.9 (s)	Ru- CH_3 $\text{C}_5\mathbf{H}_5$	10.0	$ \text{}^2\text{J}_{\text{PC}} $
^{31}P	62.8	$\mathbf{P}(\text{Ph})_3$		

* Resonances were overlapped in the ^1H NMR spectrum, and were therefore found using a $^1\text{H}/^{31}\text{P}$ HMQC NMR experiment.

Table 3.18 NMR data for $CpRu(PPh_3)(C_2H_4)Me$

				
In d_8 -THF at 198 K	δ / ppm (multiplicity, integration)	Assignment	Coupling constant / Hz	Assignment
1H	0.43 (d, 3) 0.67 (m, 1) 1.28 (m, 1) 2.54 (m, 1) 2.81 (m, 1) 4.63 (s, 5) 7.06 (m)* 7.17 (m)* 7.53 (m, 6)	Ru-CH ₃ <i>H_c</i> <i>H_b</i> <i>H_a</i> <i>H_d</i> C ₅ H ₅ <i>Para</i> - P(C ₆ H ₅) ₃ <i>Meta</i> - P(C ₆ H ₅) ₃ <i>Ortho</i> - P(C ₆ H ₅) ₃	6.7	$ ^3J_{PH} $
^{13}C	-28.3 (d) 37.8 (d) 42.5 (d) 82.3 (s) 127.3 (d) 128.4 (s) 133.2 (d) 140.2 (d)	Ru-CH ₃ C ₁ C ₂ C ₅ H ₅ <i>Meta</i> - P(C ₆ H ₅) ₃ <i>Para</i> - P(C ₆ H ₅) ₃ <i>Ortho</i> - P(C ₆ H ₅) ₃ <i>Ipsso</i> - P(C ₆ H ₅) ₃	10.2 7.6 7.6 10.5 16.3 45.4	$ ^2J_{PC} $ $ ^2J_{PC} $ $ ^2J_{PC} $ $ ^3J_{PC} $ $ ^2J_{PC} $ $ ^1J_{PC} $
^{31}P	67.7 (s)	P(Ph) ₃		

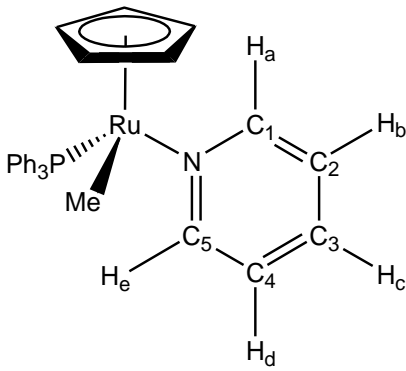
* Resonances were overlapped in the 1H NMR spectrum, and were therefore found using a $^1H/^{31}P$ HMQC NMR experiment.

Table 3.19 NMR data for $CpRu(PPh_3)(O=S(CH_3)_2)Me$ 

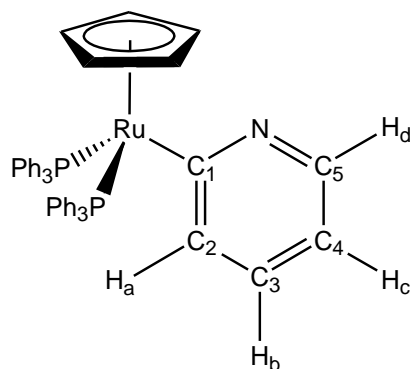
In d_8 - THF at 298 K	δ / ppm (multiplicity, integration)	Assignment	Coupling constant / Hz	Assignment
1H	-0.02 (d, 3) 2.37 (s, 3) 2.56 (s, 3) 4.43 (s, 5) 7.32 (m)* 7.34 (m)* 7.56 (m, 6)	Ru-CH ₃ S-CH ₃ (a) S-CH ₃ (b) C ₅ H ₅ Para - P(C ₆ H ₅) ₃ Meta - P(C ₆ H ₅) ₃ Ortho- P(C ₆ H ₅) ₃	5.8	$ ^3J_{PH} $
^{13}C	-27.3 (d) 46.5 (s) 48.2 (s) 83.3 (s) 127.45 (d) 128.24 (d) 137.30 (d) 141.0 (d)	Ru-CH ₃ S-CH ₃ (a) S-CH ₃ (b) C ₅ H ₅ Meta - P(C ₆ H ₅) ₃ Para - P(C ₆ H ₅) ₃ Ortho- P(C ₆ H ₅) ₃ Ipso - P(C ₆ H ₅) ₃	10.2 16.4 44.7	$ ^3J_{PC} $ $ ^2J_{PC} $ $ ^1J_{PC} $
^{31}P	59.0 (s)	P(Ph) ₃		

* Resonances were overlapped in the 1H NMR spectrum, and were therefore found using a $^1H/^{31}P$ HMQC NMR experiment.

Table 3.20 NMR data for $CpRu(PPh_3)(NC_5H_5)Me$

				
In d_8 - THF at 198 K	δ / ppm (multiplicity, integration)	Assignment	Coupling constant / Hz	Assignment
1H	0.30 (d, 3) 4.16 (s, 5) 6.77 (m)* 7.20 (m)* 7.22 (m)* 7.34 (m)* 7.38 (m)* 8.59 (m, 2)	Ru-CH ₃ C ₅ H ₅ H _b & H _d Para - P(C ₆ H ₅) ₃ Meta - P(C ₆ H ₅) ₃ H _c Ortho - P(C ₆ H ₅) ₃ H _a & H _e	5.6	$ ^3J_{PH} $
^{13}C	-28.7 (d) 85.1 (s) 127.7 (m) 127.9 (d) 128.6 (m) 128.9 (s) 134.6 (d) 141.4 (d) 157.5 (m)	Ru-CH ₃ C ₅ H ₅ C ₂ & C ₄ Meta - P(C ₆ H ₅) ₃ C ₃ Para - P(C ₆ H ₅) ₃ Ortho - P(C ₆ H ₅) ₃ Ipso - P(C ₆ H ₅) ₃ C ₁ & C ₅	10.6 162.8 10.1 147.8 16.2 45.3 176.3	$ ^2J_{PC} $ $ ^1J_{CH} $ $ ^3J_{PC} $ $ ^1J_{CH} $ $ ^2J_{PC} $ $ ^1J_{PC} $ $ ^1J_{CH} $
^{31}P	68.3 (s)	P(Ph) ₃		

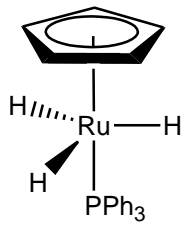
* Resonances were overlapped in the 1H NMR spectrum, and were therefore found using a $^1H/^{31}P$ HMQC NMR experiment.

Table 3.21 NMR data for $CpRu(PPh_3)_2(NC_5H_4)$ 

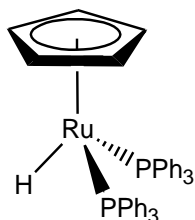
In d_8 - THF at 298 K	δ / ppm (multiplicity, integration)	Assignment	Coupling constant / Hz	Assignment
1H	4.64 (s, 5) 6.89 (t, 1) 7.00 (m)* 7.02 (m)* 7.14 (m)* 7.21 (m)* 7.51(m, 12) 8.48 (m, 1)	C_5H_5 H_c H_a <i>Para</i> - $P(C_6H_5)_3$ <i>Meta</i> - $P(C_6H_5)_3$ H_b <i>Ortho</i> - $P(C_6H_5)_3$ H_d	5.6	$ ^3J_{HH} $
^{13}C	84.5 (s) 116.5 (s) 127.3 (t) 128.1 (s) 133.7 (s) 134.1 (s) 134.5 (t) 141.8 (dd) 146.2 (t) 183.4 (t)	C_5H_5 C_5 <i>Meta</i> - $P(C_6H_5)_3$ <i>Para</i> - $P(C_6H_5)_3$ C_4 C_3 <i>Ortho</i> - $P(C_6H_5)_3$ <i>Ipsa</i> - $P(C_6H_5)_3$ C_2 C_1	10.4 16.6 13.8, 34.9 10.3 14.5	$ ^3J_{PC} $ $ ^2J_{PC} $ $ ^3J_{PC} , ^1J_{PC} $ $ ^3J_{PC} $ $ ^2J_{PC} $
^{31}P	54.7	$P(Ph)_3$		

* Resonances were overlapped in the 1H NMR spectrum, and were therefore found using a $^1H/^{31}P$ HMQC NMR experiment.

Table 3.22 NMR data for $\text{CpRu}(\text{PPh}_3)\text{H}_3$ (C_{3v})

				
In d_8 - THF at 298 K	δ / ppm (multiplicity, integration)	Assignment	Coupling constant / Hz	Assignment
^1H	-9.64 (d, 3) 4.81 (s, 5) 7.03 (m)* 7.10 (m)* 7.73 (m, 6)	Ru-H C_5H_5 <i>Para</i> - $\text{P}(\text{C}_6\text{H}_5)_3$ <i>Meta</i> - $\text{P}(\text{C}_6\text{H}_5)_3$ <i>Ortho</i> - $\text{P}(\text{C}_6\text{H}_5)_3$	19.0	$ ^2\text{J}_{\text{PH}} $
^{13}C	83.6 (s) 127.7 (d) 129.0 (s) 133.4 (d) 141.2 (d)	C_5H_5 <i>Meta</i> - $\text{P}(\text{C}_6\text{H}_5)_3$ <i>Para</i> - $\text{P}(\text{C}_6\text{H}_5)_3$ <i>Ortho</i> - $\text{P}(\text{C}_6\text{H}_5)_3$ <i>Ipsa</i> - $\text{P}(\text{C}_6\text{H}_5)_3$	10.3 16.1 44.2	$ ^3\text{J}_{\text{PC}} $ $ ^2\text{J}_{\text{PC}} $ $ ^1\text{J}_{\text{PC}} $
^{31}P	73.1 (s)	$\text{P}(\text{Ph})_3$		

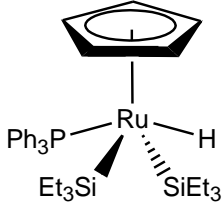
* Resonances were overlapped in the ^1H NMR spectrum, and were therefore found using a $^1\text{H}/^{31}\text{P}$ HMQC NMR experiment.

Table 3.23 NMR data for $CpRu(PPh_3)_2H$ 

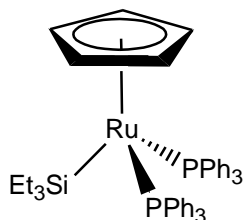
In d_8 -THF at 298 K	δ / ppm (multiplicity, integration)	Assignment	Coupling constant / Hz	Assignment
1H	-11.59 (t, 1) 4.49 (s, 5) 6.89 (m)* 6.92 (m)* 7.52 (m, 12)	Ru- <i>H</i> C_5H_5 <i>Para</i> - $P(C_6H_5)_3$ <i>Meta</i> - $P(C_6H_5)_3$ <i>Ortho</i> - $P(C_6H_5)_3$	33.8	$ ^3J_{PH} $
	81.8 (s) 127.8 (t) 128.5 (s) 130.1 (t) 141.7 (dd)	C_5H_5 <i>Meta</i> - $P(C_6H_5)_3$ <i>Para</i> - $P(C_6H_5)_3$ <i>Ortho</i> - $P(C_6H_5)_3$ <i>Ipsa</i> - $P(C_6H_5)_3$	10.5 16.3 14.4, 37.7	$ ^3J_{PC} $ $ ^2J_{PC} $ $ ^3J_{PC} , ^1J_{PC} $
^{31}P	68.3 (s)	$P(Ph)_3$		

* Resonances were overlapped in the 1H NMR spectrum, and were therefore found using a $^1H/^{31}P$ HMQC NMR experiment.

Table 3.24 NMR data for $CpRu(PPh_3)(SiEt_3)_2H$

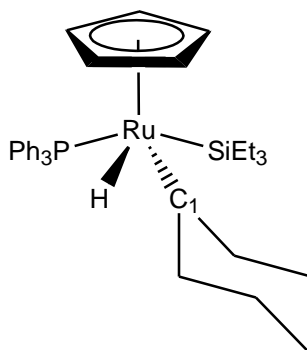
				
In d_8 -THF at 298 K	δ / ppm (multiplicity, integration)	Assignment	Coupling constant / Hz	Assignment
1H	-11.89 (d, 1) 0.97 (br, 18) 1.15 (br, 12) 4.76 (s, 5) 6.98 (m)* 7.06 (m)* 7.41 (m)*	Ru- H Si-CH ₂ CH ₃ Si-CH ₂ CH ₃ C ₅ H ₅ <i>Para</i> - P(C ₆ H ₅) ₃ <i>Meta</i> - P(C ₆ H ₅) ₃ <i>Ortho</i> - P(C ₆ H ₅) ₃	9.7	$ ^3J_{PH} $
^{13}C	12.8 (s) 14.2 (d) 85.1 (s) 127.2 (d) 128.6 (s) 133.6 (t) 140.4 (dd)	Si-CH ₂ CH ₃ Si-CH ₂ CH ₃ C ₅ H ₅ <i>Meta</i> - P(C ₆ H ₅) ₃ <i>Para</i> - P(C ₆ H ₅) ₃ <i>Ortho</i> - P(C ₆ H ₅) ₃ <i>Ipsa</i> - P(C ₆ H ₅) ₃	6.8 10.2 16.3 13.4, 45.1	$ ^3J_{PC} $ $ ^3J_{PC} $ $ ^2J_{PC} $ $ ^3J_{PC} , ^1J_{PC} $
^{31}P	58.0 (s)	P(Ph)₃		
^{29}Si	24.29 (d)	Si	14.4	$ ^2J_{PSi} $

* Resonances were overlapped in the 1H NMR spectrum, and were therefore found using a $^1H/^{31}P$ HMQC NMR experiment.

Table 3.25 NMR data for $CpRu(PPh_3)_2(SiEt_3)$ 

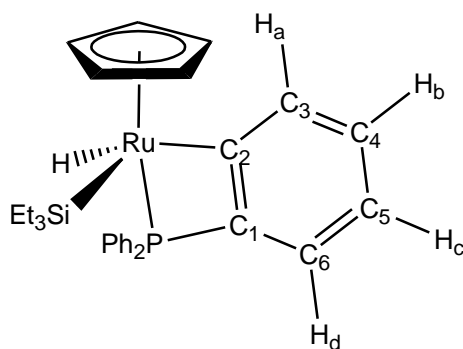
In d_8 -THF at 298 K	δ / ppm (multiplicity, integration)	Assignment	Coupling constant / Hz	Assignment
1H	1.19 (br, 9) 1.31 (br, 6) 4.53 (s, 5) 6.88 (m)* 6.97 (m)* 7.26 (m)*	Si-CH ₂ CH ₃ Si-CH ₂ CH ₃ C ₅ H ₅ <i>Para</i> - P(C ₆ H ₅) ₃ <i>Meta</i> - P(C ₆ H ₅) ₃ <i>Ortho</i> - P(C ₆ H ₅) ₃		
^{13}C	12.6 (s) 14.4 (t) 83.1 (s) 127.0 (d) 128.1 (s) 133.7 (t) 140.3 (dd)	Si-CH ₂ CH ₃ Si-CH ₂ CH ₃ C ₅ H ₅ <i>Meta</i> - P(C ₆ H ₅) ₃ <i>Para</i> - P(C ₆ H ₅) ₃ <i>Ortho</i> - P(C ₆ H ₅) ₃ <i>Ipsa</i> - P(C ₆ H ₅) ₃	6.4 10.5 16.4 14.3, 35.8	$ ^3J_{PC} $ $ ^3J_{PC} $ $ ^2J_{PC} $ $ ^3J_{PC} , ^1J_{PC} $
^{31}P	54.4 (s)	<i>P</i> (Ph) ₃		
^{29}Si	15.98 (t)	<i>Si</i>	25.6	$ ^2J_{PSi} $

* Resonances were overlapped in the 1H NMR spectrum, and were therefore found using a $^1H/^{31}P$ HMQC NMR experiment.

Table 3.26 NMR data for $CpRu(PPh_3)(SiEt_3)(C_6H_{11})H$ 

In d_8 - THF at 298 K	δ / ppm (multiplicity, integration)	Assignment	Coupling constant / Hz	Assignment
1H	-12.04 (d, 1) 0.31 (br)* 0.80 (br)* 4.58 (s, 5) 7.18 (m)* 7.21 (m)* 7.57 (m, 6)	Ru- H Si- CH₂CH₃ Si- CH₂CH₃ C₅H₅ <i>Para</i> - P(C₆H₅) ₃ <i>Meta</i> - P(C₆H₅) ₃ <i>Ortho</i> - P(C₆H₅) ₃	26.3	$ ^3J_{PH} $
^{13}C	-13.9 (d) 9.3 (s) 14.0 (s) 83.5 (s) 127.8 (s) 128.1 (d) 132.3 (d) 140.9 (d)	C₁ Si- CH₂CH₃ Si- CH₂CH₃ C₅H₅ <i>Meta</i> - P(C₆H₅) ₃ <i>Para</i> - P(C₆H₅) ₃ <i>Ortho</i> - P(C₆H₅) ₃ <i>Ipsa</i> - P(C₆H₅) ₃	15.7 10.4 16.4 44.9	$ ^2J_{PC} $ $ ^3J_{PC} $ $ ^2J_{PC} $ $ ^1J_{PC} $
^{31}P	75.3 (s)	P(Ph)₃		

* Resonances were overlapped in the 1H NMR spectrum, and were therefore found using a $^1H/^{31}P$ HMQC NMR experiment.

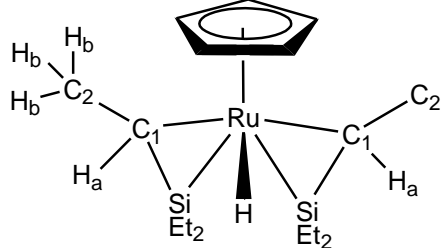
Table 3.27 NMR data for $CpRu(\kappa^2-2-C_6H_4PPh_2)(SiEt_3)H$ 

In d_8 -THF at 198 K	δ / ppm (multiplicity, integration)	Assignment	Coupling constant / Hz	Assignment
1H	-9.13 (d, 1) 0.38 & 0.54 (br)* 0.81 (br)* 4.78 (s, 5) 7.01 (m)* 7.07 (m)* 7.18 (m)* 7.37 (m)* 7.55 (m)* 7.62 (m)* 7.74 (m)*	Ru-H Si-CH₂CH₃ Si-CH₂CH₃ C₅H₅ <i>Para</i> - P(C ₆ H ₅) ₃ <i>Meta</i> - P(C ₆ H ₅) ₃ H_c <i>Ortho</i> - P(C ₆ H ₅) ₃ H_b H_d H_a	23.0	$ ^3J_{PH} $
^{13}C	9.0 (s) 13.8 (d) 83.9 (s) 127.7 (d) 128.4** 128.6** 130.6 (d) 133.8 (d) 135.4** 141.2 (d) 141.6 (d) 144.8 (d) 153.5 (d)	Si-CH₂CH₃ Si-CH₂CH₃ C₅H₅ <i>Meta</i> - P(C ₆ H ₅) ₃ <i>Para</i> - P(C ₆ H ₅) ₃ C₅ C₄ <i>Ortho</i> - P(C ₆ H ₅) ₃ C₆ <i>Ipsa</i> - P(C ₆ H ₅) ₃ C₂ C₃ C₁	6.2 10.1 4.3 16.2 44.7 16.3 11.4 43.2	$ ^2J_{PC} $ $ ^3J_{PC} $ $ ^4J_{PC} $ $ ^2J_{PC} $ $ ^1J_{PC} $ $ ^2J_{PC} $ $ ^3J_{PC} $ $ ^1J_{PC} $
^{31}P	-16.9 (s)	P(C₆H₅)₂(C₆H₄)		
^{29}Si	25.6 (d)	Ru-Si	15.8	

* Resonances were overlapped in the 1H NMR spectrum, and were therefore found using a $^1H/^{31}P$ HMQC NMR experiment.

** Peaks only observed using $^1H/^{13}C$ HMQC NMR experiment.

Table 3.28 NMR data for $CpRu(SiEt_2CH_2CH_3)_2H$

				
In d_8 -THF at 198 K	δ / ppm (multiplicity, integration)	Assignment	Coupling constant / Hz	Assignment
1H	-12.67 (s, 1) 0.26 (s, 2) 0.73 (s, 18) 0.75 (s, 6) 0.94 (s, 12) 5.09 (s, 5)	Ru- <i>H</i> <i>H_a</i> Si-CH ₂ CH ₃ <i>H_b</i> Si-CH ₂ CH ₃ <i>C₅H₅</i>		
^{13}C	-11.5 (s) 8.9 (s) 9.4 (s) 15.7 (s) 81.2 (s)	<i>C₁</i> Si-CH ₂ CH ₃ <i>C₂</i> Si-CH ₂ CH ₃ <i>C₅H₅</i>		
^{29}Si	29.8	Ru- <i>Si</i>		

Chapter 4

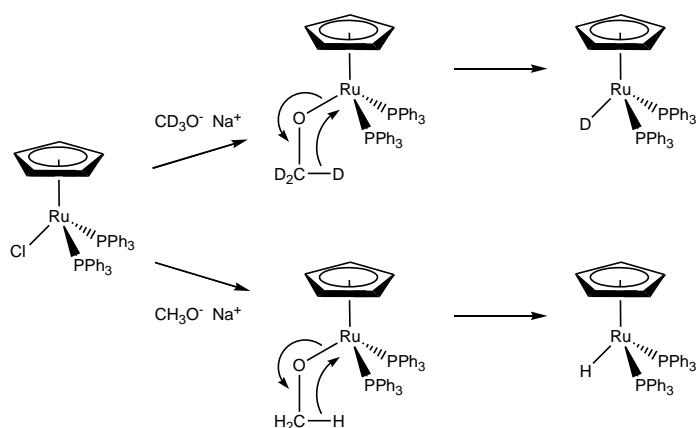
Thermal and Photochemical Reactions of $\text{CpRu}(\text{PPh}_3)_2\text{H}$

4.1 Introduction

The complex, $\text{CpRu}(\text{PPh}_3)_2\text{H}$, is readily prepared in high yield (94%) by treating $\text{CpRu}(\text{PPh}_3)_2\text{Cl}$ with sodium methoxide solution.²⁵⁹ Other preparations using sodium methylate,²⁶⁰ lithium aluminium hydride²⁶¹ or triethylamine in place of sodium methoxide have been reported, though these methods often result in lower yields (78%, 84% and 76%, respectively). Studies using sodium ethoxide were found to produce lower yields of the hydride product, which were subsequently found to be less pure than the previous reaction using sodium methoxide.

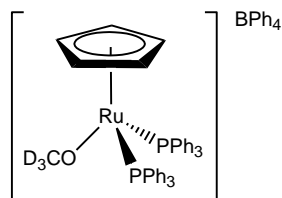
Reactions using sodium t-butoxide, however, failed to yield $\text{CpRu}(\text{PPh}_3)_2\text{H}$.²⁶² Based on the correlation of the decline in product yields with the increasing alkyl chain length of the methoxide reagent, it was believed that nucleophilic addition of an alkoxylate anion at $\text{CpRu}(\text{PPh}_3)_2\text{Cl}$ led the formation of an alkoxy complex. Subsequent β -elimination of the hydride onto the ruthenium centre led to the formation of $\text{CpRu}(\text{PPh}_3)_2\text{H}$ (Figure 4.1). Evidence for this mechanism was provided by the ^1H NMR observation of the hydride resonance when using CH_3OD , while no such observation was made when using CD_3OD , which was consequently found to form the deuteride derivative, $\text{CpRu}(\text{PPh}_3)_2\text{D}$ (Figure 4.1), and hence lack a visible hydride resonance²⁶² This mechanism bears a similarity to that proposed by Vaska and DiLuzio for iridium complexes.²⁶³

Figure 4.1 Formation of the deuteride and protio complexes, $\text{CpRu}(\text{PPh}_3)_2\text{D}$ and $\text{CpRu}(\text{PPh}_3)_2\text{H}$, via an alkoxy intermediate



Further evidence for the alkoxy intermediate was provided by the NMR observation of the “trapped” alkoxy complex, $[\text{CpRu}(\text{PPh}_3)_2(\text{OCD}_3)]^+ \text{BPh}_4^-$ (Figure 4.2), which rearranges to yield $\text{CpRu}(\text{PPh}_3)_2\text{H}$.²⁶⁴

Figure 4.2 “Trapped” alkoxy complex, $[\text{CpRu}(\text{PPh}_3)_2(\text{OCD}_3)]^+ \text{BPh}_4^-$ ²⁶⁴



Most of the literature reporting the formation of $\text{CpRu}(\text{PPh}_3)_2\text{H}$ does so as a side product of other reactions. A notable example, is the formation of $\text{CpRu}(\text{PPh}_3)_2\text{H}$ following the reaction of $\text{CpRu}(\text{PPh}_3)_2\text{Cl}$ with alkyl Grignard reagents (ClMg^iPr , $\text{ClMgCH}_2^i\text{Pr}$, ClMgBu or ClMg^tBu).²⁶⁵ Presumably, the alkyl complexes $\text{CpRu}(\text{PPh}_3)_2\text{R}$ ($\text{R} = ^i\text{Pr}$, CH_2^iPr , Bu or ^tBu) undergo β -H elimination to the metal centre, which is consistent with the mechanism reported previously for the alkoxy moiety. This is supported by the effect that increasing the reaction temperature increases the yield of $\text{CpRu}(\text{PPh}_3)_2\text{H}$.

Relatively few studies have been reported regarding the reactivity of $\text{CpRu}(\text{PPh}_3)_2\text{H}$ compared with the numbers for $\text{CpRu}(\text{PPh}_3)_2\text{Cl}$ and $\text{CpRu}(\text{PPh}_3)_2\text{Me}$. Notable reactions include the exchange of the hydride for halide (eg. $\text{CpRu}(\text{PPh}_3)_2\text{X}$, where $\text{X} = \text{Cl}$),^{259, 266}

Br,^{259, 262} or I²⁶²). However, more recent studies have determined that CpRu(PPh₃)₂H possesses catalytic behaviour in stereoselective carbene-carbene coupling,²⁶⁷ and in the ionic hydrogenation of iminium cations.²⁶⁸ Additionally via a α -hydrogen (C_{sp}³-H) activation it turns trifluoro compounds into olefins,²⁶⁹ and hydrogenation of β -N-substituted enaminoesters.²⁷⁰

4.2 Overview

As described in the previous chapter, CpRu(PPh₃)₂H is formed as a side product in a number of photochemical reactions of CpRu(PPh₃)₂Me with substrates. This was evident particularly for the reaction of CpRu(PPh₃)₂Me with HSiEt₃, which during the formation of the silyl products, CpRu(PPh₃)₂H was observed to gradually form through a side reaction. Additionally, thermally initiated ligand exchange for CpRu(PPh₃)₂H has been noted in previous literature sources as a slow process.^{259, 271} Owing to the difficulty in preventing this complex from forming in such photochemical reactions, it would be useful to determine the conditions by which CpRu(PPh₃)₂H reacts. This would enable the capability to reverse the reaction and form the precursor complexes in greater quantities, for improved characterisation, or provide routes to other novel complexes.

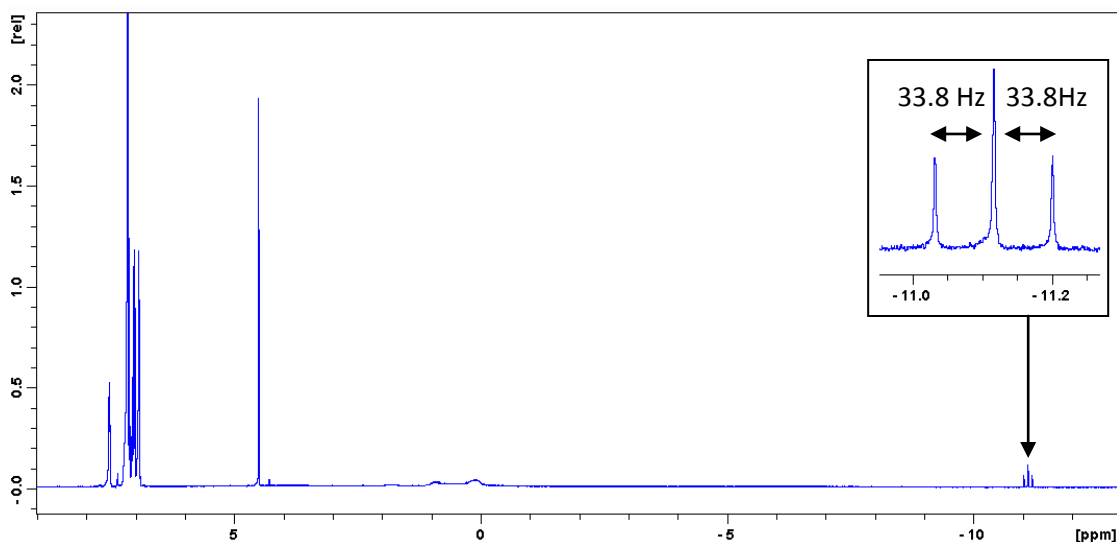
As can be inferred from the previous experiments, CpRu(PPh₃)₂H does not absorb UV light at 325 nm (the the wavelength emitted by the laser source), and so is not reactive under these conditions. If the formation of CpRu(PPh₃)₂H were a side product of a catalytic cycle, irradiation of the sample using a second frequency would be required. This would facilitate the dissociation of one of the triphenylphosphine ligands from the metal centre, and allow for further reactions. The aim of this chapter is therefore to determine the conditions by which CpRu(PPh₃)₂H will photochemically react, and demonstrate this reactivity with a range of substrates.

4.3 Synthesis and characterisation of $\text{CpRu}(\text{PPh}_3)_2\text{H}$

$\text{CpRu}(\text{PPh}_3)_2\text{H}$ was prepared by treating a sample of $\text{CpRu}(\text{PPh}_3)_2\text{Cl}$ with sodium methoxide, according to known literature methods.²⁶⁰ Full details of this synthesis are described in Chapter 7, section 7.2.3.1.

A ^1H NMR spectrum recorded for this sample in d_6 -benzene (Figure 4.3) revealed a single peak at δ 4.42, which is typical of a cyclopentadienyl ring. This signal integrated in a ratio of 5:1 with a triplet signal in the hydride region at δ -10.80 ($J_{\text{PH}} = 33.8$ Hz). The triplet splitting demonstrates that two phosphine ligands are coordinated to the metal centre. This diagnostic feature of the spectra for this complex is similar to that of $\text{CpRu}(\text{PPh}_3)_2\text{Me}$, where the number of coordinated phosphines for that complex and its products, could be determined by the multiplicity of the Ru-methyl ^1H NMR resonance.

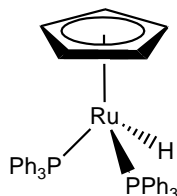
Figure 4.3 ^1H NMR spectrum recorded for $\text{CpRu}(\text{PPh}_3)_2\text{H}$ in d_6 -benzene



The recorded $^{31}\text{P}\{^1\text{H}\}$ NMR spectrum revealed only an intense singlet at δ 68.0. This signal was shown to connect through a $^1\text{H}/^{31}\text{P}$ HMQC NMR experiment to the ^1H resonances at δ 4.42 and -10.80, in addition to a third signal at δ 7.48, which is consistent with the resonance for the *ortho*-phenyl proton resonance of the coordinated triphenylphosphine ligands. The corresponding ^1H signals for the *meta* and *para*-phenyl protons (δ 7.03 and 6.93) were found using a ^1H COSY NMR experiment. These signals

are consistent with those found for $\text{CpRu}(\text{PPh}_3)_2\text{H}$ (Figure 4.4) in the previous experiments (Chapter 3, sections 3.4.9 and 3.4.10.6), and literature sources.^{259, 265} MS was also useful in the confirmation of the identity of this complex, by showing peaks corresponding to m/z $\text{M}^+ = 692$ and $\text{M}^+ - \text{PPh}_3 = 429$. Full NMR characterisation data for this complex are presented in Table 4.1.

Figure 4.4 The structure of $\text{CpRu}(\text{PPh}_3)_2\text{H}$



4.4 Thermal and photochemical reactions of $\text{CpRu}(\text{PPh}_3)_2\text{H}$ with substrates

4.4.1 Reactions of $\text{CpRu}(\text{PPh}_3)_2\text{H}$ with PEt_3

4.4.1.1 Thermally initiated reaction

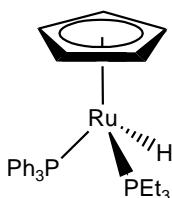
A J-Y NMR tube was charged with $\text{CpRu}(\text{PPh}_3)_2\text{H}$ in d_6 -benzene. The tube was degassed an excess of PEt_3 was added. ^1H and $^{31}\text{P}\{^1\text{H}\}$ NMR spectra were then recorded for the sample, which showed that no immediate reaction had taken place. The sample was therefore heated to 323 K for 24 hours to enable the complex to react thermally with the substrate.

The ^1H and $^{31}\text{P}\{^1\text{H}\}$ NMR spectra following heating the sample, showed no signs of reaction. The sample was then heated for a further 24 hours at 353 K. The NMR spectra then recorded failed to show the formation of any product resonances. Only after being left for a week to react thermally at 353 K, were product signals observed.

The $^{31}\text{P}\{^1\text{H}\}$ NMR spectrum now contained two new doublet resonances at δ 47.8 (41.0 Hz) and δ 65.5 (41.0 Hz). These signals were both shown in a $^1\text{H}/^{31}\text{P}$ HMQC spectrum

to couple to the same ^1H signal at δ 4.56, which is the Cp resonance for the complex. This Cp resonance integrates to 5 when compared with the integral of 1 for the new triplet hydride signal at δ -11.18 ($J_{\text{PH}} = 34.2$ Hz). These signals are consistent with those expected for $\text{CpRu}(\text{PPh}_3)(\text{PEt}_3)\text{H}$ (Figure 4.5), based on the chloride and methyl analogues (discussed in Chapters 2 and 3). There was no evidence to suggest the formation of a bis-substituted product.

Figure 4.5 Structure of $\text{CpRu}(\text{PPh}_3)(\text{PEt}_3)\text{H}$



Mono substitution product

4.4.1.2 Photochemical reaction

A second sample of $\text{CpRu}(\text{PPh}_3)_2\text{H}$ with PEt_3 in d_6 -benzene was prepared, and irradiated using the *ex situ* UV set-up for 20 hours. Following irradiation of the sample, ^1H and $^{31}\text{P}\{^1\text{H}\}$ NMR spectra were recorded, these show new product resonances which were consistent with the previously described substituted complex, $\text{CpRu}(\text{PPh}_3)(\text{PEt}_3)\text{H}$ (17 % conversion from the starting material). Evidence for the bis-substituted form (34 % conversion from the starting material) was found, with new ^1H peaks at δ 4.69 and -11.30 (t, 35.5 Hz), Cp and hydride protons, respectively. A $^1\text{H}/^{31}\text{P}$ HMQC connected a new ^{31}P signal at δ 52.8, to these ^1H peaks, in addition to new signals at δ 1.78, 1.86 and 0.94. Based on previous characterisations, these ^1H resonances correspond to the protons of the ethyl chains in the two bound PEt_3 ligands. Full NMR characterisation data for this complex appears in Table 4.2.

These two reactions demonstrate that photochemical techniques may be employed to drive the conversion of $\text{CpRu}(\text{PPh}_3)_2\text{H}$, to form products not obtained by thermal methods. The following section describes the reaction of $\text{CpRu}(\text{PPh}_3)_2\text{H}$ with CO.

4.4.2 Reactions of CpRu(PPh₃)₂H with CO

4.4.2.1 Thermally initiated reaction

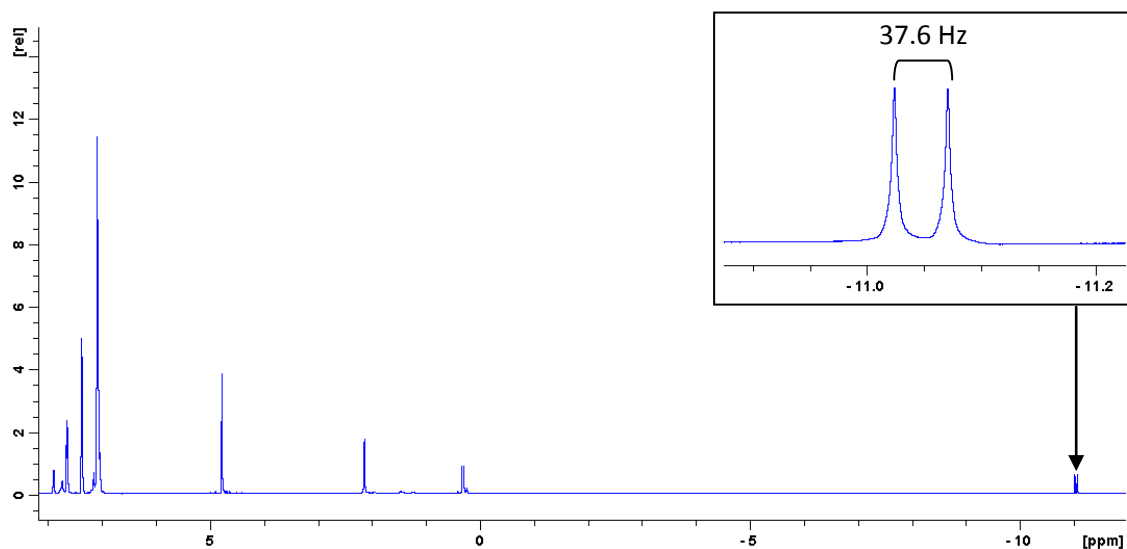
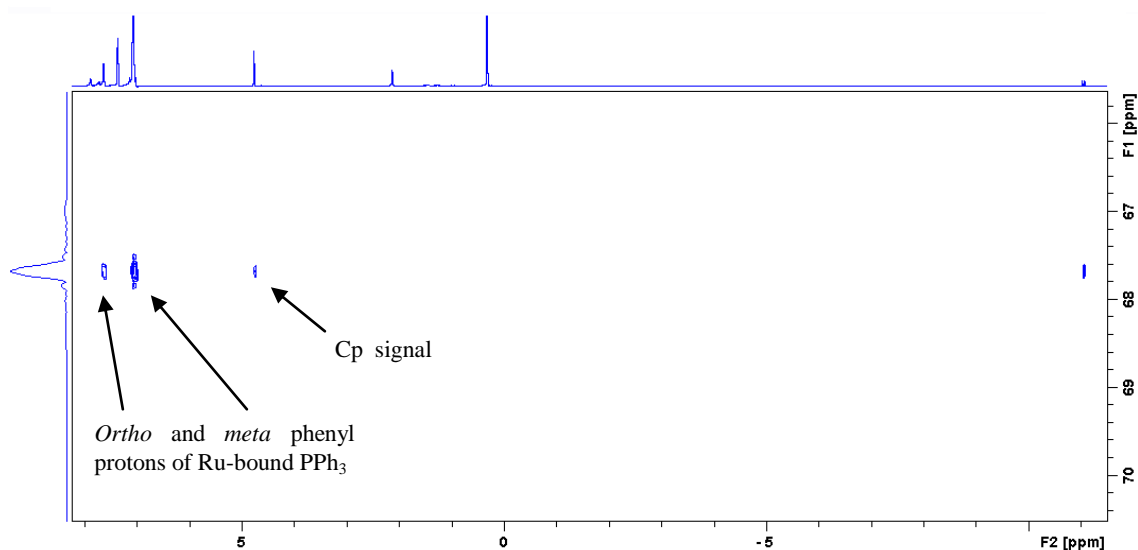
A J-Y NMR tube was charged with CpRu(PPh₃)₂H in d₆-benzene. The tube was degassed and pressurised with 1.5 bar CO. ¹H and ³¹P{¹H} NMR spectra were then recorded for the sample, which showed that no immediate reaction had taken place. The sample was therefore heated to 323 K for 24 hours to enable the complex to react thermally with the substrate.

No evidence of reaction was observed at 323 K or 353 K, even when left to react for one week. This lack of reactivity is consistent with the previously reported preparation of CpRu(PPh₃)(CO)H, which required reaction conditions of 10 atm CO, at 413 K for 16 hours, in ethylene glycol dimethyl ether.²⁵⁹

4.4.2.2 Photochemical reaction

An analogous NMR sample was prepared as described previously for the thermal reaction. Following irradiation of the sample for 20 hours, the recorded ³¹P{¹H} NMR spectrum showed only minimal conversion to the mono carbonyl product (CpRu(PPh₃)(CO)H), with no evidence of the formation of the bis-carbonyl product, as only one single new Cp resonance at δ 4.72 was found in the ¹H NMR spectrum.

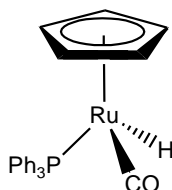
The low conversion of CpRu(PPh₃)₂H into new products made full characterisation of this sample difficult. To aid in this characterisation, CpRu(PPh₃)(CO)H was synthesised from CpRu(CO)₂H (synthesis of this complex is detailed in Chapter 7) which was subsequently reacted with an excess of PPh₃. Figures 4.6 and 4.7 show the ¹H and ¹H/³¹P NMR spectra recorded for this complex.

Figure 4.6 ^1H NMR spectrum for the synthesised $\text{CpRu}(\text{PPh}_3)(\text{CO})\text{H}$ Figure 4.7 $^1\text{H}/^{31}\text{P}$ HMQC for the synthesised $\text{CpRu}(\text{PPh}_3)(\text{CO})\text{H}$ 

The NMR data for this complex have not been previously reported, presumably owing to the difficulty in forming this product in any appreciable quantity. However IR data has been previously obtained, and therefore an IR spectrum was recorded for the present complex in order to confirm it matches with the literature values. One ν_{CO} band was obtained at 1974 cm^{-1} which correlated well with the literature value of 1976 cm^{-1} .²⁵⁹

²⁷² MS techniques also showed peaks consistent with m/z $M^+ = 457$ and $M^+ - PPh_3 = 429$, confirming the identity of the product.

Figure 4.8 Structure of $CpRu(PPh_3)(CO)H$

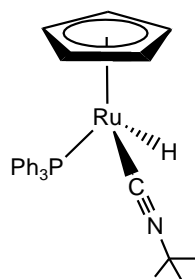


4.4.3 Reactions of $CpRu(PPh_3)_2H$ with tBuNC

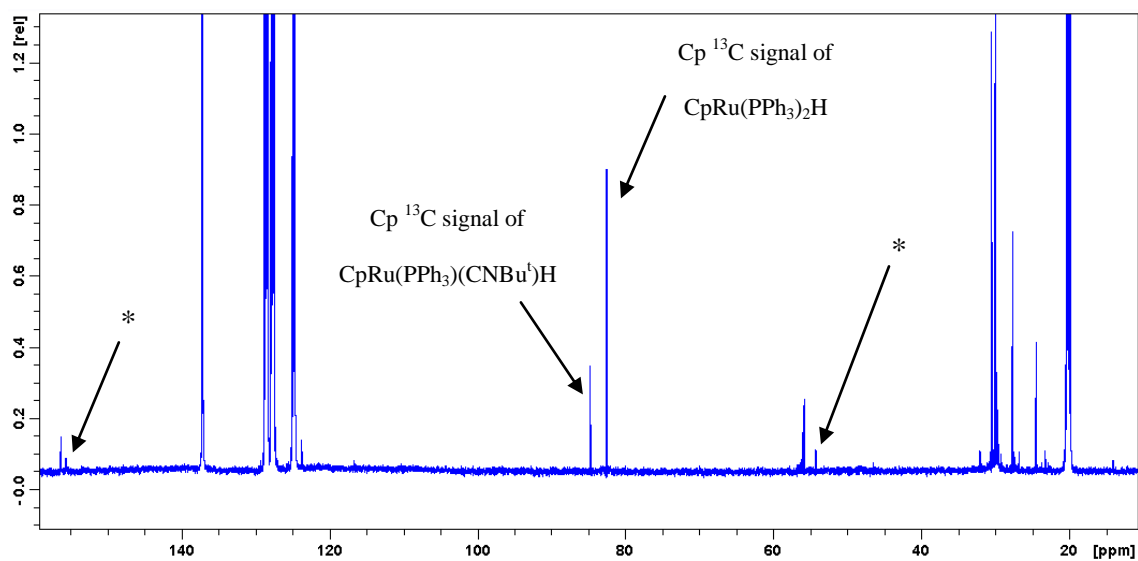
4.4.3.1 Thermal and photochemical reactions

As described for the previous experiment involving CO, no thermal reaction was observed in the recorded NMR spectra, for reactions at 323 K or 353 K, or after prolonged heating. An analogous NMR sample was prepared as described in the previous section, which was charged with $CpRu(PPh_3)_2H$ and tBuNC , in d_6 -benzene. Photochemical reaction of the sample was initiated using the *ex situ* set-up, and the sample tube was irradiated for 20 hours.

As with the previous photochemical reaction between CO and $CpRu(PPh_3)_2H$ (Section 4.4.2.2), only minimal conversion was achieved (7%, relative to the ${}^{31}P$ intensity of the starting material). The NMR signals obtained for the complex were similar to the characterisation data found in the literature for $CpRu(PPh_3)(CNBu^t)H$ (Figure 4.10), which was synthesised by treating $CpRu(PPh_3)(CNBu^t)Cl$ with $LiAlH_4$. ²⁷³ NMR data for the species obtained in this work are presented in Table 4.4.

Figure 4.9 Structure of $\text{CpRu}(\text{PPh}_3)(\text{CNBu}^t)\text{H}$ 

Mono

Figure 4.10 $^{13}\text{C}\{^1\text{H}\}$ NMR spectrum of $\text{CpRu}(\text{PPh}_3)(\text{CNBu}^t)\text{H}$, showing the relative conversion from $\text{CpRu}(\text{PPh}_3)_2\text{H}$ 

Where '*' highlights the $\text{Ru-CN-C}(\text{CH}_3)_3$ and $\text{Ru-CN-C}(\text{CH}_3)_3$ ^{13}C signals.

4.4.4 Reactions of $\text{CpRu}(\text{PPh}_3)_2\text{H}$ with HSiEt_3

4.4.4.1 Thermally initiated reaction

An NMR tube was charged with $\text{CpRu}(\text{PPh}_3)_2\text{H}$ in d_6 -benzene. The tube was degassed and an excess of HSiEt_3 was added. ^1H and $^{31}\text{P}\{^1\text{H}\}$ NMR spectra were recorded for the sample to demonstrate a reaction had taken place when compared with subsequently recorded spectra. The sample was heated to 323 K for 24 hours to enable the complex to

react thermally with the substrate. After 24 hours of heating, ^1H and $^{31}\text{P}\{^1\text{H}\}$ NMR spectra were recorded. Comparison of these spectra with the ones recorded previously revealed no signs of reactions. Heating of the sample for a further 24 hours still resulted in no change in the NMR resonances.

One of the possible products of the reaction was expected to be $\text{CpRu}(\text{PPh}_3)(\text{H}_2)\text{SiEt}_3$, as similar complexes have previously been reported as stable by Tilley *et al.*^{273, 274} Consequently, photochemical methods were considered (based on the previous reactions in Chapter 3, section 3.4.10), which would be envisioned to lead to the formation of products.

4.4.4.2 Photochemical reaction

An NMR tube was charged with $\text{CpRu}(\text{PPh}_3)_2\text{H}$ in d_6 -benzene. The tube was degassed and HSiEt_3 was added. The sample was irradiated for 12 hours at room temperature using the broadband UV Lamp set-up. Comparison of the NMR spectra recorded before and after photolysis show no differences in the resonances obtained, therefore no reaction with HSiEt_3 has occurred.

4.4.5 Reactions of $\text{CpRu}(\text{PPh}_3)_2\text{H}$ with H_2

A thermal reaction for this sample was not attempted owing to the results of the thermal reaction of $\text{CpRu}(\text{PPh}_3)_2\text{Me}$ with 1.5 bar of H_2 (Chapter 3, section 3.4.9.1), which led to only the formation of $\text{CpRu}(\text{PPh}_3)_2\text{H}$, with no evidence in the recorded NMR spectra for the formation of further products.

During the photochemical reaction of $\text{CpRu}(\text{PPh}_3)_2\text{Me}$ with H_2 , the trihydride species, $\text{CpRu}(\text{PPh}_3)(\text{H})_3$, was detected. Previous studies reported in the literature observed that $\text{CpRu}(\text{PPh}_3)(\text{H})_3$ could only be formed by treating $[\text{CpRu}(\text{PPh}_3)(\text{NCCH}_3)_2]\text{BF}_4$ with LiAlH_4 in THF.²⁶¹ The following photochemical experiment of $\text{CpRu}(\text{PPh}_3)_2\text{H}$ with H_2 outlines the attempt to access $\text{CpRu}(\text{PPh}_3)(\text{H})_3$ directly from $\text{CpRu}(\text{PPh}_3)_2\text{H}$.

An NMR tube was charged with $\text{CpRu}(\text{PPh}_3)_2\text{H}$ and H_2 in d_6 -benzene. The tube was irradiated for 12 hours at room temperature using the broadband UV lamp set-up.

Comparison of the ^1H and $^{31}\text{P}\{^1\text{H}\}$ NMR spectra recorded before and after irradiation of the sample show no new resonances were formed. This lack of new NMR resonances shows that the conversion of $\text{CpRu}(\text{PPh}_3)_2\text{H}$ to $\text{CpRu}(\text{PPh}_3)(\text{H})_3$ did not occur.

4.4.6 Reactions of $\text{CpRu}(\text{PPh}_3)_2\text{H}$ with Ethene

Based on the previous chapters which involved the reactions with ethene (Chapters 2, 3 and 5), only a photochemical reaction employing the *ex situ* UV set-up, was attempted. An NMR tube was charged with $\text{CpRu}(\text{PPh}_3)_2\text{H}$ in d_6 -benzene. The tube was degassed and pressurised with 1.5 bar ethene. The sample irradiated using a broadband UV lamp for 18 hours. Afterward the sample was transferred at an NMR spectrometer in order to record ^1H and $^{31}\text{P}\{^1\text{H}\}$ NMR spectra.

Observation of the recorded NMR spectra revealed no change in the resonances compared with the previously recorded spectra; therefore it is evident that no reaction has occurred. Further photolysis for another 18 hours also showed no signs of reaction. The literature reports the formation of $\text{CpRu}(\text{PPh}_3)(\eta^2\text{-C}_2\text{H}_4)\text{H}$ by the thermal reaction (353 K) of $\text{CpRu}(\text{PPh}_3)_2\text{Et}$, additional products formed were $\text{CpRu}(\text{PPh}_3)_2\text{H}$ and $\text{CpRu}(\kappa^2\text{-2-C}_6\text{H}_4\text{PPh}_2)(\text{PPh}_3)$.^{265, 275} Based on this research $\text{CpRu}(\text{PPh}_3)(\eta^2\text{-C}_2\text{H}_4)\text{H}$ and $\text{CpRu}(\text{PPh}_3)_2\text{Et}$ may have been expected to have formed photochemically, though this was not observed to occur.

4.4.7 Reactions of $\text{CpRu}(\text{PPh}_3)_2\text{H}$ with Naphthalene

Again, no thermal reaction was considered for $\text{CpRu}(\text{PPh}_3)_2\text{H}$ with naphthalene, owing to the low thermal instability of the resulting η^2 -naphthalene products, as observed in Chapters 2, 3 and 5, only a low temperature photochemical reaction employing the *ex situ* UV set-up, was attempted.

A J-Y NMR tube was charged with $\text{CpRu}(\text{PPh}_3)_2\text{H}$ in d_6 -benzene. The tube was degassed following the addition of naphthalene. The sample was cooled to 198 K and irradiated using a broadband UV lamp. After 18 hours the sample was transferred at an NMR spectrometer (cooled to 198 K) in order to record ^1H and $^{31}\text{P}\{^1\text{H}\}$ NMR spectra.

As with the previous reaction with ethene, no sign of new resonances for the expected product, $\text{CpRu}(\text{PPh}_3)(\eta^2\text{-C}_{10}\text{H}_8)$, were found. Resonances consistent with the activated 1,2-dihydronaphthalene complex, $\text{CpRu}(\text{PPh}_3)_2(\text{C}_{10}\text{H}_{10})$, were also absent.²⁷⁶

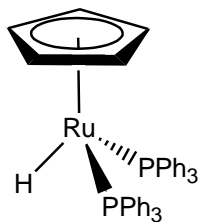
4.5 Conclusions

The original aim of the study on $\text{CpRu}(\text{PPh}_3)_2\text{H}$ was to use the greater migratory aptitude of a hydride ligand to achieve new CH bond forming reactions at ruthenium. For example the preparation of $\text{CpRu}(\text{PPh}_3)(\text{ethene})\text{H}$ might allow the controlled formation of $\text{CpRu}(\text{PPh}_3)_2(\text{Et})$.

The reactivity of $\text{CpRu}(\text{PPh}_3)_2\text{H}$ is much lower than that of the previously investigated chloride and methyl derivatives. Only after long durations of heating was the thermal reaction between the complex and PEt_3 achieved (in low yield). This slow / inability to undergo reaction (for $^t\text{BuNC}$, CO , H_2 and HSiEt_3) explains why such derivatives have not been well explored in the literature, with the formation of the majority of the complexes reported being synthesised from the chloride derivative. The chemistry of these reaction appears to bear a closer similarity to those of $\text{CpRu}(\text{PPh}_3)_2\text{Cl}$, rather than $\text{CpRu}(\text{PPh}_3)_2\text{Me}$, with the hydride complex failing to undergo the orthometallation reactions of the methyl derivative. The photochemical reactivity of $\text{CpRu}(\text{PPh}_3)_2\text{H}$ is greater than its thermal reactivity, but the conversion is still low. Previous characterisation of these photochemically formed complexes by NMR has been weak, if they have been characterised at all.

The reactions involving HSiEt_3 and H_2 do not react thermally or photochemically to form Ru(IV) activation products. This informs the reactions encountered in Chapter 3, which showed the formation of $\text{CpRu}(\text{PPh}_3)_2\text{H}$ as a by-product. This implies that formation of $\text{CpRu}(\text{PPh}_3)_2\text{H}$ cannot be reversed under the conditions tested in this chapter, to lead to the formation of larger quantities of the more interesting products discovered in Chapter 3 (particularly for the silane reactions). It is therefore concluded that $\text{CpRu}(\text{PPh}_3)_2\text{H}$ is a poor reactant for these studies.

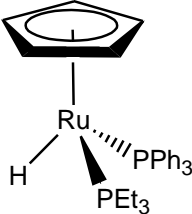
4.6 Characterisation data

Table 4.1 NMR data for $\text{CpRu}(\text{PPh}_3)_2\text{H}$ 

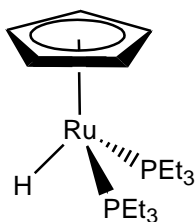
In d_8 -toluene at 298 K	δ / ppm (multiplicity, integration)	Assignment	Coupling constant / Hz	Assignment
^1H	-10.80 (t, 1) 4.42 (s, 5) 6.93 (m)* 7.03 (m)* 7.48 (m)*	Ru- H $\eta^5\text{-C}_5\text{H}_5$ <i>Para</i> - $\text{P}(\text{C}_6\text{H}_5)_3$ <i>Meta</i> - $\text{P}(\text{C}_6\text{H}_5)_3$ <i>Ortho</i> - $\text{P}(\text{C}_6\text{H}_5)_3$	33.8	$ ^2J_{\text{PH}} $
^{13}C	81.3 (s) 127.6 (t) 128.2 (s) 130.4 (t) 141.2 (t)	$\eta^5\text{-C}_5\text{H}_5$ <i>Meta</i> - $\text{P}(\text{C}_6\text{H}_5)_3$ <i>Para</i> - $\text{P}(\text{C}_6\text{H}_5)_3$ <i>Ortho</i> - $\text{P}(\text{C}_6\text{H}_5)_3$ <i>Ips</i> o- $\text{P}(\text{C}_6\text{H}_5)_3$	10.3 16.2 44.9	$ ^3J_{\text{PC}} $ $ ^2J_{\text{PC}} $ $ ^1J_{\text{PC}} $
^{31}P	68.0 (s)	$\text{P}(\text{Ph})_3$		

* Resonances were overlapped in the ^1H NMR spectrum, and were therefore found using a $^1\text{H}/^{31}\text{P}$ HMQC NMR experiment.

Table 4.2 NMR data for $CpRu(PPh_3)(PEt_3)H$

				
In d_8 -toluene at 298 K	δ / ppm (multiplicity, integration)	Assignment	Coupling constant / Hz	Assignment
1H	-11.18 (t, 1) 0.94 (m, 9) 1.72 & 1.67 (m, 6) 4.56 (s, 5) 6.98 (m)* 7.06 (m)* 7.53 (m)*	Ru-H P(CH₂-CH₃)₃ P(CH₂-CH₃)₃ η^5 - C₅H₅ <i>Para</i> - P(C₆H₅)₃ <i>Meta</i> - P(C₆H₅)₃ <i>Ortho</i> - P(C₆H₅)₃	34.2 7.9 7.5	$ ^2J_{PH} $ $ ^3J_{HH} $ $ ^3J_{HH} $
^{13}C	12.7 (t) 24.8 (t) 83.3 (s) 127.4 (t) 128.3 (s) 134.2 (t) 140.9 (dd)	P(CH₂-CH₃)₃ P(CH₂-CH₃)₃ η^5 - C₅H₅ <i>Meta</i> - P(C₆H₅)₃ <i>Para</i> - P(C₆H₅)₃ <i>Ortho</i> - P(C₆H₅)₃ <i>Ips</i> o- P(C₆H₅)₃	4.6 16.7 10.3 14.5 13.2, 34.8	$ ^2J_{PC} $ $ ^1J_{PC} $ $ ^3J_{PC} $ $ ^2J_{PC} $ $ ^3J_{PC} , ^1J_{PC} $
^{31}P	47.8 (d) 65.5 (d)	P(Et)₃ P(Ph)₃	41.0 41.0	$ ^2J_{PP} $ $ ^2J_{PP} $

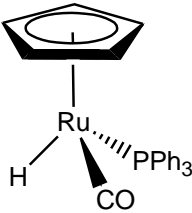
* Resonances were overlapped in the 1H NMR spectrum, and were therefore found using a $^1H/^{31}P$ HMQC NMR experiment.

Table 4.3 NMR data for $\text{CpRu}(\text{PEt}_3)_2\text{H}$ 

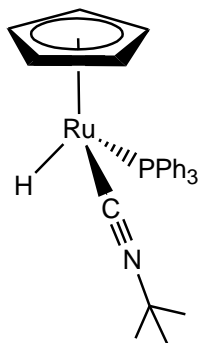
In d_8 -toluene at 298 K	δ / ppm (multiplicity, integration)	Assignment	Coupling constant / Hz	Assignment
^1H	-11.30 (t, 1) 0.94 (m, 6) 1.86 & 1.78 (m, 9) 4.69 (s, 5)	Ru- H $\text{P}(\text{CH}_2\text{-}\mathbf{CH}_3)_3$ $\text{P}(\mathbf{CH}_2\text{-CH}_3)_3$ $\eta^5\text{-C}_5\mathbf{H}_5$	35.5 7.8 7.5	$ ^2\text{J}_{\text{PH}} $ $ ^3\text{J}_{\text{HH}} $ $ ^3\text{J}_{\text{HH}} $
^{13}C	12.4 (t) 23.7 (t) 82.4 (s)	$\text{P}(\text{CH}_2\text{-}\mathbf{CH}_3)_3$ $\text{P}(\mathbf{CH}_2\text{-CH}_3)_3$ $\eta^5\text{-C}_5\mathbf{H}_5$	4.8 16.9	$ ^2\text{J}_{\text{PC}} $ $ ^1\text{J}_{\text{PC}} $
^{31}P	52.8 (s)	P (Et) ₃		

* Resonances were overlapped in the ^1H NMR spectrum, and were therefore found using a $^1\text{H}/^{31}\text{P}$ HMQC NMR experiment.

Table 4.4 NMR data for $CpRu(PPh_3)(CO)H$

				
In d_8 -toluene at 298 K	δ / ppm (multiplicity, integration)	Assignment	Coupling constant / Hz	Assignment
1H	-11.05 (d, 1) 4.72 (s, 5) 6.97 (m)* 7.08 (m)* 7.56 (m)*	Ru- <i>H</i> η^5 -C ₅ H ₅ <i>Para</i> -P(C ₆ H ₅) ₃ <i>Meta</i> -P(C ₆ H ₅) ₃ <i>Ortho</i> -P(C ₆ H ₅) ₃	37.6	$ ^2J_{PH} $
^{13}C	84.4 (s) 127.4 (d) 128.6 (s) 140.6 (d) 140.8 (d) 201.5 (d)	η^5 -C ₅ H ₅ <i>Meta</i> -P(C ₆ H ₅) ₃ <i>Para</i> -P(C ₆ H ₅) ₃ <i>Ipsa</i> -P(C ₆ H ₅) ₃ <i>Ortho</i> -P(C ₆ H ₅) ₃ C≡O	10.4 45.1 16.6 23.0	$ ^3J_{PC} $ $ ^1J_{PC} $ $ ^2J_{PC} $ $ ^2J_{PC} $
^{31}P	67.7 (s)	<i>P</i> (Ph) ₃		

* Resonances were overlapped in the 1H NMR spectrum, and were therefore found using a $^1H/^{31}P$ HMQC NMR experiment.

Table 4.5 NMR data for $CpRu(PPh_3)(^tBuNC)H$ 

In d_8 -toluene at 298 K	δ / ppm (multiplicity, integration)	Assignment	Coupling constant / Hz	Assignment
1H	-11.42 (d, 1) 0.88 (s, 9) 4.83 (s, 5) 7.00 (m)* 7.09 (m)* 7.60 (m)*	Ru- H C(CH₃)₃ η^5 - C₅H₅ <i>Para</i> - P(C₆H₅)₃ <i>Meta</i> - P(C₆H₅)₃ <i>Ortho</i> - P(C₆H₅)₃	34.3	$ ^2J_{PH} $
^{13}C	30.8 (s) 55.2 (s) 81.7 (s) 127.9 (d) 128.8 (s) 134.6 (d) 141.1 (d) 151.4 (t)	C(CH₃)₃ C(CH₃)₃ η^5 - C₅H₅ <i>Meta</i> - P(C₆H₅)₃ <i>Para</i> - P(C₆H₅)₃ <i>Ortho</i> - P(C₆H₅)₃ <i>Ips</i> o- P(C₆H₅)₃ C\equivN	10.5 16.8 45.3 19.2	$ ^3J_{PC} $ $ ^2J_{PC} $ $ ^1J_{PC} $ $ ^1J_{CN} $
^{31}P	69.2 (s)	P(Ph)₃		

* Resonances were overlapped in the 1H NMR spectrum, and were therefore found using a $^1H/^{31}P$ HMQC NMR experiment.

** Appears as a broad triplet in the $^{13}C\{^1H\}$ NMR spectrum.

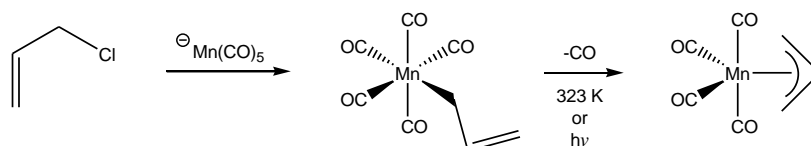
Chapter 5

Synthesis, Characterisation and Photochemistry of Ruthenium Complexes Containing η^1 and η^3 Ligands

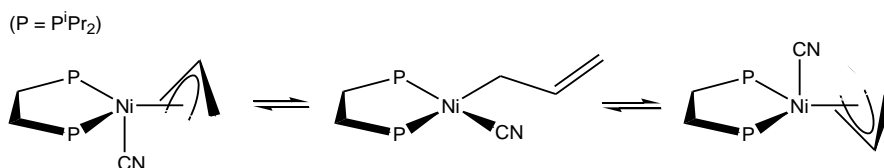
5.1 Introduction

Ligands which possess the ability to coordinate to metal centres in variable binding modes (e.g. a hapticity of 1, 2 or 3) are important in organometallic chemistry as they allow for the stabilisation of coordinatively unsaturated complexes. In this context, allyl ligands have been demonstrated to be quite versatile in this role, coordinating in either η^1 or η^3 coordination modes. Early reports of this character for the complex, $\text{Mn}(\eta^1\text{-allyl})(\text{CO})_5$, were made by Rest *et al.* (Figure 5.1, a).²⁷⁷ More recent investigations have been reported by Brunkan and Jones,²⁷⁸ who used NMR techniques to probe the isomerisation of $(\text{dippe})\text{Ni}(\eta^3\text{-allyl})\text{CN}$, which was found to occur via an η^1 -allyl intermediate (Figure 5.1, b).

Figure 5.1 Example of the binding modes for complexes containing allyl ligands



a) Conversion of η^1 -allyl to η^3 following the thermal / photochemical dissociation of CO from $\text{Mn}(\eta^1\text{-allyl})(\text{CO})_5$, reported by Rest *et al.*²⁷⁷

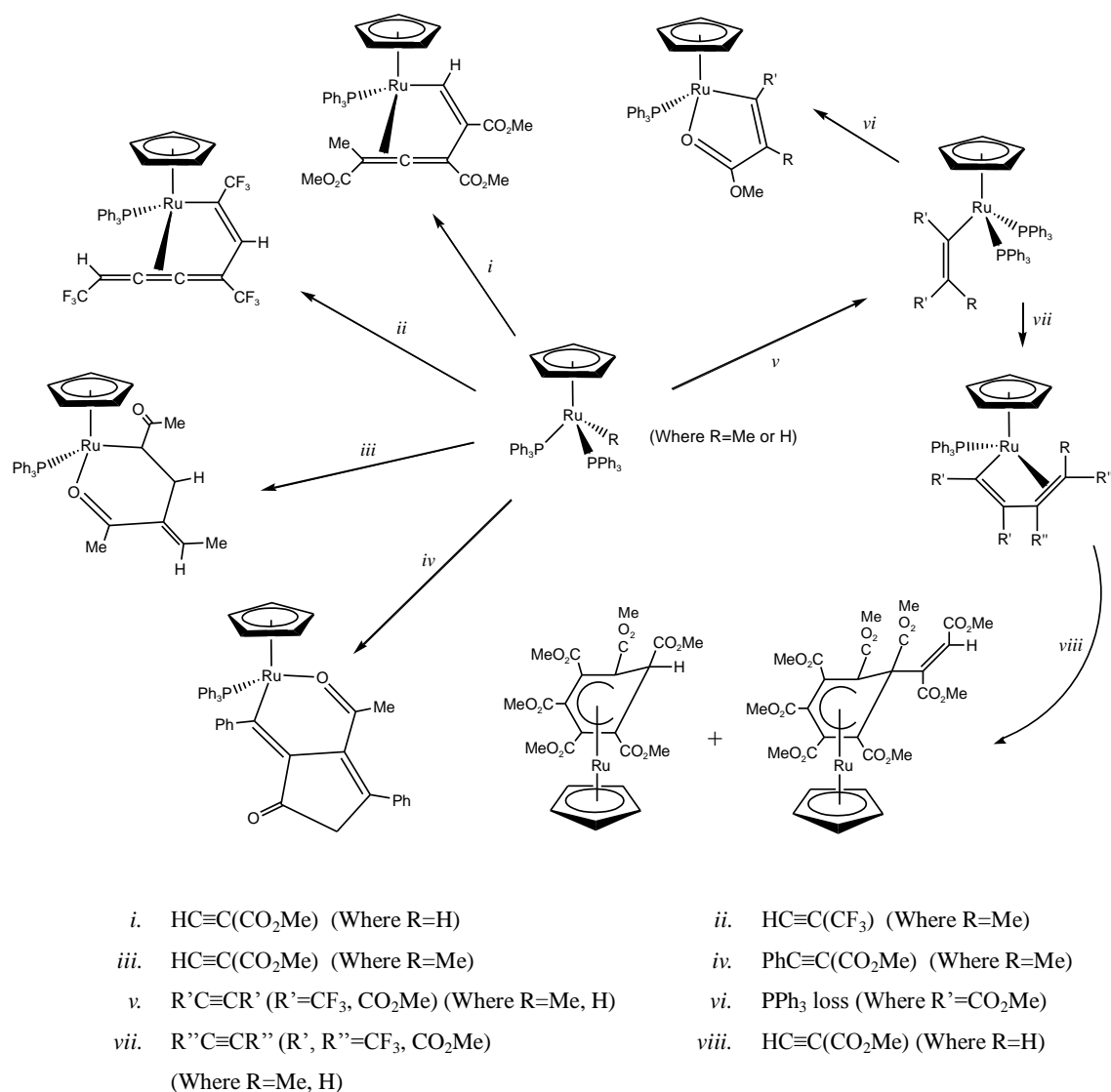


b) Isomerisation of $(\text{dippe})\text{Ni}(\eta^3\text{-allyl})\text{CN}$ via an intervening η^1 -allyl complex, reported by Brunkan and Jones²⁷⁸

In the previous examples, the allyl ligands act as tethered functionalities, which can aid in the stabilisation of the complex following the dissociation of one of the 2-electron donor ligands. This interaction is favoured by the chelate effect (discussed in chapter 1), which enhances the stability of these intermediate complexes.

For the case of cyclopentadienyl ruthenium complexes, the earliest examples which incorporate η^3 -coordinating ligands were synthesised by Bruce *et al.*²⁷⁹ Figure 5.2 summarises the reaction schemes for these η^3 ligand complexes.

Figure 5.2 Examples of known ruthenium complexes with coordinated η^3 ligands²⁷⁹

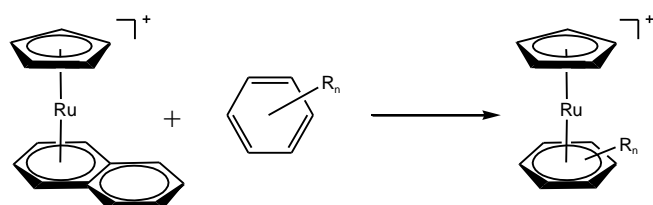


The complexes depicted in Figure 5.2 show the nature by which alkene and sigma donors coordinate to the ruthenium centre, in order to stabilise coordinatively unsaturated complexes. However, the η^3 -coordinated moieties in these complexes are

assembled at the ruthenium centre, and therefore the lability of these ligands towards forming the corresponding η^1 -ligand complexes has not been studied. Additionally, these species display relatively complex NMR spectra, which complicates the characterisation of subsequent product species, were these complexes to be used to model the reactions of ‘trapped’ 16 electron complexes.

More recent research has been undertaken by Kudinov *et al.* and Englert *et al.* to investigate the reactivity of $[\text{CpRu}(\eta^6\text{-C}_{10}\text{H}_8)]$. By probing the thermal ²⁸⁰ and photochemical ²⁸¹ reactivity of this complex, the η^6 -naphthalene ligand was found to readily dissociate from the ruthenium centre under these conditions. This character allows for the ready substitution of naphthalene for other η^6 -coordinating ligands, such as arenes (Figure 5.3). Recent developments show that this complex may be used as a convenient precursor to access other novel or previously inaccessible complexes. ²⁸²

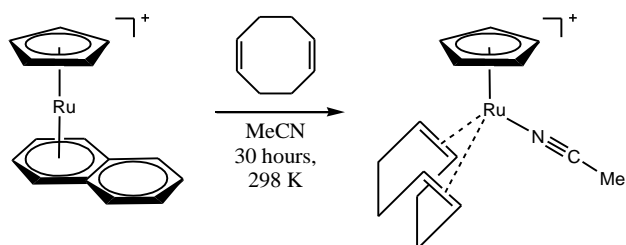
Figure 5.3 Thermal ²⁸⁰ and photochemical ^{281, 282} reactions of $[\text{CpRu}(\eta^6\text{-naphthalene})]\text{PF}_6$



Photochemically: $h\nu$ at 278 K

or thermally: MeCN & $\text{C}_3\text{H}_4\text{Cl}_2$ at 353 K

(R = H, 1,4-Me₂, 1,3,5-Me₃, 1,2,4,5-Me₄ or Me₆)



5.1.1 Context

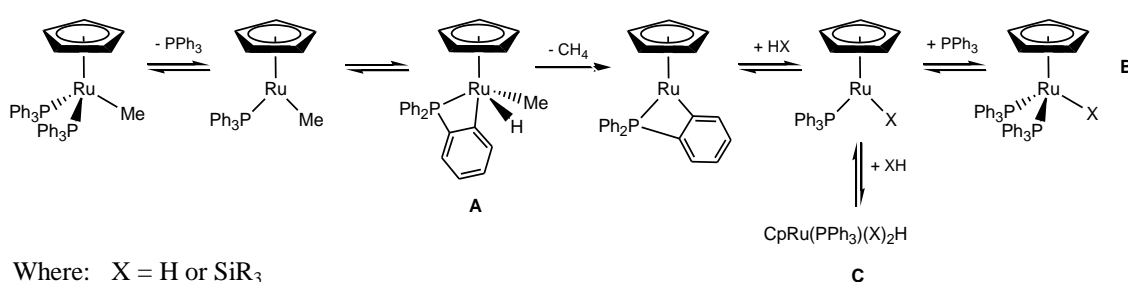
The previous chapters have focused on the thermal and photochemical elimination of one of the phosphine ligands of the parent complex, $\text{CpRu}(\text{PPh}_3)_2\text{Me}$. This process allows the subsequent binding of other substrates and hence affords new complexes.

However, the involvement of a phosphine in these reactions complicates matters as subsequent re-association of this good donor can lead to the formation of unexpected products, at the expense of the formation of the more desirable novel complexes. The increase in side reactions arising from the phosphine lead to the generation of much more complicated NMR spectra. *In situ* reactions performed on the NMR scale are particularly affected by this process, as phosphine removal is impractical, especially when dealing with air sensitive samples on such a small scale or indeed impossible when the products prove to be highly temperature sensitive.

Attempts to sequester the liberated phosphine ligand *in situ* have so far proved unreliable. While the addition of elemental sulfur leads to the formation of SPPH_3 it also decomposes the ruthenium products (refer to Chapter 3 for full discussion). When added stoichiometrically this approach works, but estimating the amount of liberated phosphine in these small scale reactions proved to be a challenge. The addition of oxygen (air) failed for similar reasons.

An alternative method that is applied in this chapter is to utilise ligands which have the capacity to change their binding mode from η^3 to η^1 in order to generate a vacant site without phosphine loss. This process is rapid partly because there is a limited entropy change.

Figure 5.4 Activation pathways of $[\text{CpRu}(\text{PPh}_3)_2\text{Me}]$ with H-H or H-Si bonds

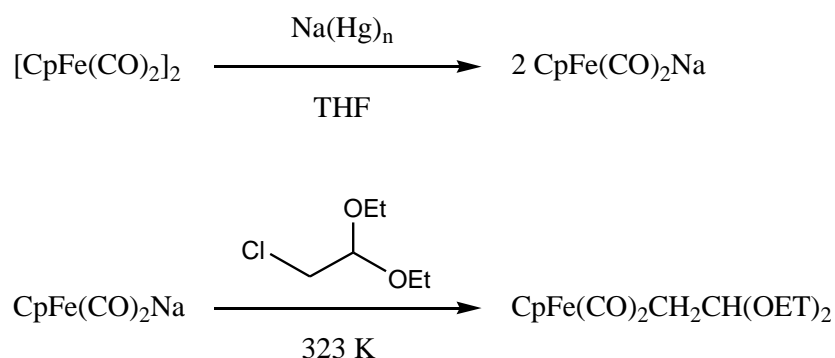


The mechanism shown in Figure 5.4 exploits the propensity of an alkyl group to undergo reductive elimination through linkage with a ruthenium hydride. This has been demonstrated in Chapter 3 as the loss of methane, and was observed when $\text{CpRu}(\text{PPh}_3)_2\text{Me}$ undergoes reaction with HSiEt_3 or H_2 . The resulting initial oxidative addition therefore yields a new Ru(IV) short-lived complex **A**, but the presence of liberated phosphine can compete with XH to form Ru(II) bisphosphine products **B**, rather than further Ru(IV) activation products **C**.

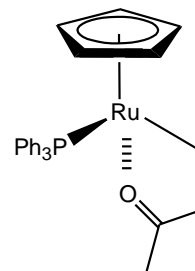
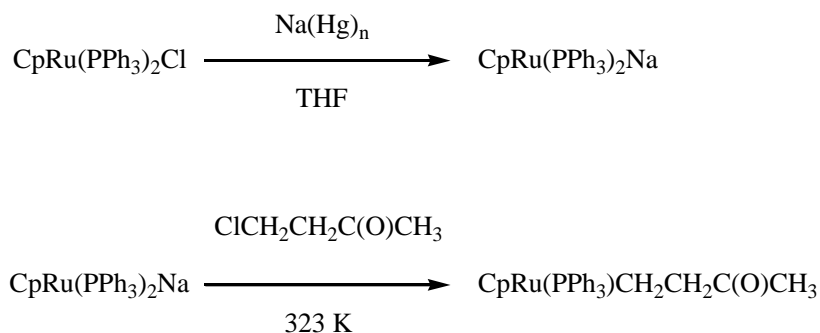
It was decided that samples of $\text{CpRu}(\text{PPh}_3)(\eta^3\text{-Si}(\text{Me}_2)\text{-CH=CH}_2)$, $\text{CpRu}(\text{PPh}_3)(\eta^3\text{-CH}_2\text{C}_2\text{H}_3)$, $\text{CpRu}(\text{PPh}_3)(\eta^3\text{-CH}_2\text{C}_6\text{H}_5)$ and $\text{CpRu}(\text{PPh}_3)(\eta^3\text{-CH}_2\text{C}_{10}\text{H}_7)$ should be prepared. For both the allyl and naphthyl derivatives, similar η^2 coordinating analogues (complexes $\text{CpRu}(\text{PPh}_3)_2(\eta^2\text{-C}_2\text{H}_4)$ and $\text{CpRu}(\text{PPh}_3)_2(\eta^2\text{-C}_{10}\text{H}_8)$) were reported in Chapter 3, which suggests the likelihood of success in the synthesis of these structures. Though the corresponding η^2 benzene structure was not determined in Chapter 3, some examples exist in the literature of η^3 – tolyl structures, which would be similar to $\text{CpRu}(\text{PPh}_3)(\eta^3\text{-CH}_2\text{C}_6\text{H}_5)$.²⁸³

5.1.2 Synthetic routes to $\text{CpRu}(\text{PPh}_3)(\eta^3\text{-Si}(\text{Me}_2)\text{-CH=CH}_2)$, $\text{CpRu}(\text{PPh}_3)(\eta^3\text{-CH}_2\text{C}_2\text{H}_3)$, $\text{CpRu}(\text{PPh}_3)(\eta^3\text{-CH}_2\text{C}_6\text{H}_5)$ and $\text{CpRu}(\text{PPh}_3)(\eta^3\text{-CH}_2\text{C}_{10}\text{H}_7)$.

New methods are therefore required to synthesise these η^3 -ligand containing species. Initially, a method employing the use of a sodium/mercury amalgam was attempted. This involves the conversion of $\text{CpRu}(\text{PPh}_3)_2\text{Cl}$ to $\text{CpRu}(\text{PPh}_3)_2\text{Na}$ and is based on the known reactions of the analogous cyclopentadienyl iron complexes with chloroacetaldehyde diethyl acetal.²⁸⁴



It was envisioned that the $\text{CpRu}(\text{PPh}_3)_2\text{Na}$ would react readily with a range of chloro compounds containing allyl and aryl moieties that could achieve an η^3 or other multiple binding modes with the ruthenium centre after phosphine dissociation. This method also allowed for the use of chloro compounds which contain oxygen and sulfur atoms which would have allowed for the investigation of possible σ complexes. This complex would have possessed bonding characteristics similar to $\text{CpRu}(\text{PPh}_3)_2(\text{OC}_4\text{H}_8)$, which was discussed in Chapter 3.



However, despite reacting $\text{CpRu}(\text{PPh}_3)_2\text{Cl}$ thermally with Na/Hg amalgam in THF (which led to a colour change from bright orange to deep red), the subsequent addition of various chloro compounds failed to give the expected products. Varying ratios of sodium to mercury were examined further, yet none led to the successful formation of the derivative when tested using ^1H and $^{31}\text{P}\{^1\text{H}\}$ NMR spectra. For this reason, an alternative procedure was employed involving the conversion of the allyl and aryl reagents to their Grignard analogues. Oxygen and sulfur-containing compounds were no longer considered as Grignard reagents formed from these compounds have a tendency to polymerise, making the synthesis of clean products difficult. This limits the diversity of the tethered functionalities which may be incorporated into these systems (thereby limiting choice of complexes), for instance, carbonyl complexes cannot be employed. This method of synthesis is similar to a known procedure that was used in the conversion of $\text{CpRu}(\text{PPh}_3)_2\text{Cl}$ to $\text{CpRu}(\text{PPh}_3)_2\text{Me}$.²⁸⁵

Another route to the formation of tethered functionalities lies with the use of a substrate which possesses a bond which may be readily activated at the ruthenium centre. As demonstrated in Chapter 3 (section 3.4.10) the Si-H adduct is one such bond that fulfils this requirement. The following section details the reaction of dimethylvinylsilane with $\text{CpRu}(\text{PPh}_3)_2\text{Me}$ to provide a route to η^3 silyl complexes.

5.2 Formation of $\text{CpRu}(\text{PPh}_3)(\eta^3\text{-Si}(\text{Me}_2)\text{-CH=CH}_2)$

The formation of $\text{CpRu}(\text{PPh}_3)(\eta^3\text{-Si}(\text{Me}_2)\text{-CH=CH}_2)$ is based on the previously discussed reaction (Chapter 3) of $\text{CpRu}(\text{PPh}_3)_2\text{Me}$ with triethylsilane, whereby the oxidative addition of the silane readily progressed to form $\text{CpRu}(\text{PPh}_3)_2\text{SiEt}_3$ and $\text{CpRu}(\text{PPh}_3)(\text{SiEt}_3)_2\text{H}$. A similar result was anticipated for an analogous reaction involving dimethylvinylsilane. Oxidative addition of the silane via breaking of the H-Si bond will effectively ‘tether’ the silane to the ruthenium centre in an η^1 binding mode. Additionally, the vinyl moiety of the ligand may also coordinate to the ruthenium centre to form an η^3 bound ligand complex after the phosphine is lost. This would essentially ‘trap’ the intervening 16 electron species, allowing for further interesting reactions that would not be feasible within the triethylsilane set of experiments. It is possible that R-Si compounds may be formed from the reductive elimination of the silane with bound organic one electron donors.

There is precedent for this chemistry on the basis of the work reported by Pannell *et al.* who described the isomerisation of $\text{CpFe}(\text{CO})_2\text{CH}_2(\text{SiMe}_2)_2\text{SiMe}_3$ to $\text{CpFe}(\text{CO})_2\text{SiMe}_2\text{CH}_2\text{SiMe}_2\text{SiMe}_3$ by photolysis experiments.²⁸⁶

$\text{CpRu}(\text{PPh}_3)_2\text{Me}$ (in C_6D_6) was added to an J-Y NMR tube, which was followed by the addition of an excess of dimethylvinylsilane. The sample was degassed using two ‘freeze-pump-thaw’ cycles and sealed under vacuum. The full details of the sample preparation are described in Chapter 7.

Photolysis of the sample for 20 hours at 320 nm, led to the observation of several new peaks in the hydride and Cp regions of the ^1H NMR spectrum. The corresponding $^{31}\text{P}\{^1\text{H}\}$ NMR spectrum showed a new major resonance at δ 66.5; the absence of a peak at δ 55.3 indicated full conversion of the starting material. It was possible to estimate that 40% of $\text{CpRu}(\text{PPh}_3)(\eta^3\text{-Si}(\text{Me}_2)\text{-CH=CH}_2)$ was formed *in situ*, with minor products accounting for the remaining 60%. To characterise this species, a $^1\text{H}/^{31}\text{P}$ HMQC NMR spectrum was recorded for a J_{HP} value of 5 Hz (CNST2). This proved to connect this resonance with five resonances in the ^1H spectrum at δ -0.33, 0.73, 1.98, 2.14, 3.53 and 7.68. None of these signals corresponded to a Cp resonance, and each of these signals were subject to selective NOE interrogation.

Most significantly, there was an observed NOE interaction between the signals at δ -0.33 and δ 0.73, both of which are of the same intensity. This piece of information, in conjunction with their chemical shift, suggests that they arise from two methyl groups bound to silicon. This was demonstrated to be correct through the use of a $^1\text{H}/^{29}\text{Si}$ HMQC experiment which showed direct coupling between the silicon resonance at δ 35.98 and these two methyl proton resonances. These resonances, however, are significantly shifted from those signals observed for the free silane in benzene (which appear at between δ 5.60 - 6.20 and at 3.56). This ^{29}Si signal also showed a 22 Hz splitting by ^{31}P NMR, confirming the grouping giving rise to it is bound to the ruthenium centre. Other weaker NOE couplings were found from the δ -0.33 signal to peaks at δ 1.98, 3.53, 7.01 and 7.68, but the Cp proton resonance was still not found.

When selective NOE irradiation of the methyl peak at δ 0.73 was employed a strong coupling to the methyl peak at δ -0.33 and also a peak at δ 4.29, which is where the Cp resonance would be expected to appear, was observed. The presence of coupling between this methyl signal and that of the expected Cp ligand suggests that the methyl group at δ 0.73 points upwards toward the Cp while the methyl group at δ -0.33 points away. This would fulfil the expectation that the bonds to silicon are arranged in a tetrahedral fashion. Given the observation of two distinct methyl resonances, displaying different orientations with respect to Cp, a locked conformation is indicated. Weaker coupling was observed to a signal at δ 1.98 and a weaker signal than the previous methyl coupling was found for the proton resonance at δ 7.68.

With the presumed Cp resonance being located, an NOE experiment positioned on that resonance would confirm which protons lie closest to it. Connections were found to signals at δ -0.33, 0.73, 1.98, 3.53, 7.01 and 7.68. Based on the previous characterisations, the signals at δ 7.01 and 7.68 correspond to the *meta* and *ortho* phenyl protons of the triphenylphosphine ligand (these two resonances were shown to mutually couple through a COSY experiment).

So far the new complex therefore contains only one ^{31}P centre, a Cp ring and a ruthenium-silicon bond. This would suggest that $\text{CpRu}(\text{PPh}_3)(\eta^1\text{-Si}(\text{Me}_2)\text{-CH=CH}_2)$ is a likely structure. However this is only a 16 electron complex, although if the vinyl were to bind to ruthenium, an $18e^-$ complex would be formed. Evidence for the binding of the vinyl moiety directly to the ruthenium centre is provided by the doublet splitting of the vinyl carbons at δ 31.0 (6.4 Hz) and δ 38.3 (6.4 Hz), by the phosphorus atom of the coordinated phosphine. The doublet splitting of 6.4 Hz, is typical of a $^2|J_{\text{CP}}|$ coupling, and so suggests that the vinyl coordinates in an η^3 manner.

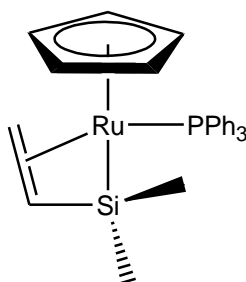
The three signals at δ 1.98, 2.14 and 3.53 are still unassigned. These are presumed to be the vinyl protons of the vinylsilane group. Each proved to couple to each other through a COSY experiment. A selective NOE interrogation at δ 2.14 shows coupling to the proton resonance at δ 1.98 which is split into a doublet with a coupling constant of 13 Hz, which would correspond to a trans splitting between the resonances at δ 2.14 and 1.98.

An NOE experiment, with irradiation centred on the Cp resonance (at δ 4.29), demonstrated magnetisation transfer to the vinyl signals at δ 1.98 and 2.14. This suggests that these protons are in geminal positions with respect to each other, and that the double bond of the vinylsilane tilts upwards towards the Cp, while the lone proton of the vinyl is positioned downward.

Confirmation of the coordination mode of the vinyl group comes from the ^{13}C and ^1H connections to ^{31}P . This coupling confirms the binding of this group to the metal.

The structure of this product is therefore confirmed as that of a half-sandwich ruthenium mono-triphenylphosphine complex with the silicon acting as a two electron donor ligand and vinyl acting as a two electron donor – forming an η^2 bond to ruthenium; in other words a negatively charged η^3 – silyl-allyl ligand. The metal therefore retains a Ru(II) oxidation state.

Figure 5.5 Structure of $\text{CpRu}(\text{PPh}_3)(\eta^3\text{-Si}(\text{Me})_2\text{-CH=CH}_2)$



The corresponding bis-phosphine product $\text{CpRu}(\text{PPh}_3)_2(\text{Si}(\text{Me})_2\text{-CH=CH}_2)$, was also characterised as a product of the previous thermal reaction of dimethylvinylsilane and $\text{CpRu}(\text{PPh}_3)_2\text{Me}$. Full NMR data for this complex are given in Table 5.2. Upon recording the MS spectra of this solution, at various stages in the reaction, only signals centred around 691 and 430 (with isotope patterns matching those of a ruthenium containing complex) were detected. These fragments were deduced to be $\text{CpRu}(\text{PPh}_3)_2$ and $\text{CpRu}(\text{PPh}_3)$ (m/z 691 and 430, respectively), which were expected for $\text{CpRh}(\text{PPh}_3)_2\text{Si}(\text{Me})_2\text{C}_2\text{H}_3$. This indicated that the silyl-ruthenium bond is readily cleaved in the mass spectrometer, and therefore neither $\text{CpRu}(\text{PPh}_3)(\eta^3\text{-Si}(\text{Me})_2\text{-CH=CH}_2)$ nor $\text{CpRu}(\text{PPh}_3)_2\text{Si}(\text{Me})_2\text{C}_2\text{H}_3$ could be detected by ESI MS.

It should be noted that the detection of both $\text{CpRu}(\text{PPh}_3)(\eta^3\text{-Si}(\text{Me}_2)\text{-CH=CH}_2)$ and $\text{CpRu}(\text{PPh}_3)_2(\text{Si}(\text{Me}_2)\text{-CH=CH}_2)$ was hampered by the abundance of the related silyl hydride tolyl complexes generated photochemically; these were described previously in Chapter 3 for Et_3SiH (section 3.4.10). The presence of these complexes was manifested by the observation of their hydride resonances in the corresponding ^1H NMR spectrum (Figure 5.6). The detailed characterisation of these species was not attempted both the full characterisation of $\text{CpRu}(\text{PPh}_3)(\eta^3\text{-Si}(\text{Me}_2)\text{-CH=CH}_2)$ and $\text{CpRu}(\text{PPh}_3)_2(\text{Si}(\text{Me}_2)\text{-CH=CH}_2)$, was achieved and data is listed in Tables 5.2 and 5.2.

Figure 5.6 ^1H NMR spectra showing the hydride signals (for the activated tolyl product, analogous to those described in Chapter 3) and the major product proton signals – highlighting the abundance of products formed

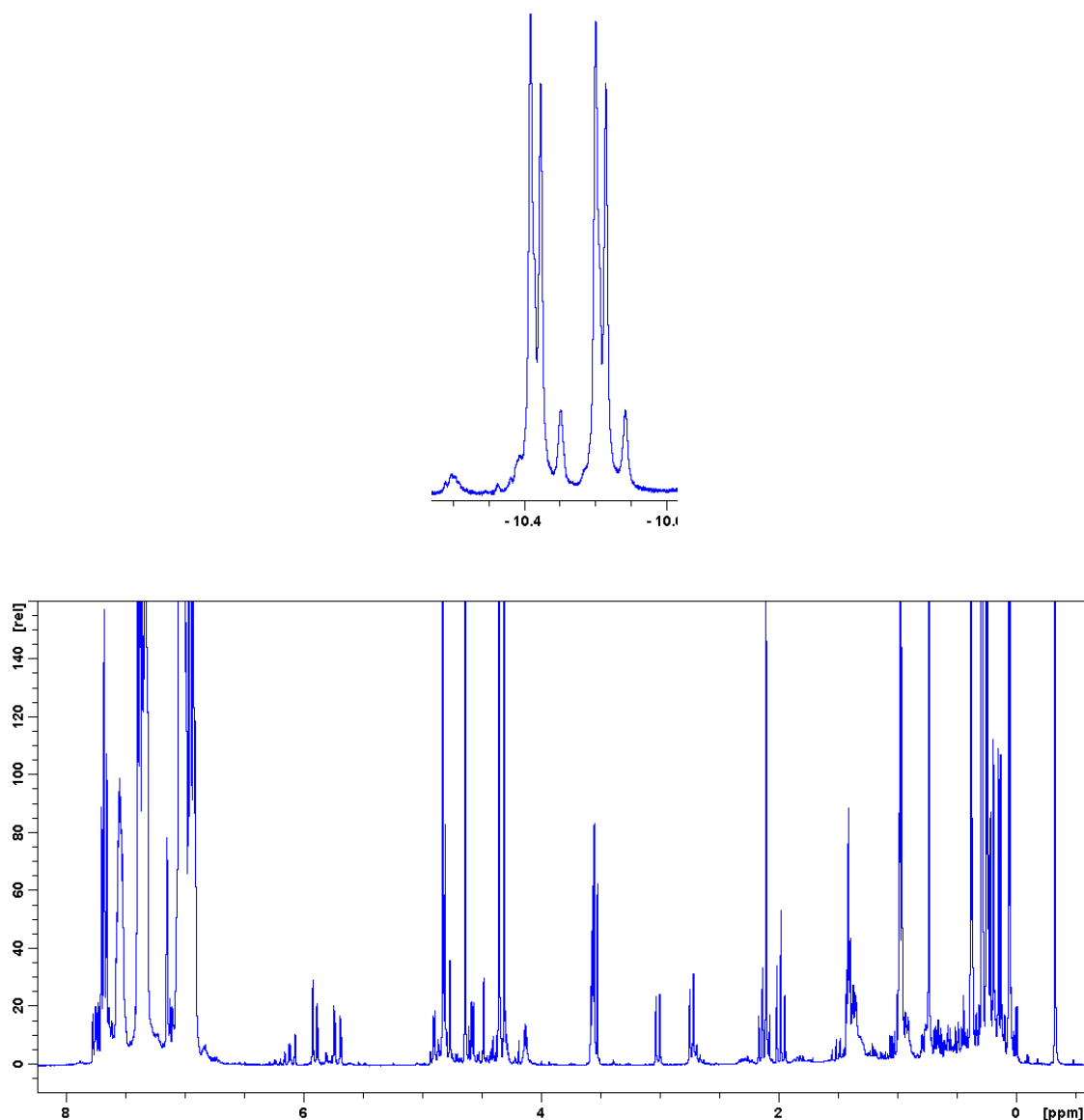
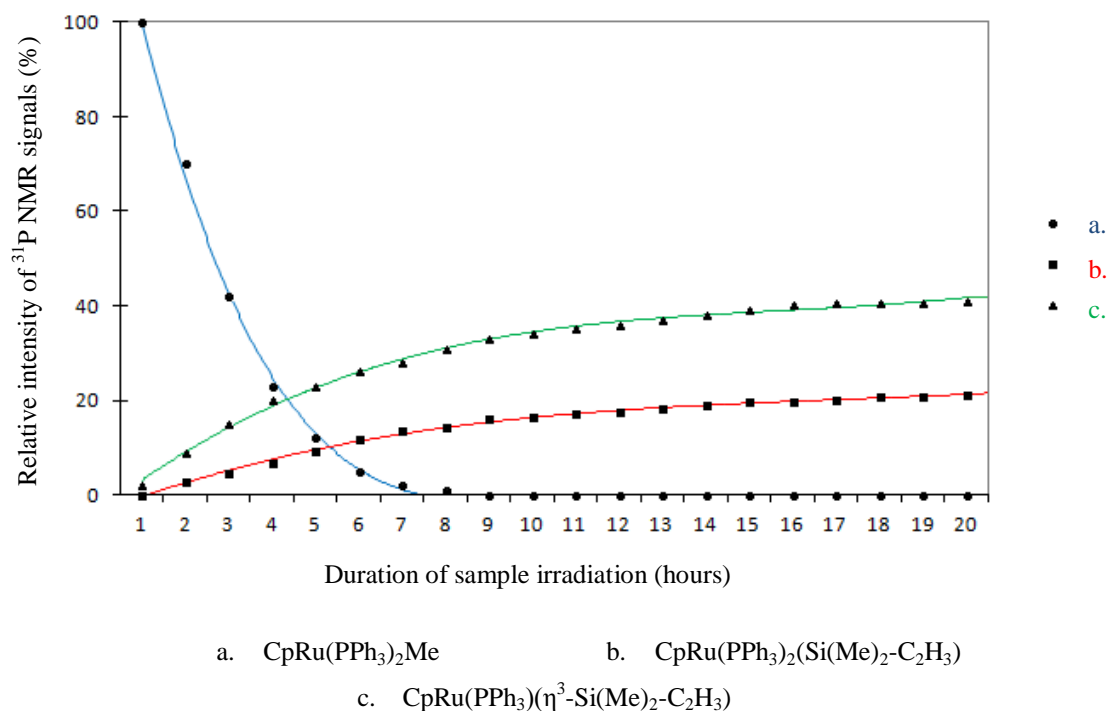


Figure 5.7 shows the time-plot for the conversion of $\text{CpRu}(\text{PPh}_3)_2\text{Me}$ to the major H-Si activation products $\text{CpRu}(\text{PPh}_3)(\eta^3\text{-Si}(\text{Me})_2\text{-CH=CH}_2)$ and $\text{CpRu}(\text{PPh}_3)_2(\text{Si}(\text{Me})_2\text{-CH=CH}_2)$. From the plot it can be noted that no interconversion between the two products takes place. The k_{obs} for these products for the processes $\text{CpRu}(\text{PPh}_3)_2\text{Me} \rightarrow \text{CpRu}(\text{PPh}_3)_2(\text{Si}(\text{Me})_2\text{-C}_2\text{H}_5)$ and $\text{CpRu}(\text{PPh}_3)_2\text{Me} \rightarrow \text{CpRu}(\text{PPh}_3)(\eta^3\text{-Si}(\text{Me})_2\text{-C}_2\text{H}_5)$ are 0.023 s^{-1} and 0.013 s^{-1} , respectively.

Figure 5.7 A plot of the relative ^{31}P resonances over time, for the photochemically formed products of the reaction between $\text{CpRu}(\text{PPh}_3)_2\text{Me}$ and dimethylvinylsilane (original illustration appears in colour)



To summarise, the activation of silanes which possess the readily activated Si-H adduct, allow for a convenient route to add functionalities capable of interacting with a metal centre to complexes (in this case, allowing for η^3 -coordination of the silane with the ruthenium centre). However, the number of side products formed detracts from the use of this method to produce large amounts of the pure $\text{CpRu}(\text{PPh}_3)(\eta^3\text{-Si}(\text{Me})_2\text{-CH=CH}_2)$ and $\text{CpRu}(\text{PPh}_3)_2(\text{Si}(\text{Me})_2\text{-CH=CH}_2)$, problematic. Such attempts were made during the course of this work (detailed in Chapter 7, section 7.2.4.2) whereby the reactions described here were scaled-up. Attempts to separate the complexes were found to be impractical, owing to the highly air sensitive nature of these silyl complexes, which

rapidly decomposed.

5.3 Synthesis and characterisation of $\text{CpRu}(\text{PPh}_3)(\eta^3\text{-CH}_2\text{-CH=CH}_2)$

Owing to the issues encountered for the previous method (Section 5.1.2), a new procedure was required. The use of Grignard reagents has been briefly mentioned in section 5.1.2. The Grignard method allows for the formation of Ru-C bonds, which can be employed to tether functionalities to the ruthenium complex; these functionalities may subsequently interact with the metal centre of a coordinatively unsaturated complex. It is envisaged that these complexes will benefit from greater stability compared with the previous silyl complexes, owing to the relatively increased strength of the M-C bonds compared with M-Si. This allows for the bulk synthesis of these complexes, unlike the silyl derivatives, and are expected to be relatively pure.

Based on the results reported in Chapter 3, C-H activation could be employed to form these products, in a similar way to the reaction of dimethylvinylsilane with $\text{CpRu}(\text{PPh}_3)_2\text{Me}$, owing to the ability of the orthometallated fragment to activate these adducts. However, it is unlikely that this method would lead to the formation of clean samples, and there is the potential for the fragment to activate the C-H / C-D bonds of the solvent (sections 3.4.10), which would further increase the complexity of the NMR spectra.

Owing to the known stability of the complex, $\text{CpRu}(\text{PPh}_3)\text{Me}(\eta^2\text{-CH=CH}_2)$, as demonstrated in Chapter 3, the similar structure, $\text{CpRu}(\text{PPh}_3)(\eta^3\text{-CH}_2\text{-CH=CH}_2)$, was considered a suitable candidate to demonstrate the role of η^1 and η^3 coordinating ligands.

The complex, $\text{CpRu}(\text{PPh}_3)(\eta^3\text{-CH}_2\text{-CH=CH}_2)$, has been mentioned previously in the literature by Lehmkuhl, where it was reported as a side product of warming $\text{CpRu}(\text{PPh}_3)_2\text{Me}$ in toluene,²⁸⁷ and was partially characterised by NMR techniques. To date, no attempts to fully characterise or explore the reactions of this complex (or the other similar η^1 and η^3 ligand containing ruthenium complexes) have been reported in the literature.

5.3.1 Synthesis of $\text{CpRu}(\text{PPh}_3)(\eta^3\text{-CH}_2\text{-CH=CH}_2)$

A sample of $\text{CpRu}(\text{PPh}_3)(\eta^3\text{-CH}_2\text{-CH=CH}_2)$ was prepared by treating $\text{CpRu}(\text{PPh}_3)_2\text{Cl}$ with $\text{ClMgCH}_2\text{-CH=CH}_2$ in toluene. The resulting yellow solid was confirmed pure and structurally characterised using ^1H , ^{31}P and ^{13}C NMR techniques (full details of the synthesis are reported in Chapter 7).

5.3.2 NMR characterisation of $\text{CpRu}(\text{PPh}_3)(\eta^3\text{-CH}_2\text{-CH=CH}_2)$

A $^{31}\text{P}\{^1\text{H}\}$ NMR spectrum recorded for the sample in d_8 -THF, showed the presence of a single peak at δ 67.8, which is characteristic of a ^{31}P resonance belonging to a ruthenium bound triphenylphosphine ligand. A number of new signals were visible in a ^1H NMR spectrum of the sample, when compared to a ^1H NMR spectrum of $\text{CpRu}(\text{PPh}_3)_2\text{Cl}$. The new peaks appeared at δ 2.92, 0.68, 4.06, 4.17, 7.36, 7.18 and 7.09 were demonstrated to couple to the ^{31}P signal at δ 68.3 through a $^1\text{H}/^{31}\text{P}$ HMQC experiment. These allyl signals were also coupled in a ^1H COSY NMR spectrum (Figure 5.8). The singlet ^1H peak at δ 4.17 is typical of the resonance associated with the protons of a ruthenium bound cyclopentadienyl ring. The three signals at δ 4.06, 0.68 and 2.92 (in a ratio of 1:2:2 respectively) belong to the bound allyl group (as shown in the ^1H COSY spectrum, Figure 5.8). These NMR signals are consistent with the partial NMR characterisation for $\text{CpRu}(\text{PPh}_3)(\eta^3\text{-CH}_2\text{-CH=CH}_2)$ (Figure 5.9) previously reported by Lehmkuhl *et al.*²⁸⁷

Figure 5.8 ^1H COSY NMR experiment showing the coupling between the coordinated allyl protons

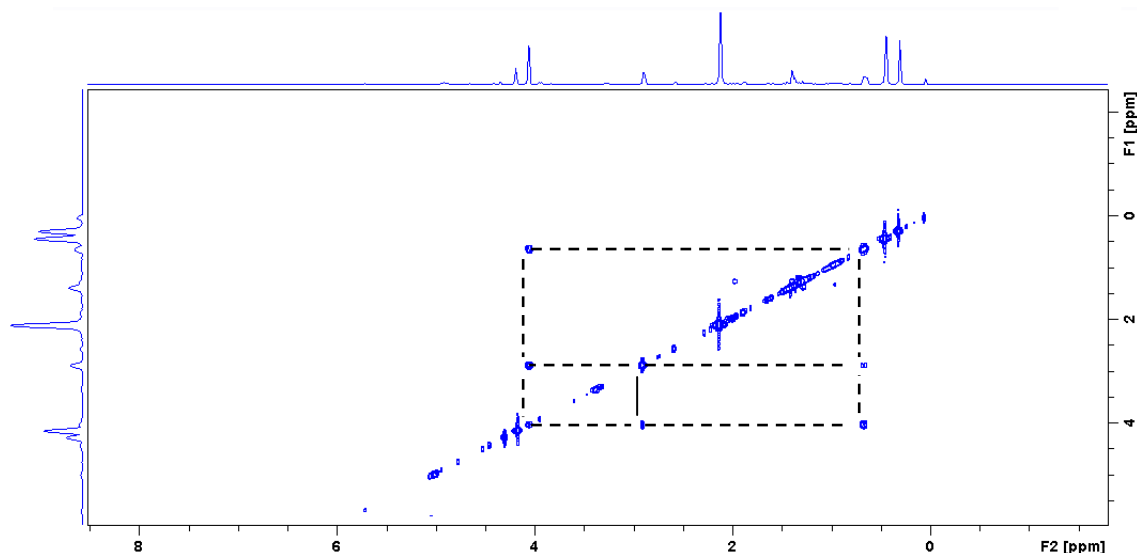
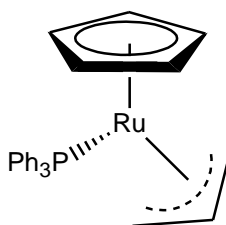


Figure 5.9 The structure of $\text{CpRu}(\text{PPh}_3)(\eta^3\text{-CH}_2\text{-CH=CH}_2)$



An η^1 analogue of this complex was not formed as the main product of the reaction, suggesting that the allyl η^3 ligand has a greater binding strength to the ruthenium centre compared with the free triphenylphosphine, and is therefore not readily displaced. Therefore the allyl η^3 ligand is not readily displaced under standard conditions to give the η^1 derivative.

The MS spectrum revealed a peak at m/z 470, corresponding to M^+ for this complex. The observation of this peak demonstrates the greater stability of these Ru-C bonded complexes compared with the previous silyl complexes $\text{CpRu}(\text{PPh}_3)(\eta^3\text{-Si}(\text{Me}_2)\text{-CH=CH}_2)$ and $\text{CpRu}(\text{PPh}_3)_2(\text{Si}(\text{Me}_2)\text{-CH=CH}_2)$, for which no M^+ peak was found, even when using a soft ionisation technique, such as ESI. No evidence for $\text{CpRu}(\text{PPh}_3)_2(\text{CH}_2\text{-CH=CH}_2)$ was seen in any of the NMR spectra recorded.

5.3.2.1 NMR Characterisation of $\text{CpRu}(\text{PPh}_3)_2(\text{CH}_2\text{-CH=CH}_2)$

$\text{CpRu}(\text{PPh}_3)(\eta^3\text{-CH}_2\text{-CH=CH}_2)$ was heated at reflux in THF in the presence of an excess of triphenylphosphine, to form the bis-phosphine product $\text{CpRu}(\text{PPh}_3)_2(\text{CH}_2\text{-CH=CH}_2)$ (full synthesis described in Chapter 7).

A single new resonance was present in the $^{31}\text{P}\{^1\text{H}\}$ NMR spectrum at δ 52.4. This singlet was demonstrated to couple to ^1H NMR signals at δ 2.93, 4.40 and 7.54, using a $^1\text{H}/^{31}\text{P}$ HMQC experiment. These three signals represented the protons of the Ru-bound CH_2 group, the Cp ring and the *ortho*-phenyl proton of the phosphine, respectively.

Through the use of a selective NOE experiment, the peak at δ 2.93 was found to lie close to the Cp protons (indicated by the peak at δ 4.40) and a second proton resonance at δ 6.21, which corresponds to the proton of the allyl group. The remaining protons of the allyl group (*E* and *Z*) were found through the use of a ^1H COSY NMR experiment, at δ 4.71 and 4.89 respectively. Additional couplings were made from the *ortho*-phenyl peak at δ 7.54 and the *meta* and *para*-phenyl protons at δ 7.18 and 7.01.

The complex is therefore readily identified as $\text{CpRu}(\text{PPh}_3)_2(\text{CH}_2\text{-CH=CH}_2)$, which has not been previously reported in the literature. Full characterisation data is listed in Table 5.3.

5.3.3 Thermal and photochemical reactions of $\text{CpRu}(\text{PPh}_3)(\eta^3\text{-CH}_2\text{-CH=CH}_2)$

5.3.3.1 Thermal reaction of $\text{CpRu}(\text{PPh}_3)(\eta^3\text{-CH}_2\text{-CH=CH}_2)$ with CO

A J-Y NMR tube was charged with $\text{CpRu}(\text{PPh}_3)(\eta^3\text{-CH}_2\text{-CH=CH}_2)$ in d_8 -toluene. The tube was degassed and pressurised with 1.5 bar CO. ^1H and $^{31}\text{P}\{^1\text{H}\}$ NMR spectra were then recorded. No reaction was evident. The sample was then heated to 323 K for 24 hours to enable the complex to react thermally with CO.

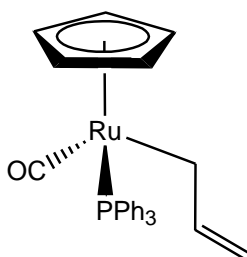
Comparison of $^{31}\text{P}\{^1\text{H}\}$ spectrum taken prior to irradiation with that recorded after showed the conversion of the original peak at δ 68.3 (corresponding to the starting material) had undergone complete conversion to the peak at δ 59.2, which is assigned to

the resonance of a new product species. A $^1\text{H}/^{31}\text{P}$ NMR spectrum connects the ^{31}P singlet at δ 59.2 with ^1H signals at δ 4.34, 7.67, 7.30 and 7.01, which are representative of resonances belonging to the Cp protons and the three resonances of the *ortho*, *meta* and *para* protons of PPh_3 . Another connection was made to a proton at δ 3.42 which subsequently connected to three further new resonances at δ 5.89, 4.82 and 4.71 through a ^1H COSY which is consistent with the protons of an allyl group. This shows that the allyl substituent has adjusted to an η^1 binding mode from an η^3 , giving the complex a 16 electron count and providing a vacant site for an incoming $2e^-$ donor ligand.

A $^{13}\text{C}\{^1\text{H}\}$ NMR spectrum revealed the presence of a single new peak at 205.8 which is consistent with a ruthenium-bound CO ligand for cyclopentadienyl ruthenium complexes. This is consistent with the η^1 binding mode of the allyl moiety, as the $2e^-$ donor CO ligand would occupy the vacant site and raise the electron count of the complex to $18e^-$. The identity of this complex based on the NMR characterisation would be $\text{CpRu}(\text{PPh}_3)(\text{CO})(\eta^1\text{-CH}_2\text{-CH=CH}_2)$ (Figure 5.10). This demonstrates that CO as a ligand is sufficiently stronger in its binding to the ruthenium centre to outcompete the allyl substituent, following the initial dissociation of the allyl substituent to an η^1 mode.

Additional reinforcement of the presence of a coordinated carbonyl ligand was provided by the observation of a νCO band at 1978 cm^{-1} , in the IR spectrum recorded for the sample. MS shows an M^+ signal at m/z 498.

Figure 5.10 Structure of $\text{CpRu}(\text{PPh}_3)(\text{CO})(\text{CH}_2\text{CH=CH}_2)$



This result demonstrates that the incoming CO ligand can displace the allyl moiety, resulting in the formation of an η^1 -allyl complex. Complexes of this type which have the ability to provide substrates with access to the metal centre have recently been of particular interest as catalysts.^{288, 289} As will be discussed later in this chapter (section 5.4.5), benzyl ligands also exhibit this ability, in some cases to a greater extent than allyl

ligands, making them useful as potential catalysts, which is evident from recent studies involving Ni-(η^3 -benzyl) catalysts to polymerise olefins.²⁹⁰⁻²⁹²

5.3.3.2 Photolysis of $\text{CpRu}(\text{PPh}_3)(\eta^3\text{-CH}_2\text{-CH=CH}_2)$ with CO

No evidence of a CO insertion product was found in the NMR spectra following thermal reaction. A second sample was prepared and irradiated using broadband UV to determine whether such insertion products could be formed.

A J-Y NMR tube was charged with $\text{CpRu}(\text{PPh}_3)(\eta^3\text{-CH}_2\text{-CH=CH}_2)$ in d_8 -toluene. The tube was degassed and pressurised with 1.5 bar CO. ^1H and $^{31}\text{P}\{^1\text{H}\}$ NMR spectra were recorded for the sample to demonstrate a reaction had taken place when compared with subsequently recorded spectra. The sample was irradiated for 12 hours at room temperature using the broadband UV Lamp set-up.

The $^{31}\text{P}\{^1\text{H}\}$ NMR spectrum recorded after photolysis shows the presence of a new peak at δ 49.2, which is consistent with the ^{31}P resonance previously reported for the complex $\text{CpRu}(\text{PPh}_3)(\text{CO})(\text{CH}_2\text{-C}_2\text{H}_5)$. The ^1H spectrum displays new resonances at δ 4.34 and 7.67, which confirm that the identity of the photoproduct matches that of the thermal product.

Additionally this similarity between the thermal and photochemical reactions demonstrates the similarity between this complex with $\text{CpRu}(\text{PPh}_3)_2\text{Me}$ (Chapter 3) and $\text{CpRu}(\text{PPh}_3)_2\text{Cl}$ (Chapter 2) whereby the triphenylphosphine ligands could not be fully substituted by the more π acidic CO ligand, owing to electronic effects of the complex.

Again, no evidence was found to suggest CO insertion, and the same product was formed both thermally and photochemically. Previous research by Forschner and Cutler²⁹³ has shown that under forcing conditions (1000 psig, 333K for 24 hours) $\text{CpRu}(\text{CO})_2\text{Me}$ can insert CO into the Ru-C bond. The current results show that the carbonyl insertion product cannot be formed for $\text{CpRu}(\text{PPh}_3)(\text{CO})(\text{CH}_2\text{-C}_2\text{H}_5)$, when using photochemical means to access the insertion product in place of high temperature and pressure. No evidence of a bis-substituted carbonyl complex was found which would be expected to show a peak at δ ~200, in the $^{13}\text{C}\{^1\text{H}\}$ NMR spectrum.

5.3.3.3 Thermal reaction of $\text{CpRu}(\text{PPh}_3)(\eta^3\text{-CH}_2\text{-CH=CH}_2)$ with H_2

A J-Y NMR tube was charged with $\text{CpRu}(\text{PPh}_3)(\eta^3\text{-CH}_2\text{-CH=CH}_2)$ in $d_8\text{-tol}$. The tube was degassed and pressurised with 1.5 bar H_2 . ^1H and $^{31}\text{P}\{^1\text{H}\}$ NMR spectra were recorded immediately after, showed no reaction had taken place. The sample was heated to 323 K for 24 hours to enable the complex to react thermally with the H_2 .

^1H and $^{31}\text{P}\{^1\text{H}\}$ NMR spectra were recorded at 298K. The $^{31}\text{P}\{^1\text{H}\}$ NMR spectrum showed only one singlet resonance at δ 68.3 which is consistent with the ^{31}P resonance of phosphorus atom of the triphenylphosphine ligand of complex $\text{CpRu}(\text{PPh}_3)(\eta^3\text{-CH}_2\text{-CH=CH}_2)$, the starting material. Comparison of the resonances in the ^1H spectra indicate no change as the previously mentioned signals associated with the protons of complex $\text{CpRu}(\text{PPh}_3)(\eta^3\text{-CH}_2\text{-CH=CH}_2)$ are present and no new signals are present after heating of the sample.

The sample was heated again at the higher temperature of 353 K for a further 24 hours. Comparison of the ^1H and $^{31}\text{P}\{^1\text{H}\}$ NMR spectra again show no evidence of thermal reaction of complex $\text{CpRu}(\text{PPh}_3)(\eta^3\text{-CH}_2\text{-CH=CH}_2)$ with H_2 , owing to the lack of any new resonance which could be attributed to a new thermally formed product.

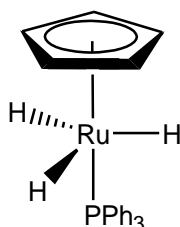
5.3.3.4 Photolysis of $\text{CpRu}(\text{PPh}_3)(\eta^3\text{-CH}_2\text{-CH=CH}_2)$ with H_2

A J-Y NMR tube was charged with $\text{CpRu}(\text{PPh}_3)(\eta^3\text{-CH}_2\text{-CH=CH}_2)$ in $d_8\text{-toluene}$. The tube was degassed and pressurised with 1.5 bar H_2 . The sample was irradiated for 12 hours at room temperature using the broadband UV Lamp set-up.

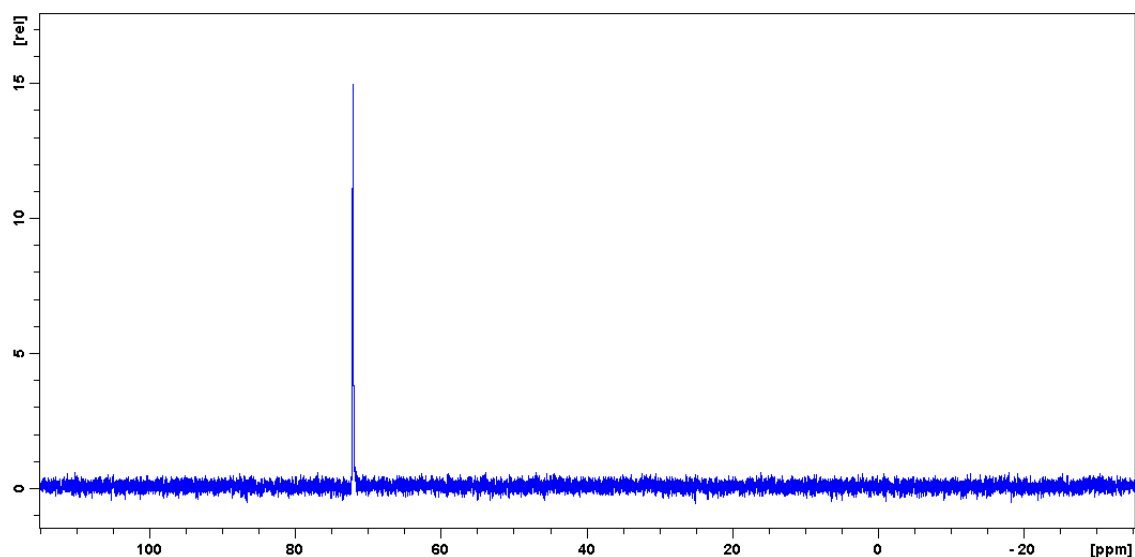
Comparison of $^{31}\text{P}\{^1\text{H}\}$ spectrum taken prior to irradiation with that recorded after showed the conversion of the original peak at δ 68.3 (corresponding to the starting material) had undergone complete conversion to the peak at δ 72.4, which denotes the resonance of a new product species. A $^1\text{H}/^{31}\text{P}$ NMR spectrum connects the ^{31}P singlet at δ 72.4 with ^1H signals at δ 4.78, 7.64, 7.09 and 6.99, which are representative of resonances belonging to the Cp protons and the *ortho*, *meta* and *para* protons of PPh_3 . Another connection was made to a proton resonance at δ -9.61 (d, 19.0 Hz), which is typical of the region where signals corresponding to hydrides appear. The resonances conform to those reported in the literature for the trihydride species, $\text{CpRu}(\text{PPh}_3)(\text{H})_3$

(Figure 5.11). This shows that the allyl substituent undergoes reductive elimination with a ruthenium bound hydride. The NMR assignment of this complex agrees with the literature sources.^{294, 295} Full characterisation for this complex in d_8 -toluene is reported in Table 5.6.

Figure 5.11 Structure of $CpRu(PPh_3)(H)_3$



This complex appears only as a product of the photochemical reaction, and is not observed in the thermal reaction of $CpRu(PPh_3)(\eta^3\text{-CH}_2\text{-CH=CH}_2)$ with hydrogen. Further characterisation was made by comparison of the recorded IR spectrum for the present complex, with bands at 1998 and 2041 cm^{-1} and the literature values, which suggest a close match.^{294, 295} This complex was previously shown to be one of the products of the photochemical reaction of $CpRu(PPh_3)_2\text{Me}$ with H_2 (Chapter 3, Section 3.4.9.2). In this case the clean and complete formation of $CpRu(PPh_3)(H)_3$ is achieved, in contrast to the previous reaction in Chapter 3. This purity is shown in the $^{31}\text{P}\{^1\text{H}\}$ NMR spectrum for the sample (Figure 5.12).

Figure 5.12 A recorded $^{31}\text{P}\{^1\text{H}\}$ NMR spectrum for $\text{CpRu}(\text{PPh}_3)(\text{H})_3$ 

5.3.3.5 Thermal reaction of $\text{CpRu}(\text{PPh}_3)(\eta^3\text{-CH}_2\text{-CH=CH}_2)$ with ethene

A J-Y NMR tube was charged with $\text{CpRu}(\text{PPh}_3)(\eta^3\text{-CH}_2\text{-CH=CH}_2)$ in d_8 -toluene. The tube was degassed and pressurised with 1.5 bar ethene. ^1H and $^{31}\text{P}\{^1\text{H}\}$ NMR spectra revealed no initial reaction occurred. The sample was heated to 323 K for 24 hours to enable the complex to react thermally with ethene.

No reaction was observed thermally, which is analogous to the previous reaction of $\text{CpRu}(\text{PPh}_3)_2\text{Me}$ with ethene (described in Chapter 3) which was found to react only under photochemical conditions.

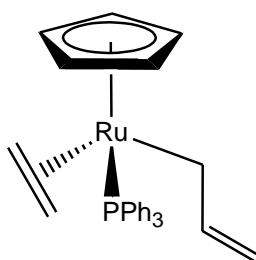
5.3.3.6 Photolysis of $\text{CpRu}(\text{PPh}_3)(\eta^3\text{-CH}_2\text{-CH=CH}_2)$ with ethene

A J-Y NMR tube was charged with $\text{CpRu}(\text{PPh}_3)(\eta^3\text{-CH}_2\text{-CH=CH}_2)$ in d_8 -toluene. The tube was degassed and pressurised with 1.5 bar ethene. The sample was irradiated for 12 hours at room temperature using the broadband UV Lamp set-up.

Comparison of $^{31}\text{P}\{^1\text{H}\}$ spectrum taken prior to irradiation with that recorded after showed the conversion of the original peak at δ 67.3 (corresponding to the starting material) had undergone partial conversion to the peak at δ 60.5 (in a ratio of 8:3, in favour of the starting material), which denotes the resonance of a new product species.

A $^1\text{H}/^{31}\text{P}$ NMR spectrum connects the ^{31}P singlet at δ 60.5 with ^1H signals at δ 4.23, 7.80, 7.43 and 7.03 which are representative of resonances belonging to the Cp protons and the *ortho*, *meta* and *para* protons of PPh_3 . Connections were also made to proton signals at 2.52, 0.73, 2.12 and 1.23, which are consistent with the data recorded in Chapter 3 (section 3.4.6) for an η^2 -bound ethene ligand. Another connection was made to a proton at 3.40 (ruthenium bound CH_2) which subsequently connected to three new resonances at δ 5.84, 4.85 and 4.69 through a ^1H COSY which is consistent with the protons of a bound allyl ligand.

Figure 5.13 Structure of $\text{CpRu}(\text{PPh}_3)(\text{CH}_2\text{-CH=CH}_2)(\eta^2\text{-C}_2\text{H}_4)$



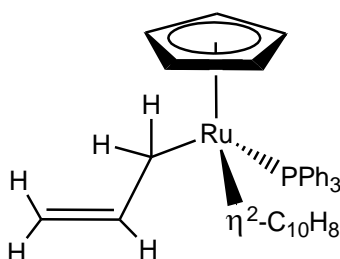
No migration of the ethene ligand was evident, as peaks corresponding to an ethene insertion product were not visible in the ^1H NMR spectrum. The polymerisation of ethene is usually facilitated through insertion into metal-alkyl bonds. $\text{CpRu}(\text{PPh}_3)(\text{CH}_2\text{-CH=CH}_2)(\eta^2\text{-C}_2\text{H}_4)$ possesses an η^2 -bound ethene ligand which is capable of undergoing insertion, but this is not observed in the NMR spectra. Upon warming of this sample to 323 K, the ethene dissociated and the starting material, $\text{CpRu}(\text{PPh}_3)(\eta^3\text{-CH}_2\text{-CH=CH}_2)$, was reformed.

5.3.3.7 Reaction of $\text{CpRu}(\text{PPh}_3)(\eta^3\text{-CH}_2\text{-CH=CH}_2)$ with naphthalene

A thermal experiment was not attempted with this reaction, owing to the similarity between the previous η^2 -naphthalene experiments discussed in Chapter 2 (section 2.4.7.2) and Chapter 3 (section 3.4.5.3). Additionally, the requirement of the ethene reaction to be carried out using low temperature photochemical methods suggests that this system will also require similar conditions to stabilise the photo-products.

To a J-Y NMR tube containing $\text{CpRu}(\text{PPh}_3)(\eta^3\text{-CH}_2\text{-CH=CH}_2)$ in d_8 -toluene, an excess of naphthalene was added. Following 12 hours of photolysis using the broad band UV setup at 193 K, a single small new peak was found in the $^{31}\text{P}\{^1\text{H}\}$ NMR spectrum at δ 62.7. $^1\text{H}/^{31}\text{P}$ HMQC and ^1H COSY NMR experiments were employed to find the peaks corresponding to the Cp (δ 4.31), allyl (δ 5.89, 4.86 and 4.75) and the *ortho*, *meta* and *para* phenyl protons (δ 7.65, 7.23 and 6.98) for this complex. Notable resonances at δ 3.69, 4.05, 6.52 and 6.74 were found to mutually couple via a ^1H COSY. As found with the previous characterisations of such η^2 -bound naphthalene complexes, these naphthyl protons are of low intensity and overlap with the other aromatic protons (in the case of the second naphthalene ring), making characterisation of these resonance impractical. Full characterisation data for this complex, $\text{CpRu}(\text{PPh}_3)(\eta^2\text{-C}_{10}\text{H}_8)(\text{CH}_2\text{-CH=CH}_2)$ (Figure 5.14), is reported in Table 5.9.

Figure 5.14 Structure of $\text{CpRu}(\text{PPh}_3)(\eta^2\text{-C}_{10}\text{H}_8)(\text{CH}_2\text{-CH=CH}_2)$



Warming this sample to 293 K led to the formation of $\text{CpRu}(\text{PPh}_3)(\eta^3\text{-CH}_2\text{-CH=CH}_2)$, the starting material. No evidence was found to suggest that C-H bond activation of the naphthalene ligand had occurred.

5.3.3.8 Thermal reaction of $\text{CpRu}(\text{PPh}_3)(\eta^3\text{-CH}_2\text{-CH=CH}_2)$ with HSiEt_3

A J-Y NMR tube was charged with $\text{CpRu}(\text{PPh}_3)(\eta^3\text{-CH}_2\text{-CH=CH}_2)$ in d_8 -toluene. The tube was degassed and charged with 10 μl of HSiEt_3 ; no thermal reaction was evident at 298K, as observed by recorded ^1H and $^{31}\text{P}\{^1\text{H}\}$ NMR spectra. The sample was then heated to 323 K for 24 hours to enable the complex to react thermally with HSiEt_3 .

^1H and $^{31}\text{P}\{^1\text{H}\}$ NMR spectra were then recorded at 298K and compared with the original spectra. The $^{31}\text{P}\{^1\text{H}\}$ NMR spectrum showed only one singlet resonance at δ 68.3 which is consistent with the ^{31}P resonance of the phosphorus atom of the triphenylphosphine ligand of complex $\text{CpRu}(\text{PPh}_3)(\eta^3\text{-CH}_2\text{-CH=CH}_2)$, the starting material.

The sample was heated again at the higher temperature of 353 K for a further 24 hours. Comparison of the ^1H and $^{31}\text{P}\{^1\text{H}\}$ NMR spectra again show no evidence of a thermal reaction between the complex $\text{CpRu}(\text{PPh}_3)(\eta^3\text{-CH}_2\text{-CH=CH}_2)$ and HSiEt_3 .

5.3.3.9 Photolysis of $\text{CpRu}(\text{PPh}_3)(\eta^3\text{-CH}_2\text{-CH=CH}_2)$ with HSiEt_3

An analogous preparation was made, as described in the previous section, where a J-Y NMR tube was charged with 5 mg of $\text{CpRu}(\text{PPh}_3)(\eta^3\text{-CH}_2\text{-CH=CH}_2)$ and 10 μl of HSiEt_3 , in d_8 -toluene. The sample was irradiated for 12 hours at room temperature using the broadband UV Lamp set-up.

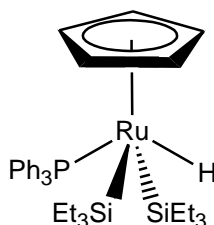
A new ^{31}P NMR signal at δ 57.4 was found using a $^1\text{H} / ^{31}\text{P}$ HMQC experiment to connect to three proton signals at δ -11.57, 4.69 and 7.38. The latter two signals correspond to the proton signals of a cyclopentadienyl ring and the *ortho*-phenyl protons of a coordinated phosphine ligand. The former signal is typical of a ruthenium bound hydride, which appears as a doublet (9.7 Hz). This doublet splitting indicates that only a single phosphine ligand is coordinated to the ruthenium centre which is responsible for the ^{31}P coupling.

To determine whether the remaining positions were filled by silane ligands, a $^1\text{H} / ^{29}\text{Si}$ HMQC experiment was used to determine that a doublet ^{29}Si resonance 24.25 (14.5 Hz) connected with two distinct proton signals at δ 0.91 and 1.04 (CH_3 and CH_2 proton

signals). To conclude whether two silane ligands were present, comparisons of the integral ratios of the cyclopentadienyl and hydride peaks were made with the peaks of the ethyl chains. The overlapping signals of the free silane were removed following the removal of the excess silane *in vacuo*. The ratio of these signals was found to confirm the presence of two coordinated silane ligands (18:5 of CH₂ to Cp). This indicates that the proton signals of the two silanes overlap. Full characterisation is reported in Table 5.7, and the proposed structure is depicted in Figure 5.15.

The product complex might be formed by a route analogous to that of the reaction between CpRu(PPh₃)₂Me and HSiEt₃. The allyl group undergoes reductive elimination with a ruthenium bound hydride, allowing the subsequent oxidative addition of a second HSiEt₃ molecule to give the product CpRu(PPh₃)(SiEt₃)₂H (Chapter 3).

Figure 5.15 Structure of CpRu(PPh₃)(SiEt₃)₂H



5.4 Synthesis and characterisation of CpRu(PPh₃)(η³-CH₂C₆H₅)

Based on the previous synthesis and reactions of the complex, CpRu(PPh₃)(η³-CH₂CHCH₂), an aryl-based moiety was considered as a replacement of the allyl group. It was expected that with the change in electronic structure of the aryl moiety (connected through the ruthenium bound CH₂) to a tolyl group, that an η³ binding mode could be achieved in a similar way to the previously discussed allyl derivative.

The complex CpRu(PPh₃)₂(CH₂C₆H₅) has been previously reported by Lemhkul as one of the minor isomeric products which arise from the thermal reaction of CpRu(PPh₃)₂Me in toluene. The characterisation of this complex remains only partially complete owing to the small quantity of the complex attained relative to the other products and the limitations of NMR techniques at the time the research was carried out. To date, no synthesis has been reported to produce this complex in a bulk quantity nor

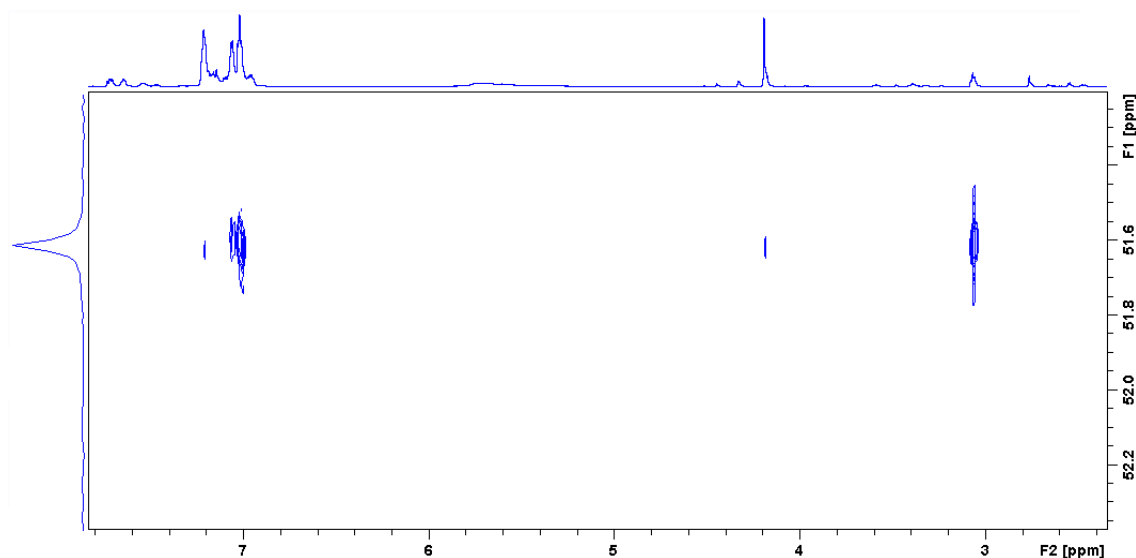
have studies been made concerning the reactivity of this complex with substrates. Additionally the η^3 bound mono phosphine derivative, $\text{CpRu}(\text{PPh}_3)(\eta^3\text{-CH}_2\text{-C}_6\text{H}_5)$, is absent from the literature.

5.4.1 Synthesis of $\text{CpRu}(\text{PPh}_3)_2(\text{CH}_2\text{C}_6\text{H}_5)$

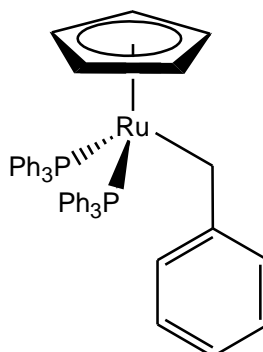
A sample of $\text{CpRu}(\text{PPh}_3)_2(\text{CH}_2\text{C}_6\text{H}_5)$ was prepared by treating $\text{CpRu}(\text{PPh}_3)_2\text{Cl}$ with $\text{ClMgCH}_2\text{C}_6\text{H}_5$ in diethyl ether, with the purity of the sample confirmed by ^1H and $^{31}\text{P}\{^1\text{H}\}$ NMR. Full details of this reaction are found in Chapter 7, section 7.2.4.4.

5.4.2 NMR characterisation of $\text{CpRu}(\text{PPh}_3)_2(\text{CH}_2\text{C}_6\text{H}_5)$

The 1D $^{31}\text{P}\{^1\text{H}\}$ NMR spectrum of the complex displayed a single peak at δ 51.6, which is typical of a ^{31}P resonance for a triphenylphosphine ligand, bound to a ruthenium centre. A $^1\text{H}/^{31}\text{P}$ HMQC NMR spectrum (Figure 5.16) connected to proton signals found at δ 4.19, 7.28, 7.07 and 6.98 which are characteristics of the proton resonances of a cyclopentadienyl ring, and the *ortho*, *meta* and *para* positions of protons of the phenyl rings of a bound triphenylphosphine ligand. An additional proton resonance was found at δ 3.07 (triplet) using the same experiment, which is typical of the protons bound to the CH_2 carbon which bridges the phenyl moiety with the ruthenium centre. The triplet splitting arises owing to the presence of two triphenylphosphine ligands bound to the ruthenium centre. This indicates that the complex in its present form binds in an η^1 mode rather than an η^3 , since the two phosphine ligands satisfy the 18 electron requirement.

Figure 5.16 A $^1\text{H}/^{31}\text{P}$ HMQC NMR spectrum for $\text{CpRu}(\text{PPh}_3)_2(\text{CH}_2\text{C}_6\text{H}_5)$ 

A connection was made via a selective NOE experiment from the triplet resonance at δ 3.07 (the irradiated peak) to the signal at δ 7.53, which belongs to a proton within the aryl structure. A ^1H COSY experiment was employed to find additional phenyl proton signals at δ 7.46 and overlapping the meta phenyl phosphine proton resonance at δ 7.07. These NMR signals are consistent with the partial NMR characterisation previously reported by Lehmkühl *et al.*²⁹⁶ Full characterisation for this complex (Figure 5.17) is presented in Table 5.10.

Figure 5.17 Structure of $\text{CpRu}(\text{PPh}_3)_2(\text{CH}_2\text{C}_6\text{H}_5)$ 

No evidence was found in the ^1H nor $^{13}\text{C}\{^1\text{H}\}$ NMR spectra for an C-H activation product, for the activation of the protons of the benzyl ring by the ruthenium centre.

5.4.3 Formation of $\text{CpRu}(\text{PPh}_3)(\eta^3\text{-CH}_2\text{C}_6\text{H}_5)$

Heating of the sample of $\text{CpRu}(\text{PPh}_3)_2(\text{CH}_2\text{C}_6\text{H}_5)$ to 353 K in toluene led to the loss of triphenylphosphine and the subsequent binding of the benzyl ligand in a η^3 mode in small quantities. The sample was exposed briefly to air, and shaken vigorously to oxidise the liberated phosphine to triphenylphosphine oxide (as discussed for similar experiments in Chapter 3, section 3.4.11.1). Following this procedure, the sample was washed with ethanol to remove the excess phosphine oxide. Further heating / washing of the sample led ultimately to a conversion to the η^3 mode of 87% (as determined by comparison of their respective ^{31}P resonances in a $^{31}\text{P}\{^1\text{H}\}$ NMR spectrum).

In the presence of free phosphine at room temperature, the sample reformed the initial bis-phosphine derivative, $\text{CpRu}(\text{PPh}_3)_2(\text{CH}_2\text{C}_6\text{H}_5)$, over a period of several days. This demonstrates that the coordination of the benzyl ring to the ruthenium centre is quite labile to exchange with other prospective ligands, relative to the allyl derivative, allowing for a more diverse range of complexes to be formed.

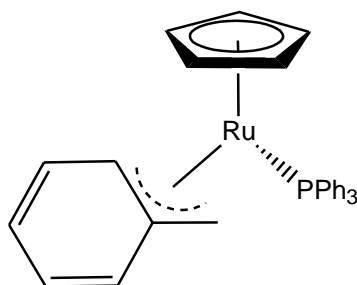
5.4.4 NMR characterisation of $\text{CpRu}(\text{PPh}_3)(\eta^3\text{-CH}_2\text{C}_6\text{H}_5)$

The $^{31}\text{P}\{^1\text{H}\}$ NMR spectrum showed a single peak at δ 60.3, which corresponds to one of the product peaks found previously for the reaction between $\text{CpRu}(\text{PPh}_3)_2\text{Me}$ and toluene (Chapter 3). A $^1\text{H}/^{31}\text{P}$ HMQC experiment showed coupling between this phosphorus peak and the five ^1H signals at δ 4.02, 4.21, 7.52, 7.05 and 6.97. The latter three signals are typical of the *ortho*, *meta* and *para* protons of a phenyl ring of a coordinated triphenylphosphine ligand.

Of the remaining two ^1H resonances, the signal at δ 4.21 is shown to correspond to the protons of a coordinated cyclopentadienyl ring, by integration of this signal with the resonance at δ 7.53 (giving a ratio of 5:6). The remaining resonance at δ 4.02 corresponds to a ^{13}C signal at δ 3.3, using a $^{13}\text{C}\{^1\text{H}\}$ HMQC experiment. This ^{13}C signal appears as a doublet of 5.0 Hz, which demonstrates that only a single phosphine ligand is coordinated to the ruthenium centre. So far, this would yield an unsaturated 16 electron complex, which is unlikely, owing to the stability of the complex. To detect the ligand which coordinates to this vacant site, a selective NOE was employed, where the irradiation was centred on the signal at δ 4.02. Strong connections were made to ^1H

signals at δ 2.67 and 7.14. These two signals were found to mutually couple using a ^1H COSY experiment, along with three signals at δ 6.24, 6.62 and 7.03. These signals are likely to be the protons of a benzyl ligand, which coordinates to the ruthenium centre via an η^3 coordination mode, similar to that previously described for the η^3 allyl complex. Confirmation of this structure was found by observation of the doublet splitting (6.4 Hz) of the carbon resonance at δ 98.8, which couples to the ^1H resonance at δ 2.67, using $^1\text{H}/^{13}\text{C}$ HMQC and $^{13}\text{C}\{^1\text{H}\}$ NMR experiments. This determines that the benzyl moiety lies coordinated to the ruthenium centre in an η^3 mode, owing to the magnitude of this $^{31}\text{P}-^{13}\text{C}$ coupling. The identity of this complex is therefore $\text{CpRu}(\text{PPh}_3)(\eta^3\text{-CH}_2\text{C}_6\text{H}_5)$ (Figure 5.18)

Figure 5.18 $\text{CpRu}(\text{PPh}_3)(\eta^3\text{-CH}_2\text{C}_6\text{H}_5)$



This complex is similar to recently reported Cp^* derivative $\text{Cp}^*\text{Ru}(\text{PPh}_3)(\eta^3\text{-CH}_2\text{C}_6\text{H}_5)$.

283

5.4.5 Thermal and Photochemical reactions of $\text{CpRu}(\text{PPh}_3)(\eta^3\text{-CH}_2\text{C}_6\text{H}_5)$

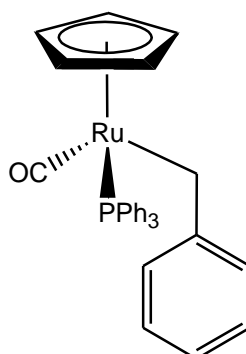
5.4.5.1 Thermal reaction of $\text{CpRu}(\text{PPh}_3)(\eta^3\text{-CH}_2\text{C}_6\text{H}_5)$ with CO

A J-Y NMR tube was charged with $\text{CpRu}(\text{PPh}_3)(\eta^3\text{-CH}_2\text{C}_6\text{H}_5)$ in d_8 -toluene. The tube was then degassed and pressurised with 1.5 bar CO, and warmed to 323 K for 24 hours to enable the complex to react thermally with CO.

Comparison of $^{31}\text{P}\{^1\text{H}\}$ spectrum taken prior to irradiation with that recorded after showed the conversion of the original peak at δ 60.3 (corresponding to the starting material) had undergone complete conversion to the peak at δ 62.1, which is assigned to the resonance of a new product species. A $^1\text{H}/^{31}\text{P}$ NMR spectrum connects the ^{31}P singlet at δ 62.1 with ^1H signals at δ 4.34, 7.43, 7.12 and 7.00, which are representative of resonances belonging to the Cp protons and the three resonances of the *ortho*, *meta* and *para* protons of PPh_3 . Another connection was made to a proton at δ 3.91 which subsequently connected to three further new resonances at δ 7.56, 7.17 and 7.05 through a ^1H COSY which is consistent with the protons of a benzyl group. This shows that the benzyl substituent has adjusted to an η^1 binding mode from an η^3 , giving the complex a 16 electron count and providing a vacant site for an incoming CO donor ligand.

A $^{13}\text{C}\{^1\text{H}\}$ NMR spectrum revealed the presence of a single new peak at 206.3 which is consistent with a ruthenium-bound CO ligand for cyclopentadienyl ruthenium complexes. This is consistent with the η^1 -binding mode of the benzyl moiety, as the $2e^-$ donor CO ligand would occupy the vacant site and raise the electron count of the complex to $18e^-$. The identity of this complex based on the NMR characterisation would be $\text{CpRu}(\text{PPh}_3)(\text{CO})(\eta^1\text{-CH}_2\text{-Ph})$ (Figure 5.19). This demonstrates that CO as a ligand is sufficiently stronger in its binding to the ruthenium centre to outcompete the allyl substituent, following the initial dissociation of the allyl substituent to an η^1 mode.

Additional reinforcement of the presence of a coordinated carbonyl ligand was provided by the observation of a νCO band at 1963 cm^{-1} , in the IR spectrum recorded for the sample. MS shows an M^+ signal at m/z 562.70.

Figure 5.19 Structure of $\text{CpRu}(\text{PPh}_3)(\text{CO})(\text{CH}_2\text{C}_6\text{H}_5)$ 

5.4.5.2 Photolysis of $\text{CpRu}(\text{PPh}_3)(\eta^3\text{-CH}_2\text{C}_6\text{H}_5)$ with CO

An analogous sample of $\text{CpRu}(\text{PPh}_3)(\eta^3\text{-CH}_2\text{C}_6\text{H}_5)$ with CO in d_8 -toluene was prepared as described for the thermal reaction. The sample was then irradiated for 12 hours at room temperature using the broadband UV Lamp set-up.

Comparison of $^{31}\text{P}\{^1\text{H}\}$ spectrum taken prior to irradiation with that recorded after showed the conversion of the original peak at δ 60.3 (corresponding to the starting material) had undergone complete conversion to the peak at δ 62.1, which is the resonance of a new product species. A $^1\text{H}/^{31}\text{P}$ NMR spectrum connects the ^{31}P singlet at δ 62.1 with ^1H signals at δ 4.34, 7.43, 7.12 and 7.00, which are representative of resonances belonging to the Cp protons and the *ortho*, *meta* and *para* protons of PPh_3 . Another connection was made to a proton at δ 7.56 which subsequently connected to two further new resonances at δ 7.17 and 7.05 through a ^1H COSY which is consistent with the protons of a bound tolyl ligand.

The NMR spectra show that no migration of the CO into the Ru-C bond has taken place, and that formation of the bis-carbonyl has not occurred.

5.4.5.3 Thermal reaction of $\text{CpRu}(\text{PPh}_3)(\eta^3\text{-CH}_2\text{C}_6\text{H}_5)$ with H_2

A J-Y NMR tube was charged with $\text{CpRu}(\text{PPh}_3)(\eta^3\text{-CH}_2\text{C}_6\text{H}_5)$ in d_8 -toluene. The tube was degassed and pressurised with 1.5 bar H_2 . No reaction was evident even when the sample was warmed to 353 K.

5.4.5.4 Photolysis of $\text{CpRu}(\text{PPh}_3)(\eta^3\text{-CH}_2\text{C}_6\text{H}_5)$ with H_2

A sample containing $\text{CpRu}(\text{PPh}_3)(\eta^3\text{-CH}_2\text{C}_6\text{H}_5)$ with H_2 (in d_8 -toluene) was irradiated for 12 hours at room temperature using the broadband UV Lamp set-up.

Comparison of the $^{31}\text{P}\{^1\text{H}\}$ spectrum taken prior to irradiation with that recorded after showed the conversion of the original peak at δ 60.3 (corresponding to the starting material) had undergone complete conversion to the peak at δ 72.4, which is the resonance of a new product species. A $^1\text{H}/^{31}\text{P}$ NMR spectrum connects the ^{31}P singlet at δ 72.4 with ^1H signals at δ 4.78, 7.64, 7.09 and 6.99, which are representative of resonances belonging to the Cp protons and the *ortho*, *meta* and *para* protons of PPh_3 . Another connection was made to a proton at δ -9.61 (d, 19.0 Hz), which is characteristic of a hydride group.

The product of the reaction is therefore $\text{CpRu}(\text{PPh}_3)(\text{H})_3$. This complex has previously been described in section 5.3.3.4 and in Chapter 3, section 3.4.9.2.

5.4.5.5 Photolysis of $\text{CpRu}(\text{PPh}_3)(\eta^3\text{-CH}_2\text{C}_6\text{H}_5)$ with ethene

After previously demonstrating for $\text{CpRu}(\text{PPh}_3)(\eta^3\text{-CH}_2\text{CH}=\text{CH}_2)$ that there was no thermal reaction with ethene, only photochemical reactivity is discussed for the reaction of the present complex, $\text{CpRu}(\text{PPh}_3)(\eta^3\text{-CH}_2\text{C}_6\text{H}_5)$, with ethene.

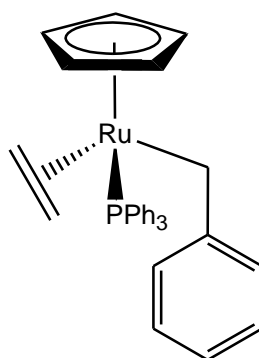
A J-Y NMR tube was charged with $\text{CpRu}(\text{PPh}_3)(\eta^3\text{-CH}_2\text{C}_6\text{H}_5)$ in d_8 -toluene. The tube was degassed and pressurised with 1.5 bar ethene. ^1H and $^{31}\text{P}\{^1\text{H}\}$ NMR spectra were recorded for the sample to demonstrate a reaction had taken place when compared with subsequently recorded spectra. The sample was then irradiated for 12 hours at room temperature using the broadband UV Lamp set-up.

Comparison of $^{31}\text{P}\{^1\text{H}\}$ spectrum taken prior to irradiation with that recorded after showed the conversion of the original peak at δ 60.3 (corresponding to the starting material) had undergone complete conversion to the peak at δ 61.3, which is the resonance of a new product species. A $^1\text{H}/^{31}\text{P}$ NMR spectrum connects the ^{31}P singlet at δ 61.3 with ^1H signals at δ 4.21, 7.78, 7.33 and 6.98, which are representative of resonances belonging to the Cp protons and the *ortho*, *meta* and *para* protons of PPh_3 . Another connection was made to a proton at δ 7.57 which subsequently connected to two further new resonances at δ 7.43 and 7.06 through a ^1H COSY which is consistent with the protons of an allyl moiety.

The presence of an η^2 -bound ethene ligand was confirmed by the two doublet signals in the $^{13}\text{C}\{^1\text{H}\}$ NMR spectrum at δ 32.4 and 39.1. Both of these signals possess a splitting of 5.8 Hz, due to the single phosphine ligand coordinated to the metal centre. A $^1\text{H}/^{13}\text{C}$ HMQC NMR experiment was employed to determine the four ^1H NMR resonances of the ethene moiety, which were found at δ 0.43, 1.12, 2.28 and 2.64.

Again, no migration of the ethene onto the Ru-C bond of the η^1 -benzyl was evident by the ^1H NMR signals observed. However, ethene clearly displaces the η^3 -benzyl interaction. Upon warming this sample to 323 K, the ethene is displaced by the benzyl moiety which interacts in an η^3 mode, to reform the starting material.

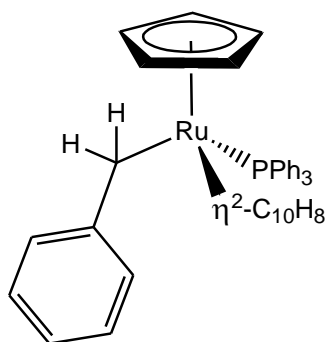
Figure 5.20 Structure of $\text{CpRu}(\text{PPh}_3)(\text{C}_2\text{H}_4)(\text{CH}_2\text{C}_6\text{H}_5)$



5.4.5.6 Photolysis of $\text{CpRu}(\text{PPh}_3)(\eta^3\text{-CH}_2\text{C}_6\text{H}_5)$ with naphthalene

Following the ability of $\text{CpRu}(\text{PPh}_3)(\eta^3\text{-CH}_2\text{-CH=CH}_2)$ to coordinate naphthalene at low temperature (section 5.3.3.7), an analogous procedure was followed for the present complex. Photolysis of the sample for 12 hours led to the formation of a single low intensity resonance at δ 63.7 in the recorded $^{31}\text{P}\{^1\text{H}\}$ NMR spectrum. ^1H signals corresponding to the Cp, η^1 -benzyl and phenyl protons were found using $^1\text{H}/^{31}\text{P}$ HMQC, NOESY and ^1H COSY NMR experiments. As noted for the previous sample signals at δ 3.74, 4.09, 6.59 and 6.77 signals were found for the coordinated naphthalene ring. The complex is therefore readily assigned as $\text{CpRu}(\text{PPh}_3)(\eta^2\text{-C}_{10}\text{H}_8)(\text{CH}_2\text{-C}_6\text{H}_5)$ (Figure 5.21), and full NMR data is reported in Table 5.14.

Figure 5.21 Structure of $\text{CpRu}(\text{PPh}_3)(\eta^2\text{-C}_{10}\text{H}_8)(\text{CH}_2\text{-C}_6\text{H}_5)$



As was found with the previous η^2 -naphthalene complex, no evidence of a C-H activation product was found. Warming the sample to 298 K led to the reformation of the original complex, $\text{CpRu}(\text{PPh}_3)(\eta^3\text{-CH}_2\text{C}_6\text{H}_5)$.

5.4.5.7 Photolysis of $\text{CpRu}(\text{PPh}_3)(\eta^3\text{-CH}_2\text{C}_6\text{H}_5)$ with HSiEt_3

After showing that no thermal reaction was evident in the reaction of $\text{CpRu}(\text{PPh}_3)(\eta^3\text{-CH}_2\text{CH=CH}_2)$ with HSiEt_3 , only the photochemical reaction is considered for the present complex. A J-Y NMR tube was charged with 5 mg of $\text{CpRu}(\text{PPh}_3)(\eta^3\text{-CH}_2\text{C}_6\text{H}_5)$ in d_8 -toluene. The tube was degassed and 10 μl of HSiEt_3 was added. ^1H and $^{31}\text{P}\{^1\text{H}\}$ NMR spectra were recorded for the sample to demonstrate a reaction had taken place when compared with subsequently recorded spectra. The sample was irradiated for 12 hours at room temperature using the broadband UV Lamp set-up.

A new ^{31}P signal at δ 57.4 was found using a $^1\text{H}/^{31}\text{P}$ HMQC experiment to connect to three proton signals at δ -11.57, 4.69 and 7.38. The latter two signals correspond to the proton signals of a cyclopentadienyl ring and the *ortho*-phenyl protons of a coordinated phosphine ligand. The former signal is typical of a ruthenium bound hydride, which appears as a doublet (9.7 Hz). This doublet splitting indicates that only a single phosphine ligand is coordinated to the ruthenium centre which is responsible for the ^{31}P coupling. These signals correspond to the previously characterised complex $\text{CpRu}(\text{PPh}_3)(\text{SiEt}_3)_2\text{H}$.

These resonances are consistent with those recorded previously for the complex $\text{CpRu}(\text{PPh}_3)(\text{SiEt}_3)_2\text{H}$, which was discussed in Chapter 3 as a product of the reaction between $\text{CpRu}(\text{PPh}_3)_2\text{Me}$ and HSiEt_3 . Unlike the previous reaction the lack of free triphenylphosphine present means that the formation of $\text{CpRu}(\text{PPh}_3)(\text{SiEt}_3)_2\text{H}$ is relatively clean compared to the previous reaction, which generated a variety of different complexes arising from the re-association of the free phosphine and solvent activation.

5.5 Synthesis and characterisation of $\text{CpRu}(\text{PPh}_3)_2(\text{CH}_2\text{C}_{10}\text{H}_7)$

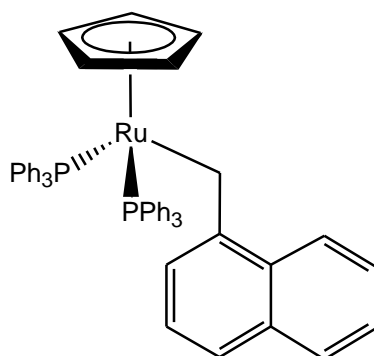
5.5.1 Synthesis of $\text{CpRu}(\text{PPh}_3)_2(\text{CH}_2\text{C}_{10}\text{H}_7)$

A sample of $\text{CpRu}(\text{PPh}_3)_2(\text{CH}_2\text{C}_{10}\text{H}_7)$ was prepared by treating $\text{CpRu}(\text{PPh}_3)_2\text{Cl}$ with $\text{ClMgCH}_2\text{C}_{10}\text{H}_7$ in diethyl ether, with the purity of the sample confirmed by ^1H and $^{31}\text{P}\{^1\text{H}\}$ NMR. Both complexes $\text{CpRu}(\text{PPh}_3)_2(\text{CH}_2\text{C}_{10}\text{H}_7)$ and $\text{CpRu}(\text{PPh}_3)(\eta^3\text{-CH}_2\text{C}_{10}\text{H}_7)$ (to be discussed later in this section) are thermally unstable and therefore this preparation was repeated numerous times in order to confirm the identity of these complexes and obtain the NMR data recorded in tables 5.15 and 5.16, and described in the following section.

5.5.2 NMR characterisation of the η^1 / η^3 methyl-naphthalene complexes

The dominant product of the sample was $\text{CpRu}(\text{PPh}_3)_2(\text{CH}_2\text{C}_{10}\text{H}_7)$, which was partially characterised by NMR techniques (Figure 5.22). The $^{31}\text{P}\{^1\text{H}\}$ NMR spectrum revealed a peak at δ 49.9, which was linked through a $^1\text{H}/^{31}\text{P}$ HMQC experiment to ^1H signals at δ 3.93, 4.17, 7.32 and 7.12. The latter three of these signals represent the cyclopentadienyl protons, and the *ortho* / *meta*-phenyl phosphine protons, respectively. The signal at δ 3.93 represents the protons of the methylene bridge, which connects the metal-centre to the naphthyl moiety. NOE interrogation of this resonance revealed transfer to three other signals at δ 7.28, 7.76 and 7.33, which comprise the protons of the first naphthyl ring. Owing to the low conversion of this complex from the starting material (and the instability of this complex, which is discussed further later in this section) only partial characterisation of this complex was achieved.

Figure 5.22 Structure of $\text{CpRu}(\text{PPh}_3)_2(\text{CH}_2\text{C}_{10}\text{H}_7)$



For the characterisation of $\text{CpRu}(\text{PPh}_3)(\eta^3\text{-CH}_2\text{C}_{10}\text{H}_7)$, 1D $^{31}\text{P}\{^1\text{H}\}$ NMR spectrum of the complex displayed a single peak at δ 68.7, which is typical of a ^{31}P resonance for a triphenylphosphine ligand, bound to a ruthenium centre. A $^1\text{H}/^{31}\text{P}$ HMQC experiment connected to proton signals found at δ 4.32, 7.76, 7.37 and 7.05 which are characteristics of the proton resonances of a cyclopentadienyl ring, and the *ortho*, *meta* and *para* positions of protons of the phenyl rings of a bound triphenylphosphine ligand. An additional proton resonance was found at δ 3.45 (triplet) which is typical of the protons bound to the carbon which bridges the naphthalene moiety with the ruthenium centre. The triplet splitting arises owing to the presence of two triphenylphosphine ligands bound to the ruthenium centre. This demonstrates that the complex in its present form binds in an η^1 mode rather than an η^3 , since the two phosphine ligands satisfy the 18 electron requirement.

Through a ^1H COSY experiment three resonance signals were found to connect at δ 2.21, 3.78 and 6.73. These resonances were connected to the naphthyl ligand which is bound to the ruthenium centre directly and through the CH_2 moiety, in a η^3 binding mode. A connection was made via a selective NOE experiment from the triplet resonance at δ 3.41 (the irradiated peak) to the signal at δ 4.09, which belongs to a proton within the naphthalene structure, chemical shifts are matched to their structural positions in Table 5.15.

Further characterisation could not be obtained for the complex owing to precipitation of the complex. Though no signs of sample decomposition were found in the ^1H NMR spectrum (numerous small peaks corresponding to the decomposed organic fragments would be expected in the δ 1-10 region of the NMR spectrum), any attempts to dissolve the solid precipitate in other solvents proved to be unsuccessful. It is likely that the complex forms clusters, by reacting with molecules of the same complex, which ultimately prove to be insoluble in solution. This unexpected occurrence meant that further reactions involving this complex and other substrates could not be completed owing to the unstable nature of the complex. In addition, due to the low quantity of $\text{CpRu}(\text{PPh}_3)(\eta^3\text{-CH}_2\text{C}_{10}\text{H}_7)$ formed within the sample (relative to $\text{CpRu}(\text{PPh}_3)_2(\eta^1\text{-CH}_2\text{C}_{10}\text{H}_7)$), only a limited characterisation of the complex was achieved.

5.6 Conclusions

This chapter described studies which led to the *in situ* preparations and characterisation of $\text{CpRu}(\text{PPh}_3)(\eta^3\text{-Si}(\text{Me})_2\text{C}_2\text{H}_3)$, $\text{CpRu}(\text{PPh}_3)_2(\text{Si}(\text{Me})_2\text{C}_2\text{H}_4)$, $\text{CpRu}(\text{PPh}_3)(\eta^3\text{-CH}_2\text{CH}=\text{CH}_2)$, $\text{CpRu}(\text{PPh}_3)_2(\text{CH}_2\text{CH}=\text{CH}_2)$, $\text{CpRu}(\text{PPh}_3)(\text{CO})(\text{CH}_2\text{CH}=\text{CH}_2)$, $\text{CpRu}(\text{PPh}_3)(\eta^2\text{-C}_2\text{H}_4)(\text{CH}_2\text{CH}=\text{CH}_2)$, $\text{CpRu}(\text{PPh}_3)(\eta^2\text{-C}_{10}\text{H}_8)(\text{CH}_2\text{CH}=\text{CH}_2)$, $\text{CpRu}(\text{PPh}_3)(\eta^3\text{-CH}_2\text{Ph})$, $\text{CpRu}(\text{PPh}_3)_2(\text{CH}_2\text{Ph})$, $\text{CpRu}(\text{PPh}_3)(\text{CO})(\text{CH}_2\text{Ph})$, $\text{CpRu}(\text{PPh}_3)(\eta^2\text{-C}_2\text{H}_4)(\text{CH}_2\text{Ph})$, $\text{CpRu}(\text{PPh}_3)(\eta^2\text{-C}_{10}\text{H}_8)(\text{CH}_2\text{Ph})$, $\text{CpRu}(\text{PPh}_3)(\eta^3\text{-CH}_2\text{C}_{10}\text{H}_7)$ and $\text{CpRu}(\text{PPh}_3)_2(\text{CH}_2\text{C}_{10}\text{H}_7)$.

$\text{CpRu}(\text{PPh}_3)_2(\eta^1\text{-CH}_2\text{-CH}=\text{CH}_2)$ and $\text{CpRu}(\text{PPh}_3)_2(\eta^1\text{-CH}_2\text{-C}_6\text{H}_5)$ react photochemically with ethene (two electron donor), H_2 and HSiEt_3 while showing no thermal reactivation up to 353 K. In contrast, CO reacts to form the same mono substitution products thermally and photochemically for the two ruthenium complexes. *In situ* irradiation studies using the 325 nm source failed to produce any photochemical conversion and therefore the photochemical studies used the broadband *ex situ* approach.

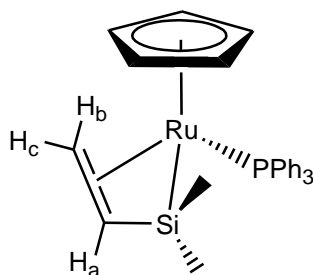
The NMR data recorded for these irradiated samples established that η^3 ligand binding is achieved after PPh_3 loss. This was determined by complete product characterisation including the observation of a P-C coupling to the coordinated moieties of the ligand (e.g. the two vinyl carbons in the allyl case have a J_{CP} value of 10.8 Hz). The chemical shifts observed in the $^{31}\text{P}\{^1\text{H}\}$ NMR spectrum for the respective η^3 allyl and naphthyl complexes are similar to those of $(\text{CpRu}(\text{PPh}_3)(\eta^2\text{-C}_2\text{H}_4)\text{Me})$ and $(\text{CpRu}(\text{PPh}_3)(\eta^2\text{-C}_{10}\text{H}_8)\text{Me})$ discussed in Chapter 3. This demonstrates that the electronic properties of each complex are similar and hence PPh_3 binding is comparable. This is of particular interest for the η^3 -naphthyl complex, as the corresponding complex, $\text{CpRu}(\text{PPh}_3)(\eta^2\text{-C}_{10}\text{H}_8)\text{Me}$, is not stable at room temperature.

The η^3 -dimethylvinylsilane complex, reported in section 5.2, is novel and few examples exist in the literature. This method of synthesis also provided a convenient route to tethering the vinyl functionality to the metal centre. However, the lack of selectivity towards forming the η^3 complex via $\text{CpRu}(\text{PPh}_3)_2\text{Me}$, the competing CH bond activation pathways of the precursor, and the photochemical activity of the products makes characterisation of these complexes by NMR a challenge, and also hinders the use of this complex in further reactions.

The photochemical reactivity of the η^3 allyl and benzyl products towards H_2 and silane substrates leads to the formation of a common product (which are also found in Chapter 3). However, owing to the lack of liberated phosphine, these products were observed to be formed in higher yields with no side products formed. In the case of ethene, no migration-based reactivity was evident even though an effective Ru(ethene)alkyl arrangement was obtained.

In terms of the stability of η^3 vs η^1 complexes, the allyl moiety binds the strongest, which is evident from the initial synthesis, where the majority of the product is the η^3 allyl complex, rather than the η^1 . The lack of thermal stability of the naphthyl complexes results in only the partial characterisation of the η^3 and η^1 forms. The benzyl forms possess similar reactivity to the allyl derivative. However, the interaction with the metal centre is weaker than the former η^3 -allyl complex, and the phenyl moiety is readily displaced from the metal centre.

5.7 Characterisation data

Table 5.1 NMR data for $CpRu(PPh_3)(\eta^3-Si(Me)_2C_2H_3)$ 

In d_6 -benzene at 298 K	δ / ppm (multiplicity, integration)	Assignment	Coupling constant / Hz	Assignment
1H	-0.33 (s, 3) 0.73 (s, 3) 1.98 (m) 2.14 (m) 3.53 (m) 4.29 (s, 5) 6.97 (m) 7.01 (m) 7.68 (m)	Si(CH ₃) ↓ * Si(CH ₃) ↑ * H_a H_b H_c C₅H₅ <i>Para</i> - P(C ₆ H ₅) ₃ <i>Meta</i> - P(C ₆ H ₅) ₃ <i>Ortho</i> - P(C ₆ H ₅) ₃	11.2 11.2 11.2 8.1	$ ^2J_{PH} $ $ ^2J_{PH} $ $ ^2J_{PH} $ $ ^1J_{PH} $
^{13}C	-3.1 (s) -3.5 (s) 31.0 (d) 38.4 (d) 81.6 (s) 127.6 (d) 128.5 (s) 133.6 (d) 141.1 (d)	Si(CH ₃) ↑ * Si(CH ₃) ↓ * Si-CHCH ₂ Si-CHCH ₂ C₅H₅ <i>Meta</i> - P(C ₆ H ₅) ₃ <i>Para</i> - P(C ₆ H ₅) ₃ <i>Ortho</i> - P(C ₆ H ₅) ₃ <i>Ipsa</i> - P(C ₆ H ₅) ₃	6.4 6.4 10.3 12.0 42.3	$ ^3J_{PC} $ $ ^3J_{PC} $ $ ^3J_{PC} $ $ ^2J_{PC} $ $ ^1J_{PC} $
^{31}P	66.5 (s)	P(Ph)₃		
^{29}Si	35.9 (d)	Si	22	$ ^2J_{PSi} $

* Where: ↑ denotes that the methyl group points towards the Cp ring and ↓ denotes that the methyl group points away from the Cp ring

Table 5.2 NMR data for $CpRu(PPh_3)_2(Si(Me)_2C_2H_3)$

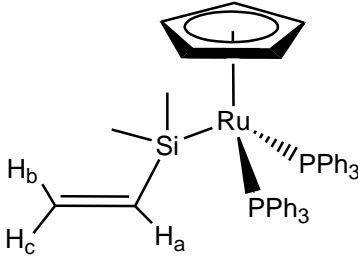
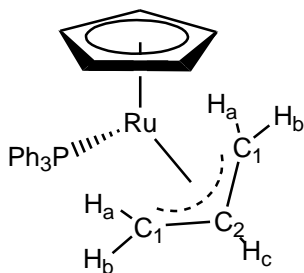
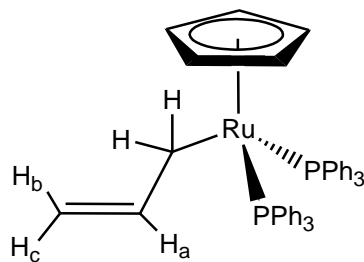
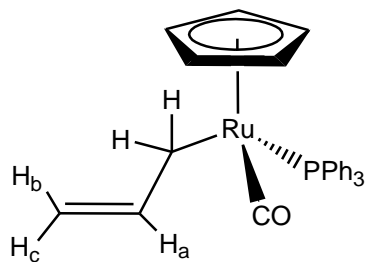
				
In d_6 -benzene at 298 K	δ / ppm (multiplicity, integration)	Assignment	Coupling constant / Hz	Assignment
1H	0.23 (s) 4.39 (s) 5.39 (m) 5.52 (m) 6.31 (m) 7.02 (m) 7.18 (m) 7.49 (m)	Si(CH ₃) C ₅ H ₅ H _c H _b H _a <i>Para</i> - P(C ₆ H ₅) ₃ <i>Meta</i> - P(C ₆ H ₅) ₃ <i>Ortho</i> - P(C ₆ H ₅) ₃	6.8 11.3 6.8, 11.3 7.8	$ ^3J_{HH} $ $ ^3J_{HH} $ $ ^3J_{HH} , ^3J_{HH} $ $ ^1J_{PH} $
^{13}C	-2.9 (s) 34.4 (s) 37.5 (s) 82.3 (s) 127.9 (d) 128.4 (s) 133.7 (t) 142.1 (dd)	Si(CH ₃) Si-CHCH ₂ Si-CHCH ₂ C ₅ H ₅ <i>Meta</i> - P(C ₆ H ₅) ₃ <i>Para</i> - P(C ₆ H ₅) ₃ <i>Ortho</i> - P(C ₆ H ₅) ₃ <i>Ipsa</i> - P(C ₆ H ₅) ₃	10.9 13.5 14.3, 37.4	$ ^3J_{PC} $ $ ^2J_{PC} $ $ ^3J_{PC} , ^1J_{PC} $
^{31}P	51.8 (s)	P(C ₆ H ₅) ₃		
^{29}Si	17.2 (t)	Si	26.8	$ ^2J_{PSi} $

Table 5.3 NMR data for $\text{CpRu}(\text{PPh}_3)(\eta^3\text{-CH}_2\text{CH=CH}_2)$ 

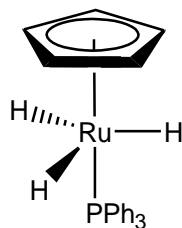
In d_8 -toluene at 298 K	δ / ppm (multiplicity, integration)	Assignment	Coupling constant / Hz	Assignment
^1H	0.68 (m) 2.92 (m) 4.06 (m) 4.17 (s) 7.05 (m) 7.09 (m) 7.36 (m)	H_a H_b H_c C_5H_5 <i>Para</i> - $\text{P}(\text{C}_6\text{H}_5)_3$ <i>Meta</i> - $\text{P}(\text{C}_6\text{H}_5)_3$ <i>Ortho</i> - $\text{P}(\text{C}_6\text{H}_5)_3$	14.7, 10.8 6.2, 10.8 6.2, 14.7, 10.8 8.6	$ \text{}^3\text{J}_{\text{HH}} , \text{}^3\text{J}_{\text{PH}} $ $ \text{}^3\text{J}_{\text{HH}} , \text{}^3\text{J}_{\text{PH}} $ $ \text{}^3\text{J}_{\text{HH}} , \text{}^3\text{J}_{\text{HH}} , \text{}^3\text{J}_{\text{PH}} $ $ \text{}^1\text{J}_{\text{PH}} $
^{13}C	32.3 (d) 38.7 (d) 78.6 (s) 127.9 (d) 128.8 (s) 133.9 (d) 141.3 (d)	C_2 C_1 C_5H_5 <i>Meta</i> - $\text{P}(\text{C}_6\text{H}_5)_3$ <i>Para</i> - $\text{P}(\text{C}_6\text{H}_5)_3$ <i>Ortho</i> - $\text{P}(\text{C}_6\text{H}_5)_3$ <i>Ipsa</i> - $\text{P}(\text{C}_6\text{H}_5)_3$	14.7 14.7 10.8 13.0 44.6	$ \text{}^2\text{J}_{\text{PC}} $ $ \text{}^2\text{J}_{\text{PC}} $ $ \text{}^3\text{J}_{\text{PC}} $ $ \text{}^2\text{J}_{\text{PC}} $ $ \text{}^1\text{J}_{\text{PC}} $
^{31}P	68.3 (s)	$\text{P}(\text{C}_6\text{H}_5)_3$		

Table 5.4 NMR data for $CpRu(PPh_3)_2(CH_2CH=CH_2)$ 

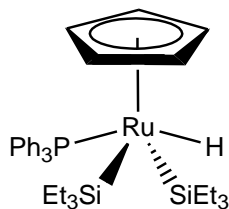
In d_8 -toluene at 298 K	δ / ppm (multiplicity, integration)	Assignment	Coupling constant / Hz	Assignment
^1H	2.93 (t) 4.40 (s) 4.71 (m) 4.89 (m) 6.21 (m) 7.01 (m) 7.18 (m) 7.54 (m)	CH_2 C_5H_5 H_b (<i>E</i>) H_c (<i>Z</i>) H_a <i>Para</i> - $\text{P}(\text{C}_6\text{H}_5)_3$ <i>Meta</i> - $\text{P}(\text{C}_6\text{H}_5)_3$ <i>Ortho</i> - $\text{P}(\text{C}_6\text{H}_5)_3$	7.3 16.4 6.3 6.3, 16.4 8.3	$^3\text{J}_{\text{PH}}$ $^3\text{J}_{\text{HH}}$ $^3\text{J}_{\text{HH}}$ $^3\text{J}_{\text{HH}}$, $^3\text{J}_{\text{HH}}$ $^1\text{J}_{\text{HH}}$
^{13}C	27.5 (t) 82.3 (s) 113.2 (s) 128.1 (d) 128.6 (s) 133.6 (t) 138.9 (s) 141.2 (dd)	$\text{CH}_2=\text{CH}-\text{CH}_2$ C_5H_5 $\text{CH}_2=\text{CH}-\text{CH}_2$ <i>Meta</i> - $\text{P}(\text{C}_6\text{H}_5)_3$ <i>Para</i> - $\text{P}(\text{C}_6\text{H}_5)_3$ <i>Ortho</i> - $\text{P}(\text{C}_6\text{H}_5)_3$ $\text{CH}_2=\text{CH}-\text{CH}_2$ <i>Ipsa</i> - $\text{P}(\text{C}_6\text{H}_5)_3$	4.4 10.3 15.8 14.5, 38.2	$^2\text{J}_{\text{PC}}$ $^3\text{J}_{\text{PC}}$ $^2\text{J}_{\text{PC}}$ $^3\text{J}_{\text{PC}}$, $^3\text{J}_{\text{PC}}$
^{31}P	52.4 (s)	$\text{P}(\text{Ph})_3$		

Table 5.5 NMR data for $CpRu(PPh_3)(CO)(CH_2CH=CH_2)$ 

In d_8 -toluene at 298 K	δ / ppm (multiplicity, integration)	Assignment	Coupling constant / Hz	Assignment
1H	3.42 (d)	CH_2	7.2	$ ^3J_{PH} $
	4.34 (s)	C_5H_5		
	4.71 (m)	H_c (<i>E</i>)	7.6	$ ^3J_{HH} $
	4.82 (m)	H_b (<i>Z</i>)	5.8	$ ^3J_{HH} $
	5.89 (m)	H_a	10.4	$ ^3J_{HH} $
	7.01 (m)	$P(C_6H_5)_3$ <i>Para</i>		
	7.30 (m)	$P(C_6H_5)_3$ <i>Meta</i>		
	7.67 (m)	$P(C_6H_5)_3$ <i>Ortho</i>	8.4	$ ^1J_{HH} $
^{13}C	5.1 (d)	CH_2	4.3	$ ^2J_{PC} $
	79.8 (s)	C_5H_5		
	116.6 (s)	$CH_2CH=CH_2$		
	127.8 (d)	$P(C_6H_5)_3$ <i>Meta</i>	10.7	$ ^3J_{PC} $
	128.5 (s)	$P(C_6H_5)_3$ <i>Para</i>		
	133.7 (d)	$P(C_6H_5)_3$ <i>Ortho</i>	12.4	$ ^2J_{PC} $
	138.2 (s)	$CH_2CH=CH_2$		
	142.5 (d)	$P(C_6H_5)_3$ <i>Ipsa</i>	42.9	$ ^1J_{PC} $
205.8 (d)	CO	22.8	$ ^2J_{PC} $	
^{31}P	59.2 (s)	$P(Ph)_3$		

Table 5.6 NMR data for $CpRu(PPh_3)H_3$ (C_{3v})

In d_8 -toluene at 298 K	δ / ppm (multiplicity, integration)	Assignment	Coupling constant / Hz	Assignment
1H	-9.61 (d) 4.78 (s) 6.99 (m) 7.09 (m) 7.64 (m)	Ru-H C_5H_5 <i>Para</i> - $P(C_6H_5)_3$ <i>Meta</i> - $P(C_6H_5)_3$ <i>Ortho</i> - $P(C_6H_5)_3$	19.0 8.4	$ ^2J_{PH} $ $ ^1J_{PH} $
^{13}C	83.1 (s) 127.6 (d) 128.4 (s) 133.2 (d) 140.9 (d)	C_5H_5 <i>Meta</i> - $P(C_6H_5)_3$ <i>Para</i> - $P(C_6H_5)_3$ <i>Ortho</i> - $P(C_6H_5)_3$ <i>Ipsa</i> - $P(C_6H_5)_3$	10.3 11.8 42.2	$ ^3J_{PC} $ $ ^2J_{PC} $ $ ^1J_{PC} $
^{31}P	72.4 (s)	$P(Ph)_3$		

Table 5.7 NMR data for $CpRu(PPh_3)(SiEt_3)_2H$ 

In d_8 -toluene at 298 K	δ / ppm (multiplicity, integration)	Assignment	Coupling constant / Hz	Assignment
1H	-11.57 (d, 1) 0.91 (br, 18) 1.04 (br, 12) 4.69 (s, 5) 6.97 (m) 7.03 (m) 7.38 (m)	Ru- H Si- CH₂CH₃ Si- CH₂CH₃ C₅H₅ <i>Para</i> - P(C₆H₅) ₃ <i>Meta</i> - P(C₆H₅) ₃ <i>Ortho</i> - P(C₆H₅) ₃	9.5 8.2	$ ^2J_{PH} $ $ ^1J_{PH} $
^{13}C	12.6 (s) 14.0 (s) 84.7 (s) 127.0 (d) 128.5 (s) 133.2 (d) 141.2 (d)	Si- CH₂CH₃ Si- CH₂CH₃ C₅H₅ <i>Meta</i> - P(C₆H₅) ₃ <i>Para</i> - P(C₆H₅) ₃ <i>Ortho</i> - P(C₆H₅) ₃ <i>Ipsa</i> - P(C₆H₅) ₃	 10.6 13.2 43.7	 $ ^3J_{PC} $ $ ^2J_{PC} $ $ ^1J_{PC} $
^{31}P	57.4 (s)	P(Ph)₃		
^{29}Si	24.25 (d)	Si	14.5	$ ^2J_{PSi} $

Table 5.8 NMR data for $CpRu(PPh_3)(\eta^2-C_2=H_4)(CH_2CH=CH_2)$

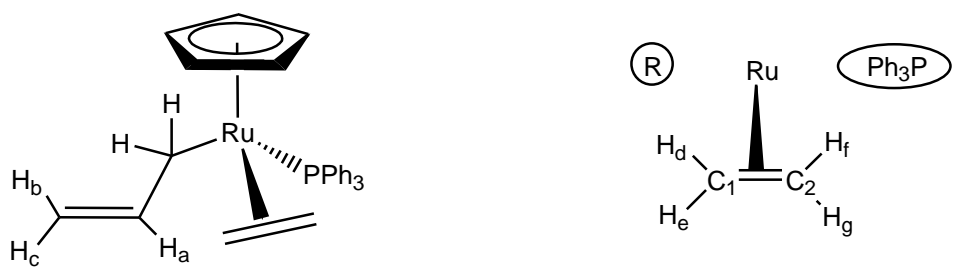
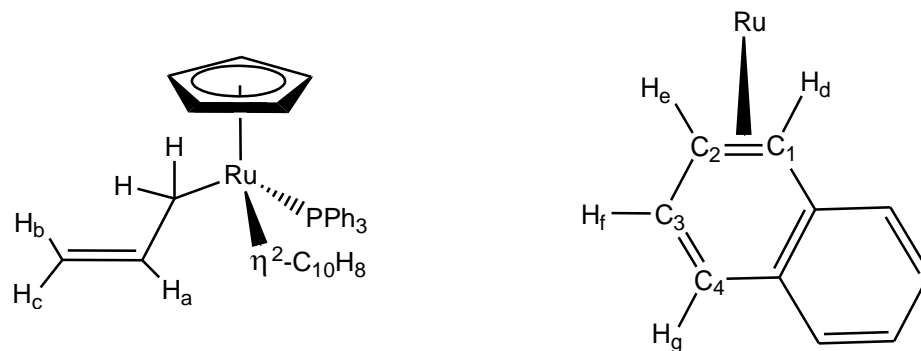
				
In d_8 -toluene at 198 K	δ / ppm (multiplicity, integration)	Assignment	Coupling constant / Hz	Assignment
1H	0.73 (m) 1.23 (m) 2.12 (m) 2.52 (m) 3.40 (d) 4.69 (m) 4.73 (s) 4.85 (m) 5.84 (m) 7.03 (m) 7.43 (m) 7.80 (m)	H_e H_g H_f H_d CH_2 H_c (<i>E</i>) C_5H_5 H_b (<i>Z</i>) H_a $P(C_6H_5)_3$ <i>Para</i> $P(C_6H_5)_3$ <i>Meta</i> $P(C_6H_5)_3$ <i>Ortho</i>	7.4	$ ^3J_{PH} $
^{13}C	4.3 (d) 38.1 (d) 44.4 (d) 77.6 (s) 117.2 (s) 127.6 (d) 128.4 (s) 134.4 (d) 137.9 (s) 142.5 (d)	CH_2 C_2 C_1 C_5H_5 $CH_2CH=CH_2$ $P(C_6H_5)_3$ <i>Meta</i> $P(C_6H_5)_3$ <i>Para</i> $P(C_6H_5)_3$ <i>Ortho</i> $CH_2CH=CH_2$ $P(C_6H_5)_3$ <i>Ipsa</i>	4.1 5.6 5.6 10.3 12.5 44.6	$ ^2J_{PC} $ $ ^2J_{PC} $ $ ^2J_{PC} $ $ ^3J_{PC} $ $ ^2J_{PC} $ $ ^1J_{PC} $
^{31}P	60.5 (s)	$P(Ph)_3$		

Table 5.9 NMR data for $CpRu(PPh_3)(\eta^2-C_{10}H_8)(CH_2CH=CH_2)$ 

In d_8 -toluene at 198 K	δ / ppm (multiplicity, integration)	Assignment	Coupling constant / Hz	Assignment
1H	3.65 (d) 3.69 (br) 4.05 (br) 4.31 (s) 4.75 (m) 4.86 (m) 5.89 (m) 6.52 (br) 6.74 (br) 6.98 (m) 7.23 (m) 7.65 (m)	CH_2 H_e H_d C_5H_5 $CH_2CH=CH_2$ $CH_2CH=CH_2$ $CH_2CH=CH_2$ H_g H_f $P(C_6H_5)_3$ Para $P(C_6H_5)_3$ Meta $P(C_6H_5)_3$ Ortho	7.3 8.7	$ ^3J_{PH} $ $ ^3J_{PH} $
^{13}C	5.2 (d) 76.7 (s) 118.6 (s) 127.7 (d) 128.2 (s) 133.4 (d) 138.4 (s) 141.3 (d)	CH_2 C_5H_5 $CH_2CH=CH_2$ $P(C_6H_5)_3$ Meta $P(C_6H_5)_3$ Para $P(C_6H_5)_3$ Ortho $CH_2CH=CH_2$ $P(C_6H_5)_3$ Ipso	3.9 10.1 11.4 44.3	$ ^2J_{PC} $ $ ^3J_{PC} $ $ ^2J_{PC} $ $ ^1J_{PC} $
^{31}P	62.7 (s)	$P(Ph)_3$		

Table 5.10 NMR data for $CpRu(PPh_3)_2(CH_2Ph)$

In d_8 -toluene at 298 K	δ / ppm (multiplicity, integration)	Assignment	Coupling constant / Hz	Assignment
1H	3.07 (t)	CH_2 -Ph	7.25	$ \ ^3J_{PH} $
	4.19 (s)	C_5H_5		
	6.98 (m)	<i>Para</i> - $P(C_6H_5)_3$		
	7.07 (m)	H_c		
	7.07 (m)	<i>Meta</i> - $P(C_6H_5)_3$		
	7.28 (m)	<i>Ortho</i> - $P(C_6H_5)_3$		
	7.46 (m)	H_b & H_d		
	7.53 (m)	H_a & H_e		
^{13}C	3.01 (t)	CH_2 -Ph	5.5	$ \ ^2J_{PC} $
	84.7 (s)	C_5H_5	10.4	$ \ ^3J_{PC} $
	120.6 (s)	C_3 & C_5		
	120.6 (s)	C_4		
	127.4 (d)	<i>Meta</i> - $P(C_6H_5)_3$	12.7	$ \ ^2J_{PC} $
	128.7 (s)	<i>Para</i> - $P(C_6H_5)_3$		
	133.5 (t)	<i>Ortho</i> - $P(C_6H_5)_3$	14.8, 37.2	$ \ ^3J_{PC} , \ ^1J_{PC} $
	138.2 (s)	C_2 & C_6		
	141.4 (dd)	<i>Ipsa</i> - $P(C_6H_5)_3$		
145.0 (s)	C_1			
^{31}P	51.6	$P(Ph)_3$		

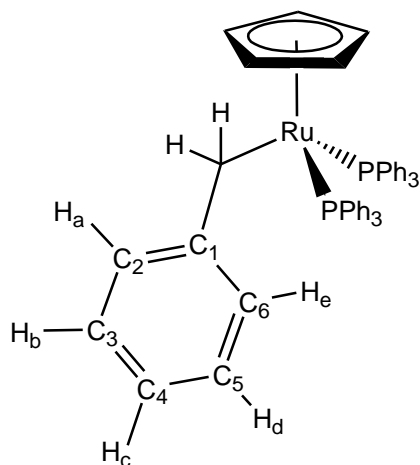


Table 5.11 NMR data for $CpRu(PPh_3)(\eta^3-CH_2Ph)$

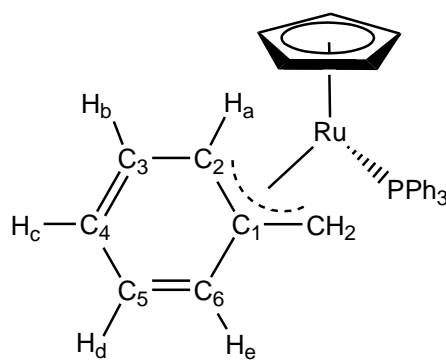
				
In d_8 -toluene at 298 K	δ / ppm (multiplicity, integration)	Assignment	Coupling constant / Hz	Assignment
1H	2.67 (m) 4.02 (m) 4.21 (s) 6.24 (m) 6.62 (m) 6.97 (m) 7.03 (m) 7.05 (m) 7.14 (m) 7.52 (m)	H_a CH_2 -Ph C_5H_5 H_b H_c <i>Para</i> - $P(C_6H_5)_3$ H_d <i>Meta</i> - $P(C_6H_5)_3$ H_e <i>Ortho</i> - $P(C_6H_5)_3$	7.2	$ ^3J_{PH} $
^{13}C	3.3 (d) 81.1 (s) 98.8 (br) 120.4 (br) 127.4 (d) 127.6 (s) 128.4 (s) 128.6 (s) 132.5 (br) 134.1 (d) 142.1 (d) 142.7 (d)	CH_2 -Ph C_5H_5 C_2 C_3 <i>Meta</i> - $P(C_6H_5)_3$ C_5 C_4 <i>Para</i> - $P(C_6H_5)_3$ C_6 <i>Ortho</i> - $P(C_6H_5)_3$ C_1 <i>Ipsa</i> - $P(C_6H_5)_3$	5.0 10.2 11.6 6.4 42.9	$ ^2J_{PC} $ $ ^3J_{PC} $ $ ^2J_{PC} $ $ ^2J_{PC} $ $ ^1J_{PC} $
^{31}P	60.3 (s)	$P(Ph)_3$		

Table 5.12 NMR data for $CpRu(PPh_3)(CO)(CH_2Ph)$

In d_8 -toluene at 298 K	δ / ppm (multiplicity, integration)	Assignment	Coupling constant / Hz	Assignment		
1H	3.91 (d)	CH_2	6.7	$ ^3J_{PH} $		
	4.34 (s)	C_5H_5				
	7.00 (m)	$P(C_6H_5)_3$ Para				
	7.05 (m)	H_c				
	7.12 (m)	$P(C_6H_5)_3$ Meta				
	7.17 (m)	H_b & H_d				
	7.43 (m)	$P(C_6H_5)_3$ Ortho				
	7.56 (m)	H_a & H_e				
^{13}C	4.4 (d)	CH_2	24.0	$ ^2J_{PC} $		
	77.8 (s)	C_5H_5	10.2	$ ^3J_{PC} $		
	120.6 (s)	C_4				
	127.1 (s)	C_3 & C_5				
	127.7 (d)	$P(C_6H_5)_3$ Meta				
	128.4 (s)	$P(C_6H_5)_3$ Para				
	133.9 (d)	$P(C_6H_5)_3$ Ortho			11.5	$ ^2J_{PC} $
	138.3 (s)	C_2 & C_6			44.5	$ ^1J_{PC} $
	141.0 (d)	$P(C_6H_5)_3$ Ipso				
154.2 (s)	C_1					
206.3 (d)	CO	22.5	$ ^2J_{PC} $			
^{31}P	62.1 (s)	$P(Ph)_3$				

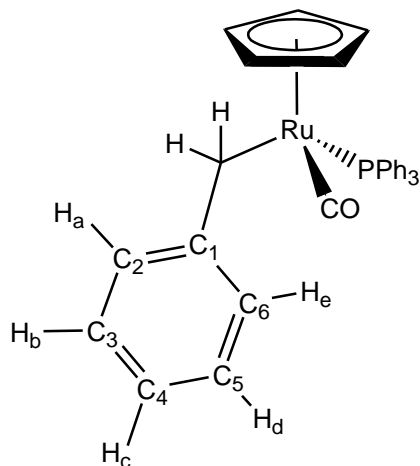


Table 5.13 NMR data for $CpRu(PPh_3)(\eta^2-C_2=H_4)(CH_2Ph)$

In d_8 -toluene at 198 K	δ / ppm (multiplicity, integration)	Assignment	Coupling constant / Hz	Assignment
1H	0.43 (m, 1) 1.12 (m, 1) 2.28 (m, 1) 2.64 (m, 1) 3.64 (d) 4.21 (s, 5) 6.98 (m) 7.06 (m) 7.33 (m) 7.43 (m) 7.57 (m) 7.78 (m)	H_g H_i H_h H_f CH_2 C_5H_5 $P(C_6H_5)_3$ <i>Para</i> H_c $P(C_6H_5)_3$ <i>Meta</i> H_b & H_d H_a & H_e $P(C_6H_5)_3$ <i>Ortho</i>	7.2	$ ^3J_{PH} $
^{13}C	4.4 (d) 32.4 (d) 39.1 (d) 79.4 (s) 120.8 (s) 127.4 (d) 127.5 (s) 128.5 (s) 133.9 (d) 138.9 (s) 141.2 (d) 154.0 (s)	CH_2 C_8 C_7 C_5H_5 C_4 $P(C_6H_5)_3$ <i>Meta</i> C_3 & C_5 $P(C_6H_5)_3$ <i>Para</i> $P(C_6H_5)_3$ <i>Ortho</i> C_2 & C_6 $P(C_6H_5)_3$ <i>Ipsso</i> C_1	4.5 5.8 5.8 10.1 11.6 44.3	$ ^2J_{PC} $ $ ^2J_{PC} $ $ ^2J_{PC} $ $ ^3J_{PC} $ $ ^2J_{PC} $ $ ^1J_{PC} $
^{31}P	61.3 (s)	$P(Ph)_3$		

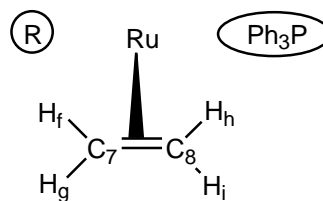
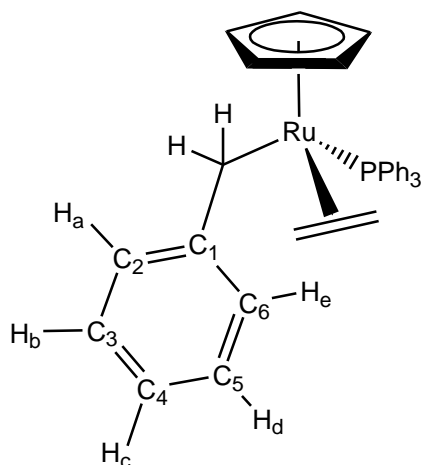
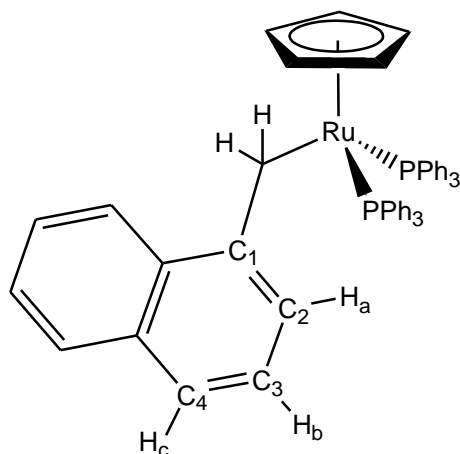
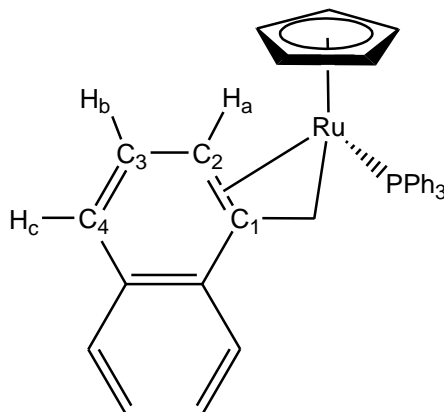


Table 5.14 NMR data for $CpRu(PPh_3)(\eta^2-C_{10}H_8)(CH_2Ph)$

In d_8 -toluene at 198 K	δ / ppm (multiplicity, integration)	Assignment	Coupling constant / Hz	Assignment
1H	3.41 (d) 3.74 (m) 4.09 (m) 4.37 (s) 6.59 (m) 6.77 (m) 7.02 (m) 7.08 (m) 7.11 (m) 7.44 (m) 7.52 (m) 7.58 (m)	CH_2 H_g H_f C_5H_5 H_i H_h $P(C_6H_5)_3$ Para H_c $P(C_6H_5)_3$ Meta H_b & H_d H_a & H_e $P(C_6H_5)_3$ Ortho	7.2	$ ^3J_{PH} $
^{13}C	5.9 (d) 30.4 (d) 43.0 (d) 84.1 (s) 121.2 (s) 127.2 (d) 127.5 (s) 128.8 (s) 129.8 (s) 133.5 (d) 137.4 (s) 140.7 (d) 147.2 (s) 154.3 (s)	CH_2 C_7 C_8 C_5H_5 C_4 $P(C_6H_5)_3$ Meta C_3 & C_5 $P(C_6H_5)_3$ Para C_9 $P(C_6H_5)_3$ Ortho C_2 & C_6 $P(C_6H_5)_3$ Ipso C_{10} C_1	4.6 15.2 15.2	$ ^2J_{PC} $ $ ^2J_{PC} $ $ ^2J_{PC} $ $ ^3J_{PC} $ $ ^2J_{PC} $ $ ^1J_{PC} $
^{31}P	63.7 (s)	$P(Ph)_3$		

Table 5.15 NMR data for $CpRu(PPh_3)_2(CH_2C_{10}H_7)$ 

In d_8 -toluene at 298 K	δ / ppm (multiplicity, integration)	Assignment	Coupling constant / Hz	Assignment
1H	3.93 (t) 4.17 (s) 6.97 (m) 7.12 (m) 7.28 (m) 7.32 (m) 7.33 (m) 7.76 (m)	$CH_2-C_{10}H_7$ C_5H_5 <i>Para</i> - $P(C_6H_5)_3$ <i>Meta</i> - $P(C_6H_5)_3$ H_a <i>Ortho</i> - $P(C_6H_5)_3$ H_c H_b	7.3	$ ^3J_{PH} $
^{13}C	4.1 (t) 79.8 (s) 122.3 (s) 127.4 (s) 133.4 (d) 138.7 (s) 150.2 (s)	$CH_2-C_{10}H_7$ C_5H_5 C_4 C_3 <i>Ortho</i> - $P(C_6H_5)_3$ C_2 C_1	4.1 12.0	$ ^2J_{PC} $ $ ^2J_{PC} $
^{31}P	49.9 (s)	$P(Ph)_3$		

Table 5.16 NMR data for $CpRu(PPh_3)(\eta^3-CH_2C_{10}H_7)$ 

In d_8 -toluene at 298 K	δ / ppm (multiplicity, integration)	Assignment	Coupling constant / Hz	Assignment
1H	2.21 (m) 3.45 (d) 3.78 (m) 4.32 (s) 6.73 (m) 7.05 (m) 7.37 (m) 7.76 (m)	H_a $CH_2-C_{10}H_7$ H_b C_5H_5 H_c <i>Para</i> - $P(C_6H_5)_3$ <i>Meta</i> - $P(C_6H_5)_3$ <i>Ortho</i> - $P(C_6H_5)_3$	6.9	$ ^3J_{PH} $
^{13}C	4.8 (d) 35.2 (d) 54.3 (d) 84.5 (s) 123.2 (s) 133.7 (d) 137.7 (s)	$CH_2-C_{10}H_7$ C_1 C_2 C_5H_5 C_4 <i>Ortho</i> - $P(C_6H_5)_3$ C_3	4.6 14.8 14.8 11.8	$ ^2J_{PC} $ $ ^2J_{PC} $
^{31}P	68.7 (s)	$P(Ph)_3$		

Chapter 6

Low Temperature Photochemical Reactions of $\text{CpRh}(\eta^2\text{-C}_2\text{H}_4)_2$

6.1 Introduction

In the same way that the complex $\text{CpRu}(\text{PPh}_3)_2\text{Cl}$ has allowed for the convenient routes to the synthesis of novel half-sandwich ruthenium complexes, $\text{CpRh}(\eta^2\text{-olefin})_2$ complexes provide comparable accessibility to cyclopentadienyl rhodium complexes. Since the initial synthesis of $\text{CpRh}(\eta^2\text{-C}_2\text{H}_4)$ in 1963 by King,²⁹⁷ such rhodium complexes have been demonstrated to take part in reactions involving C-H bond activation,²⁹⁸⁻³⁰⁰ hydrosilation processes³⁰¹⁻³⁰³ and hydrocarbon functionalisation.³⁰⁴ Rhodium complexes of this type have also recently been used in the construction of molecular boxes capable of encapsulating methanol and DCM.³⁰⁵

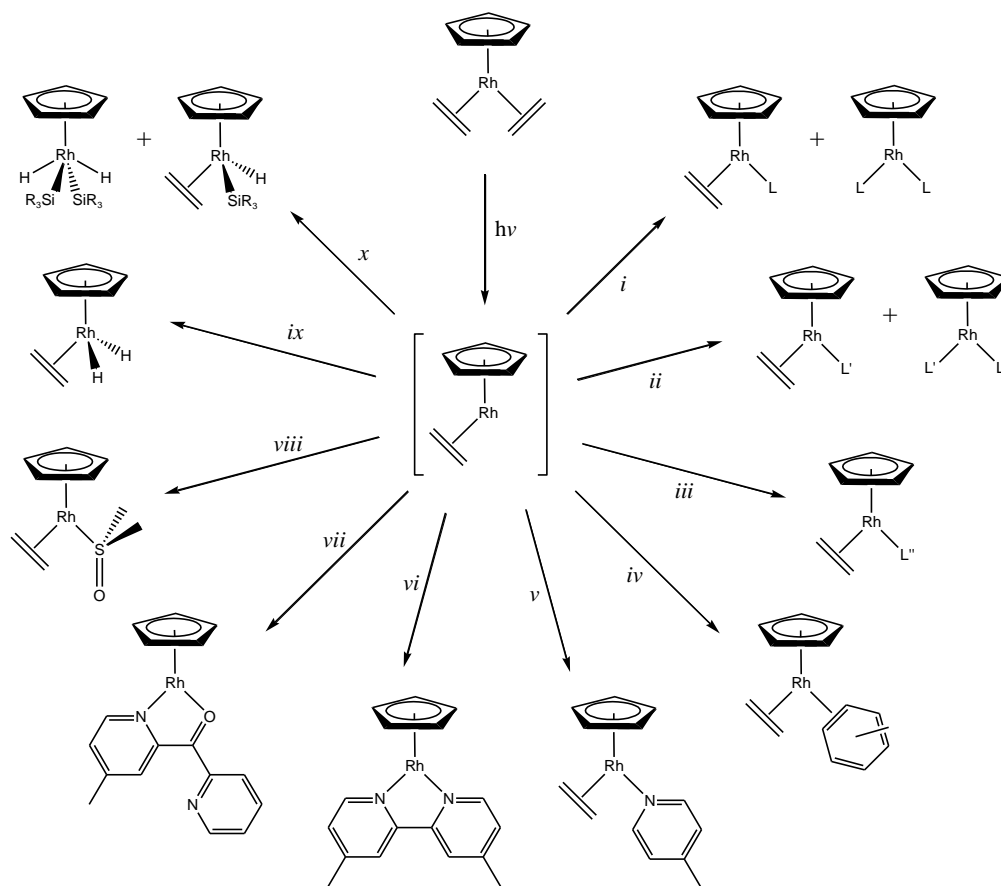
The reactivity concerning $\text{CpRh}(\eta^2\text{-olefin})_2$ complexes has widely been explored in terms of their thermal and photochemical reactivity, which accounts for their subsequent use in the synthesis of a diverse range of rhodium complexes (see Figure 6.1). However, Cramer's method³⁰⁶ (used in this thesis and outlined in Chapter 7) produces HCl as a by-product of reaction, which precludes the use of functionalised olefins as ligands, which limits the range of possible olefin complexes which can be readily made. This accounts for why "simple" olefins, such as ethene, have generally been incorporated into the structures of starting materials; however, recent research has addressed this problem.³⁰⁷

As mentioned, one of the main research areas concerning $\text{CpRh}(\eta^2\text{-C}_2\text{H}_4)$ (through the $[\text{CpRh}(\eta^2\text{-C}_2\text{H}_4)]$ fragment) is the study of its potential to activate C-H bonds. As discussed in Chapter 1, C-H activation is often a key step in the mechanism of catalytic

transformations, and such character could potentially be utilised to develop catalytic cycles, similar to those of the half-sandwich ruthenium analogues.

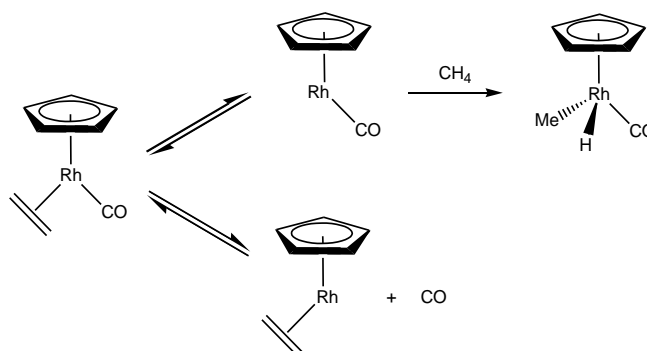
Haddon and Perutz have previously shown that cyclopentadienyl rhodium complexes are capable of C-H activation in low temperature matrices, using UV photolysis. Figure 6.2 depicts the C-H activation of methane by the $[\text{CpRh}(\text{CO})]$ fragment; such reactivity is not observed for the $[\text{CpRh}(\text{C}_2\text{H}_4)]$ fragment.^{308, 309} This was initially attributed to steric factors, but, owing to more recent examples and similarly encumbered cyclopentadienyl ruthenium analogues, it is more feasible to conclude that electronic factors are responsible for the inability of the $[\text{CpRh}(\text{C}_2\text{H}_4)]$ fragment to C-H activate.³¹⁰ More recently, kinetic studies of the $[\text{CpRh}(\text{CO})]$ fragment toward C-H activation have been made.^{310, 311}

Figure 6.1 Photochemical substitution reactions of $\text{CpRh}(\eta^2\text{-C}_2\text{H}_4)_2$



- i.* $\text{L} = \text{PR}_3$ ^{312, 313} or C_6H_{10} ³¹⁴ *ii.* $\text{L}' = \text{CO}$ ^{308, 309} *iii.* $\text{L}'' = \text{N}_2$ ³¹⁵ *iv.* C_7H_8 (198 K)³¹⁶
v. 4-Mepy³¹⁷ *vi.* 2,2'-Me₂bpy³¹⁷ *vii.* DPK³¹⁷ *viii.* DMSO³¹⁸
ix. H_2 ³¹⁵ *x.* HSiEt_3 ³⁰³

Figure 6.2 Comparison of the ability of the fragments $[\text{CpRh}(\text{CO})]$ and $[\text{CpRh}(\text{C}_2\text{H}_4)]$ to C-H activate methane³⁰⁸



Reaction conditions: low temperature (12 K) in an Ar/ CH_4 matrix, initiated by a UV source (229 nm)

The capacity of the $[\text{CpRh}(\text{PMe}_3)]$ and the $[\text{CpRh}(\text{CO})]$ fragments to also undertake C-H activation with ethene and toluene,³¹⁹ further supports the case for electronic effects. The $[\text{CpRh}(\text{C}_2\text{H}_4)]$ fragment does not form a stable activation product, but does undergo H/D exchange at the alkene. A summary of the types of photochemical reactions which $\text{CpRh}(\text{C}_2\text{H}_4)_2$ undergoes is presented in Figure 6.1.

6.1.1 Context

As previously described, the fragments $[\text{CpRh}(\text{PR}_3)]$ and $[\text{CpRh}(\text{CO})]$ are capable of activating alkanes and arenes. However, these fragments do not lend themselves to use as catalysts, as the activation products ($\text{CpRh}(\text{PR}_3)(\text{CR}_3)\text{H}$ or $\text{CpRh}(\text{CO})(\text{CR}_3)\text{H}$) do not readily release PR_3 or CO to allow for further activation at the rhodium centre. Therefore, a more labile ligand, which provides similar electronic effects to the rhodium centre, is required.

Preliminary DFT studies carried out at York by Dr. Joaquín López-Serrano (personal communication, 2008), investigated the reactions between with the $[\text{CpRh}(\eta^2\text{-C}_2\text{H}_4)]$ and $[\text{Cp}^*\text{Rh}(\eta^2\text{-C}_2\text{H}_4)]$ fragments and benzene. While these materials were found to yield stable η^2 and phenyl hydride adducts, the barrier to their interconversion was very high. Hence the lack of apparent CH activation with $[\text{CpRh}(\eta^2\text{-C}_2\text{H}_4)]$. He also replaced the phosphine (PR_3) of $[\text{CpRh}(\text{PR}_3)]$ with an amine (NR_3). He now found that the formation of $\text{CpRh}(\text{NR}_3)(\text{aryl})\text{H}$ was feasible. Given the likely lability of the amine in such complexes we decided to explore whether $\text{CpRh}(\text{NR}_3)(\text{aryl})\text{H}$ provided a route to

$\text{CpRh}(\eta^2\text{-C}_2\text{H}_4)\text{Ph}(\text{H})$. Subsequent re-association of the amine may occur and be followed by reductive elimination, perhaps to yield a functionalised aromatic molecule e.g. ethylbenzene (Figure 6.3).

Figure 6.3 Proposed scheme of reactivity for the work covered in this chapter, based on DFT calculations

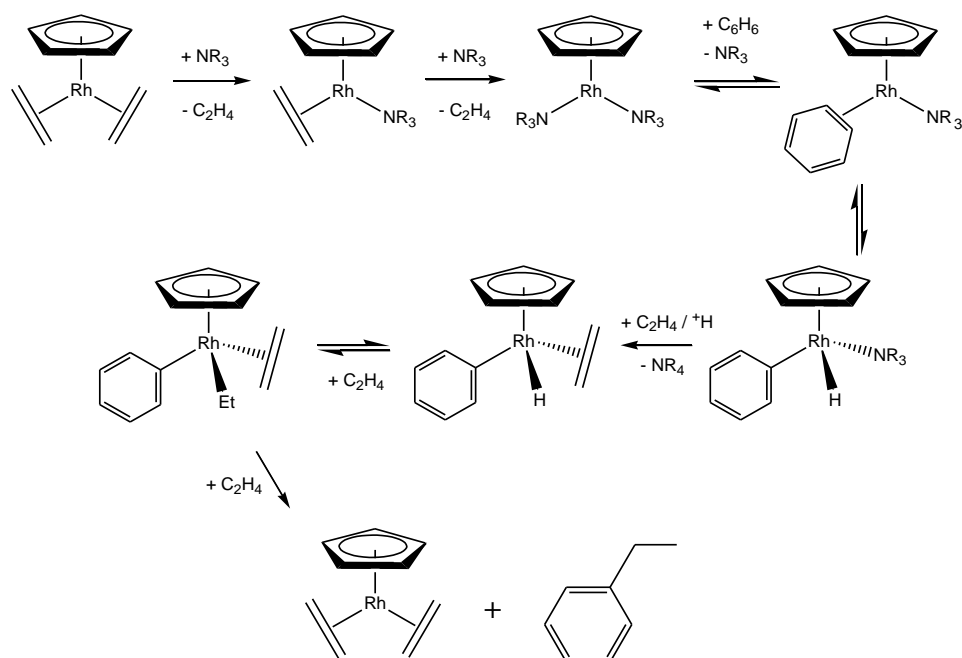
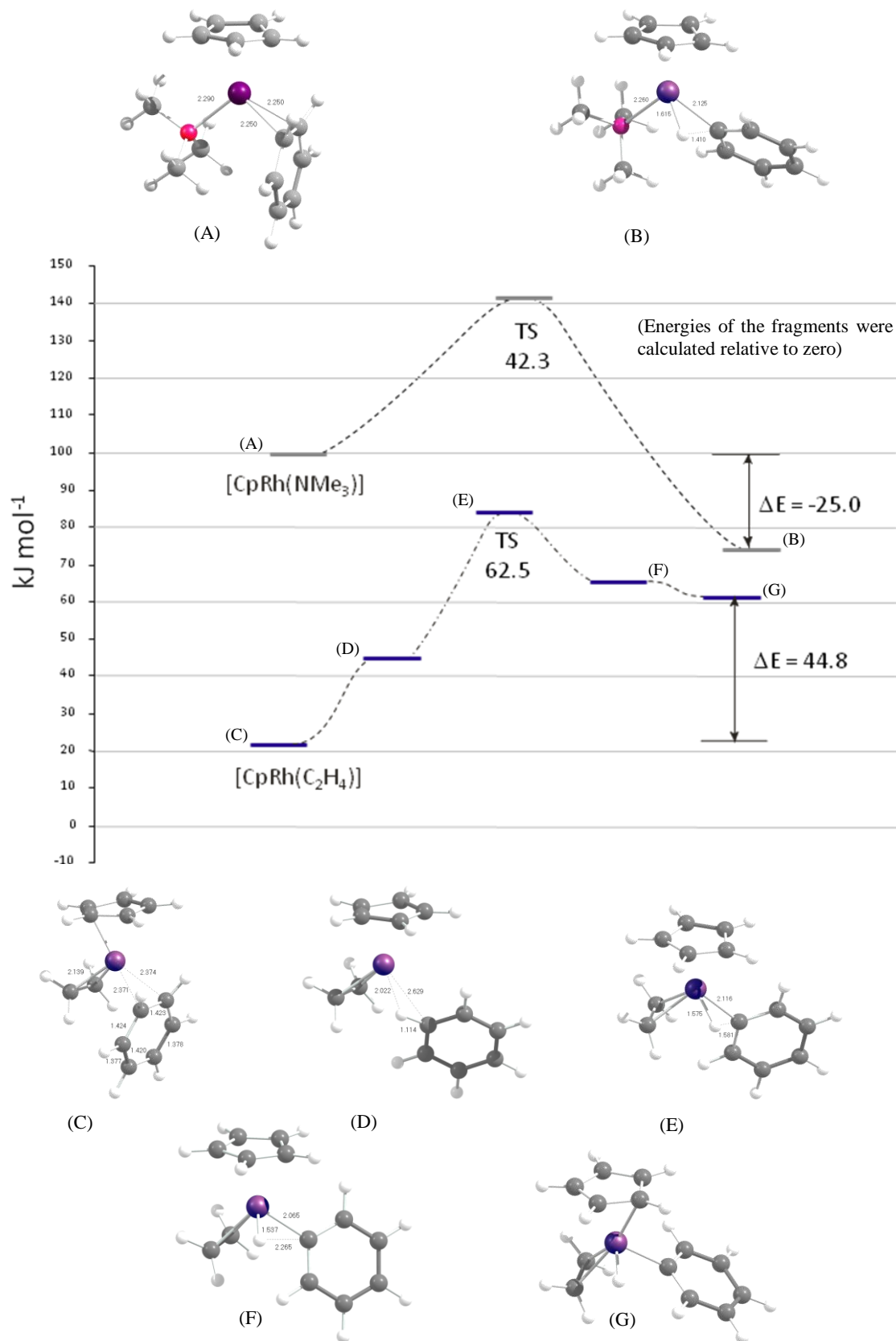


Figure 6.4 depicts the energy profiles for the reactions of the two fragments, $[\text{CpRh}(\text{NMe}_3)]$ and $[\text{CpRh}(\eta^2\text{-C}_2\text{H}_4)]$, with benzene. The pathway involving $[\text{CpRh}(\text{NMe}_3)]$ yields a more stable reaction product, which is lower in energy than $[\text{CpRh}(\text{NMe}_3)(\eta^2\text{-C}_6\text{H}_6)]$ by 25 kJ mol^{-1} . This indicates that this pathway is favourable, and therefore the products of this reaction are likely to be observable by low temperature NMR methods. The energy profile for the reaction of $[\text{CpRh}(\eta^2\text{-C}_2\text{H}_4)]$ leads to a C-H activated product which is less stable by 44.8 kJ mol^{-1} than $[\text{CpRh}(\eta^2\text{-C}_2\text{H}_4)(\eta^2\text{-C}_6\text{H}_6)]$. This suggests that the resulting complex, $\text{CpRh}(\eta^2\text{-C}_2\text{H}_4)\text{Ph}(\text{H})$, will be too unstable to be observed by low temperature NMR methods.

Figure 6.4 Energy profiles for the activation of benzene by $[\text{CpRh}(\text{C}_2\text{H}_4)]$ and $[\text{CpRh}(\text{NMe}_3)]$, calculated by Dr. Joaquín López-Serrano using DFT methods (original in colour)



6.2 Characterisation of $\text{CpRh}(\eta^2\text{-C}_2\text{H}_4)_2$

The complex, $\text{CpRh}(\eta^2\text{-C}_2\text{H}_4)_2$, was prepared in bulk according to the method reported by Cramer.³⁰⁶

Characterisation was carried out in d_8 -THF using 1D ^1H and $^{13}\text{C}\{^1\text{H}\}$ NMR techniques. A single peak was visible in the ^1H NMR spectrum corresponding to the protons of a cyclopentadienyl group at δ 4.78. Two further broad resonances were observed at δ 0.93 and 2.84. These peaks were observed to mutually couple through a ^1H COSY experiment. These resonances are consistent with the two inequivalent proton resonances of an η^2 bound ethene ligand attached to the rhodium centre in $\text{CpRh}(\eta^2\text{-C}_2\text{H}_4)_2$. The proton signals at δ 0.93 and 2.84 were found to integrate to four protons respectively, compared with the 5 proton intensity of the Cp resonance.

The signals of the upper and lower ethene protons are distinct because of the symmetry associated with the complex, and are broad because rotation allows their interconversion. This was confirmed through a $^1\text{H}/^{13}\text{C}$ HMQC measurement which linked both ^1H resonances, at δ 0.93 and 2.84, with a single ^{13}C resonance at δ 35.3. Based on these resonances the complex can be identified as $\text{CpRh}(\eta^2\text{-C}_2\text{H}_4)_2$. Table 6.1 presents the full NMR data for this complex.

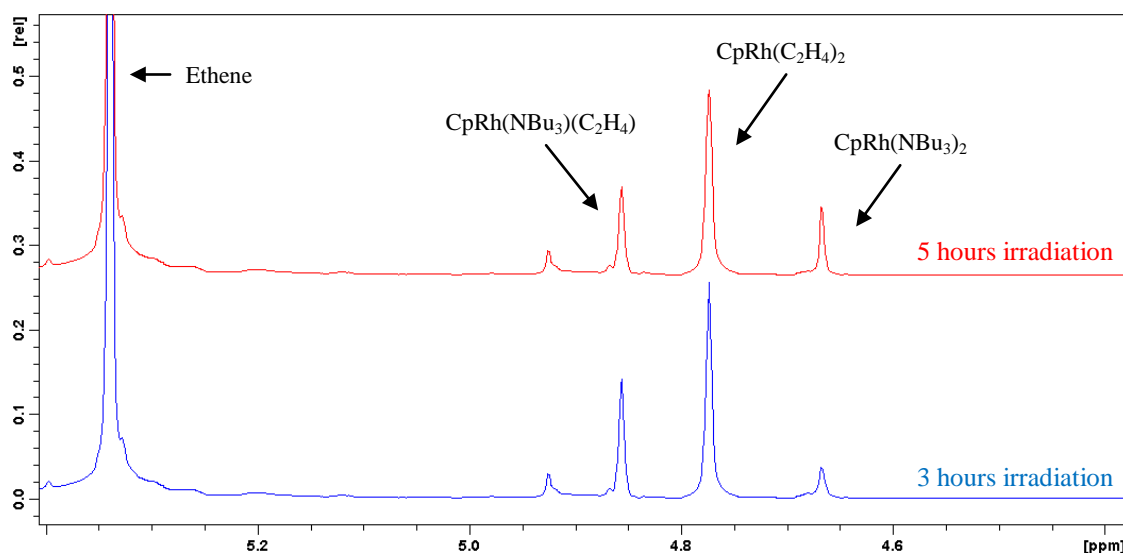
6.3 Photolysis reactions of $\text{CpRh}(\eta^2\text{-C}_2\text{H}_4)_2$ with tributylamine and tripentylamine

The mono and bis substituted amine forms ($\text{CpRh}(\text{C}_2\text{H}_4)\text{NR}_3$ and $\text{CpRh}(\text{NR}_3)_2$) do not appear in the literature and so attempts to characterise these unstable materials has been made. The characterisation of these structures will allow for easier characterisation of subsequent complexes formed through irradiation in the presence of benzene.

Two different amines have been used, tripentylamine and tributylamine, with each added in 10 μl quantities to two separate Young's tap fitted NMR tubes containing ~2 mg of $\text{CpRh}(\text{C}_2\text{H}_4)_2$, in d_8 -THF. The two samples were degassed and photolysed simultaneously for 2 hours at 233 K, using a broad-band UV lamp as an irradiation source.

A ^1H NMR spectrum of the tributylamine sample revealed a new peak at δ 5.34 corresponding to free ethene in solution.³²⁰ Two further peaks were found in the Cp region at δ 4.81 and 4.65 (<5% of the intensity of the starting material Cp resonance). The sample was photolysed a further three times for one hour, and the sample was checked by NMR in between each irradiation. Comparison of the ^1H NMR spectra show that the peak at δ 4.65 changed little over time, while the peak at δ 4.81 increased in size. This indicates that the Cp peak at δ 4.65 belongs to the bis substituted form, $\text{CpRh}(\text{NR}_3)_2$. The same sequence was repeated for the tripropylamine sample, and analogous Cp peaks were found at δ 4.86 and 4.65 for the mono and bis forms respectively.

Figure 6.5 ^1H NMR spectra showing the conversion of $\text{CpRh}(\text{NBu}_3)(\text{C}_2\text{H}_4)$ to $\text{CpRh}(\text{NBu}_3)_2$ (original in colour)



However, in each case full characterisation for the proton resonances of the alkyl portion of the amine could not be obtained owing to the high amount of free amine added, which overlaps with these new minor resonances. Attempts with less amine led to much lower amounts of product. This adds an additional challenge to the characterisation of these complexes, and ultimately means that the characterisation of the mono substituted form is unfeasible. However, for the bis substituted complex, full characterisation may in principle be obtained if the amine can be removed from the NMR tube *in vacuo*.

Preparing a sample with lower amine content (5 μ l and 2 μ l) in an attempt to observe the product peaks more clearly, compared to the free amine resonances, led to decreased conversion (indicated by barely noticeable cyclopentadienyl resonances). This suggests that when the concentration of amine is reduced, a competitive reverse reaction with the liberated ethene (which is dissolved in the solution, as evidenced by the ^1H NMR signal at δ 5.34) occurs – therefore poor conversion to the products is achieved.

The bis-complex itself is unstable and needs to be kept cold (below 223 K). There is also the possibility of a back reaction once the amine is removed. If all of the free ethene is not removed, it may be necessary to repeat cycles of add amine, photolyse and remove *in vacuo*, before full conversion of the sample to the bis form can be obtained. Starting with a sample of pure $\text{CpRh}(\text{NR}_3)_2$, would be a better starting material for further reactions, and possibly lead to easier characterisation of new products.

Two analogous samples were prepared as described previously for tributylamine and tripropylamine with $\text{CpRh}(\text{C}_2\text{H}_4)_2$. Each of the samples was irradiated for a period of 18 hours, in order to maximise conversion of the starting material to the products. Following irradiation of the sample, the ^1H NMR spectrum revealed little change in the intensity of the resonances, with the Cp proton resonance of $\text{CpRh}(\text{C}_2\text{H}_4)_2$ appearing in a greater excess compared to the minor (<5%) signals in each of the experiments which correspond to the bis-amine products. This lack of conversion for this experiment was unexpected, owing to the distinct colour change of the samples from a pale yellow to a deep (almost black) purple/brown. Upon allowing the sample to settle in an acetone/dry ice bath (193 K), a large amount of precipitate formed, presumably due to the instability of these products.

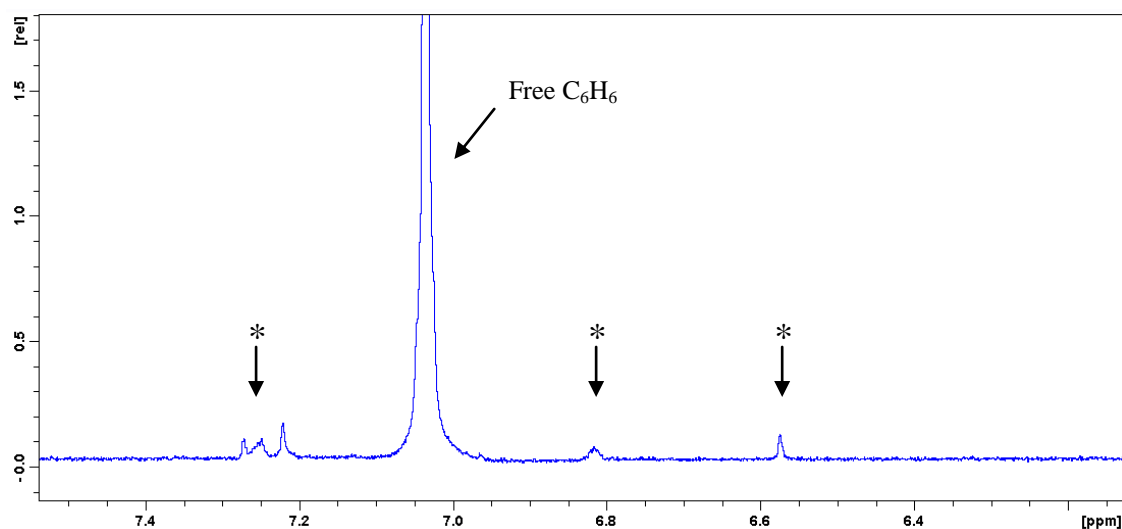
Replicates of the amine / $\text{CpRh}(\text{C}_2\text{H}_4)_2$ sample were made using d_6 -acetone and d_4 -methanol as solvents, to encourage solubility of the product amine complexes; however, the same precipitate was observed in each case. It is therefore unlikely that the full characterisation of these products is possible due to their inherent low stability.

6.3.1 Photolysis reactions of $\text{CpRh}(\eta^2\text{-C}_2\text{H}_4)_2$ with tributylamine and protio benzene

Even though the conversion of $\text{CpRh}(\text{C}_2\text{H}_4)_2$ to $\text{CpRh}(\text{NR}_3)_2$ and $\text{CpRh}(\text{NR}_3)(\text{C}_2\text{H}_4)$ was limited, a series of experiments aiming to form $\text{CpRh}(\text{NR}_3)(\text{Ph})\text{H}$ were undertaken.

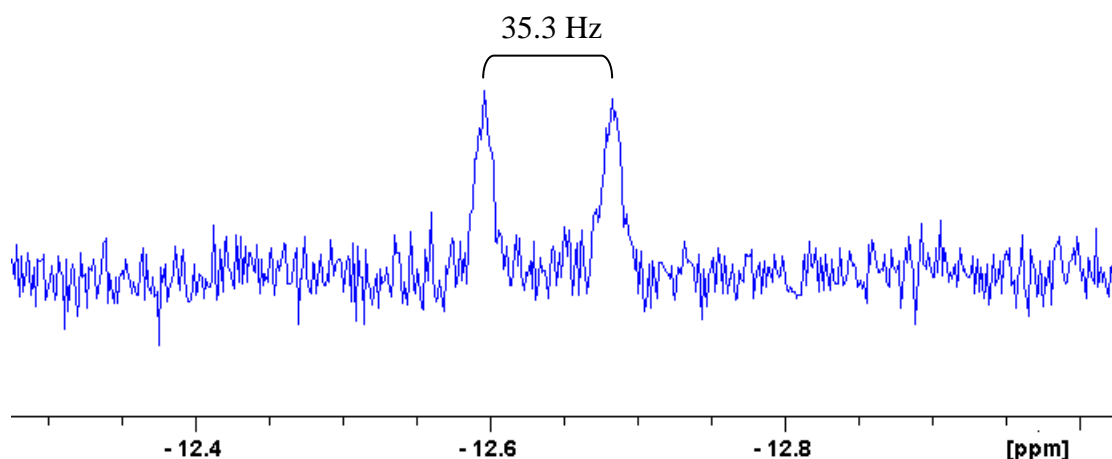
An NMR tube was therefore charged with $\text{CpRh}(\eta^2\text{-C}_2\text{H}_4)_2$ in $d_8\text{-THF}$, in addition to tributylamine and protio benzene. This sample was then degassed and stored under N_2 prior to being photolysed by a UV lamp for two hours at 233 K. The resulting ^1H NMR spectrum, recorded at 233 K, showed a doublet at δ -12.62 (Figure 6.7) thereby confirming the formation of a rhodium hydride complex. A Cp proton resonance was located at δ 4.98, which appeared in the ratio 5:1 based on this hydride signal. Several new proton signals were found, including those at δ 7.25, 6.81, and 6.58 (Figure 6.6) which are consistent with the aryl protons of a coordinated phenyl moiety. These assignments were confirmed by a ^1H COSY NMR spectrum which showed connections between each of these three signals. These data are therefore consistent with the detection of resonances in the fragment $\text{CpRh}(\text{Ph})\text{H}$. The signals for the free amine would mask those expected for a bound alkene in this sample.

Figure 6.6 ^1H NMR spectrum, focusing on the phenyl region



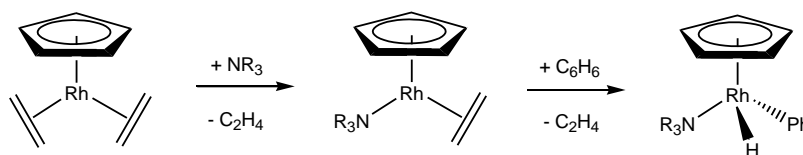
(* = proton peaks of the phenyl group; *ortho*, *meta* and *para*, respectively)

Figure 6.7 ^1H NMR spectrum focusing on the hydride doublet signal of $\text{CpRh}(\text{NBu}_3)(\text{Ph})\text{H}$

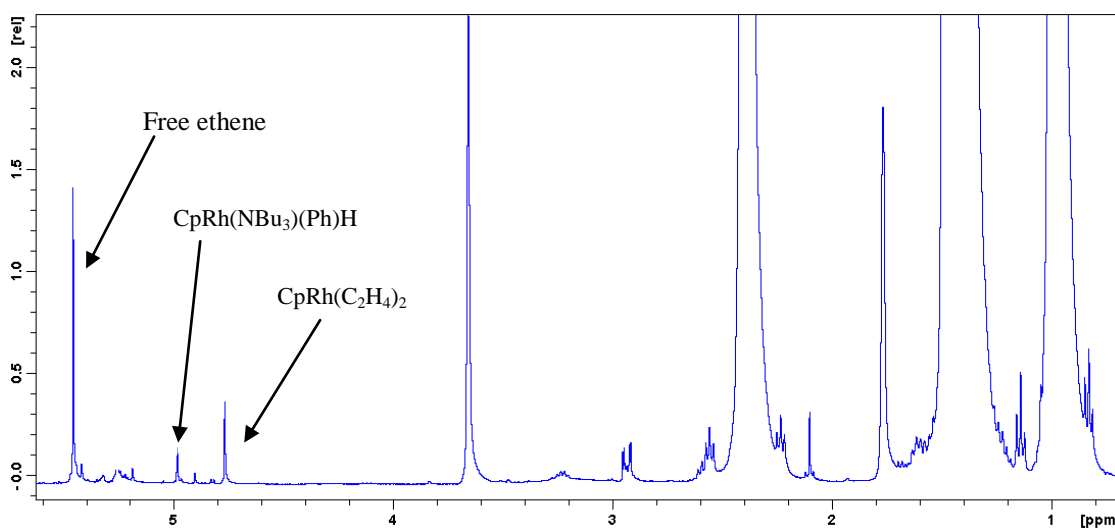


However, the presence of a new set of alkyl protons associated with a coordinated amine were found by $^1\text{H}/^{13}\text{C}$ HMQC NMR. Upon acquiring many scans, over a long time period, two small ^{13}C peaks were detected at δ 51.2 and 28.2 (which lie close to the ^{13}C carbon peaks of the free amine). The corresponding ^1H proton signals overlap with those of the free amine. Comparison of this NMR spectrum with those recorded for $\text{CpRh}(\text{C}_2\text{H}_4)_2$ and the amine show no sign of these peaks (hence no integration of these proton peaks could be achieved), therefore they are attributed as part of $\text{CpRh}(\text{NBu}_3)(\text{Ph})\text{H}$. The NMR characterisation data obtained for this complex is presented in Table 6.2. Similar results were obtained using the tripropylamine analogue (see Table 6.3 for NMR characterisation data).

Figure 6.8 General conditions for the C-H activation of benzene by this system

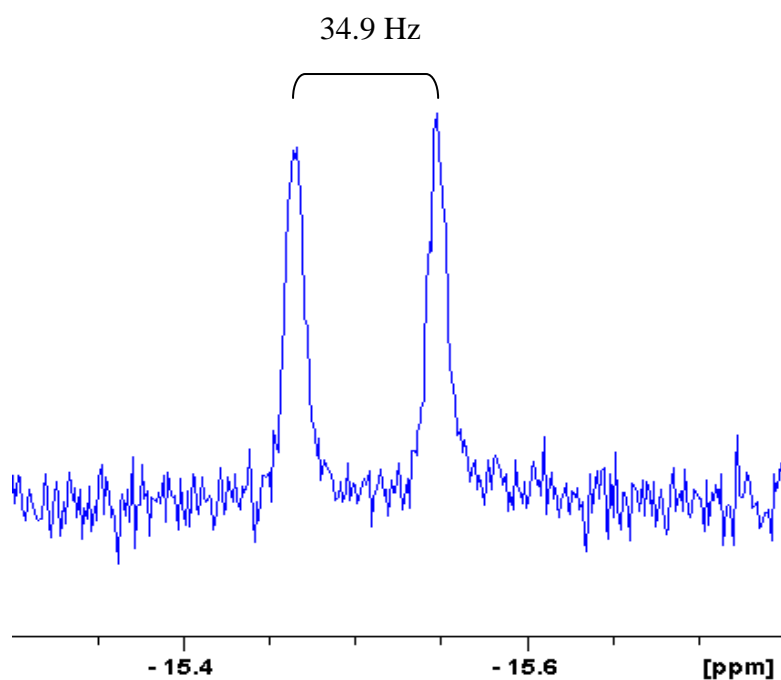


General conditions: Broadband UV photolysis at 233 K in d_8 -THF

Figure 6.9 ^1H NMR spectrum showing the product signals and free amine peaks

The complexity of the NMR spectrum is depicted by Figure 6.9, which illustrated the large intensity peaks of the free amine. This quantity of amine is required in order to achieve adequate conversion to the products, to enable characterisation by NMR. However, peaks of this intensity overlap some of the signals relating to the products, making characterisation of these products a challenge.

This experiment was then repeated, but the ratio of reactants changed to 1:1 ($\text{CpRh}(\eta^2\text{-C}_2\text{H}_4)_2$: tributylamine : benzene). After two lots of 12 hours of UV photolysis at 233 K (prolonged photolysis was required owing to the low amine content of the sample), a second minor hydride resonance (compared with the first experiment) was observed at δ -15.5 (doublet, 34.9 Hz) as shown in Figure 6.10. Owing to the large intensity of free ethene (indicated by the large resonance at δ 5.34) it is possible that the dissolved ethene within the solution displaces the amine ligand bound to the rhodium centre, forming the complex $\text{CpRh}(\eta^2\text{-C}_2\text{H}_4)(\text{Ph})\text{H}$. In order to lend further support to this assertion, the experiment was repeated and irradiated over the same 12 hour period. However, with this experiment the ethene was removed by quenching with hydrogen and pumping on the sample tube using a high-vacuum line, at regular intervals. The ^1H NMR spectrum following the 12 hour irradiation still showed the presence of this new doublet hydride resonance; however, the intensity of the signal is reduced compared to the previous example. This suggests that the removal of the majority of the liberated ethene affects the formation of this product.

Figure 6.10 ^1H NMR of hydride region

Another possible identity for this complex is $\text{CpRh}(\eta^2\text{-C}_2\text{H}_4)(\text{H})_2$. However, this assignment may be discounted when comparing the obtained ^1H NMR signals with those previously reported in the literature for $\text{CpRh}(\eta^2\text{-C}_2\text{H}_4)(\text{H})_2$.³¹⁵

As described in section 6.1.1, the formation of this product would be unfavorable from a thermodynamic perspective, owing to the increased energy of $\text{CpRh}(\eta^2\text{-C}_2\text{H}_4)\text{Ph}(\text{H})$ compared with $\text{CpRh}(\eta^2\text{-C}_2\text{H}_4)(\eta^2\text{-C}_6\text{H}_6)$ ($\Delta E = 44.8 \text{ kJ mol}^{-1}$). However, based on the barrier to interconversion between $\text{CpRh}(\eta^2\text{-C}_2\text{H}_4)(\eta^2\text{-C}_6\text{H}_6)$ and $\text{CpRh}(\eta^2\text{-C}_2\text{H}_4)\text{Ph}(\text{H})$ (as depicted previously in Figure 6.4), it is feasible that $\text{CpRh}(\eta^2\text{-C}_2\text{H}_4)\text{Ph}(\text{H})$ is formed as the kinetic product of the reaction. This is due to the relatively small energy difference between $\text{CpRh}(\eta^2\text{-C}_2\text{H}_4)\text{Ph}(\text{H})$ and the transition state (TS), compared to the larger energy difference for the TS and $\text{CpRh}(\eta^2\text{-C}_2\text{H}_4)(\eta^2\text{-C}_6\text{H}_6)$; the back-reaction. The barrier to interconversion hence leads to the appreciable conversion to $\text{CpRh}(\eta^2\text{-C}_2\text{H}_4)\text{Ph}(\text{H})$, which allows for the proton signals of this complex to be observed in the recorded ^1H NMR spectrum.

6.3.2 Photolysis reactions of $\text{CpRh}(\eta^2\text{-C}_2\text{H}_4)_2$ with tributylamine and d_6 -benzene

To check if the formed hydride was due to the oxidative addition of benzene or an intramolecular interaction with a butyl chain of the amine (hydride transfer), a second experiment using 4 mg and tributylamine (4 μl) was carried out in d_8 -THF with d_6 -benzene. The sample was photolysed (at 233 K) for a total of two hours – checked by low temperature NMR at 233 K at half-hour intervals. No hydride signals were visible thereby confirming that both of the detected hydride signals originate in benzene. It should be noted that signals consistent with $\text{CpRh}(\text{NBu}_3)(\text{Ph})\text{H}$ were found in approximately the same positions (consistent with the slight variations in chemical shift expected from deuteration). This supports the formation of $\text{CpRh}(\text{NBu}_3)(\text{Ph})\text{D}$, which would not generate a hydride signal.

6.3.3 Photolysis reactions of $\text{CpRh}(\eta^2\text{-C}_2\text{H}_4)_2$ with triethylamine and benzene

Owing to the difficulty in obtaining complete spectra for the amine complexes, an analogous procedure to the one listed in section 6.3.1 was employed for the simpler amine compound, NEt_3 . It was envisioned that the two sets of ^1H peaks associated with the free amine would obscure less of the ^1H spectrum (hence cleaner spectra), and therefore allow peaks of interest to be viewed more clearly.

Following irradiation of the sample at low temperature (233 K) the sample was subject to investigation by ^1H , $^{13}\text{C}\{^1\text{H}\}$, ^1H COSY, $^1\text{H}/^{13}\text{C}$ HMQC and NOESY NMR techniques. Similar results were obtained to those previously, the NMR confirmed that the activated product $\text{CpRh}(\text{NEt}_3)(\text{Ph})\text{H}$ had been formed, and that all the peaks were accounted for owing to the short alkyl chain length of the amine (see Table 6.4 for NMR characterisation data). Despite the use of a simpler amine, the peaks in the 3 – 0 range of the ^1H NMR were overlapped by the large, broad signals for the free amine. As discussed earlier, the challenge associated with the characterisation of these complexes is to achieve a significant conversion to the product – which requires large excesses of amine. These amine peaks overlap with the ^1H signals for the coordinated amine moieties, and therefore obscures the detail of these peaks (e.g. multiplicity and coupling constants). Though the use of this amine does improve the ability to characterise the

products to a greater extent, the inherent problems of the large excess of amine / low conversion to the products, prove to cause difficulties when studying these reactions.

6.4 Conclusion

The results obtained in this chapter show that the fragment, $[\text{CpRh}(\text{NR}_3)]$, is capable of the C-H activation of an arene, in accordance with the DFT predictions. The experiments conducted here show that the presence of the hydride is a direct result of the activation of benzene by the fragment (and not by hydride transfer from the alkyl chains of the amine). Furthermore, no hydride signals were produced when $\text{CpRh}(\text{C}_2\text{H}_4)_2$ was irradiated with an amine in d_8 -THF, in the absence of benzene.

The NMR spectra recorded during the photochemical reactions of $\text{CpRh}(\text{C}_2\text{H}_4)_2$ with amine also suggest that both the mono- and bis- substituted complexes $\text{CpRh}(\text{C}_2\text{H}_4)\text{NR}_3$ and $\text{CpRh}(\text{NR}_3)_2$, are formed. Full characterisation of these complexes could not be achieved, owing to their low stability. Varying the reaction solvent and the amine concentration did little to enhance their stability, and failed to enable their full characterisation. This shows the challenge associated with the characterisation of these compounds.

Prolonged photolysis samples with low amine concentrations and large benzene excesses led to the suspected formation of $\text{CpRh}(\text{C}_2\text{H}_4)(\text{Ph})\text{H}$. We note, the intensity of the liberated ethene peak follows the intensity of the corresponding hydride signal. These reactions were extremely hard to undertake due to the very low stability of the detected products. They do however serve to illustrate the power of this photochemical approach.

6.5 Characterisation data


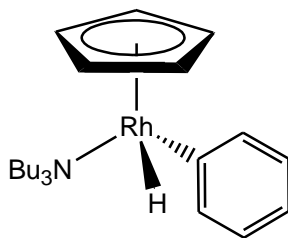
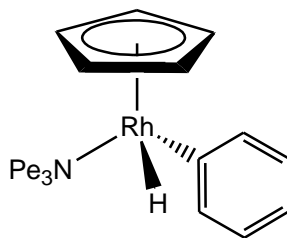
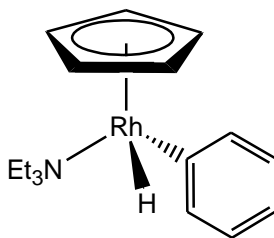
Table 6.1 NMR data for $\text{CpRh}(\text{C}_2\text{H}_4)_2$		
		
In d_8 - THF at 198 K	δ / ppm (multiplicity, integration)	Assignment
^1H	0.93 (br, 4) 2.84 (br, 4) 4.78 (s, 5)	H_a H_b C_5H_5
^{13}C	35.3 (s) 86.6 (s)	C_5H_5 C_2H_4

Table 6.2 NMR data for $CpRh(NBu_3)(Ph)H$ 

In d_8 - THF at 198 K	δ / ppm (multiplicity, integration)	Assignment	Coupling constant / Hz	Assignment
^1H	-12.62 (d) 1.21 (m) 2.28 (m) 4.98 (s) 6.81 (m) 7.25 (m)	Rh-<i>H</i> N(CH ₂ <i>H</i> ₂ CH ₂ CH ₃) ₃ N(<i>H</i> CH ₂ (CH ₂) ₂ CH ₃) ₃ C₅<i>H</i>₅ <i>Meta</i> -C ₆ <i>H</i> ₅ <i>Ortho</i> -C ₆ <i>H</i> ₅	35.3	$ ^1J_{\text{RhH}} $
^{13}C	28.2 (s) 51.2 (s) 81.5 (s) 124.2 (s) 129.4 (s)	N(CH ₂ CH ₂ CH ₂ CH ₃) ₃ N(CH ₂ (CH ₂) ₂ CH ₃) ₃ C₅<i>H</i>₅ <i>Meta</i> -C ₆ <i>H</i> ₅ <i>Ortho</i> -C ₆ <i>H</i> ₅		

Table 6.3 NMR data for $CpRh(NPe_3)(Ph)H$ 

In d_8 - THF at 198 K	δ / ppm (multiplicity, integration)	Assignment	Coupling constant / Hz	Assignment
^1H	-12.78 (d) 1.27 (m) 2.34 (m) 4.93 (s) 6.79 (m) 7.49 (m)	Rh- H N(CH ₂ CH ₂ (CH ₂) ₂ CH ₃) ₃ N(CH ₂ (CH ₂) ₃ CH ₃) ₃ C₅H₅ <i>Meta</i> -C ₆ H₅ <i>Ortho</i> -C ₆ H₅	35.7	$ ^1J_{\text{RhH}} $
^{13}C	28.9 (s) 54.2 (s) 82.1 (s) 123.1 (s) 128.8 (s)	N(CH ₂ CH ₂ (CH ₂) ₂ CH ₃) ₃ N(CH ₂ (CH ₂) ₃ CH ₃) ₃ C₅H₅ <i>Meta</i> -C ₆ H₅ <i>Ortho</i> -C ₆ H₅		

Table 6.4 NMR data for $\text{CpRh}(\text{NEt}_3)(\text{Ph})\text{H}$ 

In d_8 - THF at 198 K	δ / ppm (multiplicity, integration)	Assignment	Coupling constant / Hz	Assignment
^1H	-12.53 (d) 0.96 (m) 2.38 & 2.43 (m) 4.92 (s) 6.84 (m) 7.55 (m)	Rh-H $\text{N}(\text{CH}_2\text{CH}_3)_3$ $\text{N}(\text{CH}_2\text{CH}_3)_3$ C_5H_5 <i>Meta</i> - C_6H_5 <i>Ortho</i> - C_6H_5	34.8 7.0 7.0	$ \text{}^1\text{J}_{\text{RhH}} $ $ \text{}^3\text{J}_{\text{HH}} $ $ \text{}^3\text{J}_{\text{HH}} $
^{13}C	12.6 (s) 47.3 (s) 81.3 (s) 122.4 (s) 128.6 (s)	$\text{N}(\text{CH}_2\text{CH}_3)_3$ $\text{N}(\text{CH}_2\text{CH}_3)_3$ C_5H_5 <i>Meta</i> - C_6H_5 <i>Ortho</i> - C_6H_5		

Chapter 7

Experimental Methods

7.1 General experimental

7.1.1 Solvents. Reagents and equipment

Deuterated NMR solvents (d_6 -benzene, d_8 -toluene, d_8 -THF and d_{12} -cyclohexane) were purchased from Sigma-Aldrich and dried over potassium, under vacuum, in ampoules. Analytical / reagent grade solvents (ethanol, acetone, dibutyl ether) were obtained from Fisher Scientific and used without further purification. Toluene, diethyl ether, THF and cyclohexane were dried over sodium and distilled under nitrogen prior to storage in flame-dried ampoules.

Ruthenium trichloride, triruthenium dodecacarbonyl and rhodium trichloride were purchased from Johnson-Matthey.

Ethene, carbon monoxide, hydrogen, nitrogen and liquid nitrogen were supplied by BOC gases.

All other reagents referred to within this section were purchased from Sigma-Aldrich, and used without further purification

Throughout this work, photochemical studies (in the UV range) were carried out using either a Oriel 200 W Hg-Xe arc lamp or a Kimmon 63 mW He-Cd LASER (operating at 325 nm). This equipment is discussed in further detail in section 7.3, of this chapter.

7.1.2 NMR spectroscopy

NMR data was collected using a Bruker DRX 400, DMX 400 (^1H 400.13 MHz, ^{13}C 100.62 MHz, ^{31}P 162 MHz, ^{29}Si 79.49 MHz) or an AV 700 (^1H 700.13 MHz, ^{13}C 176.05 MHz, ^{31}P 283.46 MHz) spectrometers. The resonances of the acquired ^1H NMR spectra were referenced to the residual proton signals of the deuterated solvents ³²¹: benzene δ 7.15, toluene δ 2.09, THF δ 3.58, cyclohexane δ 1.38, acetone δ 2.05. ^{13}C NMR spectra were referenced to the signals corresponding to the solvent peaks: benzene δ 128.39, toluene δ 20.40, THF δ 25.37, cyclohexane δ 26.43, acetone δ 29.92. ^{31}P resonances were referenced to free PPh_3 , which was set to δ 7.1, and ^{29}Si signals were referenced to external TMS, at δ 0. The Topspin 1.3 software environment was used to record and process the NMR spectra.

Standard pulse sequences were used to obtain 1D ^1H , $^{31}\text{P}\{^1\text{H}\}$, $^{13}\text{C}\{^1\text{H}\}$, $^{29}\text{Si}\{^1\text{H}\}$, ^1H COSY, $^1\text{H}/^{31}\text{P}$ HMQC, $^1\text{H}/^{13}\text{C}$ HMQC and $^1\text{H}/^{29}\text{Si}$ HMQC data. ³²² For 1D selective NOE and 2D NOE experiments, the pulse sequences were used as reported in the literature. ³²³⁻³²⁵

7.1.2.1 NMR sample preparation

All NMR tubes were charged with 5 mg (unless otherwise stated) of the respective compound under test, and degassed using a high vacuum line prior to transferring to the glovebox (MBRAUN Unilab). Where possible, dried / degassed reagents were added to the NMR tube in the glove box (usually by 10 μl syringe in the case of liquid substrates), and the sample depth was then made up to a depth of 4 cm using the relevant deuterated solvent. The samples were then brought out of the glovebox and degassed using freeze/thaw methods, to place the sample under vacuum. Prior to lowering the temperature, samples were checked via 1D ^1H and $^{31}\text{P}\{^1\text{H}\}$ NMR methods at 298 K.

7.1.3 Mass spectrometry

Mass spectrometry was conducted using a Bruker-Daltonics Esquire 6000. Fragmentation of the samples was carried out using the ESI method, with ruthenium containing complexes being identified by the characteristic isotope pattern of ruthenium. GC/MS experiments were run using a Varian 3800 gas chromatograph coupled to a Varian Saturn GC/MS 2000.

Figures 7.1, and 7.2 depict sample spectra obtained for $\text{CpRu}(\text{PPh}_3)(\eta^3\text{-Si}(\text{Me})_2\text{C}_2\text{H}_3)$ and $\text{CpRu}(\text{PPh}_3)_2(\text{Si}(\text{Me})_2\text{C}_2\text{H}_3)$ (Chapter 5, section 5.2), and $\text{CpRu}(\text{}^t\text{BuNC})_2\text{Cl}$ (Chapter 1, section 2.4.3.3).

Figure 7.1 Mass spectrum obtained for the sample containing $\text{CpRu}(\text{PPh}_3)(\eta^3\text{-Si}(\text{Me})_2\text{C}_2\text{H}_3)$ and $\text{CpRu}(\text{PPh}_3)_2(\text{Si}(\text{Me})_2\text{C}_2\text{H}_3)$

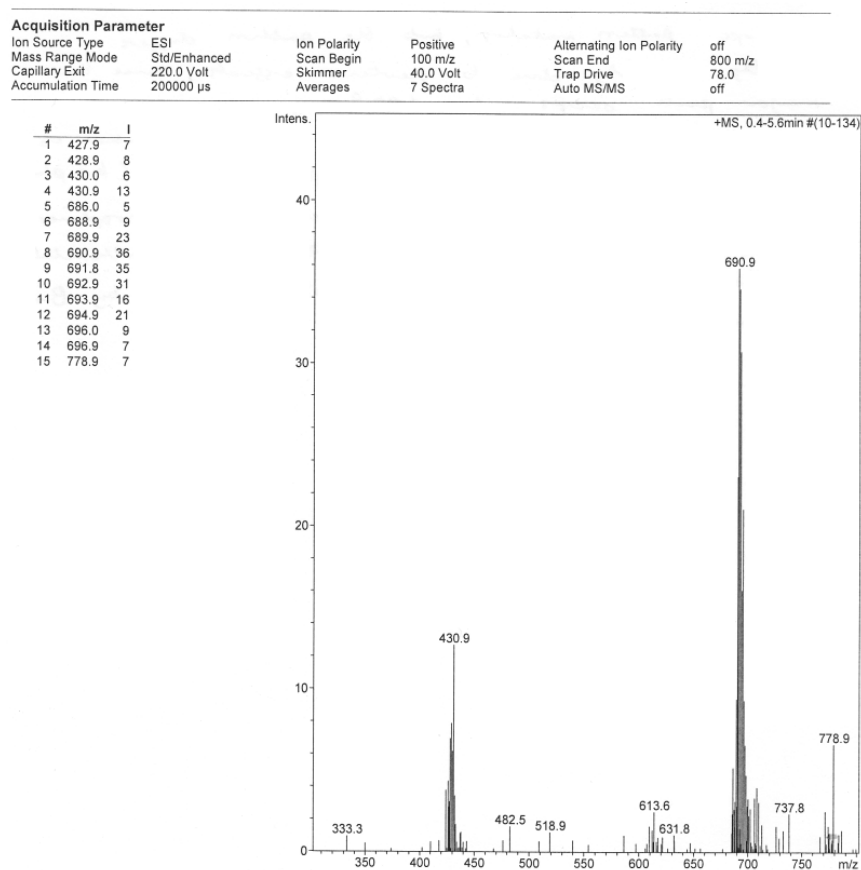
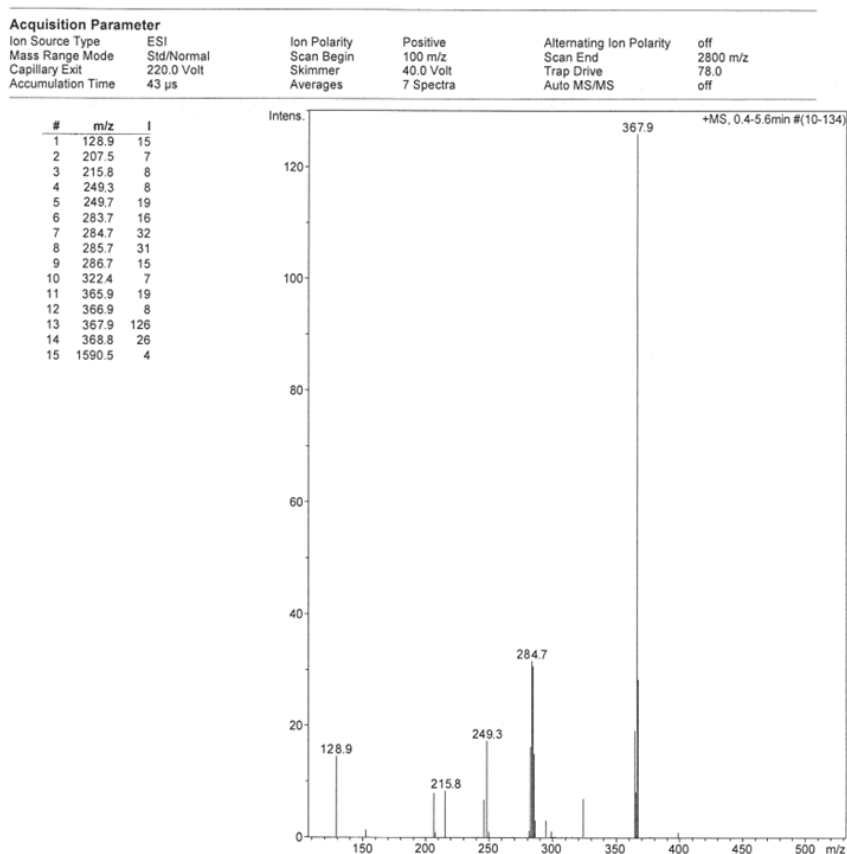


Figure 7.2 Mass spectrum obtained for the sample containing $\text{CpRu}(\text{CNBu}^i)_2\text{Cl}$ 

7.1.4 UV spectroscopy

UV spectra were recorded on a Jenway 6705 UV-Vis spectrophotometer, using quartz cuvettes.

7.1.5 Infrared spectroscopy

Infrared spectra were collected on a Perkin-Elmer Paragon 1000 FT-IR spectrometer, using NaCl plates.

Figures 7.3, 7.4 and 7.5 depict sample spectra for $\text{CpRu}(\text{PPh}_3)(\text{H})_3$ (Chapter 3, section 3.4.9.2), $\text{CpRu}(\text{PPh}_3)(\text{CO})(\text{CH}_2\text{-CH=CH}_2)$ (Chapter 5, section 5.4.5.2), and $\text{CpRu}(\text{PPh}_3)(\text{CO})\text{Me}$ (Chapter 3, section 3.4.3).

Figure 7.3 IR spectrum for $\text{CpRu}(\text{PPh}_3)(\text{H})_3$ – not isolated, contains residual $\text{CpRu}(\text{PPh}_3)_2\text{H}$, $\text{Ru}(\text{PPh}_3)_4(\text{H})_2$ and benzene

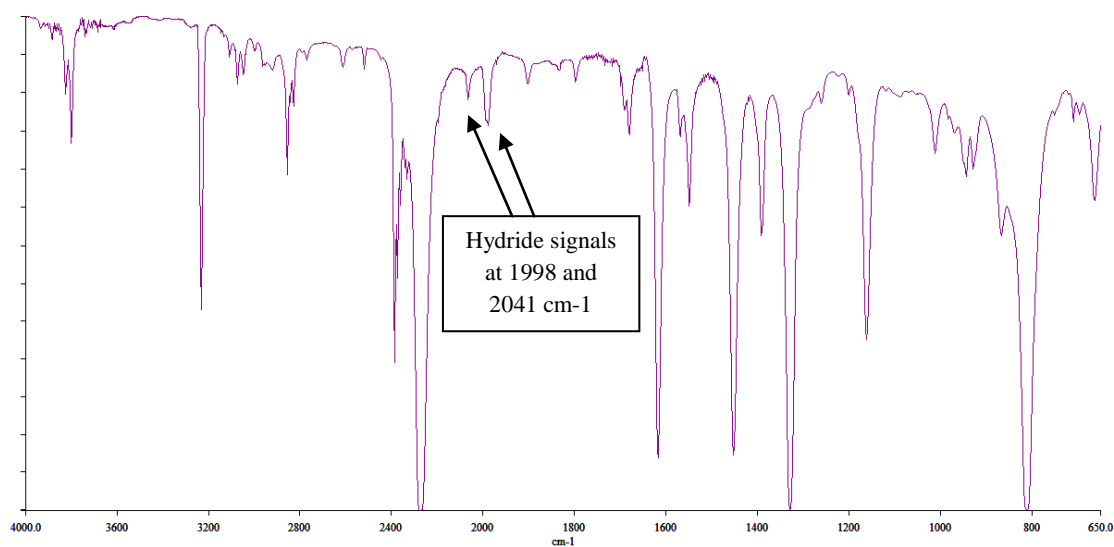


Figure 7.4 IR spectrum for $\text{CpRu}(\text{PPh}_3)(\text{CO})(\text{CH}_2\text{-CH=CH}_2)$ with residual THF

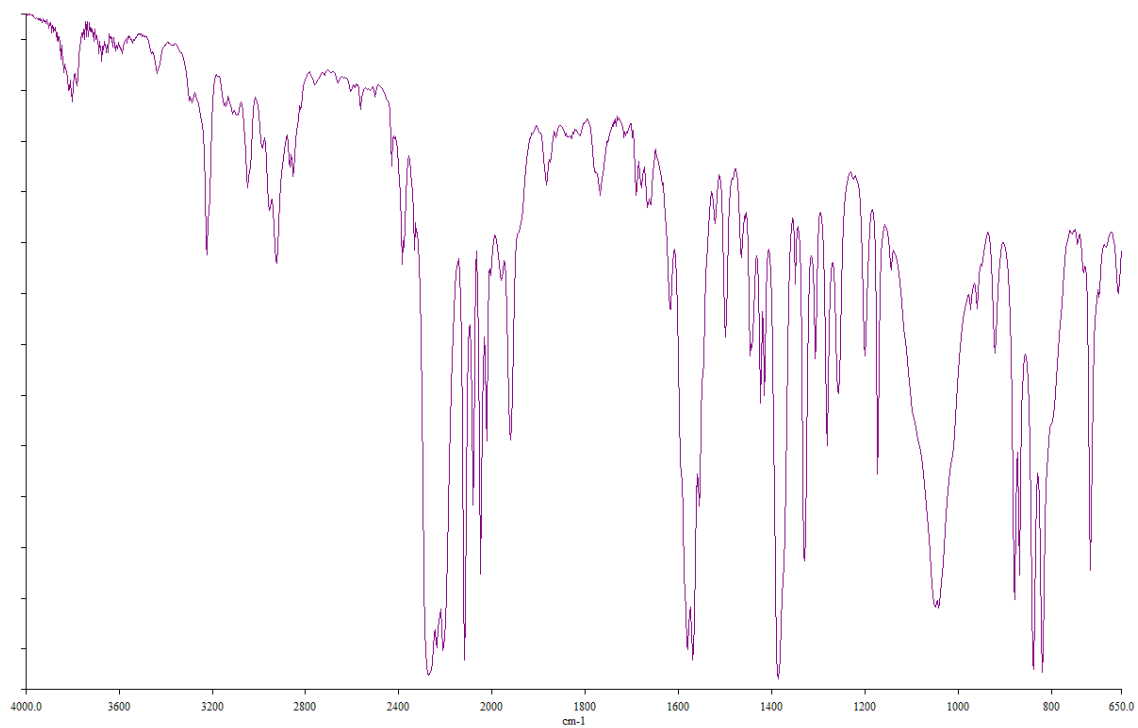
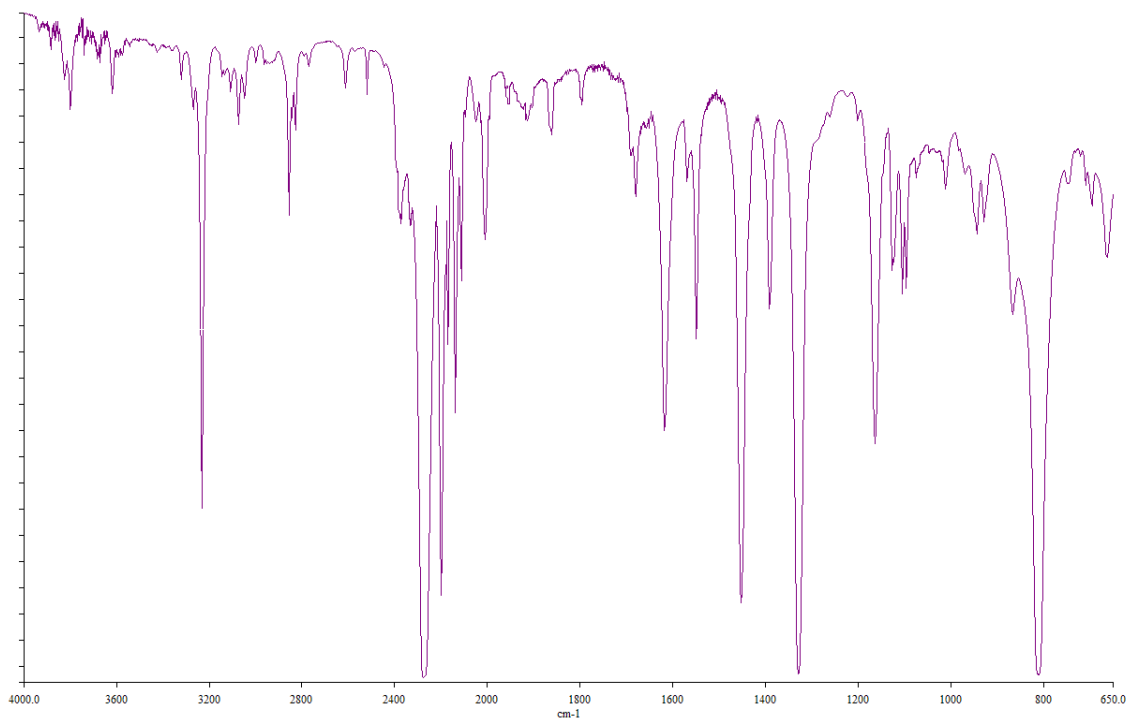


Figure 7.5 IR spectrum for $\text{CpRu}(\text{PPh}_3)(\text{CO})\text{Me}$ with residual benzene

7.2 Synthesis of starting complexes / reactions

7.2.1 Methods for Chapter 2

7.2.1.1 Preparation of $\text{CpRu}(\text{PPh}_3)_2\text{Cl}$ ³²⁶

To a 250 ml three-necked round-bottomed flask, fitted with a condenser and dropping funnel, 2.79 g of PPh_3 was added and dissolved in 200 ml of dry, degassed, ethanol. The PPh_3 solution was heated at reflux for 30 minutes under nitrogen. To a second flask, 100 ml two-necked and fitted with a condenser, 0.52 g (2.51×10^{-3} mol) of RuCl_3 was added and dissolved in 40 ml of dry and degassed ethanol – then refluxed for 30 minutes under nitrogen. The RuCl_3 solution was cooled on ice whilst maintaining stirring, and was followed by the dropwise addition of 2 ml of freshly cracked cyclopentadiene (fractionally distilled from dicyclopentadiene). The RuCl_3 solution was then transferred to the dropping funnel and slowly added to the stirring, and still under reflux, PPh_3 solution. At the end of the addition the solution remains deep brown in colour (almost black). This colour persists for half an hour before gradually beginning to lighten to a light brown/orange, and is then followed by a swift change to a deep red solution. Filtration

of the solution yields a bright orange solid ($\text{CpRu}(\text{PPh}_3)_2\text{Cl}$) which is pure enough for subsequent reactions (96% yield). Full NMR characterisation data for this complex appears in Chapter 2, Table 2.1.

7.2.1.2 Reactions of $\text{CpRu}(\text{PPh}_3)_2\text{Cl}$

Seven NMR tubes were prepared as described earlier containing d_8 -toluene and $\text{CpRu}(\text{PPh}_3)_2\text{Cl}$. For three of the tubes, liquid substrates (PEt_3 , HSiEt_3 and ${}^t\text{BuNC}$) were added in the quantities listed in Table 7.1. Following the addition of these reagents, the samples were degassed using an acetone ice bath and a high vacuum line. The same procedure was followed for the solid naphthalene substrate. For the reactions involving the gases CO and H_2 the samples were degassed using an acetone ice bath and a high vacuum line, in each case the sample tubes were then pressurised to 1.5 bar with either of the two gases.

Each of the samples were then heated for one day at 323 K, using a silicone oil bath as a heat source. The samples were then characterised using NMR techniques, prior to heating to 353 K for a further day, in order to monitor the progress of the reaction.

Table 7.1 Quantities of reagents used in the thermal and photochemical reactions with $\text{CpRu}(\text{PPh}_3)_2\text{Cl}$

Reagent	moles	Quantity
PEt_3	6.788×10^{-5}	10 μl
${}^t\text{BuNC}$	6.265×10^{-5}	6 μl
HSiEt_3	6.270×10^{-5}	10 μl
naphthalene	6.242×10^{-5}	8 mg

Analogous samples were prepared (according to the reagent quantities listed in Table 7.1) for photochemical reactions. The samples were irradiated using the *ex situ* photolysis set-up (described in section 7.3.3) prior to characterisation of the formed products using NMR techniques.

The reactions involving ethene and naphthalene were found to be unreactive using thermal and room temperature photolysis techniques. The samples were then irradiated using the low temperature in situ set-up method described in section 7.3.2, in order to initiate a reaction.

7.2.1.3 Preparation of $\text{CpRu}(\text{PEt}_3)_2\text{Cl}$

To a 100 ml two-necked round bottomed flask, fitted with a condenser, 0.052 g (2.51×10^{-4} mol) of RuCl_3 was added and dissolved in 25 ml of dry and degassed ethanol – then refluxed for 30 minutes under nitrogen. The RuCl_3 solution was cooled on ice whilst maintaining stirring, and was followed by the dropwise addition of 0.1 ml of freshly cracked cyclopentadiene (fractionally distilled from dicyclopentadiene). An excess of PEt_3 (0.7 ml) was added dropwise to the solution with continued stirring, and still under reflux. Filtration of the solution yields a yellow / orange solid ($\text{CpRu}(\text{PEt}_3)_2\text{Cl}$, yield 88%).

7.2.1.4 Preparation of $\text{CpRu}(\text{PPh}_3)(\text{CO})\text{Cl}$

A 0.2 g (2.754×10^{-4} mol) sample of $\text{CpRu}(\text{PPh}_3)_2\text{Cl}$ was dissolved in 60 ml of toluene in a Schlenk tube. A 250 ml round-bottomed flask was fitted to the top of the schlenk tube, and the vessel was degassed and re-pressurised to 1.5 bar with CO. The solution was stirred, and irradiated using the Hg-Xe arc UV lamp. At regular intervals the CO supply was replenished. After 14 hours of photolysis, the toluene was removed *in vacuo*, and the product, $\text{CpRu}(\text{PPh}_3)(\text{CO})\text{Cl}$ (stoichiometric conversion was achieved), was then recrystallised using methanol. A yield of 94% of the recrystallised $\text{CpRu}(\text{PPh}_3)(\text{CO})\text{Cl}$ was obtained.

7.2.1.5 Preparation of $CpRu(CNBu^t)_2Cl$

A 50 ml round-bottomed flask (fitted with a condenser) containing $RuCl_3$ (0.051 g, 2.46×10^{-4} mol), in 25 ml ethanol, was heated to 358 K until the solute had fully dissolved. Freshly cracked cyclopentadiene added dropwise (0.1 ml) heating of the solution was continued for half hour under stirring. tBuNC (0.1 ml) was then added dropwise to the flask. The solution was observed to change from deep red to bright yellow over the course of 15 minutes. The solution was left to react under N_2 with stirring at 358 K for further to ensure complete conversion was achieved. The resulting solution was transferred by cannula to a small Schlenk tube, where the excess tBuNC and ethanol were removed *in vacuo*, to yield a pale yellow solid (yield = 88 %), which was found to be pure by 1H and $^{13}C\{^1H\}$ NMR.

7.2.2 Methods for Chapter 3

7.2.2.1 Preparation of $CpRu(PPh_3)_2Me$ ³²⁷

To a Schlenk tube, 0.35 g (4.820×10^{-4} mol) of $CpRu(PPh_3)_2Cl$ was added and thoroughly degassed and placed under nitrogen. To this, 50 ml of dry and degassed toluene was added; the solution was stirred until all of the complex had dissolved. Approximately 6 ml of methyllithium (1.6 mol, in ether) was added dropwise, causing the solution to become more viscous and slightly lighter in colour. After 20 minutes the solution became less viscous, and was left to stir for a further 4 hours. The remaining methyllithium was quenched using degassed water. The organic layer was recovered and dried over magnesium sulphate. Volatiles were removed *in vacuo* to yield a light yellow solid which was confirmed to be pure by 1H and $^{31}P\{^1H\}$ NMR. A yield of 92% of $CpRu(PPh_3)_2Me$ was obtained.

7.2.2.2 Preparation of $\text{CpRu}(\kappa^2\text{-2-C}_6\text{H}_4\text{PPh}_2)(\text{PPh}_3)$ ³²⁸

A flask was charged with 250 mg (3.443×10^{-4} mol) of $\text{CpRu}(\text{PPh}_3)_2\text{Me}$ and degassed prior to the addition of 300 ml of dried and degassed decalin. The contents of the flask were heated to 368 K under nitrogen with stirring. After 48 hours, the solution had grown darker than the initial bright yellow colour. The decalin was removed *in vacuo* and the remaining solid was left to dry over night using a high vacuum pump. The residue was dissolved in dry cyclohexane under nitrogen and filtered through a celite plug. The cyclohexane was removed under vacuum. A 94% yield of the sand coloured product, $\text{CpRu}(\kappa^2\text{-2-C}_6\text{H}_4\text{PPh}_2)(\text{PPh}_3)$ was obtained.

An alternative method of preparing an NMR scale sample of $\text{CpRu}(\kappa^2\text{-2-C}_6\text{H}_4\text{PPh}_2)(\text{PPh}_3)$ requires the UV irradiation of a 5 mg sample of $\text{CpRu}(\text{PPh}_3)_2\text{Me}$ in $\text{d}_8\text{-cyclohexane}$, using a Hg-Xe arc UV lamp. After 12 hours the sample was observed by $^{31}\text{P}\{^1\text{H}\}$ NMR to have undergone full conversion to the product $\text{CpRu}(\kappa^2\text{-2-C}_6\text{H}_4\text{PPh}_2)(\text{PPh}_3)$.

7.2.2.3 Preparation of DSiEt_3 ³²⁹

To a Schlenk tube containing 30 ml of dry dibutyl ether, 20 ml of ClSiEt_3 was added. The solution was degassed, and placed under nitrogen. Approximately 0.2 g of LiAlD_4 was added, and the solution was stirred for two hours at 313 K. The solution was filtered through a cannula fitted with a celite plug to remove the LiAlD_4 . The DSiEt_3 was removed from the ether by fractional distillation. A yield of 84% of DSiEt_3 was obtained. The pure DSiEt_3 (as determined by ^1H and $^{29}\text{Si}\{^1\text{H}\}$ NMR) was stored in an ampoule under nitrogen until use.

7.2.2.4 Reactions of $CpRu(PPh_3)_2Me$

Nine NMR tube were prepared as described earlier (section 7.1.2.1) containing d_8 -toluene and $CpRu(PPh_3)_2Me$. For three of the tubes, liquid substrates (PEt_3 , $HSiEt_3$, pyridine, DMSO and tBuNC) were added in the quantities listed in Table 7.2. Following the addition of these reagents, the samples were degassed using an acetone ice bath and a high vacuum line. The same procedure was followed for the solid naphthalene substrate. For the reactions involving the gases CO, ethene and H_2 the samples were degassed using a acetone ice bath and a high vacuum line, in each case the sample tubes were then pressurised to 1.5 bar with either of the two gases.

Each of the samples were then heated for one day at 323 K using a silicone oil bath as a heat source. The samples were then characterised using NMR techniques, prior to heating to 353 K for a further day, in order to monitor the progress of the reaction.

Table 7.2 Quantities of reagents used in the thermal and photochemical reactions with $CpRu(PPh_3)_2Me$

Reagent	moles	Quantity
PEt_3	6.788×10^{-5}	10 μ l
Pyridine	6.207×10^{-5}	5 μ l
tBuNC	6.265×10^{-5}	6 μ l

Reagent	moles	Quantity
$HSiEt_3$	6.270×10^{-5}	10 μ l
Naphthalene	6.242×10^{-5}	8 mg
DMSO	6.425×10^{-5}	5 μ l

Duplicate samples were prepared for the photochemical reactions, which were initiated using the *in situ* LASER set-up described in section 7.3.1.

7.2.2.5 Preparation of $CpRu(PPh_3)_2(C_{10}H_7)$

A 500 ml ampoule was charged with 0.89 g of naphthalene and placed under an N_2 atmosphere. Degassed dimethoxyethane (25 ml) was added to the ampoule, and stirred until all of the naphthalene had dissolved. The ampoule was then cooled by partial submersion in a methanol / dry ice bath, prior to the addition of small slithers of sodium (0.05 g) under a strong positive nitrogen flow. The colourless solution was rapidly observed to rapidly change a very dark green (almost black). The mixture was allowed

to stir under N_2 for two more hours to ensure complete conversion. The resulting mixture contained both 1-naphthyl sodium and 2-naphthyl sodium, and was subsequently used in the subsequent reactions with $CpRu(PPh_3)_2Cl$.

A small Schlenk tube was charged with 0.36 g of $CpRu(PPh_3)_2Cl$ in 25 ml of dried / degassed toluene, under N_2 . Dropwise, 5ml of the previously made sodium-naphthyl solution was added. The solution was left to stir at room temperature for 18 hours. Degassed water was added to the solution to quench the excess sodium-naphthyl. The organic layer was separated and washed several more times before drying over magnesium sulphate. Following separation, the toluene was removed *in vacuo* to leave a yellow oil, which was triturated with dry and degassed diethyl ether to yield a pale yellow solid (yield = 76%).

7.2.3 Methods for Chapter 4

7.2.3.1 Preparation of $CpRu(PPh_3)_2H$ ³³⁰

A suspension of sodium methoxide was prepared by adding a small slither of sodium to a Schlenk tube containing 25 ml of degassed anhydrous methanol under nitrogen at 263 K. The sodium methoxide solution was transferred by cannula to a second Schlenk tube kept under nitrogen containing 0.50 g (6.885×10^{-4} mol) of $CpRu(PPh_3)_2Cl$ in 50 ml of dry, degassed toluene. The solution was stirred and heated to 323 K for 15 minutes. The solution was then cooled on ice and the yellow precipitate collected by filtration. A yield of 93% of $CpRu(PPh_3)_2H$ was obtained.

7.2.3.2 Reactions of $CpRu(PPh_3)_2H$

Seven NMR tube were prepared as described earlier containing d_8 -toluene and $CpRu(PPh_3)_2H$. For three of the tubes, liquid substrates (PEt_3 , $HSiEt_3$ and tBuNC) were added in the quantities listed in Table 7.3. Following the addition of these reagents, the samples were degassed using an acetone ice bath and a high vacuum line. The same procedure was followed for the solid naphthalene substrate. For the reactions involving the gases CO and H_2 the samples were degassed using an acetone ice bath and a high

vacuum line, in each case the sample tubes were then pressurised to 1.5 bar with either of the two gases.

Each of the samples were then heated for one day at 323 K using a silicone oil bath as a heat source. The samples were then characterised using NMR techniques, prior to heating to 353 K for a further day, to monitor the progress of the reaction.

Table 7.3 Quantities of reagents used in the thermal and photochemical reactions with $CpRu(PPh_3)_2H$

Reagent	moles	Quantity
PEt ₃	6.788×10^{-5}	10 μ l
^t BuNC	6.265×10^{-5}	6 μ l
HSiEt ₃	6.270×10^{-5}	10 μ l
Naphthalene	6.242×10^{-5}	8 mg

Duplicate samples were prepared for the photochemical reactions, which were initiated using the *ex situ* set-up described in section 7.3.3.

7.2.3.3 Preparation of $CpRu(PPh_3)(CO)H$ ³³¹

The product complex, $CpRu(CO)_2H$, is highly air sensitive and care was taken to ensure that all reagents and solvents were thoroughly degassed prior to commencing the reaction.

To a 150 ml two-necked flask, 0.5 g of $Ru_3(CO)_{12}$ was added along with a stirrer bar. The flask was purged with nitrogen prior to adding 60 ml of dry / degassed hexane, the flask was then fitted with a condenser and the remaining neck was blocked with a rubber septum. The solution was brought to reflux (340 K). Once the $Ru_3(CO)_{12}$ has fully dissolved, and the solution has become a deep red, 4 ml of freshly cracked cyclopentadiene was added to the stirring solution. After ~ 4 hours the solution began to lighten to a pale yellow.

At this stage, the $\text{CpRu}(\text{CO})_2\text{H}$ has been formed and is highly air sensitive, even using a positive pressure of nitrogen, it was found that submersing the flask in a dry ice and acetone bath, prior to further manipulations, limited further decomposition of the product. Decomposition can be seen rapidly, as the pale yellow solution darkens to an opaque orange, as the decomposed product precipitates from the solvent. The hexane was removed *in vacuo*, and the product was further dried under nitrogen and transferred to the glovebox. A 90 % yield was obtained of the pale yellow solid and was used in the listed reactions without further purification. The complex was confirmed pure by NMR techniques (d_8 -toluene: ^1H NMR signals at δ -10.70 (s, 1) and 4.72 (s, 5); hydride and Cp proton signals, respectively. $^{13}\text{C}\{^1\text{H}\}$ signals at δ 89.5 (s) and 201.2 (s); Cp and carbonyl carbon signals, respectively). These NMR signals are consistent with those reported in the literature.³³¹

Photolysis (broadband UV, using the *ex situ* set-up) of a 5 mg sample of $\text{CpRu}(\text{CO})_2\text{H}$ (2.240×10^{-5}) in d_8 -benzene, with an three fold excess of excess triphenylphosphine (17.6 mg, 6.721×10^{-5}). Irradiation of the sample for 10 hours, led to the formation of a $\text{CpRu}(\text{PPh}_3)(\text{CO})\text{H}$. This complex was identified using ^1H and $^{31}\text{P}\{^1\text{H}\}$ NMR spectra. The NMR characterisation data is recorded in Chapter 4, Table 4.4.

7.2.4 Methods for Chapter 5

7.2.4.1 Preparation of $\text{HSi}(\text{Me})_2\text{C}_2\text{H}_3$ ^{332, 333}

To a round-bottom flask fitted with a condenser containing 0.05 of lithium aluminium hydride (under nitrogen), 15 ml of dried dibutyl ether was added. The flask was cooled in an ice bath prior to the dropwise addition of 5 ml of dried / degassed chloro(dimethyl)vinylsilane. The solution was heated to 353 K for two hours with continued stirring. The solution was separated from the remaining lithium aluminium hydride using a cannula fitted with a celite plug, to filter the solution. The solution was fractionally distilled using the appropriate apparatus. The fraction collected at 315 K was found by ^1H and ^{29}Si NMR to be pure dimethylvinylsilane. The sample was stored in an ampoule under nitrogen at 193 K until required.

7.2.4.2 Reaction of $CpRu(PPh_3)_2Me$ with dimethylvinylsilane

An NMR scale sample was prepared, as described in section 7.1.2.1, for a 5 mg quantity of $CpRu(PPh_3)_2Me$ in d_8 -toluene, which was charged with 10 μ l of dimethylvinylsilane. Following 12 hours photolysis of the sample using the *ex situ* set-up (described in section 7.3.3), the sample was checked using NMR methods. NMR data recorded for the photoproducts formed for this product appears in Chapter 5, Tables 5.1 and 5.2. Attempts to scale-up and consequently separate the species within this sample were unsuccessful, owing to the highly air sensitive nature of these products; the sample rapidly decomposed on exposure to air. This was observed by the rapid darkening of the sample to a deep brown / black, and the lack of any clear resonances in the 1H NMR spectrum, and a lone signal corresponding to triphenylphosphine oxide in the corresponding $^{31}P\{^1H\}$ NMR spectrum.

7.2.4.3 Preparation of Grignard Reagents

$ClMgCH_2-CH=CH_2$, $ClMgCH_2-Ph$, and $ClMgCH_2-C_{10}H_7$ were prepared from their respective chloride derivatives, $ClCH_2-CH=CH_2$, $ClCH_2-Ph$, and $ClCH_2-C_{10}H_7$, using a standard Grignard synthesis procedure.³³⁴ A flame-dried round bottomed flask containing 0.02 g of dried magnesium turnings was placed under a nitrogen atmosphere, and fitted with a condenser. To the flask, 20 ml of dried and degassed diethyl ether was added, along with a single iodine crystal, which would initiate the reaction. The contents of the flask were stirred using a magnetic stirrer bar and were cooled to 263 K using a salt / ice bath. Dropwise, the chloride derivative (see table below for the exact quantities used for each of the four derivatives) was cautiously added to the flask over a ten minute period. The contents of the flask were then heated to reflux (308 K) and allowed to react for two hours.

Table 7.4 Quantities of chloro compounds used in the synthesis of their corresponding Gignard reagents

Reagent	Moles	Volume (ml)
$\text{ClCH}_2\text{-CH=CH}_2$	3.30×10^{-3}	0.27
$\text{ClCH}_2\text{-Ph}$	3.30×10^{-3}	0.38
$\text{ClCH}_2\text{-C}_{10}\text{H}_7$	3.30×10^{-3}	0.45

The contents of the flask were transferred to a Schlenk tube (under nitrogen) using cannula fitted with a celite plug (this was done to separate any unreacted magnesium turnings from the solution). The resulting organo-magnesium complexes were used in subsequent reactions without any further need for purification.

7.2.4.4 Preparation of $\text{CpRu}(\text{PPh}_3)_2\text{R}$ ($\text{R} = \text{vinyl, benzyl, or methyl-1-naphthyl}$)

Appropriate 5 ml of each of the four solutions containing the organo-magnesium complexes were added dropwise to Schlenk tube containing 0.2 g (2.754×10^{-4} mol) of $\text{CpRu}(\text{PPh}_3)_2\text{Cl}$ in 60 ml of dried / degassed toluene. The solution was left to react for 18 hours at room temperature, with stirring. For each of the reactions a colour change was evident, indicating that the conversion was complete. The remaining organo-magnesium reagent within the solution was quenched with 10 ml of degassed water.

The organic phase was separated and dried using magnesium sulfate. The solution was transferred to a second Schlenk via a cannula fitted with a celite plug; to filter the solution. The volatiles were removed *in vacuo* to yield the products in their respective quantities (see Table 7.5). The complexes were deemed pure by ^1H and ^{31}P NMR techniques and used in further experiments without further purification.

Table 7.5 Tabulated yield data for the product complexes

Product	Yield (%)
$\text{CpRu}(\text{PPh}_3)(\eta^3\text{-CH}_2\text{-CH=CH}_2)$	94%
$\text{CpRu}(\text{PPh}_3)_2(\text{CH}_2\text{Ph})$	92 %
$\text{CpRu}(\text{PPh}_3)(\eta^3\text{-CH}_2\text{Ph})$	4% (by-product)
$\text{CpRu}(\text{PPh}_3)_2(\text{CH}_2\text{C}_{10}\text{H}_7)$	32%
$\text{CpRu}(\text{PPh}_3)(\eta^3\text{-CH}_{10}\text{C}_6\text{H}_7)$	66%

7.2.4.5 Preparation of $\text{CpRu}(\text{PPh}_3)(\eta^3\text{-CH}_2\text{-Ph})$

Heating a 0.25 g sample of $\text{CpRu}(\text{PPh}_3)_2(\text{CH}_2\text{C}_6\text{H}_5)$ to 353 K in toluene led to the loss of triphenylphosphine, and the subsequent binding of the benzyl ligand in a η^3 mode. Small quantities of elemental sulphur were added to the solution, while stirring and heating under N_2 . This addition of sulphur “trapped” the liberated phosphine, facilitating conversion to the η^3 binding mode. The reaction was monitored at frequent intervals by recording $^{31}\text{P}\{^1\text{H}\}$ NMR spectra. More sulphur was added as required until the conversion to the η^3 form reached 90% (as determined by comparison of their respective ^{31}P resonances in a $^{31}\text{P}\{^1\text{H}\}$ NMR spectrum). The sample was then washed with ethanol to remove the free phosphine sulphide, prior to use in further reactions with substrates.

7.2.4.6 Reactions of $\text{CpRu}(\text{PPh}_3)(\eta^3\text{-CH}_2\text{-CH=CH}_2)$ and $\text{CpRu}(\text{PPh}_3)(\eta^3\text{-CH}_2\text{-Ph})$

Five NMR tube were prepared as described earlier containing d_8 -toluene and $\text{CpRu}(\text{PPh}_3)(\eta^3\text{-CH}_2\text{-CH=CH}_2)$. For three of the tubes, liquid substrates PEt_3 , HSiEt_3 and $^t\text{BuNC}$ were added in 10 μl , 10 μl and 6 μl quantities (giving molar quantities of 6.788×10^{-5} , 6.270×10^{-5} and 6.265×10^{-5} , respectively). Following the addition of these reagents, the samples were degassed using an acetone ice bath and a high vacuum line. The same procedure was followed for the solid naphthalene substrate. For the reactions involving the gases CO , ethene and H_2 the samples were degassed using a acetone ice bath and a high vacuum line, in each case the sample tubes were then pressurised to 1.5 bar with either of the two gases.

Each of the samples were then heated for one day at 323 K using a silicone oil bath as a heat source. The samples were then characterised using NMR techniques, prior to heating to 353 K for a further day, to monitor the progress of the reaction.

A second set of five NMR tubes were prepared containing $\text{CpRu}(\text{PPh}_3)(\eta^3\text{-CH}_2\text{-Ph})$. These tubes were heated thermally as described for the reactions involving $\text{CpRu}(\text{PPh}_3)(\eta^3\text{-CH}_2\text{-CH=CH}_2)$.

Duplicate samples were prepared for the photochemical reactions, which were initiated using the *ex situ* set-up described in section 7.3.3.

7.2.4.7 Preparation of sodium/mercury amalgam³³⁵

A Schlenk tube containing 7 ml of mercury was placed under a nitrogen atmosphere and suspended in an ice bath to lower the temperature to ~263 K. Slithers of sodium (0.7 g, 0.031 mol) were cautiously added to the Schlenk tube against a strong flow of nitrogen. The mixture was left to stir for several hours, after which the Na(Hg) amalgam had the appearance and colour of solid graphite. The temperature of Schlenk tube was raised to room temperature, and the amalgam was stored under a nitrogen atmosphere.

7.2.4.8 Attempted η^3 complex synthesis using sodium/mercury amalgam

A solution of $\text{CpRu}(\text{PPh}_3)_2\text{Cl}$ (0.2 g, 2.754×10^{-4} mol) in THF (25 ml) was slowly transferred by cannula, to a Schlenk tube under nitrogen, containing 0.45 g of the Na(Hg) amalgam. The solution was stirred for two hours at room temperature. The solution was separated from the Na(Hg) amalgam using a cannula fitted with a celite plug to transfer the solution to a separate Schlenk tube, which was also placed under nitrogen. The resulting solution was observed have become deep red, from a previously orange coloured solution.

The solution was then separated, and transferred to three separated shlenk tubes, under nitrogen. The following reagents $\text{ClCH}_2\text{-CH=CH}_2$, $\text{ClCH}_2\text{-Ph}$ and $\text{ClCH}_2\text{-C}_{10}\text{H}_7$, were added to one of each of the three Schlenk tubes in the quantities described in Table 7.6. These chloro reagents were added dropwise to the solutions, as a strong exothermic

reaction was anticipated. Upon stirring the solutions for 24 hours, no colour change was observed. ^1H and $^{31}\text{P}\{^1\text{H}\}$ NMR did not reveal any evidence that the anticipated products, $\text{CpRu}(\text{PPh}_3)(\eta^3\text{-CH}_2\text{C}_2\text{H}_3)$, $\text{CpRu}(\text{PPh}_3)(\eta^3\text{-CH}_2\text{C}_6\text{H}_5)$ and $\text{CpRu}(\text{PPh}_3)(\eta^3\text{-CH}_2\text{C}_{10}\text{H}_7)$, had been formed.

Table 7.6 Quantities of chloro compounds used in the amalgam reactions

Reagent	Volume / ml	Moles
$\text{ClCH}_2\text{-CH=CH}_2$	3.30×10^{-3}	0.27
$\text{ClCH}_2\text{-Ph}$	3.30×10^{-3}	0.38
$\text{ClCH}_2\text{-C}_{10}\text{H}_7$	3.30×10^{-3}	0.45

7.2.5 Methods for Chapter 6

7.2.5.1 Preparation of $\text{CpRh}(\text{C}_2\text{H}_2)_2$

$\text{CpRh}(\text{C}_2\text{H}_2)_2$ was prepared using standard literature methods.³³⁶⁻³³⁸ $\text{RhCl}_3 \cdot 3\text{H}_2\text{O}$ (1 g, 3.8 mmol) was dissolved in a degassed mixture of methanol (25 ml) and water (1.5 ml). A large round bottom flask was connected to the top of the Schlenk tube and was pressurised to 2 bar with ethene. After several hours of stirring, an orange precipitate formed. The solution was left to stir for a total duration of 48 hours, with regular top-ups to the ethene pressure. The orange solution was filtered through a celite plug and dried *in vacuo*. The recovered solid, $[\text{RhCl}(\text{C}_2\text{H}_2)_2]$ (0.63g, 1.61 mmol, 85 %) was transferred to a glovebox and dissolved in 10 ml of dry THF. LiCp was added to the mixture dropwise, and left to stir for 3 hours. The volatiles were removed *in vacuo*, outside of the glove box. The yellow / orange solid was sublimed at room temperature onto an ice-cooled cold finger. The resulting yellow solid was collected and confirmed by ^1H and ^{13}C NMR to be pure $\text{CpRh}(\text{C}_2\text{H}_2)_2$ (0.56g, 2.4 mmol, 75%)

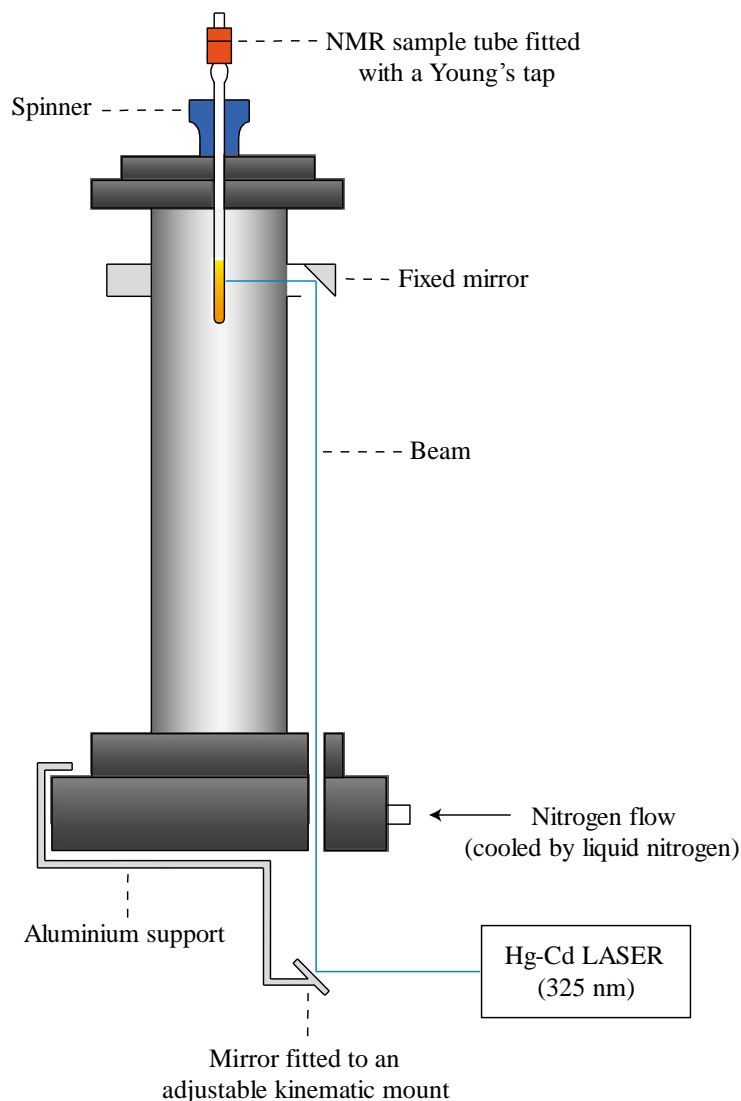
7.3 Photolysis

Three photolysis methods have been employed to conduct the experiments listed in this thesis. The two *in situ* methods allow NMR data to be collected during irradiation of the sample. Using the LASER as an initiation source provides UV light with a frequency of 325 nm, while the UV lamp provides broadband light. The *ex situ* setup lacks the ability to record data during irradiation, however, filters may be used with this system to restrict the frequency of the broadband light provided by the lamp – this can be used to selectively irradiated samples at a particular frequency.

7.3.1 *In situ* photolysis setup (LASER) ³³⁹

The *in situ* photolysis of samples was carried out using a Kimmon 63 mW He-Cd LASER (operating at 325 nm) as an irradiation source. Irradiation of the sample within the NMR probe was achieved using a modified narrow bore NMR probe, which when inserted into the wide-bore DMX (400 MHz) Bruker NMR spectrometer, allowed for a 1.5 cm cavity to permit the passage of the LASER beam. As shown in Figure 7.6, the beam is initially reflected off a mirror at the base of the probe, upwards through a drilled hole and the cavity to the second mirror, which directed the beam through a second hole to the sample.

Figure 7.6 Cut-away view of the modified NMR probe and LASER set-up used for *in situ* photolysis experiments (original in colour)



Alignment of the beam may be made approximately by directing the beam onto the mirror at the base of the probe. Using the screws on the kinematic mount, the mirror may be adjusted vertically and horizontally so that the beam travels up through the hole and into the cavity. This may be done owing to the visible reflection of the beam off of the surface of the probe's base. Fine alignment of the laser can be achieved using a sample of $\text{Ru}(\text{CO})_3(\text{dppe})$ ³⁴⁰ in d_8 -toluene, pressurised to 3 atm with *para*- H_2 .³⁴¹ Irradiation of this sample leads to the formation of $\text{Ru}(\text{CO})_2(\text{H})_2(\text{dppe})$,³²⁹ which clearly displays two *para*- H_2 enhanced signals in a ^1H NMR spectrum, at δ -7.64 and -6.44.³⁴² The continuous acquisition of NMR data may be carried out using the *gs* command in the Bruker Topspin 1.3 software environment. By adjusting the kinematic

mount while in this mode, the signal intensity for these enhanced signals can be observed to change, when a maximum intensity is achieved the beam alignment is in the optimal position relative to the sample.

For all of the samples prepared in this manner (and also for the fibre-optic and *ex situ* methods, described in the following sections) one session of time on the NMR spectrometer was not sufficient to generate the photo-products and obtain full identification and characterisation of the species by NMR. This was due in part to the limited capacity of the liquid nitrogen dewar (25 litre capacity), which provided ~ 20 hours of cooling (at 193 K), in addition to the availability of the NMR spectrometer for such lengthy experiments. Between sessions, the samples were immediately stored in a dry ice / acetone bath (193 K) before being transferred to a freezer (198 K) for longer durations. However, for many of these samples, their transfer by this method, despite careful handling, led to their decomposition in an appreciable amount. For these experiments, the photochemical generation of the species must be repeated for another sample, which subsequently led to increased characterisation times in some of the more complicated cases.

7.3.2 *In situ* photolysis setup (fibre-optic)

A further method employed to irradiate samples *in situ*, within an NMR spectrometer, was to use a fibre-optic cable to transfer UV light to the sample. This setup uses the same modified probe and spectrometer as that used in the previous *in situ* setup (Figure 7.6). The aluminium support / kinematic mount is removed from this setup, and a fibre-optic cable is run from the base of the probe and up the mirror at the top of the probe. The other end of the cable is connected to an Oriel 200 W Hg-Xe arc lamp. A water filter is placed between the mirror and the cable, to minimise heating effects on the sample. To prevent the water filter from freezing during low temperature photolysis, the probe is wrapped with insulation material.

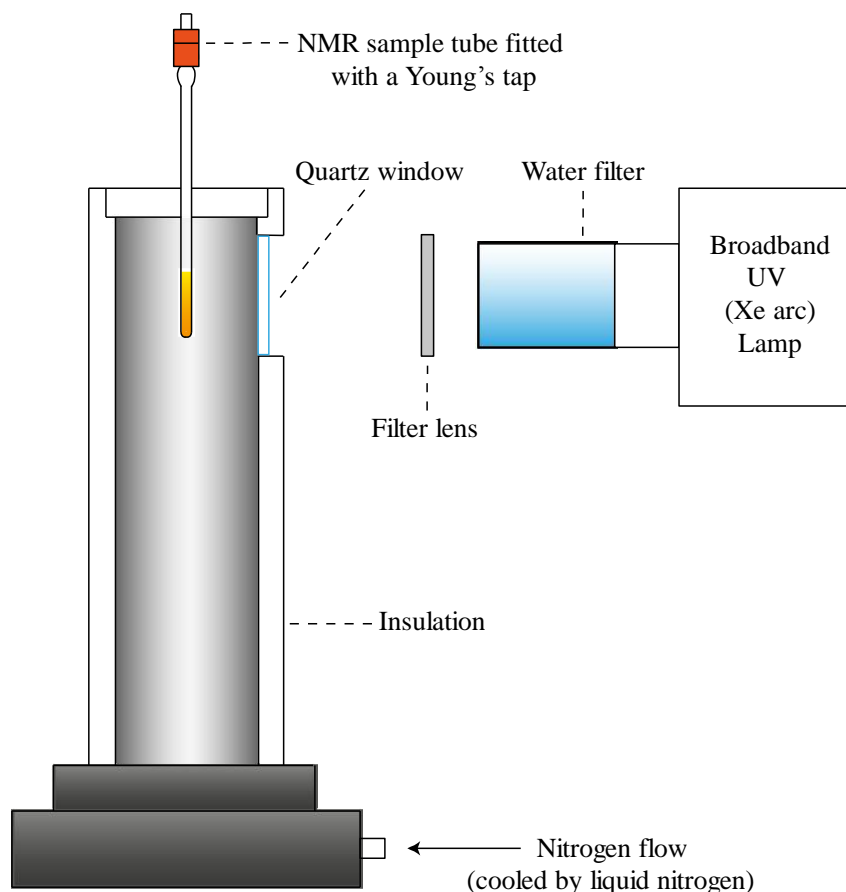
7.3.3 *Ex situ* photolysis setup

An alternative method of irradiating samples was provided by the *ex situ* photolysis setup (Figure 7.7). This equipment consists of a modified NMR probe, outside of an NMR spectrometer, which provides VT (variable temperature) cooling to the sample. A window in the side of the probe, at sample height, allows for the irradiation of the sample within the probe. The Irradiation source consists of an Oriel 200 W Hg-Xe arc lamp. The UV output from the lamp was broadband, however, in the case of some experiments a 320 nm filter lens was placed between the lamp and the sample. Additionally, a 10 cm water filter is placed in front of the UV lamp in order to minimise any unwanted heating effects on sample. Unlike the previously mentioned *in situ* setup, this method allows for the photolysis of up to three samples simultaneously. Low temperature photolysis was achieved using a continuous flow of nitrogen gas, cooled by liquid nitrogen.

However, unlike the *in situ* NMR setup the temperature control is manual. Consequently a constant temperature was difficult to achieve, though this temperature variance was only observed to be approximately 3 K within the target temperature.

Sample prepared in this manner were stored in a dry ice / acetone bath (193 K) following removal from the set-up. This was done to minimise the thermal decomposition of the sample prior to characterisation by NMR.

Figure 7.7 Cut-away view of the modified NMR probe and UV lamp setup used for *ex situ* photolysis experiments (original in colour)



7.4 Calculation of rate constants using NMR data³⁴³

The NMR data collected for rate constant determination was interpreted using the Microsoft Excel simulation package. The reversible exchange between two sites, A and B, was probed using 1D selective NOE experiments, for a range of mixing times (t_m) between 0 and 2 seconds. NOE irradiation of the resonance corresponding to site A, led to the excitation of the resonance corresponding to site B. The integrated intensity of these resonances can be obtained from the relevant NMR spectra, for each of the varying mixing times. Table 7.7 depicts example data (normalised to 100%) for the peak intensities, represented as a function of mixing time.

Table 7.7 Peak intensities (%) for the reversible conversion of resonances A to B for a range of varying mixing times.

Mixing time (s)	[A] (%)	[B] (%)
0	100	0
0.1	93	7
0.2	87	13
0.3	79	21
0.4	74	26
0.5	71	29
0.6	68	32
0.7	64	36
0.8	62	38
0.9	61	39
1.0	59	41

This data may be interpreted using an Excel based simulation package, which utilises the kinetic model presented in Equation 7.1, for the first order exchange between site A and one or more other sites. In Equation 7.1, $[A]_t$ represents the normalised intensity of the resonance A, for a time t (seconds). For every elapsed time interval (dt) between t_0 and t_{\max} , a single simulated point is calculated. During the span of dt , the sum of all processes contributing to the loss of A is covered by $i \rightarrow j$, while the processes leading to A are covered by $m \rightarrow n$.

$$\text{Equation 7.1} \quad [A]_t = [A]_{t-dt} - dt(\sum_i^j k_{loss})[A]_{(t-dt)} + dt(\sum_m^n k_{gain})[species\ yielding\ A]_{(t-dt)}$$

The percentage intensity for the sites A and B would be calculated using Equation 7.2, for a dt of 0.01 s. Ideally the value of dt should be as small as practically possible, in order to achieve the most accurate determinations of the values of $[A]_t$ and $[B]_t$.

$$\begin{aligned} \text{Equation 7.2} \quad [A]_t &= [A]_{t-0.01} - 0.01(k_{AA})([A]_{t-0.01}) + 0.01(k_{BA})([B]_{t-0.01}) \\ [B]_t &= [B]_{t-0.01} - 0.01(k_{BB})([B]_{t-0.01}) + 0.01(k_{AB})([A]_{t-0.01}) \end{aligned}$$

Since this example only considers two exchange sites as opposed to many, Equation 7.2 may be rewritten as Equation 7.3.

$$\text{Equation 7.3} \quad [A]_{0.1} = [A]_{0.09} - 0.01(k_{AB})([A]_{0.09}) + 0.01(k_{BA})([B]_{0.09})$$

Table 7.8 represents the simulated data for the peaks A and B. Only results between t_0 and $t_{0.1}$ have been listed, however, in the actual simulation data points between t_0 and t_1 would be collected.

Table 7.8 Simulated data points

Mixing time (s)	[A] (%)	[B] (%)
0	100	0
0.01	91.76	8.24
0.02	84.87	15.13
0.03	79.12	20.88
0.04	74.32	25.68
0.05	70.31	29.69
0.06	66.94	33.06
0.07	64.17	35.83
0.08	61.83	38.17
0.09	59.88	40.12
0.10	56.89	43.11

The simulation package includes a solver routine which acts to minimise the sum of the square of the differences between the experimental and the calculated peak intensities. This is achieved by varying the values of the rate constants k_{AB} and k_{BA} . For this example, $k_{AB} = k_{BA}$ since the exchange only involves two sites. The simulated data and accompanying calculated error values for the experimentally obtained results are presented in Table 7.9. Figure 7.8 illustrates the change in the relative concentrations of the species corresponding to A and B, as a function of reaction time.

Table 7.9 Calculation of error for the experimentally obtained values, for the intensities of peaks A and B, over a range of varying mixing times

Mixing time (s)	[A] (%)		[B] (%)		Calculated error values		
	Expt	Calc	Expt	Calc	Error in A	Error in B	Sum of errors
0	100	-	0	-	-	-	-
0.1	92	91.76	7	8.24	0.058	0.058	0.115
0.2	85	84.87	13	15.13	0.017	0.017	0.034
0.3	79	79.12	21	20.88	0.014	0.014	0.029
0.4	74	74.32	26	25.68	0.102	0.102	0.205
0.5	71	70.31	29	29.69	0.476	0.476	0.952
0.6	68	66.94	32	33.06	1.124	1.124	2.247
0.7	64	64.17	36	35.83	0.029	0.029	0.058
0.8	62	61.83	38	38.17	0.029	0.029	0.058
0.9	61	59.88	39	40.12	1.254	1.254	2.509
1.0	59	56.89	41	43.11	0.012	0.012	0.024
Total error =							6.231

$$\text{Error in A} = ([A]_{\text{Expt}} - [A]_{\text{Calc}})^2$$

$$\text{Error in B} = ([B]_{\text{Expt}} - [B]_{\text{Calc}})^2$$

Figure 7.8 Plot of the mixing time against the relative peak intensities for the experimentally obtained and calculated values of A and B

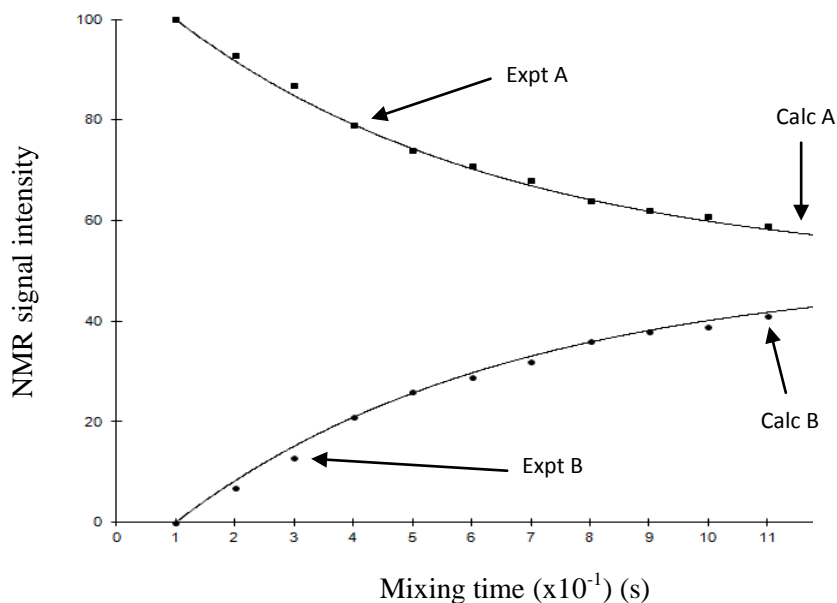


Table 7.10 Shows the calculated rate constants for the kinetic processes, k_{AB} and k_{BA} .

Table 7.10 Rate constant data for the interconversion of signals A and B

Rate constant, k (s^{-1})	A	B
A	-0.09	0.09
B	0.09	-0.09

However, this method of rate constant determination doesn't account for reactions which possess a symmetrical transition state. Such an instance would present an equal chance that a back reaction would occur, as opposed to the formation of products (and vice versa). This suggests that the rate constants calculated in Table 7.10 are half of the value for the true rate constants. Therefore, the value may be doubled to give the true rate constant for reaching the transition state³⁴³ (Table 7.11).

Table 7.11 Revised Rate constant data

Rate constant, k (s^{-1})	A	B
A	-0.18	0.18
B	0.18	-0.18

Table 7.12 Calculation of error for the experimentally obtained values, for the photochemical reaction of pyridine with $CpRu(PPh_3)_2Me$ at 198 K

Mixing time (s)	$CpRu(PPh_3)_2Me$		$CpRu(PPh_3)(Py)Me$		Calculated error values			
	Expt	Calc	Expt	Calc	Error in A	Error in B	Sum of errors	
0	100	-	0	-	-	-	-	
0.1	95.5	96.08	4.5	3.92	0.33	0.33	0.67	
0.2	92.7	92.31	7.3	7.69	0.15	0.15	0.30	
0.3	89.3	88.69	10.7	11.31	0.37	0.37	0.74	
0.4	85.5	85.21	14.5	14.79	0.08	0.08	0.17	
0.5	83.4	81.87	16.6	18.13	2.34	2.34	4.68	
0.6	78.8	78.66	21.2	21.34	0.02	0.02	0.04	
0.7	75.0	75.57	25.0	24.43	0.33	0.33	0.66	
0.8	72.5	72.61	27.5	27.39	0.01	0.01	0.02	
0.9	70.2	69.76	29.8	30.24	0.19	0.19	0.38	
1.0	67.5	67.03	32.5	32.97	0.22	0.22	0.45	
1.1	64.7	64.40	35.3	35.60	0.09	0.09	0.18	
1.2	61.8	61.87	38.2	38.13	0.01	0.01	0.01	
1.3	59.1	59.45	40.9	40.55	0.12	0.12	0.24	
1.4	56.7	57.11	43.3	42.89	0.17	0.17	0.34	
1.5	54.8	54.87	45.2	45.13	0.01	0.01	0.01	
1.6	52.5	52.72	47.5	47.28	0.05	0.05	0.10	
1.7	51.6	50.65	48.4	49.35	0.89	0.89	1.79	
1.8	48.5	48.67	51.5	51.33	0.03	0.03	0.06	
1.9	47.2	46.76	52.8	53.24	0.19	0.19	0.39	
2.0	45.3	44.93	54.7	55.07	0.15	0.15	0.31	
Total error =								11.55

Table 7.12 presents the data recorded for the photochemically induced reaction between pyridine and $\text{CpRu}(\text{PPh}_3)_2\text{Me}$ at 198 K (Chapter 3, Section 3.4.8.2). This data was subsequently used to plot the time course depicted in Figure 3.32, using the methods described here in this section. It should be noted that the magnitude of the errors obtained for this set of data are typical of those obtained using this method (i.e. for the plots reported in Chapter 3). These errors values compare well similarly recorded experiments, which use this method.^{219, 329, 339}

Abbreviations

Chemical

Me	Methyl, CH ₃
Et	Ethyl, CH ₂ CH ₃
ⁱ Pr	<i>Iso</i> -propyl, CH(CH ₃) ₂
^t Bu	Tertiary-butyl, C(CH ₃) ₃
Cp	Cyclopentadienyl, η ⁵ -C ₅ H ₅
Cp*	Pentamethylcyclopentadienyl, η ⁵ -C ₅ (CH ₃) ₅
Ph	Phenyl, C ₆ H ₅
Cy	Cyclohexyl, C ₆ H ₁₁
Py	Pyridine, NC ₅ H ₅

Units

Å	Ångström
Atm	Atmosphere
Hz	Hertz
g	Gram
mg	Milligram
K	Kelvin
mol	Mole
s	Second

Abbreviations

Techniques

ESI	Electrospray Ionisation
GCMS	Gas chromatography – mass spectrometry
MS	Mass spectrometry
M ⁺	Molecular ion
NMR	Nuclear magnetic resonance
UV	Ultra violet
IR	Infra red spectroscopy

Spectroscopy

COSY	Correlation spectroscopy
EXSY	Exchange spectroscopy
HMQC	Heteronuclear multiple quantum coherence
NOE	Nuclear Overhauser effect
NOESY	Nuclear Overhauser effect spectroscopy
δ	Chemical shift (in parts per million, ppm)
J	Coupling constant
s	Singlet
d	Doublet
dd	Doublet of doublets
ddd	Doublet of doublets of doublets
t	Triplet
q	Quartet
m	Multiplet
br	Broad

References

1. J.F. Hartwig. **2008**, *Nature*, Vol. 455, p. 314.
2. J. Hagen. *Industrial Catalysis: A Practical Approach*. Weinheim, Germany : Wiley-VCH, **2006**.
3. J.F. Hartwig. *Organotransition Metal Chemistry: From Bonding to Catalysis*. Sausalito, Calif : University Science Books, **2010**.
4. P. Jaunky, H.W. Schmalle, M. Alfonso, T. Fox and H. Berke. **2004**, *J. Organomet. Chem.*, Vol. 689, p. 801.
5. S. Bi, Z. Zhang and S. Zhu. **2006**, *Chem. Phys. Lett.*, Vol. 431, p. 385.
6. J.J. Schneider. **1996**, *Angew. Chem. Int. Ed.*, Vol. 35, p. 1068.
7. D.M. Haddleton, A. McCamley and R.N. Perutz. **1988**, *J. Am. Chem. Soc.*, Vol. 110, p. 1810.
8. S.B. Duckett, D.M. Haddleton, S.A. Jackson, R.N. Perutz, M. Poliakoff and R.K. Upmacis. **1988**, *Organometallics*, Vol. 7, p. 1526.
9. D.F. Shriver and M.I. Bruce *Comprehensive Organometallic Chemistry II*. [ed.] F.G.A. Stone and G. Wilkinson E.W. Abel. Exeter, UK : Pergamon, **1995**. Vol. 7.
10. E.A. Seddon and K.R. Seddon. *The Chemistry of Ruthenium*. Amsterdam : Elsevier, **1984**.
11. M.I. Bruce, R.C.F. Gardner and F.G.A. Stone. **1976**, *Dalton Trans.*, p. 81.
12. C. Godard, P. Callaghan, J.L. Cunningham, S.B. Duckett, J.A.B. Lohman and R.N. Perutz. **2002**, *Chem. Commun.*, p. 2836.
13. C.J. Sexton, J. López-Serrano, A. Lledós and S.B. Duckett. **2008**, *Chem. Commun.*, p. 4834.

References

14. H. Yang, M.C. Asplund, K.T. Kotz, M.J. Wilkens, H. Frei and C.B. Harris. **1998**, *J. Am. Chem. Soc.*, Vol. 120, p. 10154.
15. D.L. Lichtenberger and A. Raichaudhuri. **1989**, *J. Am. Chem. Soc.*, Vol. 111, p. 3583.
16. U. Schubert. **1990**, *Adv. Organomet. Chem.*, Vol. 30, p. 151.
17. G.S. McGrady and G. Guilera. **2003**, *Chem. Soc. Rev.*, Vol. 32, p. 383.
18. Lin, Z. **2002**, *Chem. Soc. Rev.*, Vol. 31, p. 239.
19. J.Y. Corey and J. Braddock-Wilking. **1999**, *Chem. Rev.*, Vol. 99, p. 175.
20. G.J. Kubas. **2001**, *J. Organomet. Chem.*, Vol. 635, p. 37.
21. P.I. Kaye. **1998**, *D. Phil. Thesis, University of York*.
22. S.B. Duckett. **1989**, *D. Phil. Thesis, University of York*.
23. R.H. Crabtree. **1993**, *Angew. Chem. Int. Ed.*, Vol. 32, p. 789.
24. G.I. Nikonov. **2003**, *Organometallics*, Vol. 22, p. 1597.
25. R.N. Perutz and S. Saboetienne. **2007**, *Angew. Chem. Int. Ed.*, Vol. 46, p. 2578.
26. S.M. Ng, W.H. Lam, C.C. Mak, C.W. Tsang, G. Jia, Z. Lin, and C.P. Lau. **2003**, *Organometallics*, Vol. 22, p. 641.
27. C.E. Webster, Y. Fan, M.B. Hall, D. Kunz, J.F. Hartwig. **2003**, *J. Am. Chem. Soc.*, Vol. 125, p. 858.
28. J.F. Hartwig, K.S. Cook, M. Hapke, C.D. Incarvito, Y. Fan, C.E. Webster and M.B. Hall. **2005**, *J. Am. Chem. Soc.*, Vol. 127, p. 2538.
29. A.J. Chalk and J.F. Harrod. **1965**, *J. Am. Chem. Soc.*, Vol. 87, p. 16.
30. S.B. Duckett and R.N. Perutz. **1992**, *Organometallics*, Vol. 11, p. 90.
31. C.L. Randolph and M.S. Wrighton. **1986**, *J. Am. Chem. Soc.*, Vol. 108, p. 3366.

32. S.Sakaki, M. Sumimoto, M. Fukuhara, M. Sugimoto, H. Fujimoto and S. Matsuzaki. **2002**, *Organometallics*, Vol. 21, p. 3788.
33. M.A. Schroeder and M.S Wrighton. **1977**, *J. Organomet. Chem.*, Vol. 128, p. 345.
34. M. Brookhart and B.E. Grant. **1993**, *J. Am. Chem. Soc.*, Vol. 115, p. 2151.
35. A. Millan, M.J. Fernandez, P. Bentz and P.M. Maitlis. **1984**, *J. Mol. Catal.*, Vol. 26, p. 89.
36. C.L. Reichel and M.S. Wrighton. **1979**, *J. Am. Chem. Soc.*, Vol. 101, p. 6769.
37. F. Seitz and M.S. Wrighton. **1988**, *Angew. Chem. Int. Ed.*, Vol. 27, p. 289.
38. P.B. Glaser and T.D. Tilley. **2003**, *J. Am. Chem. Soc.*, Vol. 125, p. 13640.
39. D.V. Gutsulyak and G.I. Nikonov. **2010**, *Angew. Chem. Int. Ed.*, Vol. 49, p. 7553.
40. D.V. Gutsulyak and G.I. Nikonov. **2011**, *Angew. Chem. Int. Ed.*, Vol. 50, p. 1384.
41. D.V. Gutsulyak, S.F. Vyboishchikov and G.I. Nikonov. **2010**, *J. Am. Chem. Soc.*, Vol. 132, p. 5950.
42. F. Delpech, J. Mansas, H. Leuser, S. Sabo-Etienne and B. Chaudret. **2000**, *Organometallics*, Vol. 19, p. 5750.
43. F. Gauvin, J.F. Harrod and H.G. Woo. **1998**, *Adv. Organomet. Chem.*, Vol. 42, p. 363.
44. R.D. Miller and J. Michl. **1989**, *Chem. Rev.*, Vol. 89, p. 1359.
45. J.M. Zeigler. **1986**, *Polym. Prepr.*, Vol. 27, p. 109.
46. I.A. Harrah and J.M. Zeigler. **1987**, *Macromolecules*, Vol. 20, p. 601.
47. R.D. Miller and R. Sooriyakumaran. **1988**, *Macromolecules*, Vol. 21, p. 3120.

References

48. R. Horguchi, Y. Onishi and S. Hayase. **1988**, *Macromolecules*, Vol. 21, p. 304.
49. C.T. Aitken, J.F. Harrod and E. Samuel. **1986**, *J. Am. Chem. Soc.*, Vol. 108, p. 4059.
50. T.D. Tilley. **1993**, *Accounts Chem. Res.*, Vol. 23, p. 22.
51. L. Rosenberg, D.N. Kobus. **2003**, *J. Organomet. Chem.*, Vol. 685, p. 107.
52. L. Rosenberg, M.D. Fryzuk and S.J. Rettig. **1999**, *Organometallics*, Vol. 18, p. 958.
53. M.D. Fryzuk, L. Rosenberg and S.J. Rettig. **1994**, *Inorg. Chim. Acta.*, Vol. 222, p. 345.
54. L. Rosenberg, C.W. Davis and J.Z. Yao. **2001**, *J. Am. Chem. Soc.*, Vol. 123, p. 5120.
55. R.H. Crabtree. *The Organometallic Chemistry of the Transition Metal*. New York : Wiley-Interscience, **2005**.
56. R.H. Crabtree and D.G. Hamilton. **1988**, *Adv. Organomet. Chem.*, Vol. 28, p. 299.
57. C. Elschenbroich and A. Salzer. *Organometallics: A Concise Introduction*. New York : Weinheim, **1992**.
58. F. Maseras, A. Lledos, E. Clot and O. Einstein. **2000**, *Chem. Rev.*, Vol. 100, p. 601.
59. J.Y. Saillard and R. Hoffman. **1984**, *J. Am. Chem. Soc.*, Vol. 106, p. 2006.
60. G.J. Kubas, R.R. Ryan, B.I. Swanson, P.J. Vergamini and H.J. Wasserman. **1984**, *J. Am. Chem. Soc.*, Vol. 106, p. 451.
61. G.J. Kubas. **1988**, *Accounts Chem. Res.*, Vol. 21, p. 120.
62. D.M. Heinekey and W.J. Oldham. **1993**, *Chem. Rev.*, Vol. 93, p. 913.
63. H.C. Aspinall, N. Greeves and C. Valla. **2005**, *Org. Lett.*, Vol. 7, p. 1910.

64. M. Gomberg and W.E. Bachmann. **1941**, *Org. Synth. Coll.*, Vol. 1, p. 113.
65. H. Gilman, R.G. Jones, L.A. Woods. **1952**, *J. Org. Chem.*, Vol. 17, p. 1630.
66. A. Fürstner, A. Leitner and G. Seidel. **2005**, *Org. Synth.*, Vol. 81, p. 33.
67. S. Murai, F. Kakiuchi, S. Sekine, Y. Tanaka, A. Kamatani, M. Sonoda and N. Chatani. **1993**, *Nature*, Vol. 366, p. 529.
68. G. Dyker. **1999**, *Angew. Chem. Int. Ed.*, Vol. 38, p. 1698.
69. J.J. Schneider. **1996**, *Angew. Chem. Int. Ed.*, Vol. 35, p. 1069.
70. A.D. Ryabov. **1990**, *Chem. Rev.*, Vol. 90, p. 403.
71. A.H. Janowicz and R.G. Bergman, **1983**, *J. Am. Chem. Soc.*, Vol. 105, p. 3929.
72. N.F. Gol'dshleger, M.B. Tyabin, A.E. Shilov and A.A. Shteinman. **1969**, *Zh. Fiz. Khim.*, Vol. 43, p. 2174.
73. R.H. Crabtree. **1995**, *Chem. Revs.*, Vol. 95, p. 987.
74. R.H. Crabtree. **2001**, *J. Chem. Soc. Dalton Trans.*, p. 2437.
75. M.A. Graham, R.N. Perutz, M. Poliakoff and J.J. Turner. **1972**, *J. Organomet. Chem.*, Vol. 34, p. C34.
76. R.N. Perutz and J.J. Turner. **1975**, *J. Am. Chem. Soc.*, Vol. 97, p. 4791.
77. G.L. Gould and M. Heinekey. **1989**, *J. Am. Chem. Soc.*, Vol. 111, p. 5502.
78. S. Geftakis and G.E. Ball, **1998**, *J. Am. Chem. Soc.*, Vol. 120, p. 9953.
79. T.O. Northcutt, D.D. Wick, A.J. Vetter and W.D. Jones. **2001**, *J. Am. Chem. Soc.*, Vol. 123, p. 7257.
80. D.R. Lide. *CRC Handbook of Chemistry and Physics, 82nd ed*, Boca Raton : CRC Press, **2001**.
81. M.P. Jensen, D.D Wick, S. Reinartz, P.S. White, J.L. Templeton and K.I. Goldberg. **2003**, *J. Am. Chem. Soc.*, Vol. 125, p. 8614.

References

82. S. Reinartz, P.S. White, M. Brookhart and J.L. Templeton. **2001**, *J. Am. Chem.Soc.*, Vol. 123, p. 12724.
83. W.D. Jones and F.J. Feher. **1983**, *Organometallics*, Vol. 2, p. 562.
84. W.D. Jones and F.J. Feher. **1984**, *J. Am. Chem. Soc.*, Vol. 106, p. 1650.
85. R.A. Periana and R.G. Bergman. **1986**, *J. Am. Chem. Soc.*, Vol. 108, p. 7332.
86. W.D. Jones. **2005**, *Inorg. Chem.*, Vol. 44, p. 4475.
87. A.H. Janowicz and R.G. Bergman. **1982**, *J. Am. Chem. Soc.*, Vol. 104, p. 352.
88. B.A. Arndtsen, R.G. Bergman, T.A. Mobley and T.H. Peterson. **1995**, *Accounts Chem. Res.*, Vol. 28, p. 154.
89. C.P. Lenges, P.S. White and M. Brookhart. **1999**, *J. Am. Chem. Soc.*, Vol. 121, p. 4385.
90. F.A. Cotton and V.W. Day. **1974**, *J. Chem. Soc. Chem. Commun.*, p. 415.
91. F.A. Cotton and A.G. Stanilowski. **1974**, *J. Am. Chem. Soc.*, Vol. 96, p. 5074.
92. M. Brookhart and M.L.H. Green. **1988**, *Prog. Inorg. Chem.*, Vol. 36, p. 1.
93. H.J. Wasserman, G.J. Kubas and R.R. Ryan. **1986**, *J. Am. Chem. Soc.*, Vol. 108, p. 2294.
94. I.C.M. Wehman-Ooyevaar, I.F. Luitwieler, K. Vatter, D.M. Grove, W.J.J. Smeets, E. Horn, A.L. Spek and G. van Koten. **1996**, *Inorg. Chim. Acta.*, Vol. 252, p. 55.
95. M. Brookhart and M.L.H. Green. **1983**, *J. Organomet. Chem.*, Vol. 250, p. 395.
96. W. Baratta, A.D. Zotto and P. Rigo. **1999**, *Organometallics*, Vol. 18, p. 5091.
97. A.E. Díaz-Álvarez, P. Crochet, M. Zablocka, V. Cadierno, L. Vendier, J. Gimeno and J-P. Majoral. **2007**, *Polyhedron*, Vol. 26, p. 933.

98. D. Das, P. Singh, O. Prakash and A.K. Singh. **2010**, *Inorg. Chem. Commun.*, Vol. 13, p. 1370.
99. K. Osakada. **2011**, *Angew. Chem. Int. Ed.*, Vol. 50, p. 3845.
100. B. Therrien, T-T. Thai, J. Freudenreich, G. Süß-Fink, S.S. Shapovalov, A. Pasynskii and L. Plasseraud. **2010**, *J. Organomet. Chem.*, Vol. 695, p. 409.
101. D.W. Lee and Y.S Chae. **2010**, *Organometallics*, Vol. 29, p. 3413.
102. A. Flores-Figueroa, O. Kaufhold, K-O. Feldmann and R.E. Hahn. **2009**, *Dalton Trans.*, p. 9334.
103. P.G. Hayes, R. Waterman, P.B. Glaser and T.D. Tilley. **2009**, *Organometallics*, Vol. 28, p. 5082.
104. R.C. Badger, J.S. Acchioli, T.A. Oudenhoven and B.J. Walder. **2010**, *Organometallics*, Vol. 29, p. 1061.
105. G. Vitulli, P. Pertici and P. Salvadori. **1984**, *J. Chem. Soc. Dalton Trans.*, p. 2255.
106. R.M. Fairchild and K.T. Holman. **2008**, *Organometallics*, Vol. 27, p. 1823.
107. J.W. Faller and P.P. Fontaine. **2007**, *J. Organomet. Chem.*, Vol. 692, p. 976.
108. K.H. Pannell, T. Kobayashi and R.N. Kapoor. **1992**, *Organometallics*, Vol. 11, p. 2229.
109. T.E. Bitterwolf. **2000**, *Coord. Chem. Rev.*, Vol. 419, p. 206.
110. T.E. Bitterwolf, J.C. Linehan and J.E. Shade. **2000**, *Organometallics*, Vol. 19, p. 4915.
111. N.J. Farrow and S.A.R. Knox. **1984**, *J. Chem. Soc. Chem. Commun.*, p. 679.
112. A. Eisenstadt, R Tannenbaum and A. Efraty. **1981**, *J. Organomet. Chem.*, Vol. 221, p. 317.
113. T.E. Bitterwolf, J.C. Linehan and J.E. Shade. **2001**, *Organometallics*, Vol. 20, p. 775.

References

114. C. White. **1985**, *J. Organomet. Chem.*, Vol. 287, p. 123.
115. A.H.J. Robertson, G.P. McQuillan and D.C. McKean. **1995**, *J. Chem. Soc. Dalton Trans.*, p. 3955.
116. A. Davison, J.A. McCleverty and G. Wilkinson. **1963**, *J. Chem. Soc.*, p. 1133.
117. M.F. Joseph, J.A. Page and M.C. Baird. **1984**, *Organometallics*, Vol. 3, p. 1749.
118. T.C. Forschner and A.R. Cutler. **1985**, *Organometallics*, Vol. 4, p. 1247.
119. J.D. Gilbert and G. Wilkinson. **1969**, *J. Chem. Soc. A*, p. 1749.
120. T. Blackmore, M.I. Bruce and F.G.A. Stone. **1971**, *J. Chem. Soc. A*, p. 2376.
121. M.I. Bruce, C. Hameister, A.G. Swincer and R.C. Wallis. **1991**, *Inorg. Synth.*, Vol. 28, p. 270.
122. Y. Yang, K.A. Abboud and L. McElwee-White. **2003**, *Dalton Trans.*, p. 4288.
123. R.J. Kulawiec, J.W. Faller and R.H. Crabtree. **1990**, *Organometallics*, Vol. 9, p. 745.
124. M.I. Bruce and A.G. Swincer. **1983**, *Adv. Organomet. Chem.*, Vol. 22, p. 59.
125. M.I. Bruce. **1991**, *Chem. Rev.*, Vol. 91, p. 197.
126. T. Wilczewski, M. Bochenska and J.F. Biernat. **1981**, *J. Organomet. Chem.*, Vol. 215, p. 87.
127. M.I. Bruce, M.P. Cifuentes, M.G. Humphrey, E. Poczman, M.R. Snow and E.R.T. Tiekink. **1988**, *J. Organomet. Chem.*, Vol. 338, p. 237.
128. H. Lehmkuhl, J. Grundke and R. Mynott. **1983**, *Chem. Ber.*, Vol. 116, p. 159.
129. J-P. Djukic, J-B. Sortais, L. Barloy, and M. Pfeffer. **2009**, *Eur. J. Inorg. Chem.*, Vol. 817.

130. M. Lail, C.M. Bell, D. Conner, T.R. Cundari, T.B. Gunnoe and J.L. Petersen. **2004**, *Organometallics*, Vol. 23, p. 5007.
131. S.-I. Murahashi. *Ruthenium in Organic Synthesis*. Weinheim : Wiley-VCH, **2004**.
132. C. Bruneau and P.H. Dixneuf. *Ruthenium Catalysts and Fine Chemistry*. Berlin : Springer, **2004**.
133. B.M. Trost, F.D. Toste and A.B. Pinkerton. **2001** : s.n., *Chem. Rev.*, Vol. 101, p. 2067.
134. A.G. Orpen. **1985**, *J. Am. Chem. Soc. Chem. Commun.*, p. 1310.
135. P.B. Dias, M.E.M. Depiedade and J.A.M. Simoes. **2004**, *Coord. Chem. Rev.* Vol. 135, p. 737.
136. Tolman, C.A. **1977**, *Chem. Rev.*, Vol. 77, p. 313.
137. P.K. Maples and C.S. Kraihanzel. **1968**, *Inorg. Chem.*, Vol. 7, p. 1806.
138. M.S. Sanford, J.A. Love and R.H. Grubbs. **2001**, *J. Am. Chem. Soc.*, Vol. 123, p. 6543.
139. T. Fanjul, G. Eastham, N. Fey, A. Hamilton, P.G. Pringle and M. Waugh. **2010**, *Organometallics*, Vol. 29, p. 2292.
140. P.R. Elowe, C. McCann, P.G. Pringle, S.K. Spitzmesser and J.E. Bercaw. **2006**, *Organometallics*, Vol. 25, p. 5255.
141. M.I. Bruce, F.S. Wong, B.W. Skelton and A.H. White. **1981**, *J. Chem. Soc. Dalton Trans.*, p. 1398.
142. W. Strohmeier. **1964**, *Angew. Chem. Int. Ed.*, Vol. 3, p. 730.
143. T.A. Manuel. **1965**, *Adv. Organomet. Chem.*, Vol. 3, p. 181.
144. D. Sellmann. **1972**, *Angew. Chem. Int. Ed.*, Vol. 11, p. 534.
145. R.H. Hill and M.S. Wrighton. **1987**, *Organometallics*, Vol. 6, p. 632.

References

146. D.M. Haddleton and R.N. Perutz. **1985**, *J. Chem. Soc. Chem. Commun.*, p. 1372.
147. D.M. Haddleton. **1986**, *J. Organomet. Chem.*, Vol. 311, p. C21.
148. G.E. Ball, T.A. Darwish, S. Geftakis, M.W. George, D.J. Laws, P. Portius and J.P. Rourke. **2005**, *PNAS*, Vol. 102, p. 1853.
149. D.J. Lawes, S. Geftakis and G.E. Ball. **2005**, *J. Am. Chem. Soc.*, Vol. 127, p. 4134.
150. C.J. Elsevier. **2004**, *Magn. Reson. Chem.*, Vol. 42, p. 719.
151. J.M. Brown. **2004**, *J. Organomet. Chem.*, Vol. 689, p. 4006.
152. B.E. Mann. **1988**, *Adv. Organomet. Chem.*, Vol. 28, p. 397.
153. S. Berger and S. Braun. *200 and More NMR Experiments: A Practical Course*. Weinheim : Wiley-VCH, **2004**.
154. H. Gunther. *NMR spectroscopy: Basic Principles, Concepts and Applications in Chemistry*. Chichester : John Wiley & Sons, **1995**.
155. H. Brunner, J. Wachter, I. Bernal, G.M. Reisner and R. Benn. **1983**, *J. Organomet. Chem.*, Vol. 243, p. 179.
156. A.D. Bain. **2003**, *Prog. Nucl. Magn. Reson. Spectrosc.*, Vol. 43, p. 63.
157. G.D. Gilbert and G. Wilkinson. **1969**, *J. Chem. Soc. A*, p. 1749.
158. M.I. Bruce, C. Hameister, A.G. Swincer and R.C. Wallis. *Inorg Synth*. John Wiley & Sons, Inc., **1991**, Vol. 28.
159. S.G. Davies, J.P. McNally and A.J. Smallridge. **1990**, *Adv. Organomet. Chem.*, Vol. 30, p. 1.
160. T. Blackmore, M.I. Bruce and F.G.A. Stone. **1971**, *J. Chem. Soc. A*, p. 2376.
161. M.I. Bruce and N.J. Windsor. **1977**, *Aust. J. Chem.*, Vol. 30, p. 1601.
162. G.S. Ashby, M.I. Bruce, I.B. Tomkins and R.C. Wallis. **1979**, *Aust. J. Chem.*, Vol. 32, p. 1003.

163. M.I. Bruce, F.S. Wong, B.W. Skelton and A.H. White. **1981**, *J. Chem. Soc. Dalton Trans.*, p. 1398.
164. M.I. Bruce, M.G. Humphery, J.M. Patrick and A.H. White. **1983**, *Aust. J. Chem.*, Vol. 36, p. 2065.
165. Y. Wakatsuki and A.Horiuchi. **2001**, *J. Am. Chem. Soc.*, Vol. 123, p. 11917.
166. D.B. Grotjahn and D.A. Lev. **2004**, *J. Am. Chem. Soc.*, Vol. 126, p. 12232.
167. V. Cadierno, P.Crochet, S.E. García-Carrido and J. Gimeno. **2004**, *Dalton Trans.*, p. 3635.
168. A. Varela-Fernández, C. García-Yebra, J.A. Varela, M.A. Esteruelas and C. Saá. **2010**, *Angew. Chem. Int. Ed.*, Vol. 49, p. 4278.
169. I.R. Whittall, M.G. Humphrey, M. Samoc, J. Swiatkiewicz and B. Luther-Davies. **1995**, *Organometallics*, Vol. 14, p. 5493.
170. C. Ornelas, C. Gandum, J. Mesquita, J. Rodrigues, M.H. Garcia, N. Lopes, M.P. Robalo, K. Nättinen and K. Rissanen. **2005**, *Inorg. Chim. Acta.*, Vol. 358, p. 2482.
171. B. Wardle. *Principles and Applications of Photochemistry*. Cornwall : John Wiley & Sons Ltd, **2009**.
172. P.C. Ford, J.D. Petersen and R.E. Hintze. **1974**, *Coord. Chem. Rev.*, Vol. 14, p. 67.
173. T.R. Ward, O. Schafer, C. Daul and P. Hofmann. **1997**, *Organometallics*, Vol. 16, p. 3207.
174. H. Brunner, H. Ike, M. Muschiol, T. Tsuno, N. Umegaki and M. Zabel. **2011**, *Organometallics*, Vol. 30, p. 414.
175. H. Brunner, M. Muschiol, T. Tsino, T. Takahashi and M. Zabel. **2008**, *Organometallics*, Vol. 27, p. 3514.
176. T.M. Douglas, S.K. Brayshaw, R. Dallanegra, G. Kociok-Köhn, S.A. Macgregor, G.L. Moxham, A.S. Weller, T. Wondimagegn and P. Vadivelu. **2008**, *Chem. Eur. J.*, Vol. 14, p. 1004.

References

177. S-I. Aizawa, T. Kawamoto, S. Nishigaki and A. Sasaki. **2011**, *J. Organomet. Chem.*, Vol. 696, p. 2471.
178. N.E. Jacobsen. *NMR spectroscopy explained: simplified theory, applications and examples for organic chemistry and structural biology*. New Jersey : Wiley-Interscience, **2007**.
179. A. Coto, M.J. Tenorio, M.C. Puerta and P. Valerga. **1998**, *Organometallics*, Vol. 17, p. 4392.
180. T. Wilczewski, M. Bocheńska and J.F. Biernat. **1981**, *J. Organomet. Chem.*, Vol. 215, p. 87.
181. M.F. Joseph, J.A. Page and M.C. Baird. **1984**, *Organometallics*, Vol. 3, p. 1749.
182. M. Cao, L.V. Do, N.W. Hoffman, M-L. Kwan, J.K. Little, J.M. McGilvray, C.B. Morris, B.C. Söderberg, A. Wierzbicki, T.R. Cundari, C.H. Lake and E.J. Valente. **2001**, *Organometallics*, Vol. 20, p. 2270.
183. M.I. Bruce and R.C. Wallis. **1981**, *Aust. J. Chem.*, Vol. 34, p. 209.
184. J.C.A. Boeyens, N.J. Coville and K. Soldenhoff. **1984**, *S. Afr. J. Chem.*, Vol. 37, p. 153.
185. F.M. Conroy-Lewis and S.J. Simpson. **1989**, *J. Organomet. Chem.*, Vol. 332, p. 221.
186. Y. Yang, K.A. Abboud and L. McElwee-White. **2003**, *Dalton Trans.*, p. 4288.
187. R.J. Kulawiec, J.W. Faller and R.H. Crabtree. **1990**, *Organometallics*, Vol. 9, p. 745.
188. R.J. Haines and A.L. Dupreez, **1975**, *J. Organomet. Chem.*, Vol. 84, p. 357.
189. R.M. Chin, L. Dong, S.B. Duckett and W.D. Jones. **1991**, *Organometallics*, Vol. 11, p. 871.
190. M.I. Bruce, R.C.F. Gardner and F.G.A. Stone. **1976**, *J. Chem. Soc. Dalton Trans.*, p. 81.

191. L. Pauling, *The Nature of the Chemical Bond*. USA: Cornell University, **1960**.
192. A.J. Vanderwielen and M.A. Ring. **1972**, *Inorg. Chem.* Vol. 11, p. 246
193. H. Lemkuhl, M. Bellenbaum and J. Grundke. **1987**, *J. Organomet. Chem.*, Vol. 330, p. C23
194. H. Lehmkuhl, M. Bellenbaum, J. Grundke, H. Mauermann and C. Kruger. **1988**, *Chem. Ber.*, Vol. 121, p. 1719.
195. M. Lail, C.M. Bell, D. Conner, T.R. Cundari, T.B. Gunnoe and J.L. Petersen. **2004**, *Organometallics*, Vol. 23, p. 5020.
196. M.I. Bruce, R.C.F. Gardner and F.G.A. Stone. **1976**, *J. Chem. Soc. Dalton Trans.*, p. 81.
197. M.I. Bruce, M.P. Cifuentes, M.G. Humphrey, E. Proczman, M.R. Snow and E.R.T Tiekink. **1988**, *J. Organomet. Chem.*, Vol. 338, p. 237.
198. M. Bassetti, S. Marini, F. Tortorella, V. Cadierno, J. Diez, M.P. Gamasa and J. Gimeno. **2000**, *J. Organomet. Chem.*, Vol. 593, p. 292.
199. P. Novak and M. Kotora. **2009**, *Collect. Czech. Chem. Commun.*, Vol. 74, p. 433.
200. T. Blackmore, M.I. Bruce and F.G.A. Stone. **1971**, *J. Chem. Soc. A*, p. 2376.
201. C. Pejp, H. Pardo, A. Mombru, M.F. Cerda, J.S. Gancheff, R. Chiozzzone and R. Gonzalez. **2011**, *Inorg. Chim. Acta.*, Vol. 736, p. 105.
202. J-Q. Yu. *Topics in Current Chemistry: C-H activation*. Heidelberg : Springer, **2010**.
203. M.K. Whittlesey, R.N. Perutz, I.G. Virrels and M.W. George. **1997**, *Organometallics*, Vol. 16, p. 145.
204. W.D. Jones, and F.J. Feher. **1984**, *J. Am. Chem. Soc.*, Vol. 106, p. 1650.
205. W.D. Jones, V.L. Chandler and F.J. Feher. **1990**, *Organometallics*, Vol. 9, p. 164.

References

206. M. Brookhart, D.M. Lincoln, M.A. Bennett and S. Pelling. **1990**, *J. Am. Chem. Soc.*, Vol. 112, p. 2691.
207. M. Ogasawara, K. Aoyagi and M. Saburi. **1993**, *Organometallics*, Vol. 12, p. 3393.
208. M. Ogasawara and M. Saburi. **1994**, *Organometallics*, Vol. 13, p. 1911.
209. J.A. Calladine, O. Torres, M. Anstey, G.E. Ball, R.G. Bergman, J. Curley, S.B. Duckett, M.W. George, A.I. Gilson, D.J. Lawes, R.N. Perutz, S. Xue-Zhong and K.P.C. Vollhardt. **2010**, *Chem. Sci.*, Vol. 1, p. 622.
210. J.A. Calladine, S.B. Duckett, M.W. George, S.L. Matthews, R.N. Perutz, O. Torres and K.Q. Vuong. **2011**, *J. Am. Chem. Soc.*, Vol. 133, p. 2303.
211. G. Garrido, E. Koort, C. Raols, E. Bosch, T. Rodima, I. Leito and M. Roses. **2006**, *J. Org. Chem.*, Vol. 71, p. 9062.
212. K.C. Mcleod, J.L. Conway, B.O. Patrick and K.M. Smith. **2010**, *J. Am. Chem. Soc.*, Vol. 132, p. 17325.
213. H. Adams, N.A. Bailey, P. Cahill, D. Rogers and M.J. Winter. **1986**, *J. Chem. Soc. Dalton Trans.*, p. 2119.
214. G.R. Fulmer, A.J.M. Miller, N.H. Sherden, H.G. Gottlieb, A. Nudelman, B.M. Stoltz, J.E. Bercaw and K.I. Goldberg. **2010**, *Organometallics*, Vol. 29, p. 2176.
215. J.A.S. Howell and A.J. Anthony. **1980**, *J. Chem. Soc. Dalton Trans.*, p. 1845.
216. M.F. Joseph, J.A. Page and M.C. Baird. **1982**, *Inorg. Chim. Acta.*, Vol. 64, p. L121.
217. M.F. Joseph, J.A. Page and M.C. Baird. **1984**, *Organometallics*, Vol. 3, p. 1749.
218. H. Lehmkuhl, M. Bellernbaum and J. Grundke. **1987**, *J. Organomet. Chem.*, Vol. 330, p. C23.
219. C.J. Sexton. **2008**, *Ph.D. Thesis, University of York*.

220. C.D. Tagge and R.G. Bergman. **1996**, *J. Am. Chem. Soc.*, Vol. 118, p. 6908.
221. S.H. Meiere, J.M. Keane, T.B. Gunnoe, M. Sabat and W.D. Harman. **2003**, *J. Am. Chem. Soc.*, Vol. 125, p. 2024.
222. R.E. Jilek, M. Jang, E.D. Smolensky, J.D. Britton and J.E. Ellis. **2008**, *Angew. Chem. Int. Ed.*, Vol. 47, p. 8692.
223. S.H. Meiere, B.C. Brooks, T.B. Gunnoe, M. Sabat and W.D. Harman. **2001**, *Organometallics*, Vol. 20, p. 1038.
224. R.M. Chin, L. Dong, S.B. Duckett and W.D. Jones. **1992**, *Organometallics*, Vol. 11, p. 871.
225. C.J. Sexton, J. Lopez-Serrano, A. Lledos and S.B. Duckett. **2008**, *Chem. Commun.*, p. 4834.
226. H. Lehmkuhl, J. Grundke, G. Schroth and R. Benn. **1984**, *Z. Naturforsch. B*, Vol. 39, p. 1050.
227. B.A. Sexton, N.R. Avery and T.W. Turney. **1983**, *Surface. Sci.*, Vol. 124, p. 162.
228. W. Zierkiewicz and T. Privalov. **2005**, *Organometallics*, Vol. 24, p. 6019.
229. J.D. Fotheringham, G.A. Heath, A.J. Lindsay and T.A. Stephenson. **1986**, *J. Chem. Res. -S*, Vol. 3, p. 82.
230. D.A. Cheshkov, B.A. Belyaev, A.P. Belov and V.B. Rybakov. **2004**, *Acta Cryst.*, Vol. E60, p. m300.
231. G.J. Baird, S.G. Davies, S.D. Moon and S.J. Simpson. **1985**, *J. Chem. Soc. Dalton Trans.*, p. 1479.
232. S.G. Davies, S.D. Moon and S.J. Simpson. **1983**, *J. Chem. Soc. Chem. Commun.*, p. 1278.
233. M.I. Bruce, A. Catlow, M.G. Humphrey, G.A. Koutsantonis, M.R. Snow and E.R.T. Tiekink. **1988**, *J. Organomet. Chem.*, Vol. 338, p. 59.

References

234. D.M. Heinekey, N.G. Payne and C.D. Sofield. **1990**, *Organometallics*, Vol. 9, p. 2643.
235. R. Martinez, M-O. Simon, R. Chevalier, C. Pautigny, J-P. Genet and S. Darses. **2009**, *J. Am. Chem. Soc.*, Vol. 131, p. 7887.
236. V. Montiel-Palma, R.N. Perutz, M.W. George, O.S. Jina and S. Sabo-
Etienne. **2000**, *Chem. Commun.*, p. 1175.
237. A.W. Holland and R.G. Bergman. **2002**, *J. Am. Chem. Soc.*, Vol. 124, p.
14684.
238. F.R. Lemke and C. Chaitheerapakul. **1996**, *Polyhedron*, Vol. 15, p. 2559.
239. K.H. Pannell, T. Kobayashi and R.N. Kapoor. **1992**, *Organometallics*, Vol.
11, p. 2229.
240. W.D. Jones and F.J. Feher. **1984**, *J. Am. Chem. Soc.*, Vol. 106, p. 1650.
241. T. Sakakura and M. Tanaka. **1987**, *Chem. Lett.*, p. 1113.
242. M. Tanaka and T. Sakakura. **1990**, *Pure & Appl. Chem.*, Vol. 62, p. 1147.
243. P-C. Nam, M.T. Nguyen and A.K. Chandra. **2005**, *J. Phys. Chem. A*, Vol.
109, p. 10342.
244. W.D. Jones. **2005**, *Inorg. Chem.*, Vol. 44, p. 4475.
245. B. Rajagopalan, H. Cai, D.H. Busch and B. Subramaniam. **2008**, *Catal. Lett.*,
Vol. 123, p. 46.
246. S. Rayne and K. Forest. *Nature Precedings*. [Online] 7 May **2010**,
<http://precedings.nature.com/documents/4425/version/1>.
247. W.D. Jones and F.J. Feher. **1989**, *Acc. Chem. Res.*, Vol. 22, p. 91.
248. P.E.M. Siegbahn. **1995**, *J. Phys. Chem.*, Vol. 99, p. 12723.
249. A.H. Janowicz and R.G. Bergmann. **1983**, *J. Am. Chem. Soc.*, Vol. 105, p.
3929.

250. J.M. Buchanan, J.M. Stryker and R.G. Bergman. **1986**, *J. Am. Chem. Soc.*, Vol. 108, p. 1537.
251. M.B. Sponsler, B.H. Weiller, P.O. Stoutland and R.G. Bergman. **1989**, *J. Am. Chem. Soc.*, Vol. 111, p. 6841.
252. R.A. Periana and R.G. Bergman. **1986**, *J. Am. Chem. Soc.*, Vol. 108, p. 7332.
253. N.A. Jasim, R.N. Perutz, A.C. Whitwood, T. Braun, J. Izundu, B. Neumann, S. Rothfeld and H-G. Stammer. **2004**, *Organometallics*, Vol. 23, p. 6140.
254. G.E. Ball, C.M. Brookes, A.J. Cowan, T.A. Darwish, M.W. George, H.K. Kawanami, P.Portius and J.P. Rourke. **2007**, *PNAS*, Vol. 104, p. 6927.
255. D. Bravo-Zhivotovskii, H. Peleg-Vasserman, M. Kosa, G. Molev, M. Botoshanskii and Y. Apeloig. **2004**, *Angew. Chem. Int. Ed.*, Vol. 43, p. 745.
256. C. Belon, X. Allonas, C. Croutxe-Barghorn and J. Lalevee. **2010**, *J. Polym. Sci. Pol. Chem.*, Vol. 48, p. 2462.
257. B.A. Moyer, B.K. Sipe and T.J. Meyer. **1981**, *Inorg. Chem.*, Vol. 20, p. 1475.
258. C.M. Che and K.Y. Yong, **1989**, *J. Chem. Soc. Dalton Trans.*, p. 2065.
259. M.I. Bruce, M.G. Humphrey, A.G. Swincer and R.C. Wallis. **1984**, *Aust. J. Chem.*, Vol. 37, p. 1747.
260. G.J. Baird, S.G. Davies, S.D. Moon, S.J. Simpson and R.H. Jones. **1985**, *J. Chem. Soc. Dalton Trans.*, p. 1479.
261. D.V. Gutsulyak, A.L. Osipov, L.G. Kuzmina, J.A.K. Howard and G.I. Nikonov. **2008**, *Dalton Trans.*, p. 6850.
262. T. Wilczewski, M. Bochenska and J.F. Biernat. **1981**, *J. Organomet. Chem.*, Vol. 215, p. 87.
263. L. Vaska and J.W. DiLuzio. **1962**, *J. Am. Chem. Soc.*, Vol. 84, p. 4989.
264. A.D. Zotto, W. Baratta, M. Sandri, G. Verado and P. Rigo. **2004**, *Eur. J. Inorg. Chem.*, p. 524.
265. H. Lehmkuhl, J. Grundke and R. Mynott. **1983**, *Chem. Ber.*, Vol. 116, p. 159.

References

266. R.F.N. Ashok, M. Gupta, K.S. Arulsamy and U.C. Agarwala. **1985**, *Inorg. Chim. Acta.*, Vol. 98, p. 169.
267. W. Baratta, A.D. Zotto and P. Rigo. **1999**, *Organometallics*, Vol. 18, p. 5091.
268. H. Guan, M. Iimura, M.P. Magee, J.R. Norton and G. Zhu. **2005**, *J. Am. Chem. Soc.*, Vol. 127, p. 7805.
269. Y. Guo, X. Zhao, D. Zhang and S-I. Murahashi. **2009**, *Angew. Chem. Int. Ed.*, Vol. 121, p. 2081.
270. H. Hebbache, T. Jerphagnon, H. Thomas, Z. Hank, C. Bruneau and J-L. Renaud. **2010**, *J. Organomet. Chem.*, Vol. 695, p. 870.
271. M.I. Bruce, A. Catlow, M.G. Humphrey, G.A. Koutsantonis, M.R. Snow and E.R.T. Tiekink. **1988**, *J. Organomet. Chem.*, Vol. 338, p. 59.
272. T. Wilczewski, Z. Dauter. **1986**, *J. Organomet. Chem.*, Vol. 312, p. 349.
273. B.K. Champion, R.H. Heyn and T.D. Tilley. **1992**, *J. Chem. Soc. Chem. Commun.*, p. 1201.
274. B.K. Champion, R.H. Heyn, T.D. Tilley and A.L. Rheingold. **1993**, *J. Am. Chem. Soc.*, Vol. 115, p. 5527.
275. H. Lehmkuhl, J. Grundke, R. Benn, G. Scroth and R. Mynott. **1981**, *J. Organomet. Chem.*, Vol. 217, p. C5.
276. Y. Guo, X. Zhao, D. Zhang and S-I. Murahashi. **2009**, *Angew. Chem.*, Vol. 121, p. 2081.
277. R. B. Hitam, K. A. Mahmoud and A. J. Rest. **1985**, *J. Organomet. Chem.*, Vol. 291, p. 321.
278. N.M. Brunkan and W.D. Jones. **2003**, *J. Organomet. Chem.*, Vol. 683, p. 77.
279. M.I. Bruce, R.C.F. Gardner, J.A.K. Howard, F.G.A. Stone, M. Welling and P. Woodward. **1977**, *J. Chem. Soc. Dalton Trans.*, p. 621.
280. E.E. Karslyan, D. S. Perekalin, P. V. Petrovskii, K. A. Lyssenko and A. R. Kudinov. **2008**, *Russ. Chem. Bull. Int. Ed.*, Vol. 57, p. 2201.

281. E.E. Karslyan, D.S. Perekalin, P.V. Petrovskii, A.O. Borisova, and A.R. Kudinov. **2009**, *Russ. Chem. Bull. Int. Ed.*, Vol. 58, p. 586.
282. L. Hintermann, L. Xiao, A. Labonne and U. Englert. **2009**, *Organometallics*, Vol. 28, p. 5739.
283. P.G. Hayes, R. Waterman, P.B. Glaser and T.D. Tilley. **2009**, *Organometallics*, Vol. 28, p. 5082.
284. T.C.T. Chang, M. Rosenblum and N. Simms. **1993**, *Org. Synth.*, Vol. 8, p. 479.
285. T. Blackmore, M.I. Bruce and F.G.A. Stone. **1971**, *J. Chem. Soc. A*, p. 2376.
286. K.H. Pannell, T. Kobayashi and R.N. Kapoor. **1992**, *Organometallics*, Vol. 11, p. 2229.
287. H. Lehmkuhl, J. Grundke and R. Mynott. **1983**, *Chem. Ber.*, Vol. 116, p. 176.
288. J. Campora, J.A. Lopez, P. Palma, C. Ruiz and E. Carmona. **1997**, *Organometallics*, Vol. 16, p. 2709.
289. J. Campora, J.A. Lopez, C.M. Maya, P. Palma and E. Carmona. **2000**, *Organometallics*, Vol. 19, p. 2707.
290. B.Y. Lee, G.C. Bazan, J. Vela, Z.J.A. Komon and X. Bu. **2001**, *J. Am. Chem. Soc.*, Vol. 123, p. 5352.
291. Z.J.A. Komon, G.M. Diamond, M.K. Leclerc, V. Murphy, M. Okazaki and G.C. Bazan. **2002**, *J. Am. Chem. Soc.*, Vol. 124, p. 15280.
292. I. Albers, E. Alvarez, J. Campora, C.M. Maya, P. Palma, L.J. Sanchez and E. Passaglia. **2004**, *J. Organomet. Chem.*, Vol. 689, p. 833.
293. T.C. Forschner and A.R. Cutler. **1985**, *Organometallics*, Vol. 4, p. 1247.
294. M.I. Bruce, A. Catlow, M.G. Humphrey, G.A. Koutsantonis, M.R. Snow and E.R.T. Tiekink. **1988**, *J. Organomet. Chem.*, Vol. 338, p. 59.

References

295. G.J. Baird, S.G. Davies, S.D. Moon, S.J. Simpson and R.H. Jones. **1985**, *J. Chem. Soc. Dalton Trans.*, p. 1479.
296. H. Lehmkuhl, M. Bellenbaum and J. Grundke. **1987**, *J. Organomet. Chem.*, Vol. 330, p. C23.
297. R.B. King. **1963**, *Inorg. Chem.*, Vol. 2, p. 528.
298. W.D. Jones. **2005**, *Inorg. Chem.*, Vol. 44, p. 4475.
299. H. Chen, S. Schlecht, T.C. Semple and J.F. Hartwig. **2000**, *Science*, Vol. 287, p. 1995.
300. J.F. Hartwig, K.S. Cook, M. Hapke, C.D. Incarvito, Y. Fan, C.E. Webster and M.B. Hall. **2005**, *J. Am. Chem. Soc.*, Vol. 127, p. 2538.
301. M.J. Fernandez, P.M. Bailey, P.O. Bentz, J.S. Ricci, T.F Koetzle and P.M. Maitlis. **1984**, *J. Am. Chem. Soc.*, Vol. 106, p. 5458.
302. G.J. Nikonov. **2005**, *Adv. Organomet. Chem.*, Vol. 53, p. 217.
303. S.B. Duckett and R.N Perutz. **1991**, *J. Chem. Soc. Chem. Commun.*, p. 28.
304. J.F. Hartwig. *Activation and Functionalization of C-H Bonds; ACS Symposium Series 885*. [ed.] K.I. Goldberg and A.S. Goldberg. Washington : American Chemical Society, **2004**.
305. Y-F. Han, Y-J. Lin and G-X. Jin. **2011**, *Dalton Trans.*, Vol. 40, p. 10370.
306. R. Cramer. **1974**, *Inorg. Synth.*, Vol. 15, p. 14.
307. A.C. Esqueda, S. Conejuro, C. Maya and E. Carmona. **2010**, *Organometallics*, Vol. 29, p. 5481.
308. D.M. Haddleton. **1986**, *J. Organomet. Chem.*, Vol. 311, p. C21.
309. D.M. Haddleton, A. McCamley and R.N. Perutz. **1988**, *J. Am. Chem. Soc.*, Vol. 110, p. 1810.
310. M.W. George, M.B. Hall, O.S. Jina, P. Portius, S. Xue-Zhong, M. Towrie, H. Wu, X. Yang and S.D. Zaric. **2010**, *PNAS*, Vol. 107, p. 20178.

311. M.W. George, M.B. Hall, P. Portius, A.L. Renz, S. Xue-Zhong, M. Towrie and X. Yang. **2011**, *Dalton Trans.*, Vol. 40, p. 1751.
312. J.M. Mayer and J.C. Calabrese. **1984**, *Organometallics*, Vol. 3, p. 1292.
313. M.V. Campian, J.L. Harris, N. Jasim, R.N. Perutz, T.B. Marder and A.C. Whitwood. **2006**, *Organometallics*, Vol. 25, p. 5093.
314. S.T. Belt, D.M. Haddleton, R.N. Perutz, B.P.H. Smith and A.J. Dixon. **1987**, *J. Chem. Soc. Chem. Commun.*, p. 1347.
315. S.B. Duckett, D.M. Haddleton, S.A. Jackson, R.N. Perutz, M. Poliakoff and R.K. Upmacis. **1988**, *Organometallics*, Vol. 7, p. 1526.
316. C. Godard, P. Callaghan, J.L. Cunningham, S.B. Duckett, J.A.B. Lohman and R.N. Perutz. **2002**, *Chem. Commun.*, p. 2836.
317. C. Godard, S.B. Duckett, S. Parsons and R.N. Perutz. **2003**, *Chem. Commun.*, p. 2332.
318. S.T. Belt, S.B. Duckett, D.M. Haddleton and R.N. Perutz. **1989**, *Organometallics*, Vol. 8, p. 748.
319. T.W. Bell, D.M. Haddleton, A. McCamley, M.G. Partridge, R.N. Perutz and H. Willner. **1990**, *J. Am. Chem. Soc.*, Vol. 112, p. 9212.
320. S.T. Belt, S.B. Duckett, D.M. Haddleton and R.N. Perutz. **1989**, *Organometallics*, Vol. 8, p. 752.
321. H.E. Gottlieb, V. Kotlyar and A. Nudelman. **1997**, *J. Org. Chem.*, Vol. 62, p. 7512.
322. S. Berger and S. Braun. *200 and more NMR experiments: A practical course*. Weinheim : Wiley-VCH, **2004**.
323. K. Stott, J. Stonehouse, J. Keeler, T.L. Hwang and A.J. Shaka. **1995**, *J. Am. Chem. Soc.*, Vol. 117, p. 4199.
324. R. Wagner and S. Berger. **1996**, *J. Magn. Reson. Ser. A*, Vol. 123, p. 119.

References

325. J. Stonehouse, P. Adell, J. Keeler and A.J. Shaka. **1994**, *J. Am. Chem. Soc.*, Vol. 116, p. 6037.
326. M.I. Bruce, C. Hameister, A.G. Swincer and R.C. Wallis. **1991**, *Inorg. Synth.*, Vol. 28, p. 270.
327. T. Blackmore, M.I. Bruce and F.G.A. Stone. **1971**, *J. Chem. Soc. A*, p. 2376.
328. M.I. Bruce, M.P. Cifuentes, M.G. Humphrey, E. Proczman, M.R. Snow and E.R.T. Tiekink. **1988**, *J. Organomet. Chem.*, Vol. 338, p. 237.
329. D. Schott. **2002**, *D. Phil. Thesis, University of York*.
330. T. Wilczewski, M. Bochenska and J.F. Biernat. **1981**, *J. Organomet. Chem.*, Vol. 215, p. 87.
331. J.W. Curry. **1956**, *J. Am. Chem. Soc.*, Vol. 78, p. 1686.
332. P. Klæboe, C.J. Richard, V. Aleksa, C.J. Nielsen, G.A. Guirgis and J.R. Durig. **2003**, *J. Mol. Struct.*, Vol. 661, p. 81.
333. M. Weinmann, T.W. Kamphowe, P. Fischer and F. Aldinger. **1999**, *J. Organomet. Chem.*, Vol. 592, p. 115.
334. A.I. Vogel, B.S. Furniss, A.J. Hannaford, P.W.G. Smith and A.R. Tatchell. *Vogel's Textbook of Practical Organic Chemistry*. 5th Edition. Essex : Pearson - Prentice Hall, **1989**.
335. T.C.T. Chang, M. Rosenblum and N. Simms. **1993**, *Org. Synth.*, Vol. 8, p. 479.
336. R.B. King. **1963**, *Inorg. Chem.*, Vol. 2, p. 528.
337. R. Cramer. **1974**, *Inorg. Synth.*, Vol. 15, p. 14.
338. S.T. Belt, S.B. Duckett, D.M. Haddleton and R.N. Perutz. **1989**, *Organometallics*, Vol. 8, p. 748.
339. C. Godard, P. Callaghan, J.L. Cunningham, S.B. Duckett, J.A.B. Lohman and R.N. Perutz. **2002**, *Chem. Commun.*, p. 2836.

340. R.A. Sanchez-Delgado, J.S. Bradley and G. Wilkinson. **1976**, *J. Chem. Soc. Dalton Trans.*, p. 399.
341. S.B. Duckett and N.J. Wood. **2008**, *Coord. Chem. Rev.*, Vol. 252, p. 2278.
342. D. Schott, C.J. Sleigh, J.P. Lowe, S.B. Duckett, R.J. Mawby and M.G. Partridge. **2002**, *Inorg. Chem.*, Vol. 41, p. 2960.
343. W.D. Jones, G.P. Rosini and J.A. Maguire. **1998**, *Organometallics*, Vol. 18, p. 1754.
344. M.L.H. Green, L.L. Wong and A. Sella. **1992**, *Organometallics*, Vol. 11, p. 2660.